PB97-172464

EARTHQUAKE ENGINEERING RESEARCH AT BERKELEY, 1996

CALIFORNIA UNIV., RICHMOND

FEB 97

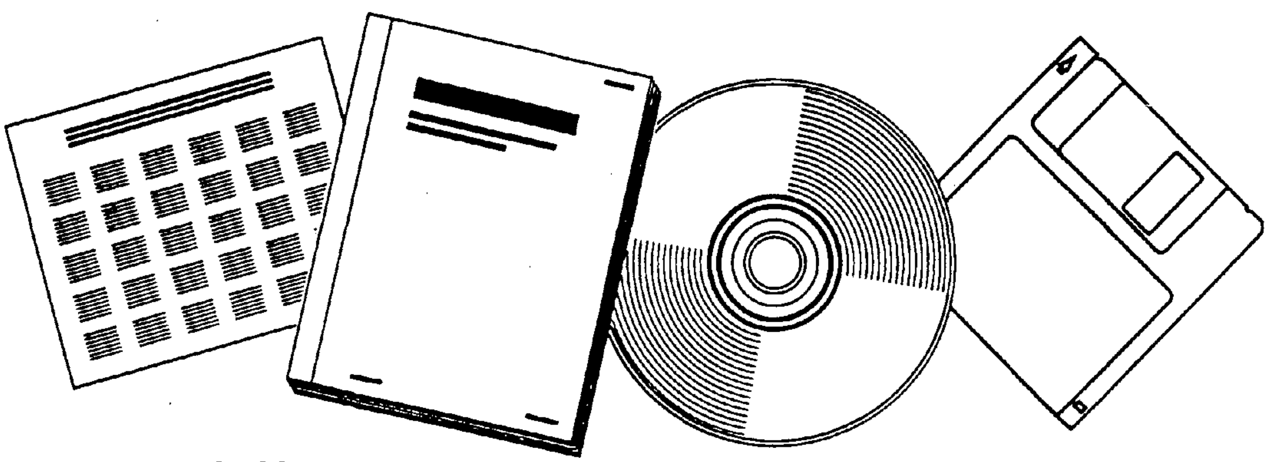

U.S. DEPARTMENT OF COMMERCE
National Technical Information Service

REPORT NO.
UCB/EERC-96/01
MAY 1996

EARTHQUAKE ENGINEERING RESEARCH CENTER

EARTHQUAKE ENGINEERING RESEARCH AT BERKELEY — 1996:

PAPERS PRESENTED AT THE 11TH WORLD CONFERENCE ON EARTHQUAKE ENGINEERING

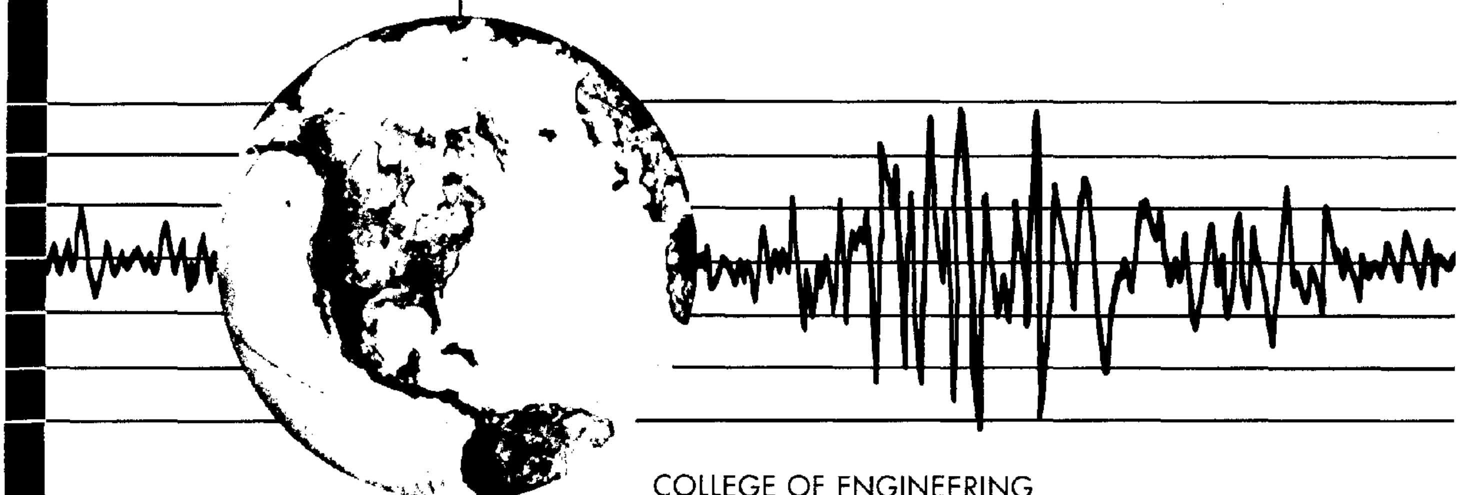

COLLEGE OF ENGINEERING

UNIVERSITY OF CALIFORNIA AT BERKELEY

For sale by the National Technical Information Service, U.S. Department of Commerce, Springfield, Virginia 22161

See back of report for up to date listing of EERC reports.

EARTHQUAKE ENGINEERING RESEARCH AT BERKELEY -- 1996:

PAPERS PRESENTED AT THE 11TH WORLD CONFERENCE ON EARTHQUAKE ENGINEERING

Report No. UCB/EERC-96/01
Earthquake Engineering Research Center
College of Engineering
University of California at Berkeley

May 1996

50272-101

PB97-172464

REPORT DOCUMENTATION PAGE	1. REPORT NO.	2.

4. Title and Subtitle Papers Presented at the 11th World Conference on Earthquake Engineering	5. Report Date May 1996
	6.
7. Author(s)	8. Performing Organization Rept. No. UCB/EERC-96/01
9. Performing Organization Name and Address Earthquake Engineering Research Center University of California at Berkeley 1301 S. 46th Street Richmond, CA 94804	10. Project/Task/Work Unit No.
	11. Contract(C) or Grant(G) No. (C) UCB/EERC-96/01 (G)
12. Sponsoring Organization Name and Address Earthquake Engineering Research Center University of California at Berkeley 1301 S. 46th Street Richmond, CA 94804	13. Type of Report & Period Covered Final
	14.

15. Supplementary Notes

16. Abstract (Limit: 200 words)

Twenty-seven papers by faculty participants and research personnel associated with the Earthquake Engineering Research Center of the University of California at Berkeley will be presented at the Eleventh World Conference on Earthquake Engineering to be held in Acapulco, Mexico, June 23-28, 1996. The papers have been compiled in this report to illustrate some of the research work in earthquake engineering being conducted at the University of California at Berkeley.

17. Document Analysis a. Descriptors

b. Identifiers/Open-Ended Terms

c. COSATI Field/Group

18. Availability Statement	19. Security Class (This Report) unclassifed	21. No. of Pages 240
	20. Security Class (This Page) unclassfied	22. Price

(See ANSI-Z39.18) See Instructions on Reverse

OPTIONAL FORM 272 (4-
(Formerly NTIS-35)
Department of Commerce

FORWARD

Twenty-seven papers by faculty participants and research personnel associated with the Earthquake Engineering Research Center of the University of California at Berkeley will be presented at the Eleventh World Conference on Earthquake Engineering to be held in Acapulco, Mexico, June 23-28, 1996. The papers have been compiled in this report to illustrate some of the research work in earthquake engineering being conducted at the University of California at Berkeley. The research has been sponsored by the following agencies:

Applied Technology Council
California Department of Transportation
California Division of Mines and Geology
California Seismic Safety Commission
Caltrans
ERICO U.S.A.
Federal Emergency Management Agency
Headed Reinforcement Canada
National Science Foundation
National Science Research Foundation of Chile
Strong Motion Instrumentation Program
3M Company

TABLE OF CONTENTS

Preceding page blank

PERFORMANCE-BASED EARTHQUAKE-RESISTANT DESIGN BASED ON COMPREHENSIVE DESIGN PHILOSOPHY AND ENERGY CONCEPTS

RAUL D. BERTERO[1], VITELMO V. BERTERO[2] and AMADOR TERAN-GILMORE[3]

1 Larrea 1224 6^{O}B, Capital Federal 1117, R. Argentina
2 Earthquake Engineering Research Center, UC Berkeley, 1301 S. 46th St., Richmond CA 94804, U.S.A.
3 Universidad Autonoma Metropolitana, Av. San Pablo #180, Col. Reynosa, 02200 Mexico, D.F. Mexico

ABSTRACT

The main objectives of this paper are: to discuss the need for earthquake-resistant design (EQ-RD) and EQ-resistant construction (EQ-RC) approaches that will result in buildings with more predictable performance under EQ ground motions (EQGMs) than structures built according to current approaches; to present a general conceptual framework for performance-based EQ-RD and EQ-RC; to review a general comprehensive performance-based EQ-RD approach based on the use of energy concepts, performance (or damage) indices, and fundamental principles of structural dynamics and comprehensive design philosophy; to compare the general approach to current code; and to identify research needs for improving the proposed approach and its implementation in practice.

KEYWORDS

Comprehensive design; conceptual design; energy balance equation; energy-based design; damage index; damage spectra; performance-based seismic design; performance design objectives; performance levels; performance objective matrix.

INTRODUCTION

A review of the performance of facilities during the EQs of the last decade, particularly the 1989 Loma Prieta, the 1994 Northridge, and especially the 1995 Great Hanshin, clearly shows the need for EQ-RD and EQ-RC approaches that will result in civil engineering facilities that perform more predictably under EQGMs. The number of people made homeless and the level of economic loss from physical damage to nonengineered houses and engineered facilities, and particularly from functional and indirect damages, are socially and economically unacceptable. This is not surprising in view of the insistence of current seismic codes on EQ-RD approaches that are based on just a life-safety performance level which has no clear quantitative definition, and on following procedures that ***satisfy only strength requirements***. Although the understanding of the basic problems created by EQs and of the behavior of structures subjected to EQGMs has improved significantly, and this improvement has been reflected in the formulation of improved code requirements for the design and particularly the detailing of structural members, current seismic code design approaches fall short of realizing the goals and objectives of the worldwide-accepted philosophy of EQ-RD. Present seismic codes are not transparent, i.e., their regulations do not present in a visible way the basic concepts that govern the EQ performance of civil engineering facilities. Arising from the above need, already pointed out by the 1989 Loma Prieta EQ and emphasized by the 1994 Northridge EQ, the Structural Engineering Association of California (SEAOC), established the Vision 2000 Committee to develop a conceptual comprehensive framework for seismic codes. This framework, which is called ***performance-based seismic engineering***, regulates all areas that a seismic code should: conceptual overall design, preliminary numerical design, acceptability analysis, final design and detailing, quality assurance during construction and monitoring of occupancy and maintenance. The authors, based on studies they conducted previously, have developed and incorporated into this performance-based seismic engineering a ***comprehensive EQ-RD approach.*** It considers four performance levels (service or fully operational, operational, life safety, and impeding collapse) and four levels of EQGMs (frequent, moderate, rare, and very rare or extreme). The iterative procedure involved in this general comprehensive approach is reviewed below in some detail. The conceptual methodology for the comprehensive performance-based EQ-RD was developed in accordance with the comprehensive design philosophy and in compliance with the worldwide-accepted EQ-RD philosophy, and is based on the use of energy concepts and fundamental principles of structural dynamics. It takes into account from the beginning of the EQ-RD procedure the simultaneous demands for strength (C_y), deformation (δ) and rate of deformation (including torsional effects), and their combined effects on the energy input (E_I), on the demanded and supplied energy capacities [E_E (elastic energy) = E_K (kinetic) + E_S (elastic strain), and the E_D (dissipated energy) = $E_{H\mu}$ (hysteretic plastic deformations) and $E_{H\xi}$ (damping)] of the entire facility system and on the acceptable damage at the different limit states associated with the desired performance levels. Before discussing this comprehensive EQ-RD approach, it is convenient to define and discuss briefly what is understood by performance-based seismic engineering.

PERFORMANCE-BASED SEISMIC ENGINEERING

The Vision 2000 Committee of SEAOC in its 1995 report has defined performance-based seismic engineering as *"a process that begins with the first concepts of a project and lasts throughout the life of the building. It includes identification of seismic hazards, selection of the performance levels and design performance objectives, determination of site suitability, conceptual design, numerical preliminary design, final design, acceptability checks during design, design review, quality assurance during construction, and maintenance during the life of the building."* A conceptual framework for performance-based seismic engineering has been developed. This framework, which focuses on the case that seismic hazards control the design of building facilities, encompasses the full range of seismic engineering issues to be addressed in the design, construction and maintenance of structures for predictable and controlled seismic performance within established levels of risk. Herein only the methodology of the proposed comprehensive EQ-RD approach will be discussed.

COMPREHENSIVE EQ-RD APPROACH

Selection of Performance Objectives

The first step of the comprehensive design approach is the ***selection of the performance objectives.*** These are selected and expressed in terms of expected levels of damage resulting from expected levels of EQGMs. This selection is made by the client in consultation with the design professional based on consideration of the client's expectations, the seismic hazard exposure, economic analysis and acceptable risk. A design performance objective couples expected performance level with levels of possible seismic hazard, as illustrated in the Performance Objective Matrix (Fig.1). Performance levels are defined in terms of damage to the structure and nonstructural components, and in terms of consequences to the occupants and functions of the facility. The performance levels in Fig. 1 are as follows: *Fully Operational or Serviceable* (facility continues in operation with negligible damage); *Operational or Functional* (facility continues in operation with minor damage and minor disruption in non-essential services); *Life Safety* (life safety is substantially protected, damage is moderate to extensive); and *Near Collapse or Impending Collapse* (life safety is at risk, damage is severe, and structural collapse is prevented). The seismic hazard at a given site is represented as a set of EQGMs and associated hazards with specified probabilities of occurrence (*frequent, occasional, rare* and *very rare*).

Performance objectives typically include multiple goals. For example, for a given site they may be: fully operational in the 43-year event, operational in the 72-year event, life-safe in the 475-year event, and collapse prevention in the 970-year event. Two set of objectives are identified. *(i) Minimum objectives*: within this set, the *Basic Objective* is defined as the minimum acceptable performance objective for typical new buildings, while *Essential/Hazardous Objectives* and *Safety Critical Objectives* are defined as minimum objectives for facilities such as hospitals and nuclear material processing, respectively. These three minimum objectives are illustrated in Fig. 1 as diagonal lines in the *Performance Objective Matrix. (ii) Enhanced objectives*: other objectives providing better performance or lower risk than the minimum objectives may be selected at the client's discretion.

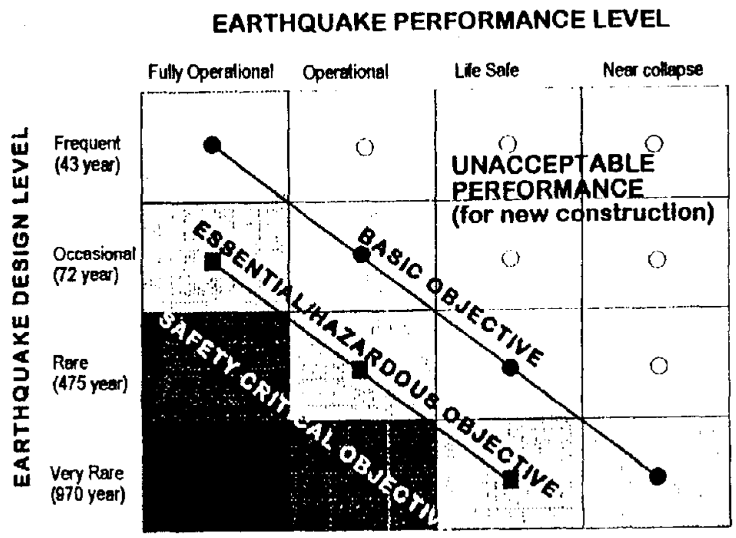

Figure 1. Recommended Seismic Performance Objectives for Buildings (SEAOC, 1995)

These objectives are termed "*enhanced objectives.*" The selection of performance objectives sets the acceptability criteria for the design. The performance objectives represent performance levels, or damage levels, expected to result from the selected corresponding design EQGMs. The performance levels are keyed to limiting values of measurable structural response parameters, such as drift, deformation rates, and ductility (monotonic and cumulative) demands. When the performance levels are selected, the associated limiting values become the acceptability criteria to be checked in later stages of the design.

Site Suitability

Before starting the structural design process, site suitability and seismic hazard analysis must be undertaken considering the proposed performance objectives. The EQGM design criteria are established and characterized in a form suitable for the anticipated structural analysis and design methods. Seismic hazard analysis determines the design EQGMs and other significant actions for the specified design events considering all critical seismic sources. It has to be decided whether it is economically possible to build the building on the selected site.

Conceptual Overall Seismic Design

Once the performance objectives are selected and the site suitability and seismic ground motions are established, the structural design process begins with the conceptual overall seismic design of the facility and acceptability checks of the conceptual overall design. Since the conceptual design is closely tied to the desired performance of a building, guidelines specifying appropriate limitations for configuration, structural layout, structural system, structural materials, and nonstructural components and their materials are needed for each performance objective. These must be defined in terms that are usable at the conceptual design stage. The level of restriction should increase in severity with the level of performance objective, and should reflect the excellent historical performance of regularly configured structural systems composed of well-detailed ductile materials properly constructed and maintained. A list of guidelines for overall seismic design of the entire building system is given in Appendix B of the SEAOC 1995 report.

Selection of the structural system and the design strategy to be used in the preliminary EQ-RD and the final sizing and detailing of the structural members should consider application of energy concepts through the use of the energy balance equation, which can be written as:

$$E_I = E_E + E_D = E_K + E_S + E_{H\xi} + E_{H\mu} \tag{1}$$

where E_I is the energy input at the foundation of the building due to the EQGMs, E_E is the stored elastic energy, E_D is the dissipated energy, E_K is the kinetic energy, E_S is the strain energy, $E_{H\xi}$ is the energy dissipated through hysteretic damping and $E_{H\mu}$ is the energy dissipated through hysteretic plastic deformation. The designer analyzes whether it is technically and economically possible to balance the seismic demand (E_I) using only the elastic behavior of the structure (E_E), or whether it is better to attempt to reduce E_E by dissipating the effects of E_I as much as possible using E_D. As shown in Eq. 1, there are three ways to increase E_D: one is to increase the linear viscous damping, $E_{H\xi}$; another is to increase the plastic hysteretic energy, $E_{H\mu}$; and third is a combination of increasing both. It is common practice to try to increase $E_{H\mu}$ as much as possible through inelastic behavior through the use of deformation ductility ratio, which implies damage of structural members throughout the structure. Only recently has it been recognized that it is possible to increase $E_{H\xi}$ significantly and control damage through the use of *energy dissipation devices* at proper locations throughout the structure. Increasing E_D by increasing $E_{H\xi}$ rather than $E_{H\mu}$ has the great advantage of providing control of the structure's behavior through all of its limit states (impending collapse, safety, operational or fully operational performance levels). Increasing $E_{H\mu}$ by just increasing μ will not improve behavior at the service limit state. If it is technically or economically impossible to balance the required E_I by E_E alone or through $E_E + E_D$, the designer has the option of attempting to decrease the E_I to the structure. This can be done by *seismic base isolation techniques*.

Comprehensive Numerical EQ-RD

In accordance with the comprehensive design philosophy, in the comprehensive EQ-RD approach ***an iterative procedure*** that starts with an efficient preliminary EQ-RD is recommended. The preliminary EQ-RD is divided into two main phases: ***establishment of the design EQGMs***, and ***numerical preliminary design procedure***.

First Phase: Establishment of the Design EQGMs. The essential information needed is the time history of the expected EQGMs at the different recurrence periods of the performance levels to be considered. Because of the uncertainties in predicting such EQGMs, it is necessary to specify for each recurrence period a suite of EQGM time histories. With this information, engineers can compute the specified detailed information needed to conduct the preliminary EQ-RD and acceptability analysis. The specific information to be obtained from processing the time history of the EQGMs at each of the recurrence periods are the *Smoothed Inelastic Design Response Spectra (SIDRS)* for strength, total acceleration, velocity, displacement, energy input and energy dissipation corresponding to the predicted or established suite of EQGMs. These spectra have to be computed considering the different levels of displacement ductility ratio, μ_δ , that can be accepted according to the desired performance (damage) at the recurrence period under consideration. These spectra should include as a particular case the *Smoothed Linear Elastic Design Spectra (SLEDRS)* for $\mu_\delta = 1$, and the SLEDRS corresponding to the EQGMs inducing allowable stress.

Second Phase: Numerical Preliminary Design Procedure. In order to arrive at the desired final design, it is necessary to start with a preliminary numerical design procedure, whose main objective is a design that is as close as possible to the desired final design. The numerical preliminary design phase consists of three main groups of steps: ***(i) preliminary analysis, (ii) preliminary sizing and detailing and (iii) acceptability checks of the preliminary design.***

In the preliminary design, the structural framing elements are sized and checked against selected criteria. The sizing is accomplished using a systematic design approach, which usually involves designing to at least meet two performance design objectives, one for full operation (service) and one for life-safety.

(i) Preliminary analysis. The preliminary analysis can be formulated using an equivalent single-degree-of-freedom (SDOF) system as follows:
GIVEN: Function of building and desired performance design objectives; general configuration, structural layout, structural system, structural materials and nonstructural components and contents; gravity, wind, snow and other possible loads or excitations; and SLERS, SIRS and γ-spectra for frequent minor and rare major EQGMs. The parameter γ is defined by Fajfar (1992) as:

$$\gamma = \left(\sqrt{\frac{E_{H\mu}}{m}}\right) \omega \delta \tag{2}$$

where ω is the frequency associated with the fundamental period of translation (T_1) of the structure, and **m** is

the reactive mass.
REQUIRED: Establishment of design criteria (acceptable damage levels under the established EQGM levels), minimum stiffness (or maximum period T) and minimum strength of the building capable of controlling the damage, the design seismic forces; and the critical load combinations.
SOLUTION: based on a transparent approach that take into account from the beginning that the building structure is a multi-degree-of-freedom (MDOF) system and that there can be important torsional effects even under service EQGMs (i.e., in the linear elastic response), and that for safety EQGMs these effects can be different; and that it is also necessary to consider the desired damage index (control of damage) corresponding to the hysteretic behavior of critical regions of members and connections, and the ductility ratio that can be used, as well as the expected overstrength.

Figure 2 shows a flow chart of the steps involved in the preliminary analysis. As shown in this figure, to initiate the preliminary analysis it is necessary to quantify the performance objectives by setting limits to the maximum value of all relevant response parameters, which for the case illustrated in this paper are: interstory drift demands for the service and safety limit states (IDI_{SER} and IDI_{SAF}, respectively); damage, through the use of damage indexes (DM_{SER} and DM_{SAF}); and probability of failure (PF_{SER} and PF_{SAF}). This quantification is possible through the knowledge of the qualitative definition of the Performance Objectives and through initial estimates of some of the relevant mechanical characteristics of the building, which should be established during the Conceptual Overall Seismic Design. For example, consider the limiting value assigned to IDI_{SER} or IDI_{SAF}: these values depend not only on the performance objectives, but also on the mechanical characteristics of the nonstructural elements and the detailing of their connection to the structure.

Because the preliminary analysis is formulated using an equivalent SDOF system, and this model cannot provide direct estimates of the local seismic demands, it is necessary to consider limits to the maximum value of the relevant response parameters at the global level. Thus, it is necessary to set limits to the global displacement demands in the building for service ($S_{d\ SER}$) and safety ($S_{d\ SAF}$) from their corresponding limits for IDI_{SER} and IDI_{SAF}. As shown, this is done by using the available estimates of the mechanical characteristics of the building to establish: a first mode shape, torsional effects, deviation from first mode shape, and concentration of plastic rotation demands over height.

Next, it is necessary to establish a value of target displacement ductility ratio, $\mu_{\delta TAR}$, defined as the maximum value of μ_δ that the structure can undergo during the safety limit state as limited by the requirement that the demanded $E_{H\mu}$ for this $\mu_{\delta TAR}$ will not exceed the supplied $E_{H\mu}$ capacity. As shown, establishing $\mu_{\delta TAR}$ requires using the available estimates of the mechanical characteristics to consider: concentration of nonlinear deformation demands, ultimate deformation capacity under monotonically increasing deformation, stability of hysteretic cycle, and $E_{H\mu}$ demands. The $E_{H\mu}$ demands can be estimated through the use of a γ-spectra obtained according to the estimated equivalent damping coefficient for safety (ξ_{SAF}) and the return period associated with the design ground motion for safety (T_{R2}). Although in many cases the value of γ is practically independent of the T_1 and μ_δ (provided $\mu_\delta \geq 2$), in some cases, such as EQGMs with very narrow frequency content, it may be necessary to consider the dependence of γ on T_1. Using the Park-Ang damage model (1985) and the parameter γ, estimates of $\mu_{\delta TAR}$ can be obtained from the following equality:

$$\frac{DM_{SAF}\ \theta_{u\ mon}}{\beta_2\ \theta} = 1 + \beta\,\gamma^2\,\mu_{\delta TAR} \tag{3}$$

where θ is the maximum rotation at the critical section during the seismic response; $\theta_{u\ mon}$ the ultimate monotonic rotation for the critical section; β_2 a parameter that quantifies the IDI increase due to concentration of plastic rotations in one story; and β a parameter that characterizes the stability of the hysteretic behavior of the frame members. In general, $\theta \approx$ maximum IDI in multistory frames, so that $\theta \approx IDI_{SAF}$ can be considered as an upper bound for θ. On the other hand, $\theta_{u\ mon}$ and β depend on the designer's decision about the kind of connections, detailing, level of axial load and shear at critical regions (plastic hinges), and aspect ratio of members. For example, for RC structures the designer could increase the amount of stirrups at critical plastic hinges (increasing $\theta_{u\ mon}$) to increase the value of $\mu_{\delta TAR}$ considered in the design of the EQ-resisting structure.

Once the $\mu_{\delta TAR}$ has been established, it is necessary to estimate the value of T_{1TAR}, which is defined as the maximum value of T_1 that the structure can have to limit the deformation demands to values equal to or smaller than those imposed by the performance objectives for structural and nonstructural damage (i.e., according to the values of IDI_{SER} and IDI_{SAF}). As shown in Fig. 2, this is possible through the use of the displacement limits established for the service and safety limit states and their corresponding displacement spectra. Note that the service displacement spectra is computed using a μ_δ of 1 and according to the return period associated with the design EQGM for service (T_{R1}). As indicated in Fig. 2, the values of T_1 obtained for service and safety are denoted as T_{SER} and T_{SAF}, respectively, and once they have been established, T_{1TAR} is established in turn as the smaller of the two. Before proceeding to the next step, it is necessary to check if the initially selected value of γ is consistent with the obtained value of T_{1TAR}. If not, the value of γ should be actualized and a new iteration attempted.

In the example shown in Fig. 2, the value of T_{1TAR} is established according to displacement control requirements; nevertheless, in some cases the critical value of T_{1TAR} may arise from the need to control also the maximum velocity and/or total acceleration demands. In the latter cases, it is necessary to establish, besides the displacement design spectra, the spectra for velocity and/or total acceleration. Similar needs arise in the case that energy demands are relevant for the design of the building (e.g., buildings with passive energy dissipating devices). A simple method to estimate these demands for safety can be established if, as suggested by preliminary statistical analysis of the response of SDOF systems to synthetic and real EQGMs, it is possible to estimate the E_I, $E_{H\xi}$ and velocity demands in the equivalent SDOF from the values of T_{1TAR}, $\gamma(T_{1TAR})$, and $S_{d\ SAF}$. Further research needs to be carried to confirm this observation as well as to find a simple way to estimate the total acceleration in the structure.

As will be discussed in detail later, once T_{1TAR} and $\mu_{\delta TAR}$ have been established, the designer may size the frame members (design for stiffness) and estimate their longitudinal reinforcement (design for strength). It should be noted that by carrying out the proposed preliminary analysis procedure, the designer may obtain a fair idea of which are the limit states that control the design, such that early decisions can be made to optimize the design. For example, if the stiffness required to control damage to the partitions of the building is too high, the designer could decide to isolate the partitions from the structure or use other partitions less sensitive to structural distortions; or to use special devices to reduce the displacements of the structure (e.g., energy-dissipating devices). The explicit relationship between selected performance and design can improve the owner's understanding that the expected level of damage and economic losses after an EQ is directly related to his or her initial investment. This can facilitate the communication between the designer and the owner, and the recognition by the owner that an extra small amount of money invested in the initial construction can result in significant savings during the life of the structure.

Note that recently proposed "displacement-based design methods" can be adapted to satisfy the requirements for performance-based design and considered as a particular case of the comprehensive method presented here, in which $\beta = 0$. In this case, damage is assumed to depend on maximum displacement and not on dissipated energy. However, as was clearly shown by the Loma Prieta and Northridge EQs, a minimum strength (or maximum ductility) is needed for most structures to control damage under moderate EQGMs. This minimum strength depends on the hysteretic behavior and energy dissipation capacity of the structure, represented in the comprehensive method given herein by the parameter β.

(ii) Preliminary Sizing and Detailing. The preliminary sizing and detailing step may be stated as follows:
<u>GIVEN</u>: gravity, wind, snow and other possible loads or excitations; minimum stiffness and strength of an equivalent SDOF system required to satisfy the selected seismic performance; critical load combinations; and mechanical characteristics of the structural and nonstructural materials.
<u>REQUIRED</u>: Preliminary sizing and detailing of both the structural elements [beam and columns sizes and their flexural reinforcement (in the case of moment-resisting space frames)], and the unintentional structural (sometimes called nonstructural) components, which can affect the seismic response of the building.
<u>SOLUTION</u>: Select a first period, T_1, that is less than or equal to T_{1TAR}. Using T_1 and the selected first mode shape, to obtain a preliminary sizing for stiffness. Based on these preliminary member sizes, select a minimum equivalent SDOF strength using the service and safety strength design spectra according to the values of T_1 and $\mu_{\delta TAR}$. Consider MDOF and torsional effects, as well as the expected overstrength, to obtain the seismic design loads for service and safety limit states. Based on the application of linear optimization theory and plastic and capacity design, design beams and columns in each story to minimize the volume of flexural reinforcement (in the case of RC), using practical requirements and service forces and moments as constraints so that the preliminary design simultaneously considers the demands for serviceability and safety.

Note that estimation of design forces, overstrength, and elastic moments to be used as constraints in the optimization design are in fact part of the preliminary analysis rather than of the design step. However, since they are intermediate steps between preliminary sizing for stiffness and preliminary sizing and detailing for strength, they are included in the preliminary design of sizes and reinforcement for the sake of simplicity in the discussion.

(iii) Acceptability Checks. An acceptability check is performed to verify that the selected performance objectives are met. The structural response as measured by certain quantifiable parameters must be consistent with the performance objectives and associated acceptability criteria. The acceptability criteria consist of limiting values in structural response parameters, associated with selected performance levels or damage levels for specified levels of EQGM. In a particular building, the design of specific components may be controlled by the same or different response parameters for the same or different performance objectives. Typical response parameters may include: stress ratios, deformation and interstory drift ratios, structural accelerations, ductility demand ratios, damage index, and energy dissipation demand vs. capacity.

Typical limiting values for these response parameters must be established for each performance level through research, including laboratory testing of specific components and calibrating the limiting values by analyzing buildings whose EQGMs and responses, and therefore damages, have been measured (recorded) in past EQs. Then, in a specific design, the appropriate parameters must be checked at the governing performance levels. Typically, the design should at least be checked at the fully operational level and at the life-safety level, after both the preliminary and the final design. In many cases, nonstructural components can be pre-qualified by being prescriptively designed to meet the target parameters of the structural design. Acceptability checks will involve both elastic and inelastic analysis methods. Elastic analysis procedures for checking stress ratios and drift are currently well known and widely used. Several simplified nonlinear inelastic procedures, such as those based on the use of pushover analysis, are also proposed.

CONCLUSIONS

The general comprehensive performance-based EQ-RD approach has been applied successfully to the design of a RC building similar to an existing 30-story building (Bertero *et al.*, 1992) and to a ten-story RC building. The main advantage of the proposed comprehensive performance-based general EQ-RD is that, notwithstanding great uncertainties in the numerical quantification of some of the concepts involved, this quantification can be improved without changing the format of the codified methodology as new and more reliable data are acquired. The relationships between E_I and other relevant seismic demands are usually stable and can be expressed in a simple manner. The use of these relationships simultaneously with performance indices or functions makes it possible to establish a rational and simple EQ-RD procedure that accounts for performance considerations. One such method, which conciliates the analysis and design phases of the overall EQ-RD procedure, is based on energy concepts. This method provides a simple way to estimate the relevant seismic demands in a building while allowing the designer to be an active part of the overall EQ-RD procedure. Nevertheless, at this stage there is still a considerable amount of experimental, field and analytical research that needs to be carried out to create a solid basis on which the proposed method can be properly implemented in practice.

REFERENCES

Bertero, R. D., and Bertero, V. V. (1992) Tall reinforced concrete buildings: conceptual earthquake resistant design methodology. *Report No. UCB/EERC-92/16*, 243 pp., Earthquake Engineering Research Center, University of California at Berkeley.

Fajfar, P. (1992). Equivalent ductility factors, taking into account low-cycle fatigue. *Earthquake Engineering & Structural Dynamics*, Vol. 21, No. 10, pp. 837-848, October.

Park, Y. J. and Ang, A. H. S. (1985). Mechanistic seismic damage model for reinforced concrete. *Journal of the Structural Division*, ASCE, 111(ST4), April.

SEAOC Vision 2000 Committee (1995). Performance-based seismic engineering. Report prepared by Structural Engineers Association of California. Sacramento, California, U.S.A.

STATE-OF-THE-ART REPORT ON: DESIGN CRITERIA

VITELMO V. BERTERO

Earthquake Engineering Research Center, University of California at Berkeley
1301 S. 46th St., Richmond CA 94804-4698, USA

ABSTRACT

The main objectives of this paper are: first, to discuss the ***main purpose of seismic design***, and to clarify what is understood by "***design criteria***" by discussing their role in the ***overall design process*** and the importance of properly selecting and establishing them to ensure that the main objectives of the design are satisfied; and second, to discuss the state of the art in earthquake-resistant design (EQ-RD) criteria. After a review of the general philosophy of EQ-RD and the available design philosophies and approaches, it is concluded that the most attractive design philosophy for EQ-RD appears to be the ***comprehensive design philosophy***. Recent proposals for new approaches to EQ-RD of buildings aimed at designing buildings with more predictable performance are reviewed. Then the paper focusses on the recently proposed ***performance-based seismic engineering of buildings*** and the design criteria involved in the different approaches that have been suggested for conducting ***performance-based EQ-RD***. Emphasis is placed on discussing the multi-level design criteria that need to be adopted to cover the main performance design objectives recommended in the proposed ***comprehensive EQ-RD approach***. The difficulties encountered in the practical application of this approach are discussed, and some recommended procedures for ***acceptability checks*** involved in a proposed ***simple force/strength approach*** are critically reviewed. The need to develop EQ-RD approaches that are based on ***multi-level probabilistic structural performance criteria*** is stressed, and recent studies in this area by Wen and his associates are briefly reviewed. Recommendations for research to improve the state of the art in EQ-RD criteria, and consequently the state of the practice in EQ-RD, are formulated.

KEY WORDS

Allowable stress design; comprehensive design; design criteria; design philosophy; earthquake-resistant design; life-safety; limit design; multi-level design criteria; performance-based seismic design; performance design objectives; performance levels; plastic design; probability of failures; reliability; structural safety.

INTRODUCTION

Main Purpose of Design. From the structural engineering point of view, the main purpose of design is to devise a technically and economically ***efficient system*** to resist and transmit the forces and/or deformations induced by the excitations imposed by the environment in which the facility is to be built. Thus, ***the purpose of structural design is to produce optimum structures***, as has long been stated clearly by several authors (Gallagher, 1973; Rosenblueth, 1974; Esteva, 1980). As pointed out by Rosenblueth (1974), "*Optimization should consider not only the initial cost of the structure, but also: the benefits to be derived from the structure while it survives; the present values of maintenance, damage and failure costs; and the probabilities that the structure might suffer damage or failure as a function of time.*" Thus, a rational approach to design requires computing the probabilities that a structure will undergo given degrees of damage and the probability that it will suffer failure. Generically, these quantities are referred to as ***probabilities of failure***. Their complements, or probabilities of survival, are called ***reliabilities***. Gallagher (1973) pointed out that, "*In contrast to analysis technology, optimal structural design technology has not yet enjoyed the predicted and/or expected acceptance in practical design, and that it is difficult to ascertain the full range of considerations responsible for the slow acceptance of the available design technologies in the computational aspects of practical design.*" This statement is still valid today.

Esteva (1980) discussed the nature and objectives of EQ-RD as follows: "*Engineering design is rooted in society's need to optimize. It implies considering alternate lines of action, assessing their consequences, and making the best choice. In earthquake engineering, every alternate line of action includes the adoption of both a structural system and a* ***seismic design criterion***, *while the assessment of consequences implies estimating structural response and hence expected cost of damage. The choice is based on comparison of initial, maintenance and repair costs for the various alternatives.*" After also considering the approximations implicit in conventional criteria for prediction of structural response and the general goal of optimization in terms of direct particular objectives, Esteva concludes that: "*Achievement of the foregoing objectives requires much more than dimensioning structural members for given internal forces. It implies explicit consideration of those objectives and of the problems related to nonlinear structural response and to the behavior of materials, members and connections when subjected to several cycles of high-load reversals. It implies as well the identification of serviceability conditions and formulation of acceptance criteria with respect to them.*" Esteva's publications make it clear that achievement of optimum EQ-RD and EQ-resistant construction (EQ-RC) requires more than independent structural analysis, studies of the mechanical behavior of a structure, and dimensioning of structural members for given internal forces. It requires both a clear understanding of the role of each of the above aspects and an overall grasp of their intimate relationship in each phase of the ***total design process***.

<u>Total Design Process</u>. As is discussed in two companion papers (Bertero, R.D. *et al.*, 1996; Bertero, V.V., 1996), the total design process of a civil engineering facility usually involves several phases, of which the following four are the most important: ***(1) conceptual overall design, or planning phase; (2) preliminary design phase, which usually involves approximate analysis; (3) rigorous analysis and final design phase; and (4) acceptability check of final design and detailing phase.*** The first, and perhaps most difficult, technical problem in carrying out this total process is the formulation of the ***design criteria***.

<u>Design Criteria</u>

Biggs (1986) defines design criteria as those rules and guidelines which must be met to ensure that the objectives of the design are satisfied. The three major objectives are ***(1) safety, (2) performance of function, and (3) economy***. ***Safety*** is the most important objective, because structural failure usually endangers human life and always involves economic losses due to physical and functional damages. It must be recognized that no structure is totally safe: that is, there is always some finite probability of failure due to human error in design and construction, or unforeseen natural catastrophe. The required degree of safety depends on the function of the structure, which determines the uncertainties in performance and the penalty for failure. Even if a structure is safe against collapse, it may deflect or vibrate excessively and interfere with its intended use. ***Functional requirements*** must be met if the structural design is to be satisfactory. Having satisfied objectives (1) and (2), the structure must be designed for minimum cost. However, there may be a trade-off between objectives (2) and (3), and a final decision must be based on a ***minimum cost/benefit ratio***. The cost of the structure may not be considered in isolation. The important consideration is the cost of the total project, and the most economical structure may result in higher costs of other nonstructural systems.

<u>EQ-RD Criteria and Their Function</u>. In discussing the problems of EQ-RD, Housner *et al.* (1982) noted that when formulating the ***design criteria*** it is necessary to keep in mind that, fundamentally, ***they are a means of specifying the desired earthquake-resistant capability of the structures and the facilities***. The objectives of the criteria are twofold: first, to provide levels of EQ resistance for the various parts of the project that are consistent relative to each other; and second, to provide a level of EQ resistance that is appropriate to ***the desired performance of the facility***. The above authors pointed out that the primary function of design criteria in general, and EQ-RD design criteria in particular, is to ***restate a complex problem that has unknowns and uncertainties in an unambiguous, simplified form having no ambiguities***. The design criteria should provide clearly stated guidelines for the designers. In the preparation of the design criteria, allowances must be made for the uncertainties, and it is necessary to be cognizant of all the unknowns for which allowances must be made.

The ideal philosophy of EQ-RD should attempt to realize all of the objectives of the above general philosophy by providing all the needed stiffness, strength and energy dissipation capacity with the minimum possible extra cost in initial construction as well as in its maintenance during its service life and the slightest possible sacrifice in the architectural features required for the design of the building for just gravity loads.

U.S. Code EQ-RD Philosophy and Criteria. The primary function of a building code is *to provide minimum standards to assure public safety.* In view of this, it is not surprising that SEAOC has established a seismic code philosophy that is in accordance with the above primary function of building codes. *Thus, the basic philosophy of the SEAOC seismic code, as well as of most of the other seismic codes, has been to protect the public in and about buildings from loss of life and serious injury during major EQs.* ***In few words, current code design methodology is based on a one-level design EQ.*** Moreover, the SEAOC commentary states that, "*the protection of life is reasonably provided but not with complete assurance.*" To summarize, ***the primary goal of the U.S. seismic provisions is to protect life.*** *The secondary goal is to reduce (not eliminate) property damage.* The questions that need to be answered are: First, ***Does the application of current seismic code provisions accomplish the above goals?***; and second, ***Are these goals sufficient?***

Uang *et al.* (1991) have shown that the UBC- (or SEAOC-) specified seismic design procedure cannot adequately control the general demands that can be imposed by service EQGMs. The author has long believed that it will be very difficult to satisfy the criteria for all three objectives of seismic design philosophy by keeping the present building code design methodology, which requires only one level of design EQ (life-safety level), and thus there is a need ***to move from the current code one-level design EQ criteria and methodology to multi-level criteria and methodology based on at least two distinct levels of design EQs: the service-level (functional adequacy) and the life-safety level EQs.*** In 1974, Bertero *et al.* developed and applied a nonlinear EQ-RD procedure for multi-story steel frames based on two levels of design EQs. This procedure was extended to the optimal EQ-RD of RC ductile moment-resisting frames employing a computer-aided iterative technique (Zagajeski *et al.*, 1977). The idea of using two levels of design EQ is not new. In the U.S., its application and introduction into seismic codes were discussed in the 1970s. The 1981 Japanese Building Standard Law (BSL) explicitly specifies a *two-level design EQ: moderate EQGMs*, which occur several times during the service life of the building with almost no damage, and *severe EQGMs*, which occur less than once during the use of the building and would not cause collapse or harm to human lives. While buildings not higher than 31 m (102 ft.) can be designed under just moderate EQGMs, buildings higher than 31 m must be designed for the both levels.

Recently, SEAOC, recognizing the need to design structures with more predictable performance, has developed a conceptual framework for what is called **Performance-Based Seismic Engineering of Buildings (PBSEOB)** (SEAOC, 1995), which considers multi-level EQ-RD criteria.

MAIN ISSUES IN IMPROVING THE DESIGN CRITERIA FOR EQ-RD OF STRUCTURES

As discussed earlier, the information needed to improve prediction of EQ responses of structures can be grouped into the following three basic elements: *EQ input, demands on the structure, and supplied capacities to the structure.* These three basic elements of the EQ response problem are discussed briefly below.

EQ Input: Establishment of Design EQs and Design Criteria. The design EQs depend on the design criteria, or *the limit states controlling the design.* Conceptually, the design EQ should be that EQGM, out of all probable EQGMs at the site, which will drive a structure to its critical response. In practice, the application of this simple concept meets with serious difficulties because, firstly, there are great difficulties in predicting the main dynamic characteristics of ground EQGMs which have yet to occur, and, secondly because even the critical response of a specific structural system will vary according to the various limit states (performance levels) that could control the design. Seismic codes specify design EQs in terms of a building code zone, a site intensity factor, or a peak site acceleration. Reliance on these indices, however, is generally inadequate, and methods using *ground motion spectra (GMS), and Smoothed Linear Elastic Design Response Spectra (SLEDRS)* based on *effective peak acceleration (EPA)* have been recommended (ATC 3-06, 1978). While this has been a major improvement conceptually, great uncertainties regarding appropriate values for EPA and GMS, as well as for other recommended parameters, persist.

Estimation of Reliable Demands. The major uncertainties in the estimation of the potential demands are due to difficulties in predicting the following: (1) the critical seismic excitations and hazards at the site during the service life of the structure (lack of properly established design EQGMs and critical load combinations); (2) the state of the entire soil-foundation-superstructure-nonstructural components and contents system when the critical EQGM occurs [proper selection of the mathematical model(s) to be analyzed]; (3) internal forces, deformation, stresses and strains induced in the model (structural and stress analysis); and (4) realistic supplies of stiffness, strength, stability, and capacity to absorb and dissipate energy (i.e., realistic hysteretic behavior) of the entire facility system.

Prediction of Supplies. The supplies to a facility include not only supplies to its bare superstructural system, but also supplies that result from the interaction of the bare superstructural system with the soil-foundation and the so-called *nonstructural components* of the facility. When such interactions occur, *neglecting them in the selection of numerical characteristics for the design of the structure could lead to completely unrealistic evaluation of the demands, and consequently could result in a poor final design of the entire building system.* In considering the basic general design equation (***Demands ≤ Supplies***), the designer might be tempted to increase *supplies* in order to overcome the problems created by the uncertainties in the values of *demands*. However, supply must be increased very carefully, because it may considerably increase the demands.

Directions Toward Solutions of the Main Issues in Establishment of Design EQs and Design Criteria

General Remarks Regarding the Need for Reliable Site Seismic Hazard Assessment. Before embarking on the design of a structure at a given site, it is necessary to conduct *an analysis of the seismic suitability of the selected site* i.e., a reliable site seismic hazard assessment is needed. Recent EQs have shown that in order to improve the reliability of this analysis and definition, it is necessary to: (1) improve the *identification of all possible sources of EQs* that can affect the site; (2) *describe fully and reliably the dynamic characteristics of the ground motions at the source*; (3) quantify how the source ground motions are modified (attenuated or amplified) as they propagate from the source to the site (i.e., *improve the so-called Attenuation Law*); (4) identify the types of EQ hazards at the selected site; and (5) estimate the return periods of these EQ hazards at different intensity levels.

Establishment of Design EQ. For any given building to be constructed on a selected site, present U.S. codes define just one level of hazard (EQGM). Analyses of the damages from recent EQs clearly show the need to consider more than one level of EQGM for the design of structures. Since damage involves nonlinear response (inelastic deformation), ***the only way to estimate damage and the actual behavior of a facility under severe EQ excitation is to consider its inelastic behavior***. Guided by this basic concept and by the fact that the damage potential of any given EQGM at the foundation of a structure depends on the interaction of its intensity, its frequency content, and its duration with the dynamic characteristics of the structure, the author believes that one of the most reliable ways to define the damage potential of an EQGM is to compute its energy input, E_I, to the foundation of the structure, together with the other associated parameters which can be obtained through the use of energy concepts (Bertero, 1992).

Use of Energy Concepts in Establishing EQ-RD Criteria

Traditionally, displacement ductility ratio has been used as a criterion to establish *Inelastic Design Response Spectra (IDRS)* for EQ-RD of buildings. The minimum required *lateral strength* of a building is then based on the selected IDRS. As an alternative to this traditional design approach, an energy-based design method was proposed by Housner (1956). However, it is only recently that this approach has gained extensive attention (Akiyama, 1985). This design method is based on the premise that the *energy demand* during an EQ (or an ensemble of EQs) can be predicted, and that the *energy supply* of a structural element (or structural system) can be established. In a satisfactory design, the energy supply is larger than the energy demand. To develop reliable design methods based on an energy approach, it is necessary to derive the energy equations.

Derivation of Energy Equations. Uang *et al.* (1988) give a detailed discussion of the derivation of the two basic energy equations (absolute and relative), and have shown that the maximum values of the absolute and relative energy input, E_I , for any given constant displacement ductility ratio are very close in the period range of practical interest for EQ-RD of buildings, which is 0.3 to 5.0 seconds. Thus, the two energy equations can be written as:

$$E_I = (E_E) + (E_D) \quad \textbf{(1a)} \qquad\qquad E_I = (E_K + E_s) + (E_{H\xi} + E_{H\mu}) \quad \textbf{(1b)}$$

Where: E_I= energy input, E_E = the stored elastic energy, E_D = the dissipated energy, E_K = kinetic energy, E_s = elastic strain energy, $E_{H\xi}$ = dissipated energy due to hysteretic equivalent linear viscous damping, and $E_{H\mu}$ = dissipated energy due to hysteretic plastic deformation.

Comparing this equation with the design equation (**Demands ≤ Supplies**), it becomes clear that E_I represents the *demands*, and the summation of $E_E + E_D$ represents the *supplies*. ***An understanding of Eq. (1) will guide the designer in establishing the design criteria.*** Equation (1a) points out clearly to the designer that to obtain an efficient seismic design, the first step is to have a good estimate of the E_I for the critical EQGM. Then the designer has to analyze whether it is possible to balance this demand with just the elastic behavior of the structure to be designed, or if it will be convenient to attempt to dissipate as much as possible of the E_I using E_D. As revealed by Eq. (1b), there are three ways of increasing E_D: one is to increase $E_{H\xi}$ by increasing the equivalent linear viscous damping, $E_{H\xi}$; another is to increase the hysteretic energy, $E_{H\mu}$; and the third is a combination of increasing $E_{H\xi}$ and $E_{H\mu}$. At present it is common practice to just try to increase the $E_{H\mu}$ as much as possible through inelastic (plastic) behavior of the structure, which implies damage of the structural members. Only recently it has been recognized that it is possible to increase the $E_{H\mu}$ significantly and control damage throughout the structure through the use of *energy dissipation devices*. Furthermore, as discussed by Bertero (1992), increasing E_D by increasing $E_{H\xi}$ has the great advantage that it can control the behavior of the structure under both safety and service levels of EQGMs.

If technically or economically (or both) it is not possible to balance the required E_I either through E_E alone or E_E+E_D, the designer has the option of attempting to control (decrease) the E_I to the structure. This can be done by *base isolation techniques*. A combination of controlling (decreasing) the E_I by base isolation techniques and increasing the E_D by the use of energy dissipation devices is a very promising strategy not only for achieving efficient EQ-RD and EQ-RC of new structures, but also for the seismic upgrading of existing hazardous structures. To use this energy approach reliably, it is essential to be able to select the critical EQGM (design EQ); in other words, the ground motion that has the largest damage potential for the structure being designed. E_I is a promising parameter for assessing the damage potential of these motions, but this parameter alone is not sufficient to evaluate (visualize) the E_D that has to be supplied to balance the E_I for any specified acceptable damage. Additional information is needed.

Information Needed to Conduct Reliable EQ-RD Criteria and Thus EQ-RD of Buildings. Currently, for structures that can tolerate a certain degree of damage, the *Safety or Survival-Level Design EQ* is defined through *Smoothed Inelastic Design Response Spectra, SIDRS*. Most of the SIDRS that are used in practice (seismic codes) have been obtained directly from *Smoothed Elastic Design Response Spectra, SEDRS*, through the use of the *displacement ductility ratio,* μ_δ , or *reduction factors, R*. The validity of such procedures has been questioned, and it is believed that at present such SIDRS can be obtained directly as the mean or the mean plus different values of standard deviation of the *IRS*, corresponding to all the different time histories of the severe EQGMs that can be induced at the given site from EQs that can occur at all of the possible sources affecting the site (Bertero, 1991). While the above information is *necessary* to conduct reliable design for safety, it is *not sufficient*. In other words, *the maximum global ductility demand by itself does not give an appropriate definition of the damage potential of EQGMs*. As discussed previously, it has been shown that a more reliable parameter than those presently used in assessing damage potential is the E_I. This damage potential parameter depends on the dynamic characteristics of both the shaking of the foundation and the whole building system (soil-foundation-superstructure and nonstructural components). Now the question is: ***Does the use of the SIDRS for a specified global μ_δ and the corresponding E_I of the critical EQGM give sufficient information to conduct a reliable seismic design for safety?***

From recent studies (Uang *et al.*, 1988; Bertero, 1991) it has been shown that the energy dissipation capacity of a structural member, and therefore of a structure, depends upon both the loading and deformation paths. Although the energy dissipation capacity under monotonic increasing deformation may be considered as a lower limit of energy dissipation capacity under cyclic inelastic deformation, the use of this lower limit could be too conservative for EQ-RD. This is particularly true when the ductility deformation ratio, say μ_δ , is limited, because of the need to control damage of structural and nonstructural components or other reasons, to low values compared to the ductility deformation ratio reached under monotonic loading. Thus, effort should be devoted to determining experimentally the energy dissipation capacity of main structural elements and their basic subassemblages as a function of the maximum deformation ductility that can be tolerated, and the relationship between energy dissipation capacity and loading and/or deformation history. From the above studies, it has also been concluded that damage criteria based on the simultaneous consideration of E_I and μ_δ (given by SIDRS), and the $E_{H\mu}$ are promising parameters for defining rational EQ-RD criteria and procedures. From the above discussion, it is clear that when significant damage can be tolerated, *the search for a single parameter to characterize the EQGM or the design EQ for safety is doomed to fail.* ***If future codes perpetuate simple procedures for seismic design specifying only smoothed strength response spectra, it will be necessary to place more stringent limitations on the type of structural systems that could be used and on how such procedures can be applied, and to have very conservative regulations in the sizing and detailing for ductility and in the maximum acceptable deformations.***

NEED FOR FORMULATION OF CONCEPTUAL EQ-RD CRITERIA AND METHODOLOGY

Current seismic codes, in their attempt to be simple (as they should be), have tried hard to simplify the complex problem of EQ-RD by developing design criteria and procedures based on just one parameter. The result is codes that are not transparent because their regulations do not present in a visible way the basic concepts which govern the EQ-RD of structures. Although it is generally recognized that damage is due to deformation, there is no agreement regarding the main criterion for preliminary EQ-RD of structures. Perhaps as a consequence of past and present code requirements, present practice emphasizes the use of strength in the preliminary design of structures. The reasons for and drawbacks of the insistence on using only strength as primary criterion has been discussed by Bertero (1992). For a long time already it has been recognized by researchers and practitioners that ***to produce serviceable, safe and economical facilities, EQ-RD criteria and methods must incorporate drift (damage) control in addition to lateral displacement ductility as design constraints.*** The question is how to achieve such control at the different levels of EQ shaking that can occur during the life of the structure. Bertero *et al.* (1991) discuss in detail the issues involved in achieving such control at the serviceability and safety limit states.

The control of the drift of a structural system under EQ excitation is important for at least three different reasons: (1) to maintain architectural integrity, thereby avoiding unacceptable damage to nonstructural components; (2) to limit structural damage and avoid structural instability (P-Δ) problems; and (3) to avoid human discomfort under frequent minor or even occasional moderate EQ shaking. Story drifts and drift ductility factors may also be useful in providing information on the distribution of structural damage. Unfortunately, conventionally computed story drifts may not adequately reflect the potential structural or nonstructural damage to multistory buildings. In some structures, a substantial portion of the horizontal displacements results from axial deformations in the columns. Story drifts due to these deformations are not usually a source of damage. A better index of both structural and nonstructural damage is the tangential story drift index, R_T (Mahin *et al.*, 1976). Furthermore, some of the nonstructural damages are caused by deformation rates (velocity and/or acceleration), rather than just deformation. For example, the failure of partitions out of their plane is due to the acceleration perpendicular to their plane. Damage to equipment and contents of buildings are also due to deformation rates. Thus, it is also of importance to control the deformation rates to achieve good performance of nonstructural elements, equipment, contents and, in some cases (e.g., when viscous dampers are used) the structure itself.

In response to the noted weakness of present seismic code EQ-RD procedures based on base shear strength, which is insensitive to damage in the inelastic (plastic) range, there have been proposals that preliminary design be based only on lateral stiffness, i.e., only on controlling interstory drift.

Recommended Practical Methods for Designing Considering IDI

Recently, Bonacci (1994) has reviewed the methods useful for estimating response of yielding RC systems to EQs with special emphasis on a comprehensive method that enables the designer to evaluate and control member damage on the bases of an inelastic estimate of nonlinear displacement response. Bonacci's review is a vote of confidence for the method proposed by Gulkan *et al.* (1974) and for that used by Shibata *et al.* (1976) in the well-known proposed ***substitute structural method.*** A simplified method for estimating lateral drift of RC structures has been suggested by Sozen (1983). The method is intended to be used for interpreting experience and evaluating relative merits of different structural schemes and member sizes on the basis of a tolerable damage criterion. The method is conveniently used in preliminary evaluation by simple estimates of the base shear capacity coefficient. Shimazaki (1984, 1988) investigated the effects of strength and stiffness and of the type of EQGM on nonlinear displacement response of SDOF systems. *The results obtained show that the nonlinear displacement response is equal to the linear response spectral values if the system has a certain strength which is determined by dimensionless parameters for strength, initial period, and type of EQGM.*

Recently Qi *et al.* (1991) and Moehle (1992) developed two simple and practical EQ-RD procedures based on displacement (drift) information. One uses displacement information directly, and the other, a ductility-ratio approach, uses it indirectly, establishing ductility requirements as a function of the provided strength and the strength required for elastic response. Priestley (1993), after examining current practice in seismic analysis and design, suggested that our current emphasis on strength-based design and ductility lead us in directions that are not always rational, and advanced a ***pure displacement-based design approach.*** This approach is comparatively straightforward for a simple multi-column bridge pier. To carry out the proposed procedure a set of elastic displacement response spectra for different levels of equivalent viscous-damping coefficient, ξ, are required. These spectra are called the ***elastic design displacement spectra for the building site.*** An initial estimate must be made of the structural yielding displacement, which could be based on a drift angle, and then the limit to acceptable plastic rotation of critical hinges has to be determined. Priestley claims this approach has considerable flexibility, since plastic hinge rotational capacity can be related to transverse detailing (or vice versa) and their design is not dictated by a somewhat arbitrary decision about force-reduction factors. According to Priestley (1993), it would appear that the above method of displacement-based design could also be applied to multi-story frame or shear wall buildings, provided some additional assumptions are made. The two critical pieces of information required are: (1) *the relation between maximum interstory drift and structural displacement* at the height of the center of seismic force; and (2) the shape of the lateral force vector to be applied. Although the displacement-based design approach appears attractive in principle, it will need to be checked by specific examples covering a wide range of structural types and periods.

The author believes that some of the assumptions made in the proposed displacement-based design methods that have been proposed can be seriously questioned. One of the questioned assumptions is that inelastic displacements are equal to those obtained from a linear elastic response. Because of the limitations involved (due to the assumptions made to simplify the design procedure) in applying each of the practical methods on the basis of the use of just one parameter, whether strength (as in present codes), or lateral drift, and because of the difficulties in specifying very clearly the limitations on the application of these proposed methods, the author believes that to achieve an efficient preliminary EQ-RD, there is a need to consider the following requirements simultaneously: the ***strength*** (based on rational use of μ_δ and ξ), the ***deformation*** (based on the limitation of IDI), the ***deformation rate***, and their combined effect on the ***energy capacity*** of the whole facility system. The need for a rational and transparent approach to the issue of improving EQ-RD criteria and procedures for new facilities and for upgrading existing hazardous facilities has motivated the author and his research associates to attempt to develop and apply ***conceptual comprehensive criteria and methodology for EQ-RD of structures.***

Conceptual Criteria and Methodology for EQ-RD of Buildings

As described by Bertero *et al.* (1993), a new conceptual framework for a seismic code based on the state of the art in EQ engineering has been formulated. This code framework includes "***conceptual criteria and methodology for EQ-RD.***" The methodology consists of: (1) guidelines for conceptual overall design of entire building systems; and (2) a conceptual methodology for numerical EQ-RD of building systems in compliance with the worldwide-accepted EQ-RD philosophy and based on energy concepts, fundamental principles of structural dynamics, mechanical behavior of entire building facilities, and comprehensive design. The numerical EQ-RD methodology considers the desired seismic performance of the entire building system explicitly from the beginning of the EQ-RD process, and concludes by evaluating whether such performance would be achieved. Detailed discussions of the conceptual methodology for EQ-RD are given elsewhere (Bertero *et al.*, 1993), and in a companion paper at this WCEE (Bertero, R. D., *et al.*, 1996). This methodology was also used in the "comprehensive EQ-RD approach" proposed as the most general and comprehensive approach of those included in the conceptual framework for "***performance-based seismic engineering of buildings***" recently proposed by the Vision 2000 Committee of the Structural Engineering Association of California (SEAOC, 1995). The proposed comprehensive EQ-RD approach is illustrated in the flow chart in Fig. 1. As discussed in detail in the SEAOC 1995 report, ***although the proposed approach can be applied for all kinds of structures, its main use will be for carrying out studies to develop simplified practical methods of performance-based EQ-RD of certain types of facilities, such as low-rise buildings having relatively regular structural configurations and***

systems and constructed on normal sites. This comprehensive methodology should be used to calibrate simpler practical performance-based criteria and EQ-RD approaches. Therefore, in practice, the application of this comprehensive approach will be limited to buildings with irregular configurations, structural layout or structural systems; or very tall slender building located on normal or abnormal sites. The importance of the detailed chart in Fig. 1 is that it can be used for the development of any other simplified performance-based EQ-RD approach.

NEED FOR SIMPLIFIED BUILDING CODE EQ-RD CRITERIA AND PROCEDURES

Priestley (1993) stated that, "*Given the wide range and occasional gross nature of the assumptions and approximations inherent in seismic design, we might be better keeping the design and analysis processes simple enough so that we still understand what we are doing.*" The author strongly supports Priestley's cautionary note about the tendency for increased complexity in analysis. What is needed is the development of simplified criteria and numerical EQ-RD procedures for engineered buildings which, backed up by strict code provisions regarding site conditions, load combinations, building configuration, superstructure, nonstructural components and their materials and detailing, and the foundation to be considered, can result in construction with seismic performance that complies with all the performance levels and performance design objectives envisioned in the general EQ-RD philosophy on which the comprehensive performance-based EQ-RD approach has been based.

Proposed Simple Codified Performance-Based EQ-RD Procedures. The author believes that there are two different routes to the development of simplified performance-based EQ-RD procedures that can be codified in current building codes. These two different routes are: (1) ***Use of a Deformation (Displacement) Approach***; and (2) ***Use of a Force/Strength Approach.***

Deformation or Displacement Approach. Discussion of performance-based EQ-RD and the proposed comprehensive approach leaves no doubt that performance, particularly degree of damage, of an entire building system is more a consequence of deformations than of forces, and consequently it appears logical that the design should be based on deformation (displacement or drift spectra) rather than on forces (acceleration spectra). This is how the comprehensive EQ-RD approach starts the sizing of the structure (Bertero, R. *et al.*, 1996). For cases of one-story buildings, the displacement approach proposed by Priestley is attractive. Efforts should be devoted to improving the proposed methodology, particularly the development of reliable design displacement spectra and relationships between equivalent viscous damping and displacement ductility level. Regarding the application of the proposed method to multistory buildings, as pointed out by Priestley (1993) this would need to be checked out by specific examples, covering a wide range of structural types and periods. Furthermore, attempts should be made to extend the proposed methodology to include simultaneous design for at least two performance levels.

Simplified Force/Strength Approach. Inspection of the behavior of engineered buildings during previous EQs around the world shows that there are certain types of buildings, usually low-rise buildings, that can have excellent performance under different levels of EQGMs, even if their design used a very simple force/strength numerical design approach based on just the ***static equivalent lateral force (ELF)*** and ***linear elastic analysis and design procedure.*** This excellent performance has been observed when the very simple numerical design approach has been backed up by strict enforcement of very restrictive code regulations regarding the siting conditions, relative importance of the EQGMs among other excitations, and the characteristics of the entire building system. Thus, what is proposed herein is the development of a simplified numerical design procedure for engineered buildings which, backed up by strict code provisions regarding the applicability of such an approach (covering the site conditions, building configuration, superstructure, nonstructural components and their material and detailing, the foundation and the load combinations to be considered) can result in construction with seismic performances that comply with all the performance levels and performance design objectives envisioned in the general philosophy that has been formulated by the Vision 2000 Committee (SEAOC, 1995) and on which the comprehensive performance-based EQ-RD approach illustrated in Fig. 1 has been developed.

Considering that at present the simplest practical design procedure for the design of engineered buildings is based on the use of the ***linear elastic ELF*** procedure that considers just one performance level (the life safety level), it has been proposed to keep this numerical design procedure but to find out how to improve the regulations and their enforcement in the field regarding when and how such a procedure can be applied and result in construction that complies with the general philosophy of the performance-based EQ-RD and EQ-RC. A discussion of the needed simplifications and improvements is given in the SEAOC 1995 report. Herein is presented only a review of some methods of analysis that have been recommended lately for conducting the acceptability checks.

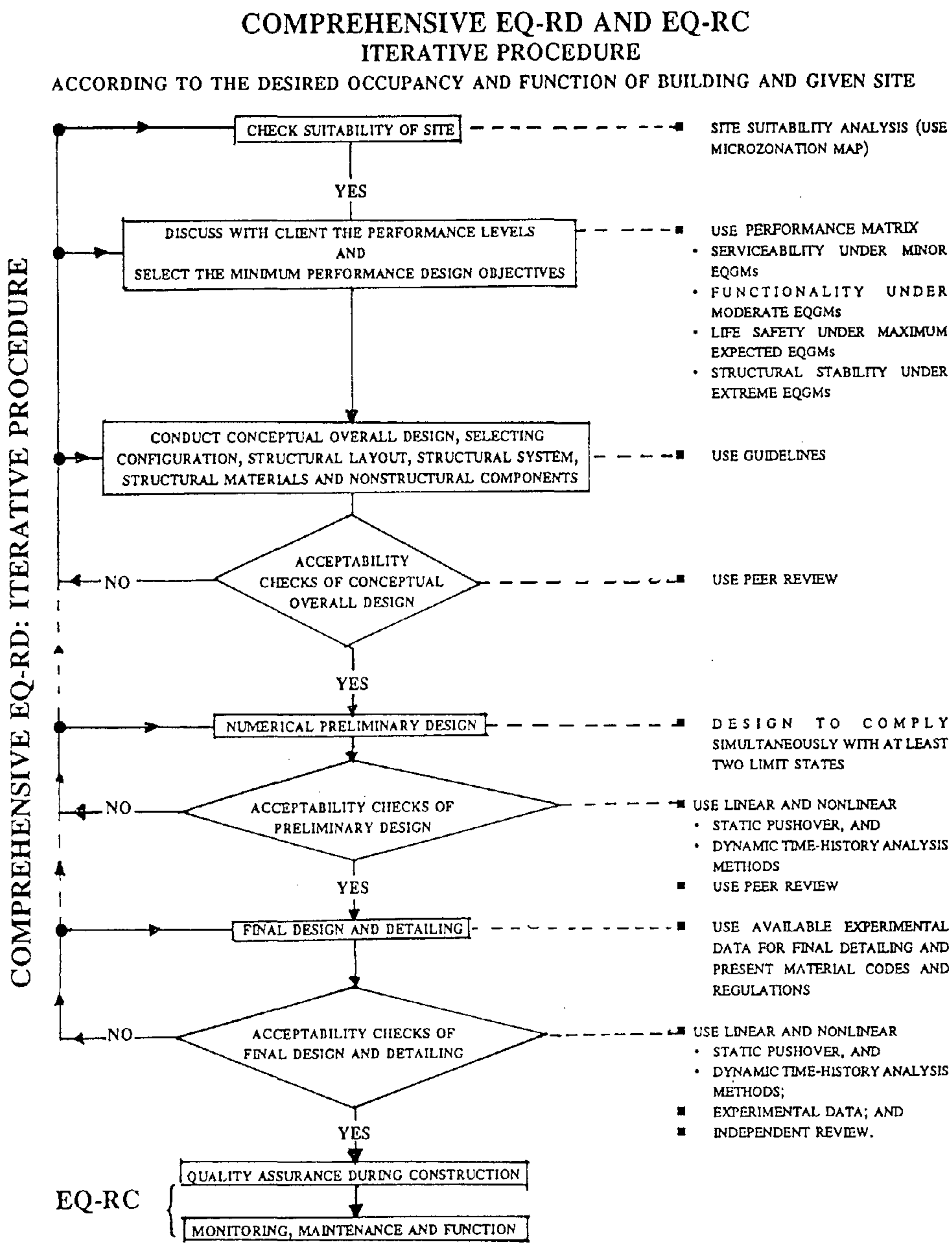

Fig. 1 Flow chart for comprehensive EQ-RD and EQ-RC

Acceptability Checks: Acceptance Criteria. The acceptability checks under the EQGMs (in combination with other loads that can act simultaneously) corresponding to *the service performance level* are straightforward because as the building should remain essentially in its linear elastic range, deformations are directly related to forces, and the principle of superposition applies. On the other hand, for the other three performance design objectives considered in the performance-based EQ-RD (Fig. 1), particularly for *the life safety and impending collapse performance levels*, considerable judgement should be employed in interpreting the results obtained using just linear elastic analyses and when these results are compared with the established values for the parameters controlling the performance (damage) at each of these performance levels.

In the ATC 33-03 project, significant efforts were devoted to the development of simplified procedures, including some empirical equations using just linear elastic analysis to determine component acceptability (Shapiro *et al.*, 1996). While the author recognizes the need for such development and applauds efforts to develop such simplified procedures, usually these simplifications use empirical equations that are based on assumptions that limit their applications to real situations. In the determination of the component acceptability, ATC 33-03 proposed that the component actions be classified as being either ***force-controlled*** or ***deformation-controlled***, which are defined as follows: ***Deformation-controlled action*** (an action for which deformation can exceed yield, and the maximum permissible deformation is limited by ductility); and ***Force-controlled action*** (an action for which force cannot exceed yield, and the maximum permissible force is limited by strength).

Recommended Procedure for Determination of Component Acceptability. ***For deformation-controlled actions*** on primary and secondary components, the demanded internal forces shall satisfy the following equations.

$$Q_G \pm Q_E \le m\, Q_C \quad (2) \qquad \text{and} \qquad Q_G \le Q_C \quad (3)$$

where: Q_G = internal force due to gravity forces acting on component; Q_E = component force action due to earthquake loads determined from the linear elastic structural analysis model subjected to the seismic force V; Q_C = the strength capacity of the structural component action represented by the *expected* strength at the demand deformation level; and m = a component demand modifier to account for the expected ductile response capacity of the component. The m factor represents the ratio of permissible component deformation to yield deformation. It is related to ductility and is obtained from hysteretic data from laboratory cyclic tests and engineering judgment considering Performance Levels (i.e., acceptable levels of damage).

For force-controlled actions:

$$Q_G \pm Q_{EF} \le Q_{CF} \tag{4}$$

where: Q_{EF} = an estimate of the maximum force that can be delivered to the component; and Q_{CF} = the strength capacity of the structural component represented by a *lower bound* strength. In order to emphasize the importance of avoiding blind application of the demands resulting from the static linear elastic pushover analysis or even from the dynamic linear elastic modal spectra response analysis, some of the unexpected and undesirable inelastic behavior (performance) that can occur is illustrated with results presented in the following discussion of a simple one-story, one-bay special moment-resistant frame.

Statement of Problem. Consider a MRF building on a site in ***a region of low seismicity and very heavy environmental gravity loads (Live and Snow)***. Assume that: (1) the columns are very strong and stiff compared to the strength and stiffness of the beam, but that the flexibility of the columns is enough to allow that the moment diagram under the gravity loads, P_G, to be the same as the one shown in Fig. 2a, i.e., the moments at the ends of the girder (i.e., at B and D) when compared to the plastic moment capacity, M_P, of the girder are:

$$|(M_B)|_G = |(M_D)|_G = \frac{1}{2}|M_p| \tag{5}$$

and the moment at midspan of the girder, i.e., at M $(M_M)_G$ is

$$|(M_M)_G| = \frac{3}{2}|(M_B)_G| = \frac{3}{2}|(M_D)_G| = \frac{3}{4}|M_p| \tag{6}$$

The moments induced by the statically equivalent seismic lateral force, $(V_E)_{el}$ are those shown in Fig. 2b, i.e.,

$$|(M_B)_E| = |(M_D)_E| = \frac{3}{2}|M_P| \tag{7}$$

From examination of the linear elastic analyses of the MRF under P_G and $(V_E)_{el}$ shown in Figs. 2a and 2b, respectively, and their superimposed effects, shown in Fig. 2c, it is clear that the critical section of the girder appears to be either the end D or the end B, depending on the selected direction of the $(V_E)_{el}$. For the direction adopted in the plots of Fig. 2, the critical section is D, and a check of the deformations at this section, blindly applying Eqs. 2 and 3, leads to the following results.

Eq. 2 requires that:

$$(M_D)_G + (M_D)_E \le m\,(M_D)_C \tag{8}$$

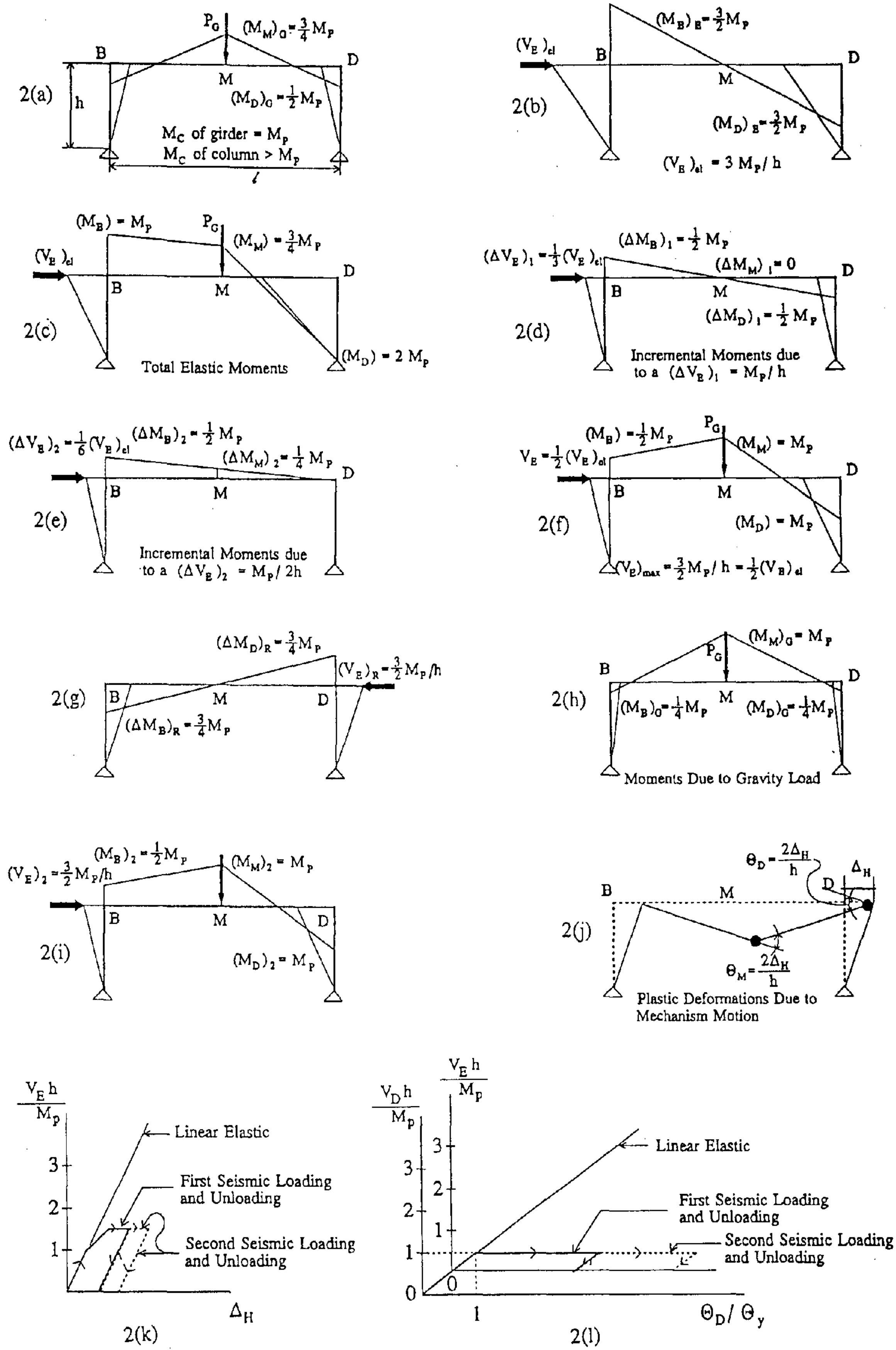

Fig. 2 Linear elastic vs. elastic/plastic demands for a MRF

Using the above values and assuming $m = 2$: $\frac{1}{2}M_P + \frac{3}{2}M_P = 2M_P$ **(9)**

I.e., Eq. 2 is satisfied. Eq. 3 requires that: $(M_D)_G \leq (M_D)_C$ **(10)**

As: $(M_D)_G = \frac{3}{4}M_P$ and $(M_D)_C = M_P$ **(11)** $\therefore\ \frac{3}{4}M_P < M_P$ **(12)**

Thus Eq. 3 is also satisfied. Therefore, it can be concluded that the existing MRF is adequate to resist the estimated effects of the EQGMs.

Fallacy of the Conclusions That Have Been Drawn. The fallaciousness of the above conclusions from linear elastic analysis can be demonstrated by estimating the expected inelastic behavior of the MRF when subjected to the given P_G and the expected V_E.

■ ***Nonlinear (Inelastic) Behavior***. For the sake of simplicity, consider that the moment rotation (M vs. θ) relationships for the critical regions of the MRF are linear-elastic/perfectly-plastic. Then it is clear that as soon as the gravity load MRF is subjected to the effects of the EQGMs (Fig. 2b), the moment at D will increase and reach the M_p capacity of this section D, when $(\Delta V_E)_1 = (1/3)(V_E)_{el}$, as can be seen by adding the moments of the diagrams shown in Fig. 2a and 2d. After this, a plastic hinge (PH) will be developed at the end of the girder. Because of the development of this plastic hinge (PH) at D, the moments induced by an increased $(\Delta V_E)_2$ due to the EQGM excitation will be those shown in Fig. 2e. Thus, in this case it appears that as soon as $(V_E) > (1/3)(V_E)_{el}$ the lateral stiffness of the MRF when subjected to the EQ lateral force will be significantly smaller than that of the original linear elastic MRF and for which the expected linear elastic lateral deformations and consequently the inelastic deformations have been estimated.

The Moment Diagrams shown in Figs. 2a, 2d and 2e show that the maximum lateral EQ resistance, i.e.. $(V_E)_{max}$, is controlled by the formation of a new PH at M and which led to the formation of a type of sidesway mechanism with PHs at D and M that could not have been anticipated just from the linear elastic analysis. ***The linear elastic analysis does not give any hint that a PH can be developed at the midspan of the girder, and consequently no need for special detailing for ductility of the girder at this section would have been required.*** The resulting $(V_E)_{max}$ as given in Fig. 2f is shown to be equal to half of the equivalent linear elastic base shear that was estimated using the ATC guidelines (Shapiro *et al.*, 1996). Other important observations regarding the danger of blind use of the results obtained just from linear elastic analyses for judging the expected nonlinear (inelastic) behavior can be drawn by analyzing ***what could happen after the effects of the first severe EQGMs cease and then the MRF is subjected to any one of the following new loading conditions: (a) An increase in gravity load; (b) A new impulsive EQGM inducing deformations and therefore a V_E in the same direction as the original pulse; and (c) A reversal of EQGM, and consequently a reversal of the V_E.***

Earthquake Unloading of the MRF. If the EQGM is just a pulse represented by the statically equivalent lateral force, $(V_E)_{max}$, when this EQGM ceases the MRF will unload and during this unloading will respond with a linear elastic behavior. The changes in the moments throughout the frame are illustrated in Fig. 2g, and the final moment diagram under gravity alone is illustrated in Fig. 2h. Analysis of this moment diagram shows that the critical section of the beam under gravity load alone is at M, i.e., at the midspan of the girder, rather than at the ends of the girders. This change in the moment diagram indicates that the girder will end with an increase in its vertical deflection at the center. Furthermore, because the moment at M is equal to the plastic moment capacity, M_p , of the girder, a small increase in gravity load can induce significant plastic deformations at this midspan region of the girder, which could not be predicted using just linear elastic analysis as is discussed below in some detail.

(a) An increase in gravity loads. *Can this realistically be expected?* Yes, it can if one uses the load combinations in the NEHRP (1994) recommendations (which are based on probabilistic studies). From analysis of the moment diagram shown in Fig. 2h, it is clear that any increase in P_G will lead to the development of a PH at section M, i.e., at the center of the girder span, ***with an extra significant increase in the vertical deflection, which is very undesirable and would not have been suspected from the linear elastic analysis alone.***

(b) A new impulsive EQGM inducing deformations and therefore a V_E in the same direction as the original pulse. In this case, the MRF will behave linear-elastically, with a lateral stiffness equal to the original linear elastic stiffness and the change in moments are given in Fig. 2i. When the V_E reaches a value of

$(V_E)_2 = (3/2)(M_p /h)$, the moment at D reaches again its plastic capacity, M_p, and therefore a PH will be developed at this section and the MRF cannot resist any extra significant lateral resistance under the V_E in this direction because an extra PH will also develop at M and a sidesway mechanism, as shown in Fig. 2j, is formed. Due to this mechanism, significant inelastic (plastic) rotations will be developed at sections D and M, as is illustrated in Fig. 2j. It should be noted that for any given mechanism lateral deformation, the corresponding mechanism rotations will be twice those that would have been developed if the PHs had developed at the ends of the girder. Thus, significant plastic rotations will accumulate at D (Fig. 2l), as well as at M with the application of a new EQGM pulse having the same direction and also significant increase in lateral deformation, Δ_H, will take place as illustrated in Fig. 2k. This performance cannot be predicted using just linear elastic analysis; nor, therefore, with Eq. 2.

(c) A reversal EQGM and consequent reversal of V_E. In this scenario, once again the MRF will perform in its linear elastic range with a lateral stiffness equal to that of the original MRF until the moment at B reaches its plastic moment capacity, M_p, which will occur under a $(V_E)_2 = (3/2)(M_p/ h)$. This $(V_E)_2$ is also the maximum seismic lateral resistance for the MRF under this reversal of seismic loading, and the frame will start deforming as a sway mechanism with large plastic rotations at sections B and M.

The above results and discussion make it clear that under a time-history EQGM containing several severe acceleration pulses capable of demanding the inelastic (plastic) behavior of the frame, there will be a severe accumulation of plastic rotations, particularly at the midspan of the girder, i.e., at section M, ***which linear elastic analysis alone would not be able to predict.***

NEED FOR THE DEVELOPMENT OF EQ-RD PROCEDURES AND FORMATS BASED ON MULTI-LEVEL PROBABILISTIC STRUCTURAL PERFORMANCE CRITERIA

As discussed in the Introduction, it has long been recognized by practitioners and researchers that there is large variability in the type and degree of seismic hazards (particularly EQGMs) that can develop during an EQ, as well as in the response of entire facility systems to these hazards. The variability of the response of the entire facility system is due to the variability of mechanical characteristics of these systems. In spite of this awareness, these variabilities are not fully accounted for in current EQ-RD code procedures. Thus, it is not surprising that since the 1989 Loma Prieta and the 1994 Northridge EQs, a strong sentiment has developed among researchers and practitioners that there is a need to develop EQ-RD formats with explicit treatment of the variables and uncertainties. Based on this need, Wen (1995) evaluated the reliability of current code provisions and developed and calibrated reliability design procedures. Furthermore, he proposed a bi-level reliability and performance-based design procedure in which satisfactory performance of the building is enforced at both the serviceability and life safety levels.

Wood *et al.* (1995) proposed and applied a dual-level design procedure in which a building structure is designed for both an ultimate and a serviceability level force. This procedure is applied to the design of a seven-story RC MRF, which is also designed according to the 1991 NEHRP provisions. The reliability of the two designs at different response levels is evaluated. The dual-level design procedure resulted in better drift and damage control for severe EQGMs. Collins *et al.* (1995) developed a reliability-based dual-level seismic design procedure to address some of the shortcomings of current seismic design procedures. The proposed procedure attempts to enable designers to achieve code-specified target performance objectives for moderate and severe EQGMs. Although the procedure is more complicated than current ones, it should help designers to appreciate the consequences of various design assumptions and to identify critical regions of the structure that require careful design and detailing. The procedure was developed for steel building structures, but it should be applicable (appropriately modified) to other types of building structures as well. The procedure requires the designer to consider two levels of EQGMs. An equivalent system methodology and uniform hazard spectra are used to evaluate the performance of building structures. Performance is quantified in terms of the probability of exceeding displacement-based limit state criteria.

CONCLUSIONS AND RECOMMENDATIONS

In formulating the main conclusions of the discussion of the state of the art in EQ-RD criteria, as well as in formulating recommendations for improving it, it is convenient to distinguish the following two different purposes for establishing such criteria: one includes the design of very important and/or complex structures, as well as investigations in the search for reliable and simplified EQ-RD that can be codified; and the other purpose is to provide, in an unambiguous and simplified form, reliable rules and guidelines that the average designer can use in practice, i.e., that can be codified.

Conclusions. In the state of the art in the EQ-RD criteria for conducting research or for the practical design of important and complex structures, significant progress has been made in the last five years in the development of EQ-RD procedures that follow the sophisticated EQ-RD criteria that were discussed and proposed in the 1970s and 1980s. The main accomplishments have been: (1) the development of the ***conceptual framework for performance-based seismic engineering whose performance design objective matrix is based on multi-level design EQGMs and performance levels design criteria***; (2) the development of a ***comprehensive EQ-RD approach*** whose preliminary design phase is based on satisfying simultaneously the requirements for at least two performance design objective levels and attempting to produce optimum building structures using energy concepts; and (3) the development of a ***reliability-based dual-level seismic design procedure*** that uses uniform hazard spectra and an equivalent SDOF system to account for the variability and uncertainties in the EQGMs and inelastic response of the structures.

In the state of the art in the EQ-RD criteria that can be codified for use in practice by average designers, although code format, at least in the U.S., has not changed significantly in the 1980s and 1990s, there have been some attractive proposals for improvement such as: (1) the Department of Energy (DOE) guidelines (Kennedy *et al.*, 1994), which specify building performance goals in terms of probability of exceedance of some measure of damage; (2) attractive displacement-based EQ-RD approaches; and (3) simple codified EQ-RD procedures based on application of elastic ELF.

Recommendations. Many unresolved problems need to be addressed before the recently developed EQ-RD criteria and approaches can be implemented in practice, which is what is needed to reduce in the short run the seismic risk in our urban and rural areas. Recommendations for research, development and implementation of the EQ-RD criteria involved in performance-based EQ-RD are given by the SEAOC Vision 2000 Committee (SEAOC, 1995). Suggestions and recommendations for future research for improving the basic framework for reliability-based dual seismic design procedures are given by Collins *et al.* (1995), Elwood *et al.* (1995) and Wen (1995). Because of length restrictions on this paper, the reader is referred to these publications.

REFERENCES

Akiyama, H. (1985). Earthquake resistant limit-state design for buildings. University of Tokyo Press. Japan.

ATC 3.06 (1978). Tentative provisions for the development of seismic regulations for buildings. Applied Technology Council, Redwood City, California, U.S.

Bertero, R. D., V. V. Bertero and A. Teran-Gilmore (1996). Performance-based earthquake-resistant design based on comprehensive philosophy and energy concepts. *Proc. 11WCEE*, Acapulco, Mexico, June. Elsevier Science Ltd. Oxford, U.K.

Bertero, V. V. (1996). The need for multi-level seismic design criteria. *Proc. 11WCEE*, Acapulco, Mexico, June. Elsevier Science Ltd. Oxford, U.K.

Bertero, V. V. and R. D. Bertero (1993). Formulation of a conceptual seismic code. *Proc. Tom Paulay Symp.* American Concrete Institute *SP 157*: 255-288. Detroit, Michigan, U.S.

Bertero, V. V. (1992). Major issues and future directions in earthquake-resistant design. *Proc.* 10WCEE. 11: 6407-6444. A. A. Balkema, Rotterdam, Netherlands.

Bertero, V. V., J. C. Anderson, H. Krawinkler, E. Miranda (1991). Design guidelines for ductility and drift limits: Review of the state of the practice and state of the art in ductility and drift-based earthquake-resistant design of buildings. *Report No. UCB/EERC-91/15*, Earthquake Engineering Research Center, Univ. of California at Berkeley, U.S.

Bertero, V. V. (1991). Structural engineering aspects of seismic zonation. *Proc.*, 4th Int. Conf. Zonation: 1: 261-321. Earthquake Engineering Research Institute, Oakland, California, U.S.

Bertero, V. V. and H. Kannil (1974). Nonlinear seismic design of multistory frames. *Canadian J. Civ. Engrg.* University of Waterloo Press.

Bertero, V. V. (1982). State of the art in seismic resistant construction of structures. *Proc.*, 3rd Int. Microzonation Conf.: II: 767-808.

Bonnacci, J. F. (1994). Design forces for drift and damage control: a second look at the substitute structure approach. *EQ Spectra* 71: 4: 601-609.

Biggs, J.M. (1986). Introduction to structural engineering. Prentice Hall, Englewood Cliffs, New Jersey, U.S.

Collins, K. R., Y K. Wen and D. A. Foutch (1995). Investigation of alternative seismic design procedures for standard buildings. Tech. Report, Dept. of Civil Engineering, Univ. of Illinois, Urbana, U.S.

Elwood, K. and Y. K. Wen (1995). Performance evaluation of a dual-level design using 1994 Northridge earthquake records. Tech. Report, Dept. of Civil Engineering, Univ. of Illinois, Urbana, U.S.

Esteva, L. (1980). *Design: General*, 54-97 in Design of earthquake resistant structures. Ed. Rosenblueth. E. John Wiley & Sons, New York NY, U.S.

Gallagher, R. H. (1973). *Introduction*, Optimum structural design, Ed. Gallagher, R.H. and Zienkiewicz, O. C. John Wiley & Sons, New York NY, U.S.

Gulkan, P., and M. A. Sozen (1974). Inelastic response of RC structure to earthquake motions. *J. Struct. Div. ACI*: 71: 4: 601-609.

Housner, G. W., and P. C. Jennings (1982). *Earthquake design criteria.* Earthquake Engineering Research Institute, Oakland CA, U.S.

Housner, G. W. (1956). Limit design of structures to resist earthquakes. *Proc.* 1st WCEE: 5.1-5.13, Berkeley CA, U.S.

Kennedy, R. P. *et al.* (1994). Natural phenomena hazards design and evaluation criteria for Department of Energy facilities. *DOE-STO-1010-94.* U.S. Department of Energy.

Mahin, S. A. and V. V. Bertero (1976). Problems in establishment and prediction of ductility in aseismic design. *Proc. Int. Symp. EQ Struct. Engrg.* University of Missouri, Rolla, Missouri, U.S. I: 613-628.

Moehle, J. P. (1992). Displacement based design of RC structures. *Proc.* 10WCEE: 8: 4297-4302.

NEHRP (1991, 1994). Recommended provisions for the development of seismic regulations for new buildings. Building Seismic Safety Council, Washington, D.C., U.S.

Priestley, M. J. N. (1993). Myths and fallacies in earthquake engineering -- conflicts between design and reality. *Proc. Tom Paulay Symp.* Publication *SP-157*, American Concrete Institute, Detroit MI, U.S. 231-254.

Rosenblueth, E. (1974). *Safety and structural design*, Chap. 7 in Reinforced concrete engineering, ed. Bresler, B. John Wiley & Sons, New York NY, U.S.

Shapiro, D. *et al.* (1996). Application of case studies of buildings damaged by the Northridge earthquake to development of U.S. guidelines for seismic rehabilitation of buildings. *Proc. 7th U.S.-Japan Workshop on Improvement of Struct. Design and Construction Practices.* Japan Structural Consultants Assoc., Tokyo, Japan; and Applied Technology Council, Redwood City CA, U.S.

Shibata, A. and M. A. Sozen (1976). Substitute-structure method for seismic design in RC. *J. Struct. Div. ACI*: 102: 1: 1-18.

Shimazaki, K. and M. A. Sozen (1984). Seismic drift of reinforced concrete structures. Technical Research Report, Hazama-Gumi, Ltd.: 145-166.

Shimazaki, K. (1988). Strong motion drift and base shear coefficient for R/C structures. *Proc.* 9WCEE: V: 165-170.

Sozen, M. A. (1983). Lateral drift of reinforced concrete structures subjected to strong ground motions. Univ. Illinois, Urbana, U.S.

SEAOC Vision 2000 Committee (1995). Report on performance-based seismic engineering. Structural Engineers Association of California, Sacramento, U.S.

SEAOC Seismology Committee, 1957-1990. Recommended lateral force requirements and commentary. (SEAOC Blue Book). Structural Engineers Association of Northern California, San Francisco, U.S.

Qi, X. and J. P. Moehle (1991). Displacement design approach for reinforced concrete structures subjected to earthquakes. *Report No. UCB/EERC-91/02*, Earthquake Engineering Research Center, Univ. of California at Berkeley, U.S.

Uang, C.-M. and V. V. Bertero (1988). Use of energy as a design criterion in earthquake-resistant design. *Report No. UCB/EERC-88/18* Earthquake Engineering Research Center, Univ. of California at Berkeley, U.S.

Uang, C.-M. and V. V. Bertero (1991). UBC seismic serviceability regulations: A critical review. *J. Struct. Engrg.*, ASCE: 1: 7: 2055-2068. New York, NY, U.S.

Wen, Y. K. (1995). Building reliability and code calibration. *EQ Spectra*: 11: 2. May. Earthquake Engineering Research Institute, Oakland, California, U.S.

Zagajeski, S. W. and V. V. Bertero (1977). Computer-aided optimum design of ductile R/C moment-resisting frames. *Proc.*, Workshop on EQ-resistant RC Building Construction: III: 1140-1174. Univ. of California Extension, Berkeley, U.S.

THE NEED FOR MULTI-LEVEL SEISMIC DESIGN CRITERIA

VITELMO V. BERTERO

Earthquake Engineering Research Center, University of California at Berkeley
1301 S. 46th St., Richmond CA 94804-4698, USA

ABSTRACT

This paper gives the reasons why **there is a need to develop an Earthquake-Resistant Design (EQ-RD) methodology based on multi-level EQ-RD criteria**. It briefly reviews the available philosophies and approaches for the design of civil engineering facilities subjected to normal types of excitations, and then discusses the problems of designing against significant Earthquake Ground Motions (EQGMs), which are considered to be abnormal excitations. The worldwide accepted general philosophy of EQ-RD is discussed, and a critical review of current code procedures follows. The SEAOC Vision 2000 Committee's recent attempt to formulate a conceptual framework for Performance-Based Seismic Engineering (PBSE) of buildings subjected to significant EQGMs is discussed in tandem with a discussion of information needed for conducting Performance-Based EQ-RD (PB EQ-RD). A conceptual comprehensive approach for PB EQ-RD based on multi-level criteria is proposed. A minimum of four discrete performance EQ-RD objectives are recommended. At least two of the four performance levels are recommended for preliminary EQ-RD, and all four performance levels are necessary to check the acceptability of the final design.

KEY WORDS

Comprehensive design; design earthquake ground motions; multi-level design criteria; performance-based earthquake-resistant design; performance design objectives; performance levels.

INTRODUCTION

The total design process of a civil engineering facility usually involves several phases, of which the following four are the most important: ***(1) conceptual overall design, or planning phase; (2) preliminary design phase, which usually involves approximate analysis; (3) rigorous analysis and final design phase; and (4) acceptability check of final design and detailing phase.*** Before starting the design process, it is necessary to establish the design criteria. Biggs (1986) defines design criteria as those rules and guidelines which must be met to ensure that the objectives of the design are satisfied. There are three major objectives: ***(1) safety; (2) performance of function; and (3) economy.***

Safety must be regarded as the most important objective, because structural failure usually endangers human life and always involves economic losses due to physical and functional damages. It must be recognized that no structure is totally safe; that is, there is always some finite probability of failure due to human errors in design and construction, or unforeseen natural catastrophe. The degree of safety required depends on the function of the structure, which determines the uncertainties in performance and the penalty for failure. Even though a structure is safe against collapse, it may deflect or vibrate excessively so as to interfere with the intended use. ***Functional requirements*** must be met if the structural design is to be satisfactory.

Having satisfied objectives (1) and (2), the structure must be designed for minimum cost. However, there may be a trade-off between objectives (2) and (3), and a final decision must be based on a ***minimum cost/benefit ratio***. The cost of the structure may not be considered in isolation. The important consideration is the cost of the total project and the most economical structure may result in higher costs of other nonstructural systems. The structural cost consists of the total for materials, fabrication, erection and maintenance. Minimizing the amount of material used does not necessarily ensure minimum cost, because this may result in excessive fabrication (e.g., steel connections) and erection costs, which are a large part of the total, as well as increased costs of maintenance (repairs) and loss of function during the service life of the structure.

REVIEW OF DESIGN PHILOSOPHIES AND APPROACHES

In the available literature on design, different terms such as "Design Requirements," "Design Principles," "Fundamental Basis of Design," and "Design Philosophy" have been used to denote the total design process, including selection of the design criterion or criteria. Herein the term "Design Philosophy and Design Approaches" will be used, with intended emphasis on the numerical analysis and design phases of the total process. Before discussing the importance of selecting a rational design philosophy and design approach when the potential sources of earthquake hazards, particularly when the excitations due to EQ ground motions (EQGMs) dominate the design, it is convenient to do a critical review of the main design philosophies and design approaches that have been proposed and used in practice for normal excitations.

Linear Elastic Design Philosophy

The two following approaches, which have been developed and used in present codes and therefore in practice, are based on the assumption that the structure will behave in its linear elastic range: ***Allowable-Stress or Working Stress or Service Stress Design Approach*** (according to this approach, the structure and its members are designed to support the working or service loads without exceeding certain specified allowable stresses); ***Strength Design Approach*** [although this approach is based on the assumption of linear elastic behavior of the structure, the structural members are designed on the basis of their critical section yielding strength capacity when subjected to factored service or working loads (excitations)].

Limit Design or Plastic Design or Collapse Design Philosophy

According to this philosophy, the structure is designed on the basis of its collapse strength against properly factored service or working loads (excitations): ***Rigid-Plastic Design Approach*** (this approach is based on the assumption that the structure's members have sufficient ductility to allow the development of a collapse mechanism ignoring the elastic deformations); ***Elastic-Plastic Design Approach*** (in this approach, the elastic and plastic deformations are considered in the redistribution of the internal forces due to the plastic deformations).

Serviceability Limit States Philosophy

This philosophy considers the performance of the structure under the normal service or working excitations as in the case of allowable stress approach, but is also concerned with the other requirements besides the stresses for ensuring a satisfactory use of the building according to its occupancy, including the possible consequences of excessive deformations and/or deformation rates and vibrations on the persons occupying the building, and on the nonstructural components (such as cracking, slipping etc.). *Note that the limit state defines a deformation condition of the structure at which it or any part of it ceases to perform its intended function. Thus, limit states are usually called limits of usefulness.*

Strength Limit States Philosophy

The design based on this philosophy will consider the safety or load-carrying capacity of the building when it is subjected to the critical combinations of the factored service loads, including not only the plastic strength of the members but also the effects of normal classic fatigue, low cyclic fatigue, incremental collapse, fracture etc. The LRFD approach for steel structures has been developed based on this philosophy.

Comprehensive Design Philosophy

In a discussion of the problem of strength and deformation capacities of buildings under extreme environments, Bertero (1980) points out that the possible occurrence of a severe event, such as an earthquake, poses special problems in the design of new buildings and the evaluation of the adequacy of existing buildings. The question is whether is it necessary only to prevent collapse and subsequent loss of life, or whether the expense of damage should be limited as well. A solution is offered by the philosophy of comprehensive design, which was discussed by Sawyer (1964), who proposed *a comprehensive design procedure that correlates the resistance of a structure at various failure stages (limit states or limits of usefulness) to the probability that possible disturbances can reach the intensity required to induce such failure stages, so that the total cost (including the first cost and the expected losses from all the limit stages) is minimized.* As illustrated in Fig. 1, under increasing loads structures generally fail at successively more severe failure stages with increasingly less probability that the load will reach the required intensity levels. The relationship shown in Fig. 1 gives possible structure failure states versus a monotonically increasing pseudo-static load for a typical statically indeterminate reinforced concrete building. For EQ disturbances, the relationship is more complicated because of the effect of the cumulative damage induced by repeated cycles of reversal deformations. Owing to the variability of loss for a given load (or the variability of load for a given loss), this relationship represents the mean values of the random variables involved. The full distribution, as shown in Fig. 2, can sometimes involve large variances (Tichy *et al.*, 1964). This should be clearly understood by the analysts and designers so that they will not put all their trust in numerical results obtained via just one deterministic analysis, no matter how sophisticated a computer program is used.

COMPREHENSIVE EQ-RD: NEED FOR MULTI-LEVEL DESIGN CRITERIA

For buildings whose design is dominated by severe environmental conditions such as EQGMs, it is required that the strength, deformation and energy dissipation capacities of the building be established at each main limit state. Furthermore, to improve seismic hazard abatement, existing buildings must be continuously assessed for danger under the extreme environmental conditions that can be induced by EQs, necessitating comprehensive analyses of the buildings to predict their strength, deformation and energy dissipation capacities at each of the main limit states (performance levels). Thus, to tackle these problems efficiently it is clear that multi-level analysis and design criteria are needed, and from the above brief discussion of the existing design philosophies it appears that the comprehensive design philosophy is the most attractive one for solving them. As is shown below, the comprehensive design philosophy covers not only all the requirements for the worldwide accepted philosophy for EQ-RD, but also the more detailed performance design objectives that have been included in the definition of the PB EQ-RD adopted recently by the Vision 2000 Committee (SEAOC, 1995).

General Philosophy of EQ-RD

The general philosophy of EQ-RD for nonessential facilities has been well established and accepted worldwide, and it proposes to prevent: ***(1) structural and nonstructural damage in frequent minor earthquake ground shaking, (2) structural damage and minimization of nonstructural damage during occasional moderate earthquake ground shaking, and (3) collapse or serious damage in rare major earthquake ground-shaking***.

This general philosophy demands the use of multi-level design criteria and it qualitatively agrees with the comprehensive design concept or philosophy but, as is discussed below, present practical applications of this general philosophy fall short of realizing its objectives, mainly because it does not define specifically (quantitatively) the earthquake ground-shaking and the degree of damage that has to be prevented, and also because seismic code EQ-RD procedures, following the traditional design procedures for normal types of excitations (loading), emphasize the use of just the life-safety performance level as a design criterion. To remedy this, the Vision 2000 Committee has adopted the following more detailed and specific definition of PB EQ-RD.

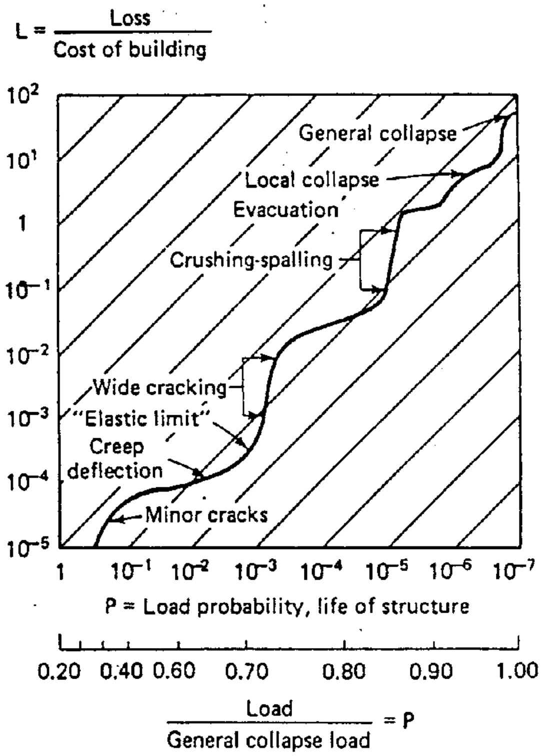

Fig. 1. Losses versus load probabilities during the service life of a RC structure (after Sawyer 1964)

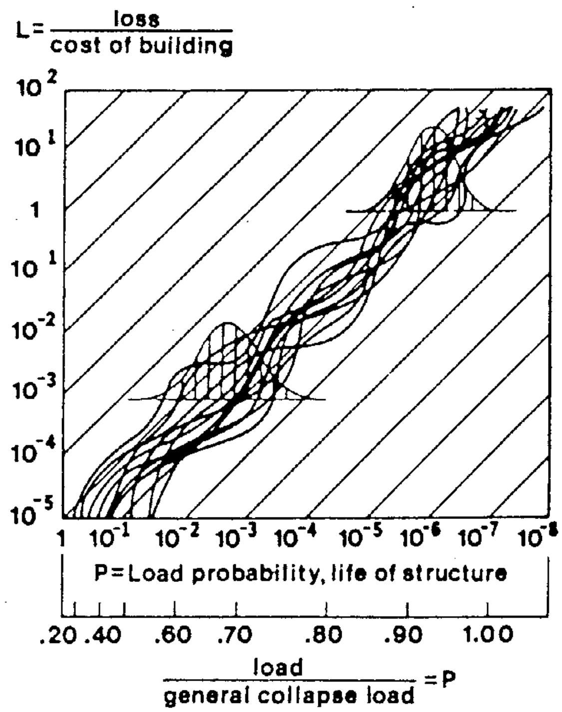

Fig. 2. Distribution of losses versus load probabilities during the service life of a RC structure (after Tichy *et al.* 1964)

Definition of PB EQ-RD

Performance-based EQ-RD consists of selection of appropriate systems, layout, proportioning and detailing of a structure and its nonstructural components and contents so that at specified levels of ground motion and with defined levels of reliability, the structure will not be damaged beyond certain limiting states. At any particular EQ demand level, a given structure will respond within a particular damage state. An infinite spectrum of limiting damage states, ranging from no damage to complete collapse, exists. For purposes of PB EQ-RD, four specific limiting damage states, or performance levels, are defined. ***The performance level is by itself independent of the seismic hazard***; however, when coupled with a specific ground motion criterion, it becomes a ***performance design objective***. Typically, a project should be designed for a spectrum of seismic design objectives, ***ranging from no damage for earthquake ground-shaking which is likely to affect the building relatively frequently to avoiding collapse for infrequent extreme events.*** The SEAOC Vision 2000 Committee has defined four performance levels: ***Fully Operational, Operational, Life-Safe*** and ***Near Collapse***. Furthermore, this Committee has defined as a minimum ***three standard design objectives***. Thus, it is obvious that PB EQ-RD involves multi-level seismic design criteria.

From the above definitions and discussion, it is clear that earthquake-resistant design must involve consideration of serviceability and strength limit states and should include the cost of losses. Furthermore, in view of the uncertainties involved in defining the levels of the EQGMs and in predicting the real mechanical behavior, it will be necessary to use a probabilistic approach in such a design. ***Thus, it becomes clear that among the different existing design philosophies the ideal one for PB EQ-RD is the comprehensive design philosophy.***

Current Seismic EQ-RD Approaches: A Critical Review from the Point of View of the Accepted EQ-RD Philosophy on Which PB EQ-RD Approaches Should Be Based

When Vision 2000 began to develop the work plan to produce design and construction standards that will yield buildings with predictable EQ performance, one of the first questions and problems that needed to be tackled was whether it will be possible to conduct PB EQ-RD using the present seismic codes' EQ-RD approaches, which in the U.S. are based on just a one-level design objective. To answer this question, it is necessary to review first what is needed to be able to produce EQ-RD and construction of predictable performance.

Information Needed for Conducting PB EQ-RD of Buildings. As briefly discussed above, the ideal design philosophy for conducting a PB EQ-RD seems to be the comprehensive design philosophy. According to this philosophy, *the ideal design is that which results in minimum total cost of the facility, which includes not only the initial cost of construction but the cost of all possible losses (physical and functional) at all the possible limit states that the facility can reach or be subjected to during its service life and the needed repair and/or upgrading work, as well as the cost of its demolition.* Thus, it is clear that the comprehensive design philosophy and consequently the PB EQ-RD are based on the use of the so-called limit states design philosophy, but goes beyond this philosophy. The comprehensive design philosophy that recognizes the uncertainties involved in defining each of the different excitations to which a facility can be subjected, and particularly their critical combinations (i.e., the design excitations) at each of the different limit states as well as the uncertainties in defining the engineering parameters controlling the mechanical behavior of the facility, is a ***probabilistically formulated limit state design philosophy***. To summarize: to conduct PB EQ-RD it is necessary to apply the comprehensive design philosophy, which is a probabilistically formulated Limit State Design philosophy based on the use of ***multi-level design criteria***, and the use of this philosophy requires the following information:

- The different sources of excitations (loads) to which the facility to be designed can be subjected during its service life.
- Definitions of the limit states (performance levels) that need to be considered.
- The variation in the intensity of each of the excitations that can act on the facility during its service life and the probability that the combinations of these excitations can reach the required intensity to induce each of the limit states (failure stages) that need to be considered.
- The types of failures (limit states) of the different components, structural and nonstructural, of the entire facility system, associated with the types of excitation and the increasingly small probability that the excitations will reach the intensity levels required to induce such failures.
- The costs of the losses (physical and functional) and repairs associated with each of the different limit states (failure stages) that need to be considered.

Thus, as is the case with any type of engineering design, the most important information for PB EQ-RD is that concerning the sources of excitations, their variation in intensity with time and their corresponding probability of reaching the intensity required to induce any of the limit states that have to be considered. Once this information is available, the owner, together with the designer, has to decide on the performance levels (limit states) that should be considered in the design together with the recurrence periods over which such levels are reached in accordance with the controlling excitations at these levels. For example, the owner may desire a design and construction that will perform as stated in Table 1. According to the expected intensity and duration of the EQGM excitations and the combination of other significant potential seismic hazards and loading conditions in the owner-desired recurrence periods, the designer has to analyze whether it will be economically feasible to design for such requirements and then to offer alternative recurrence periods for the different limit states. Assuming that a compromise is reached on the recurrence period of the limit states as indicated in Table 1, ***the design criteria*** in the form of ***PB EQ-RD objectives*** has been established, and the next step is to conduct the necessary analysis and preliminary design to comply with the established ***multi-level design criteria***.

The necessary analysis and preliminary designs are commonly based on idealized mechanical behavior under simplified excitations because it is not usually possible to consider actual behavior and the true history of disturbances. Sources, treatment and effects of the different types of excitations are summarized in Fig. 3. Structures are usually subjected to unpredictable fluctuations in the magnitude, direction and/or position of each of the individual excitations that may act on them during their service life, and the extreme values between which each of these excitations will oscillate are the only characteristics that can be estimated with some accuracy. These types of action are classified in Fig. 3 as generalized or variable-repeated excitations. The types of failures associated with variable-repeated excitations are classified as long-endurance fatigue, low-cycle fatigue, and incremental collapse. Long-endurance fatigue is only critical for very special structures. Failure prediction is clearly essential in designing against extreme environments and requires knowledge of the strength ***at different levels of structural deformation***. The discussion above points out the difficulty in predicting strength and deformation capacities and the need for a probabilistic approach, or, at least, for considering the bounds and ranges of probable mechanical behavior and possible excitations.

Table 1. Initial selection of performance levels (SEAOC 1995)

Performance Levels	No Damage	Damage Control			
		No struct. damage, minor nonstruct. damage	Minor struct. damage, moderate nonstruct. damage	Life safety and economic repairability	Life safety but no economic repairability
Limit States	Service	Continuous Operation	Immediate Occupancy	Life Safety	Impending Collapse
Owner desired recurrence period*	10 years	30 years	50 years	450 years	900 years
Compromise recurrence period	8 years	20 years	40 years	450 years	700 years

* note that the values of recurrence periods given herein are arbitrarily selected to illustrate the procedure

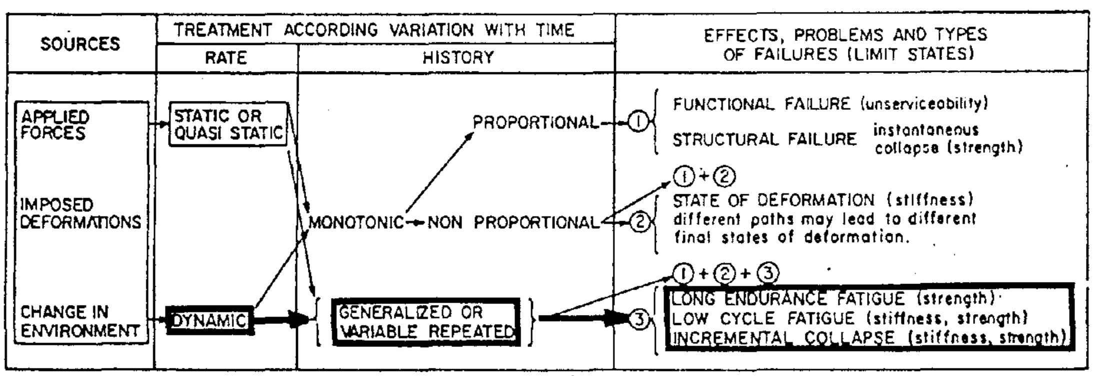

Fig. 3. Sources, treatment and effects of excitations on structures (Bertero 1980)

Based on the possible different types (dynamic characteristics) of EQGMs, such as impulsive or harmonic, and on the relative intensity of the other types of excitations, such as the gravity loads that can be acting simultaneously with the expected future EQGMs, Bertero *et al.* (1991) give a detailed discussion of what is needed regarding the EQGMs, as well as the prediction of the mechanical behavior (dynamic response) up to each of the limit states involved in the desired performance design objectives of PB EQ-RD. This is done considering the different types of failures illustrated in Fig. 3. From this information, it is clear that: except for the rare case in which it is desired to keep the entire building serviceable under even the maximum capable EQGM, in which case ***linear elastic analysis and design based on one-level design criteria***, can be used; in all the other cases estimation of the damage potential of the EQGMs and preliminary design and analysis of the entire building demand the use of approaches and procedures ***based on multi-level design criteria and on nonlinear dynamic analyses***. Regarding the expected EQGMs, the essential information needed is: ***the time history of the expected EQGMs at the different recurrence periods corresponding to the performance levels that should be considered.*** Note that because of the uncertainties in predicting such EQGM time histories it is necessary to specify for each recurrence period a suite of EQGM time histories. With this information, engineers can compute the specific detailed information needed to conduct the preliminary EQ-RD and the needed acceptability analyses. The specific information to be obtained from the processing of the time history of the EQGMs at each of the recurrence periods that need to be considered are the following ***smoothed inelastic design response spectra (SIDRS)*** for: strength, total acceleration, velocity, displacement, energy input, and energy dissipation. These spectra have to be computed considering the different levels of ductility ratio, μ, and damping coefficient, ξ, that can be developed and accepted according to the desired performance at the recurrence period under consideration. These spectra should include as a particular case the ***Smoothed Linear Elastic Design Response Spectra (SLEDRS)*** which is for μ=1.

From the above discussion it becomes clear that the use of multi-level design criteria requires the consideration and processing of a lot of information, which makes it difficult for practical application. However, its use is needed for calibrating the practical simplified design procedures that have been used or proposed based on the use of just one design criterion, which usually is formulated considering the minimum requirements of life safety.

CRITICAL REVIEW OF CURRENT U.S. CODE EQ-RD APPROACHES

As discussed in detail in Bertero *et al.* [1991], the current code EQ-RD approaches for most buildings are based on the use of a strength (base shear) SLEDRS for just one performance level, the Life Safety level corresponding to a return period of 475 years. Taking advantage of the dissipation of energy that can be developed through plastic deformation of ductile structures, the U.S. seismic codes have introduced an EQ-RD approach that reduces the demanded linear elastic strength (base shear) through ***a reduction factor called the response modification factor, R, by the NEHRP recommendations (FEMA, 1992), or the structural system factor, R_w, by the SEAOC blue book (1990).*** To keep code design procedure as simple as possible using only linear elastic methods of analysis (which allows use of the principle of superposition), the U.S. codes base their design on either the allowable or service stress approach (UBC), or the first significant yielding of the most stressed section (NEHRP). There is no doubt that this is the simplest approach, except for the case of buildings where prescriptive EQ-RD can be used. However, as shown by Bertero *et al.* (1991), blind use of the current linear elastic code approaches, ***the so-called static equivalent lateral force*** (ELF) and even ***the linear dynamic response spectrum***, which are based on the use of R factors whose values depend only on the type of structural system, independent of the period of the structure and of the EQGMs' dynamic characteristics, and of the relative importance of the other types of excitations (loads) that can act simultaneously with the effects of the EQGMs, can result in designs that can have quite different performance, and in several cases in undesirable performance. Furthermore, a main weakness of the ELF approach, as well as of any other of the current code EQ-RD approaches, is that ***they are based on just one performance design objective: life safety***. Although the code requires checking the deformations (lateral interstory drift indices) from elastic analysis under the design lateral forces against the specified values of the maximum allowable lateral drift values under working load conditions, and these deformations, modified by a factor that the NEHRP recommendations called the deflection amplification factor, C_d, and by a factor $3(R_w/8)$ in the 1994 UBC code regulations, have to be equal to or smaller than specified maximum acceptable values, it has to be noted that: first, the deformations obtained from the elastic analysis under the reduced forces for the life safety EQGMs with a return period of 475 years do not in general represent the deformations that can be expected under the service EQGMs, i.e., the EQGMs that can occur with a lower return period; and secondly that these elastic deformations amplified by the specified or recommended deflection amplification factor in general do not result in a reliable prediction of the actual inelastic deformation that will occur under the critical EQGMs with a return period of 475 years.

In judging the different code EQ-RD approaches that are based on designing for strength (base shear), as well as for those new approaches that have been suggested as promising for PB EQ-RD and which are also based on just using strength as the main design criterion or parameter, the following should be kept in mind: first, that the defined performance levels are based on different degrees of acceptable damage and damage is more a consequence of the history of deformation and rate of deformation than of strength, and secondly that for the performance levels accepting damage through the yielding of the structure as a mechanism, the use of the yielding strength as a design parameter is completely insensitive to the amount of deformation, i.e., to the amount of damage, and therefore cannot be used alone to conduct the required PB EQ-RD.

From the above discussion, it is obvious that the current code ELF EQ-RD approach, based on just one performance level and design objective and on the use of specified linear elastic strength spectrum that is reduced through specified values for the R factor cannot result in general in the design of buildings with predictable performance. Because this ELF approach is the most used approach for EQ-RD of buildings, it would be highly desirable first to investigate the kind of buildings to which it can be applied to achieve predictable performance, and secondly, what simple modifications can be introduced to extend the applications of this ELF approach to the PB EQ-RD of other types of buildings. There is no doubt that this is one of the most challenging tasks for the practical implementation of performance-based EQ-RD. To accomplish this, it will be necessary to calibrate the needed simplifications to reduce the actual multi-level requirements of the comprehensive design philosophy to the use of just one performance level and linear elastic analyses. This calibration can be done through the use of a ***comprehensive EQ-RD approach*** based on multi-level performance design objectives that the author and his associated researchers have developed and applied (Bertero *et al.*, 1994). A detailed description of the proposed comprehensive EQ-RD approach has been presented by the author in the report of SEAOC Vision 2000 Committee (1995), where it is pointed out that the preliminary design of the building based on multi-level criteria (performance design objectives) can be carried out: designing for just the one limit state (performance level) that appears to control the design, and then checking for all the others; or designing simultaneously for the demands of two or all the main limit states. It is recommended to design simultaneously for at least two limit states: for example, for the design of a tall building in the San Francisco Bay Area it is recommended to carry out the preliminary EQ-RD for service (or fully operational) and life safety. No matter how many levels are used in the preliminary design, the acceptability check of the final design should be conducted considering all the recommended levels, which for the PB EQ-RD are four.

It should be clearly noted that the author is not proposing that the comprehensive EQ-RD approach, which is based on multi-level design criteria, be implemented immediately in present seismic codes. This approach is proposed for use in investigating how reliable, simple and practical seismic code procedures based on just a single design criterion (single performance design objective) can be developed.

REFERENCES

Bertero, V. V. and R. D. Bertero (1994). Formulation and application of a conceptual code procedure for earthquake-resistant design of building structures. *Proc.*, 5th U.S. Nat'l. Conf. on Earthquake Engineering. Earthquake Engineering Research Institute, Oakland, California, U.S.A. **11**, 391-400.

Bertero, V. V., J. C. Anderson, H. Krawinkler, E. Miranda, and the CUREe and Kajima Research Teams (1991). Design guidelines for ductility and drift limits. Earthquake Engineering Research Center, *UCB/EERC-91/15*. Univ. of California at Berkeley, U.S.A.

Bertero, V. V. (1980). Strength and deformation capacities of buildings under extreme environments. In Structural Engineering and Structural Mechanics, a volume honoring Egor P. Popov. Prentice-Hall, 188-237.

Bertero, V.V. (1971). Research needs in limit design reinforced concrete structures. Earthquake Engineering Research Center, *UCB/EERC-71/04*. Univ. of California at Berkeley, U.S.A.

Biggs, J. M. (1986). Introduction to structural engineering. Prentice-Hall, New Jersey.

FEMA (Federal Emergency Management Aggency) (1992). "NEHRP recommended provisions for the development of seismic regulations for new buildings." *FEMA 222*, Washington, D.C., U.S.A.

Sawyer, H. A., Jr. (1964). Comprehensive design of reinforced concrete frames by plasticity factors. *9th Planning Session of CED Symposium*. Ankara, Turkey.

SEAOC (Structural Engineers Association of California) (1990). "Recommended lateral force requirements and commentary." Sacramento, California, U.S.A.

SEAOC Vision 2000 Committee (1995). "Performance-based seismic engineering." Report prepared by Structural Engineers Association of California. Sacramento, California, U.S.A.

Tichy, M. and N. Vorlicek, (1964). Flexural mechanics of reinforced concrete frames by plasticity factors. *Proc., Int'l. Symp. Flexural Mechanics of RC, ACI SP-12*. Miami, Florida, U.S.A.

IMPLICATIONS OF OBSERVED POUNDING OF BUILDINGS ON SEISMIC CODE REGULATIONS

VITELMO V. BERTERO

Earthquake Engineering Research Center, University of California at Berkeley
1301 S. 46th St., Richmond CA 94804-4698, USA

ABSTRACT

The main objectives of this paper are: to review the history of observed damage after significant earthquake ground motions (EQGMs) due to adjacency hazards, of which pounding of buildings is just one potential source, as well as the conclusions and recommendations formulated after the 1985 Mexico City experience; to discuss briefly the technical and socio-economic problems created by adjacency hazards, with particular emphasis on pounding, for the earthquake-resistant design (EQ-RD) of new adjacent buildings and for the seismic evaluation and upgrading of existing hazardous adjacent buildings; to assess the rationality and reliability of present seismic code regulations for EQ-RD of new adjacent buildings, as well as the standards and/or procedures for the upgrading of existing adjacent buildings; and to formulate recommendations regarding what is needed to improve the state of the art and particularly the state of the practice by improving and/or developing new seismic code regulations for the abatement of the seismic risks that can be generated by adjacency hazards.

KEY WORDS

Adjacency hazards; adjacent buildings (structures); earthquake-resistant design; hammering; pounding; seismic code regulations; and seismic upgrading.

INTRODUCTION

Introductory Remarks

Pounding Between Buildings. Field inspections of the performance of buildings after significant earthquake ground motions (EQGMs) in urban areas reveal that pounding between adjacent buildings is technically one of the main sources of damage among the different types of damage that can result from ***seismic adjacency hazards***.

Seismic Adjacency Hazards. In the glossary used in the *Standards of Seismic Safety for Existing Federally Owned or Leased Buildings (ICSSC RP4) and Commentary* developed by the Interagency Committee on

Seismic Safety in Construction (ICSSC) (Todd, 1994), the ***seismic adjacency hazards*** are defined as follows:

> *Hazards caused when adjacent buildings interact during an earthquake. Includes pounding, effects of one building buttressing another, falling hazards from an adjacent building, and the consequences of damage to common structural elements, such as party walls (single bearing walls supporting two adjacent buildings constructed on separately defined parcels of land).*

The above potential sources of danger can create complex technical and socio-economic problems. The complexity of these problems varies depending on whether the problem at hand is one of design and construction of new adjacent buildings, or one of evaluation of the presence and relative seismic risk of any one of the above adjacency hazards in existing buildings and, if one exists, how to remedy it with technical and economical efficiency. In general, the problems involved in seismic evaluation and upgrading existing buildings with an adjacency hazard are more complex than those involved in the earthquake-resistant design (EQ-RD) and earthquake-resistant construction (EQ-RC) of new adjacent buildings. This is particularly true when the adjacent buildings have different owners and even worse if one or more of the adjacent buildings under consideration are condominiums. As pointed out by Arnold (1995) and discussed later, the socio-economic problems that can arise because of the need to involve owners of adjacent buildings in costly studies, design and construction work in which they may not wish to participate can be very complex and difficult to resolve. Although only the technical problems due to pounding between adjacent buildings will be discussed herein, it should be clearly noted that the other problems of adjacency must also be addressed if we are to achieve effective mitigation of seismic risks in our urban areas.

Review of the History of Pounding Between Adjacent Buildings. Adjacency effects due to EQGMs have been noted because they caused some building distress in most of the past significant EQs that have shaken urban areas, and the existence of the problem created by these effects, particularly due to pounding, was brought to the attention of the engineering community by building codes in the 1950s (UBC, 1955 and SEAOC, 1959). Pounding is a problem related to the separation between adjacent buildings, and occurs when the spacing between buildings is not sufficient to allow them to vibrate or move freely laterally. In 1961 Blume *et al.* wrote, "The question of what width of separation is sufficient must be considered primarily a matter of engineering judgement. Arbitrary rules could cause severe hardship in some cases, and would be inadequate in others." However, perhaps because of the lack of dramatic collapse and/or severe damage, professionals and researchers did not pay the needed attention to the importance of this problem until the 1971 San Fernando EQ, when severe structural damage to the basement of the main building at a separation joint and the collapse of a stair tower of the then recently constructed Olive View Hospital (Bertero, 1973 and Mahin *et al.*, 1976). Researchers' interest in conducting detailed studies on this kind of seismic hazard was triggered by the high number of engineered buildings that suffered severe damage and even collapse in Mexico City as a consequence of pounding during the 1985 Michoacan earthquakes. As reported by Bertero (1986), analysis of the information available on the observed damage of buildings in Mexico City reveals that in over 40% of the collapsed or severely damaged buildings, pounding between adjacent buildings occurred, and in at least 15% pounding was the primary cause of building collapse.

Although pounding has been observed in most of the significant EQGMs that have occurred in urban areas since the 1985 Michoacan EQs, and particularly after the 1989 Loma Prieta EQ and the recent 1995 Kobe EQ, the number of *adjacent engineered buildings* severely damaged and dramatically suffering from partial collapse due to pounding in Mexico City in 1985 may in fact be the highest in the history of this kind of EQ damages. As a consequence of the observed dramatic failures, the following questions were raised: What are the main reasons for the observed damaging and in many cases devastating pounding of adjacent buildings? Considering that the historic center of Mexico City is crowded with adjacent buildings without any significant separation, why did only a relatively small number of these buildings suffer severe damage? An attempt to answer these questions motivated the preliminary study reported by Bertero (1986).

Types of Observed Pounding Damage. In analyzing the observed damage due to pounding, the damaged buildings were grouped by Bertero (1986) according to their types and relative separations into the following three categories: ***(1) adjacent units of the same building separated through expansion (or construction) joints; (2) units of the same buildings or adjacent different buildings which are far apart but connected by***

one or more pedestrian bridges; and (3) adjacent different buildings. In connection with this way of grouping the damaged buildings, it is of interest to note that during the 1995 Kobe EQ the damage to the bridges in the above category (2) was very high in amount as well as severity. Furthermore, the number of medium-rise buildings that underwent severe overturning was large, and in several cases buildings overturned across the street, inducing damage to the building across the street. Another type of damage due to interaction of adjacent buildings, i.e., pounding, which was observed after the Kobe EQ and which was already noted after the Loma Prieta EQ (EERC, 1989), was the "*pushing*" of the end (usually the corner) building of a series of buildings built very closely adjacent to each other along a block.

<u>Conclusions From Analyses of the Observed Pounding Damages in Mexico City</u>. From the observed performance of adjacent buildings in Mexico City during the 1985 earthquakes and the results of the preliminary studies, the following preliminary conclusions were drawn: (1) In over 40% of the collapsed or severely damaged buildings, pounding between adjacent buildings occurred, and in at least 15% pounding was the primary cause of collapse. Relative to the total number of adjacent buildings with very small separations that exist in the center of Mexico City, the number of buildings severely damaged by pounding is very small. (2) Although severe pounding was the result of insufficient separation between adjacent buildings, this insufficiency in general cannot be attributed to just one specific reason. It was the result of a combination of several of the following factors: (a) the unexpected severity of the ground motion and the consequent insufficiency of the minimum seismic code requirements for the design of structures, particularly for lateral and torsional stiffnesses and strengths; (b) inadequate building configuration and structural system to resist lateral shaking and particularly torsional effects (lack of redundancy of structural defense lines, particularly against inelastic torsional deformations); (c) cumulative tilting due to foundation movement; and (d) improper maintenance. (3) Comparison of Mexican and U.S. earthquake regulations indicates that if buildings were designed and constructed to satisfy just the minimum code requirements, and if ground motions like those recorded at the SCT station could occur in U.S. cities, the problem of pounding between adjacent buildings located in soft soils could be even more serious in the U.S. than in Mexico City.

<u>Recommendations Formulated After the 1985 Michoacan EQs</u>. (1) Thorough studies should be conducted of the performance of adjacent buildings in Mexico City in order to investigate the primary causes of such performance and to improve present code requirements by determining proper separations between the different types of adjacent buildings. This will require integrated analytical and field experimental studies. (2) The probabilities of ground motions like those recorded at SCT happening in U.S. cities should be investigated so that a more thorough assessment can be made of the implications of the observed performance of adjacent buildings in Mexico City on U.S. EQ-RD and EQ-RC practices. Furthermore, in order to conduct a thorough assessment, it would be necessary to study the differences between the building technology used in Mexico City and that used in U.S. regions of high seismic risk, particularly regarding the type of RC structural system and proportioning and detailing of its critical regions, foundation, nonstructural elements, workmanship, inspection and maintenance, all of which are important factors in the seismic response of the entire soil-foundation-building system. (3) Economical solutions for retrofitting existing adjacent buildings which do not have adequate separation to avoid severe damage due to pounding should be investigated.

<u>Studies on Pounding and Other Adjacency Problems Conducted After the 1985 Mexico City Experiences</u>. As a consequence of the great importance of pounding damage on the observed severe damage of buildings in Mexico City after the 1985 Michoacan EQs, several researchers have conducted analytical studies and lately even integrated analytical and experimental studies on the pounding problem. Special technical sessions have been held on this problem in world and national conferences on earthquake engineering, and numerous papers have been published on this topic in the pertinent literature. Some recent studies, such as those by Filiatrault *et al.* (1995a and 1995b), Papadrakis *et al.* (1995), Athanassiadou *et al.* (1994), Anagnostopoulos *et al.* (1992) and Jeng *et al.* (1992) contain extensive lists of references. A search conducted by the author at the EERC library showed 57 publications on this problem since 1988. On the other hand, the damages caused by the two other problems of adjacency hazards that have been identified previously have not yet been well documented and studied.

Objectives and Scope

Objectives. Besides the above brief review of the observed EQ damage due to adjacency hazards, the main objectives of this paper are: to discuss briefly the technical and socio-economic problems that can be created by adjacency hazards in the EQ-RD of new adjacent buildings as well as for the seismic evaluation and upgrading of existing hazardous adjacent buildings; to assess the implications of the observed pounding damage on current practice by analyzing the rationality and reliability of present seismic code regulations regarding the EQ-RD of new adjacent units of the same building or new different adjacent buildings as well as of the technical standards and/or procedures for the upgrading of existing adjacent buildings; and to formulate recommendations regarding what is needed to improve the state of the art and particularly the state of the practice through the improvement of current code provisions and/or the development of new seismic codes or technical standards for the abatement of the seismic risks that can be generated by adjacency hazards.

Scope. To achieve the above objectives, this paper has been divided into four main parts. The ***first part*** is the above ***Introduction***, which briefly reviews the observed EQ damage due to adjacency hazards, their different types, and the conclusions and recommendations formulated as a consequence of the 1985 Mexico City experience. The ***second part*** is devoted to identifying the ***primary technical reasons*** for the different problems created by adjacency hazards, as well as the ***socio-economic issues*** involved. In the light of the identified technical reasons for the observed damage due to pounding, the ***third part*** of the paper is devoted to analyzing the ***implications of the observed damage on the state of the practice as reflected in the current seismic code regulations and standards*** in the EQ-RD of new adjacent buildings and the seismic evaluation and upgrading of existing hazardous adjacent buildings. The ***fourth part*** is devoted to formulation of ***recommendations regarding what is needed to improve the state of the art and particularly the state of the practice in mitigating the seismic risks that can be generated by adjacency hazards.***

PRIMARY CAUSES OF DAMAGE DUE TO POTENTIAL SOURCES OF ADJACENCY HAZARDS: TECHNICAL AND SOCIO-ECONOMIC ISSUES

Technical Issues. Obviously the primary reason for damage due to adjacency hazards is insufficient separation. This is the case when the adjacency hazards in one building are created by deficiencies in an adjoining building through common elements (walls and/or columns), as well as in the case of pounding of buildings separated by a relatively large distance but linked by bridges at certain stories, and in some cases the danger that a medium-rise building will overturn across a street. A series of questions arise from the observation of damage due to adjacency hazards: What could constitute a sufficient separation? What parameters control sufficiency of separation? Is the damage the result of inadequate code regulations regarding minimum separation? Is it due to violations of the minimum code requirements? These are very difficult questions to answer (Bertero, 1986). As mentioned earlier in the conclusions offered in the Introduction, in the case of the observed damage in Mexico City after the 1985 EQs, after preliminary analysis of the available data it appeared that the insufficient separation between the adjacent buildings that suffered severe damage due to pounding was the result of a combination of several factors, and could not be attributed to any one factor.

To summarize: the experiences from inspection of adjacency damages, particularly those due to pounding, appear to confirm that the minimum separation required by seismic codes, or the separation resulting from designer judgement or design practice not mandated by the enforced seismic codes, is usually adequate for avoiding severe pounding damage in adjacent well designed, constructed and maintained buildings. On the other hand, the rationality and reliability of the current requirements of the U.S. seismic codes, as well as those of other countries, are questionable in the case of two adjacent buildings located on or near the sources of very severe EQGMs (near-source effects) and in which one or both offer significant irregularity in plan and/or elevation.

Socio-Economic Issues. As pointed out in the Introduction, in EQ-RD of new adjacent buildings in urban areas located in regions of high seismicity, the separation that would be required to avoid the effects of hammering of adjacent medium and tall adjacent buildings could lead to serious socio-economic problems, particularly in urban areas because of the high cost of land. The socio-economic issues, as well as the technical issues, become significantly more complicated when seismic evaluation and upgrading of existing adjacent buildings is needed, particularly if the adjacent buildings have different owners, because usually this will require the owner who sees the need for upgrading his or her building either to conduct the needed and costly studies of the seismic vulnerability of the adjacent building, or to convince the other owner to pay. If the different owners do not agree, or if one of them refuses to finance the needed upgrading, it becomes very difficult for one owner to have the upgrading work done. As pointed out by Arnold (1995), the socio-economic problems involved in the upgrading of adjacent buildings are particularly critical when adjoining buildings have common structural elements along the property line. *In this case, upgrading is very difficult, if not impossible, without the neighbor's involvement, and probably some degree of rehabilitation to his or her property. While in engineering terms it may seem obvious that it is in the adjoining owners' best interest to cooperate in evaluation and mitigation, in socio-economic terms there may be many reasons, valid or otherwise, for reluctance (Arnold 1995).*

IMPLICATIONS OF OBSERVED POUNDING FOR CURRENT SEISMIC CODES

The implications of observed effects of pounding between adjacent buildings in Mexico City after the 1985 Michoacan EQs for the Mexico EQ-RD code requirements enforced at the time of the EQs and for the 1985 Emergency Regulations, as well as for U.S. EQ-RD and construction practices as reflected in the 1985 UBC and SEAOC recommendations have been discussed elsewhere (Bertero, 1986). Herein, only the implications of the observed pounding damage and the results of some of the numerous studies that have been conducted on pounding of adjacent buildings since 1986, for the present 1994 UBC and the 1995 SEAOC proposed changes for the 1997 UBC will be briefly discussed.

1994 UBC Requirements

As pointed out previously, the technical problems created by pounding are traditionally associated with minimum separations between buildings, which is how the seismic codes deal with them. Section 1631.2.11 of the 1994 UBC states:

> *All structures shall be separated from adjoining structures. Separation shall allow for $3(R_w/8)$ times the displacement due to seismic forces. When a structure adjoins a property line not common to a public way, that structure shall be set back from the property line by at least $3(R_w/8)$ times the displacement of that structure.* ***EXCEPTION:*** *Smaller separations or property line setbacks may be permitted when justified by rational analyses based on maximum expected ground motions. As a minimum, building separations or property line setbacks shall not be less than $(R_w/8) \geq 1$ times the sum of displacements due to code-specified seismic forces.*

Allowable Displacement Due to Seismic Forces. According to the 1994 UBC, section 1628.8.2, the "*calculated story drift shall not exceed $0.04/R_w$ or 0.005 times the story height for structures having a fundamental period of less than 0.7 second. For structures having a fundamental period of 0.7 second or greater, the calculated story drift shall not exceed $0.03/R_w$ or 0.004 times the story height.*" **EXCEPTIONS** are given that permit these drift limits to be exceeded.

From analysis of the above 1994 UBC regulations, the following observations can be made: (1) these regulations are very similar to the SEAOC 1985 Tentative Lateral Requirements (SEAOC Seismology Committee, 1985), which have already been discussed (Bertero, 1986); (2) the UBC regulations address only the problems of potential adjacency hazards for the EQ-RD of new buildings, and neglect the problems that these hazards can create in existing adjacent buildings, which the author considers are the most pressing problems that need to be solved to reduce the seismic risks of our urban areas (there is a huge inventory of existing adjacent buildings with insufficient separation in most cities); and (3) the rationality and reliability of the established minimum separation and of the drift limits through the empirical expressions based on the use of the numerical coefficient R_w have been seriously questioned [a more rational establishment of the drift limit is the one recommended in the 1991 and 1995 editions of the NEHRP provisions (FEMA, 1992 and 1995)], and these regulations do not address the large lateral displacement that can be induced by near-source effects (Iwan 1994, Hall *et al.* 1995), which were revealed by the EQGMs recorded during the 1994 Northridge and 1995 Kobe EQs. Furthermore, these regulations do not address properly the effects of subsoil on the dynamic characteristics of the entire building system (superstructure, nonstructural components and contents, foundation and soil), and consequently on the possible pounding response between adjacent buildings. As noted recently by Chouw *et al.* (1995), "***Depending on the subsoil conditions, a building system on subsoils can behave very differently than a system built with fixed base.***"

As already discussed by Bertero (1986), application of the above regulations results in very large required separations. For example, for two ten-story (35 m tall) SMRF buildings, the 1994 required gap between these two adjacent buildings should be ≥ (0.0225)35m ≐ 0.79m. Despite this apparently huge spacing, compliance with this code regulation may not guarantee that pounding will not occur, firstly because the code required lateral yielding strength for these two buildings is low, and secondly because of the other possible primary causes of pounding damage that have been discussed previously, to which near-source and subsoil effects sometimes also have to be added.

<u>SEAONC 1995 Strength Design Code Change Proposal for the 1997 UBC</u>. Ten years after the 1985 Mexico City experience, the Seismology Committee of the SEAONC has taken an important step toward improving UBC regulations regarding the required minimum separation for adjacent buildings by proposing to replace 1994 UBC section 1631.2.11 with the following one (section 1648.2.11):

> *All structures shall be separated from adjoining structures. Separation shall allow for the displacement, Δ_M. Adjacent buildings on the same property shall be separated by at least Δ_{MT}, where*
>
> $$\Delta_{MT} = \sqrt{(\Delta_{M1})^2 + (\Delta_{M2})^2}$$
>
> *where Δ_{M1} and Δ_{M2} are the displacement of the adjacent buildings.*
>
> *When a structure adjoins a property line not common to a public way, that structure shall also be set back from the property line by at least the displacement, Δ_M, of that structure. **EXCEPTION:** Smaller separations on property line setbacks may be permitted when justified by rational analysis based on maximum expected ground motions.*

<u>Section 1645.9.2 Determination of Δ_M</u>. *Except as modified by section 1645.5.5, the Maximum Inelastic response Displacement, Δ_M, shall be computed as follows*

$$\Delta_M = 0.7\, R_d R_o \Delta_s$$

where:

- $R_d \equiv$ *numerical coefficient representative of the global ductility capacity of lateral force resisting systems (given in tables)*
- $R_o \equiv$ *numerical coefficient representing the overstrength inherent in the lateral force resisting system (given in tables)*
- $\Delta_s \equiv$ *Design Level Response Displacement, which is the total drift that occurs when the structure is subjected to the design seismic forces*

The equation proposed by SEAONC to compute Δ_{MT} can be considered as a compromise between the requirements of the static method of the 1990 National Building Code of Canada (NBCC) (Filiatrault *et al.* 1995b) and the approximate method proposed by Jeng *et al.* (1992), which is based on random vibration concepts. The 1990 NBCC requires that adjacent buildings be separated by the sum of the anticipated maximum deflection. The study conducted by Kasai *et al.* (1991) showed that the required separations, which ignore the phase between the building motions, are excessive.

CONCLUSIONS AND RECOMMENDATIONS

From the above discussions, the author believes that the following concluding remarks made in 1986 (Bertero) are still valid:

> *To avoid the effects of hammering of adjacent tall buildings, separation would be required that could lead to serious problems in the economical use of usually very expensive real estate. Thus, it appears that to avoid damage between adjacent buildings it is necessary to develop other regulations or requirements than just to specify adequate separation, such as including in the design and detailing of adjacent buildings the possibility of such hammering. One such regulation should be that for two adjacent buildings with inadequate separation, the floor systems of the two buildings should be at the same level. The use of proper dampers between the adjacent buildings could also be effective. A simple solution has been suggested by Rosenblueth and Esteva (Newmark* et al., *1971). The problem of proper separation between adjacent buildings urgently requires consideration in our codes. Economical solutions for retrofitting existing adjacent buildings which do not have adequate separation should be researched immediately.*

In view of the results obtained from the analytical and experimental studies conducted after the 1985 Mexico City experience, it is recommended that further investigations be conducted considering both the ***technical problems*** that can be created by ***near-source EQGMs*** and by the ***interaction between buildings with foundation and subsoil*** and the ***interaction between buildings via the subsoil***, and the ***socio-economic problems*** that pounding can generate, particularly in cases where an existing adjacent building needs to be seismically upgraded. There is also a need to investigate the technical and socio-economic problems that can be generated by the other types of adjacency hazards, which unfortunately have not been seriously considered before now.

REFERENCES

Anagnostopoulos, S. A. and K. V. Spiliopoulos (1992). An investigation on earthquake induced pounding between adjacent buildings. *Earthquake Engrg. and Struct. Dynamics*, **21**, 289-302

Arnold, C. (1995). Are adjacency issues appropriately addressed? *Proc. EERI Tech. Seminar on the Kobe Earthquake: Impact on the Executive Order for Existing Buildings*, Dec. 5, 1995, Alexandria VA. EERI, Oakland CA, U.S.A.

Athanassiadou, C. J. *et al.* (1994). Seismic response of adjacent buildings with similar or different dynamic characteristics. *Earthquake Spectra*, **10**, 2. EERI, Oakland CA, U.S.A.

Bertero, V. V. (1986). Observation of structural pounding. *Proc. ASCE Int'l. Conf. on the 1985 Mexico City Earthquake*. Sept. 1986. 264-278. ASCE. NY, NY, U.S.A.

Bertero, V. V. and R. G. Collins (1973). Investigation of the failures of the Olive View stairtowers during the San Fernando earthquake and their implications on seismic design. *Report No. UCB/EERC-73/26*, Earthquake Engrg. Research Center, Univ. of California at Berkeley. California, U.S.A.

Blume, J. A. *et al.* (1961). Design of multistory reinforced concrete buildings for earthquake motions. Portland Cement Association, Chicago, Illinois, U.S.A.

Chouw, N, and G. Schmid (1994). Influence of soil-structure interaction on pounding between buildings during earthquakes. *Proc. 10th European Conf. on Earthquake Engrg.*, Vienna, Austria, August-September 1994, **1**, 553-558. Balkema, Rotterdam.

FEMA (Federal Emergency Management Agency (1992, 1995). *NEHRP recommended provisions for the development of seismic regulations for new buildings*. Washington, D.C., U.S.A.

Filiatrault, A. *et al.* (1995a). Analytical prediction of experimental building pounding. *Earthquake Engrg. and Struct. Dynamics*. **24**, 8, Aug. 1131-1154.

Filiatrault, A. and M. Cervantes (1995b). Separation between buildings to avoid pounding during earthquakes. *Canadian J. Civ. Engrg.* **22**, 1, Feb., 164-179.

Hall, J. F. *et al.* (1995), Near-source ground motion and its effects on flexible buildings. *Earthquake Spectra*, **11**, 4, 569-606. Earthquake Engineering Research Institute. Oakland, California, U.S.A.

Iwan, W. D. (1995), "Near-field Considerations in Specification of Seismic Design Motion for Structures," *Proceedings of the 10th European Conference on Earthquake Engineering*, Vienna, Austria August-

Sept. 1994, V. 1 pp. 257-267, Balkema, Rotterdam, Netherlands.
Jeng, V. *et al.* (1992). A spectral method to estimate buildings separation to avoid pounding. *Earthquake Spectra*, **8**, 2, Earthquake Engineering Research Institute. Oakland, California, U.S.A.
Kasai, K. *et al.* (1991). A study on earthquake pounding between adjacent structures. *Proc. 6th Canadian Conf. on Earthquake Engrg.*, Toronto, Ontario, Canada, 93-100.
Mahin, S. *et al.* (1976). Response of the Olive View Hospital main building during the San Fernando earthquake. *Report No. UCB/EERC-76/22*, Earthquake Engrg. Research Center, Univ. of California at Berkeley. Berkeley, California, U.S.A.
NBCC (1990). *National building code of Canada.* National Research Council of Canada. Ottawa, Ontario, Canada.
Newmark, N. and E. Rosenblueth (1971). Fundamentals of earthquake engineering. Prentice-Hall, Englewood Cliffs, New Jersey, U.S.A.
Papadrakis, M. and H. P. Mouzakis (1995). Earthquake simulator testing of pounding between adjacent buildings. *Earthquake Engrg. and Struct. Dynamics*, **24**, 6, June, 811-834.
SEAOC Seismology Committee (1985). Tentative lateral force requirements. Structural Engineering Association of California, Sacramento, California, U.S.A.
SEAONC Seismology Committee (1995). Strength design code change proposal for the 1997 UBC. Structural Engineers Association of Northern California, Dec., San Francisco, California, U.S.A.
Todd, D. (Ed.) (1994). Standards of seismic safety for existing federally owned or leased buildings, *ICSSC RP4, NISTIR 5382*, National Institute of Standards and Technology, Feb., Gaithersburg, Maryland, U.S.A.
UBC (Uniform Building Code) (1982, 1985, 1988, 1991 and 1995 editions). International Conference of Building Officials. Whittier, California, U.S.A.

EMILIO ROSENBLUETH'S SELECTED RESULTS IN STRUCTURAL DYNAMICS

Anil K. Chopra

Department of Civil and Environmental Engineering
707 Davis Hall, University of California, Berkeley, CA 94720, U.S.A.

ABSTRACT

A historical perspective is presented for three important contributions of Emilio Rosenblueth to structural dynamics: (1) two modal combination rules; (2) a rule to combine effects of ground motion components; and (3) a response analysis procedure for multiple-support excitation.

KEY WORDS

Dynamics; earthquakes; linear analysis; modal combination rules; multiple excitations; response spectrum; Rosenblueth.

INTRODUCTION

Emilio Rosenblueth, through his contributions to research in earthquake engineering, had a profound influence on earthquake analysis and design of structures. His many seminal contributions have covered an amazingly wide variety of subjects, and many have become an integral part of textbooks and engineering practice.

They are so well integrated into earthquake engineering as we know it today that many researchers and engineers using these procedures are unaware of their origins. This paper provides a historical perspective of three of the perhaps most important contributions of Emilio Rosenblueth to the analysis of the dynamic response of structures. The contributions selected are (1) two rules for combining the peak modal responses to estimate the peak response of multi-degree-of-freedom (MDF) systems; (2) a rule to combine the peak responses due to various components of ground motion; and (3) a response analysis procedure for multiple support excitation.

Modal Analysis: A Review (Chopra, 1995)

The response of a viscously damped system described by the vector $\mathbf{u}$ of nodal displacements relative to the moving base is governed by the N (= number of degrees of freedom) differential equations

$$\mathbf{m}\ddot{\mathbf{u}} + \mathbf{c}\dot{\mathbf{u}} + \mathbf{k}\mathbf{u} = \mathbf{p}_{\text{eff}}(t) \tag{1}$$

where the effective earthquake forces are

$$\mathbf{p}_{\text{eff}}(t) = -\mathbf{m}\boldsymbol{\iota}\ddot{u}_g(t) \tag{2}$$

In Eqs. (1) and (2) $\mathbf{m}$, $\mathbf{c}$, and $\mathbf{k}$ are the mass, damping, and stiffness matrices, $\ddot{u}_g(t)$ is the ground acceleration, and $\boldsymbol{\iota}$ is the influence vector representing the displacements of the masses resulting from static application of a unit-ground displacement, $u_g = 1$.

The spatial distribution $\mathbf{s} = \mathbf{m}\boldsymbol{\iota}$ of the effective earthquake forces is expanded as

$$\mathbf{m}\boldsymbol{\iota} = \sum_{n=1}^{N} \mathbf{s}_n = \sum_{n=1}^{N} \Gamma_n \mathbf{m}\boldsymbol{\phi}_n \tag{3}$$

where $\boldsymbol{\phi}_n$ are the natural vibration modes of the system and

$$\Gamma_n = \frac{L_n}{M_n} \qquad L_n = \boldsymbol{\phi}_n^T\mathbf{m}\boldsymbol{\iota} \qquad M_n = \boldsymbol{\phi}_n^T\mathbf{m}\boldsymbol{\phi}_n \tag{4}$$

The contribution of the nth mode to $\mathbf{s}$ is

$$\mathbf{s}_n = \Gamma_n \mathbf{m}\boldsymbol{\phi}_n \tag{5}$$

which is independent of how the modes are normalized. Equation (3) may be viewed as an expansion of $\mathbf{m}\boldsymbol{\iota}$ in terms of inertia force distributions $\mathbf{s}_n$ associated with natural vibration modes.

The nth-mode contribution $r_n(t)$ to any response quantity $r(t)$ is

$$r_n(t) = r_n^{st} A_n(t) \tag{6}$$

where r_n^{st} denotes the *modal static response*, the static value of r due to external forces $\mathbf{s}_n$. The algebraic sign of r_n^{st} is a property of the structure and the selected response quantity r. In Eq. (6),

$$A_n(t) = \omega_n^2 D_n(t) \tag{7}$$

$D_n(t)$ and $A_n(t)$ are the displacement and pseudo-acceleration response of the nth-mode single-degree-of-freedom (SDF) system, an SDF system with vibration properties—natural period T_n (natural frequency ω_n) and damping ratio ζ_n—of the nth mode of the MDF system excited by ground acceleration $\ddot{u}_g(t)$.

Combining the response contributions of all the modes gives the total response:

$$r(t) = \sum_{n=1}^{N} r_n(t) = \sum_{n=1}^{N} r_n^{\mathrm{st}} A_n(t) \tag{8}$$

Peak Modal Responses

The *peak* value of the nth-mode contribution $r_n(t)$ to response $r(t)$ can be obtained from the earthquake response spectrum or design spectrum:

$$r_{no} = r_n^{\mathrm{st}} A_n \tag{9}$$

where the subscript "o" denotes the peak value, defined as the maximum of the absolute value, and $A_n \equiv A(T_n, \zeta_n)$ is the pseudo-acceleration response spectrum ordinate corresponding to natural period T_n and damping ratio ζ_n. The algebraic sign of r_{no} is the same as that of r_n^{st} because A_n is positive by definition. Although it has an algebraic sign, r_{no} will be referred to as the peak modal response because it corresponds to the peak value of $A_n(t)$.

The peak value r_o of the total response $r(t)$ is estimated by combining the peak modal responses r_{no} $(n = 1, 2, \ldots, N)$ according to the well known modal combination rules: *square-root-of-sum-of-squares (SRSS)* rule or *complete quadratic combination (CQC)* rule, as appropriate. The algebraic sign of r_{no} is relevant in the CQC rule, but inconsequential in the SRSS rule.

SRSS Rule

The SRSS rule for modal combination is

$$r_o \simeq \left(\sum_{n=1}^{N} r_{no}^2 \right)^{1/2} \tag{10}$$

The algebraic signs of r_{no} do not affect the value of r_o given by the SRSS rule.

The basis for Eq. (10) was developed by Rosenblueth in his Ph.D. thesis (1951); contained on page 97 is the following equation (in different notation):

$$E(r_o) = \left(\sum_{n=1}^{N} [E(r_{no})]^2 \right)^{1/2} \tag{11}$$

where $E(x)$ denotes the expectation of x.

Based on this thesis, an ASCE paper (Goodman, Rosenblueth, and Newmark, 1953) contains the result:

$$r_d = \left(\sum_{n=1}^{N} r_{nd}^2\right)^{1/2} \tag{12}$$

where the subscript "d" denotes the design response.

Considering that, in the early 1950's, the subject of earthquake dynamics of structures was in its infancy and random vibration theory was unknown to structural engineers, Rosenblueth's results are especially impressive. Equations (11) and (12) were derived by expressing structural response as a convolution integral of ground acceleration and the unit impulse response function, idealizing the ground acceleration as white noise, and using probability theory. Although the "white noise" terminology was apparently not used, it was implied by the assumptions (Goodman, Rosenblueth. and Newmark, 1953):

> ". . . the writers consider motions consisting of random arrays of concentrated acceleration pulses. . . . The pulses are assumed to be distributed in time in a random order, either at small, uniformly spaced intervals or at randomly spaced instants of time."

Now contained in textbooks and taken for granted in engineering practice, the SRSS rule was first applied in the design of the Latino Americana tower in Mexico City in 1950. In a letter to me dated August 3, 1993, Rosenblueth stated:

> "If I'm not mistaken, when the Holy Ghost descended on me one cold night in early 1950 in Urbana and told me about SRSS combination of modal responses, He hadn't told anyone else. This allowed me to devote the sultry summer to computing the combined responses (which I had computed in pre-Illiac [computer] days) for the Latino Americana tower, of which Nate [Newmark] was consultant, and so SRSS was applied in design for the first time. SRSS was proposed in my Ph.D. thesis, presented in 1951."

This modal combination rule usually provides excellent response estimates for structures with well-separated natural frequencies. This limitation has not always been recognized in applying this rule to practical problems, and at times it has been misapplied to systems with closely spaced natural frequencies, such as piping systems in nuclear power plants and multistory buildings with asymmetric plan.

CQC Rule

The CQC rule for modal combination is applicable to a wider class of structures as it overcomes the limitations of the SRSS rule. According to the CQC rule,

$$r_o \simeq \left(\sum_{i=1}^{N}\sum_{n=1}^{N} \rho_{in} r_{io} r_{no}\right)^{1/2} \tag{13}$$

Each of the N^2 terms on the right side of this equation is the product of the peak responses in the ith and nth modes and the correlation coefficient ρ_{in} for these two modes; ρ_{in} varies between 0 and 1 and $\rho_{in} = 1$ for $i = n$. Thus, Eq. (13) can be written as

$$r_o \simeq \left(\sum_{n=1}^{N} r_{no}^2 + \underbrace{\sum_{i=1}^{N} \sum_{n=1}^{N}}_{i \neq n} \rho_{in} r_{io} r_{no} \right)^{1/2} \tag{14}$$

to show that the first summation on the right side is identical to the SRSS combination rule of Eq. (10); each term in this summation is obviously positive. The double summation includes all the cross ($i \neq n$) terms; each of these terms may be positive or negative. A cross term is negative when the modal static responses r_i^{st} and r_n^{st} assume opposite signs. Thus, the estimate for r_o obtained by the CQC rule may be larger or smaller than the estimate provided by the SRSS rule.

The preceding modal combination rule was first derived by E. Rosenblueth and J. Elorduy (1969). although they did not give it the CQC name, which is due to A. Der Kiureghian (1981). This result was based on an idealization of earthquakes as stationary Gaussian processes, but modified to recognize the transient character of actual ground motions. The methods that led to this result were extensions of Rosenblueth's early work underlying the SRSS rule.

The 1971 textbook *Fundamentals of Earthquake Engineering* by N. M. Newmark and E. Rosenblueth gives the Rosenblueth-Elorduy equations for the correlation coefficient:

$$\rho_{in} = \frac{1}{1 + \epsilon_{in}^2} \tag{15}$$

where

$$\epsilon_{in} = \frac{\omega_i \sqrt{1 - \zeta_i^2} - \omega_n \sqrt{1 - \zeta_n^2}}{\zeta_i' \omega_i + \zeta_n' \omega_n} \qquad \zeta_n' = \zeta_n + \frac{2}{\omega_n s} \tag{16}$$

s is the duration of the segment of white noise. Equations (15) and (16) show that $\rho_{in} = \rho_{ni}$; $0 \leq \rho_{in} \leq 1$; and $\rho_{in} = 1$ for $i = n$ or for two modes with equal frequencies and equal damping ratios.

Although used in some research studies (e.g. Kan and Chopra, 1977), this important result was not used very widely in engineering practice for many years perhaps for two reasons. First, the statement defining the algebraic sign of r_{no} may have been too subtle. This definition (with appropriate change in notation) appeared in Newmark and Rosenblueth, 1971:

> ". . . r_{no} is to be taken with the sign that ψ_{rn} [defined by the authors as the transfer function for r_n, but generally known as the unit impulse response function for r_n] has when it attains its maximum numerical value."

Second, it was not obvious how to define the duration s for an actual ground motion or a given design spectrum (Villaverde, 1984), and the recommendations for s (e.g., 12.5 sec. for earthquakes on the west coast of the United States) were not widely recognized (Rosenblueth and Esteva, 1964; Newmark and Rosenblueth, 1971, page 275).

Later, using a different approach based on random vibration theory in the frequency domain, Eq. (13) was derived together with the following equation for the correlation coefficient (Der Kiureghian, 1981):

$$\rho_{in} = \frac{8\sqrt{\zeta_i\zeta_n}(\zeta_i + \beta_{in}\zeta_n)\beta_{in}^{3/2}}{(1-\beta_{in}^2)^2 + 4\zeta_i\zeta_n\beta_{in}(1+\beta_{in}^2) + 4(\zeta_i^2+\zeta_n^2)\beta_{in}^2} \tag{17}$$

where $\beta_{in} = \omega_i/\omega_n$. This equation also implies that $\rho_{in} = \rho_{ni}$, $\rho_{in} = 1$ for $i = n$ or for two modes with equal frequencies and equal damping ratios. For equal modal damping $\zeta_i = \zeta_n = \zeta$ this equation simplifies to

$$\rho_{in} = \frac{8\zeta^2(1+\beta_{in})\beta_{in}^{3/2}}{(1-\beta_{in}^2)^2 + 4\zeta^2\beta_{in}(1+\beta_{in})^2} \tag{18}$$

This form of the correlation coefficient was easier to use relative to Eqs. (15) and (16), and it gained widespread popularity.

In order to compare the two equations for the correlation coefficient, Eq. (15) is specialized for systems with same damping ratio in all modes subjected to earthquake excitation with duration s long enough to replace Eq. (16b) by $\zeta_n' = \zeta_n$. We substitute $\zeta_i = \zeta_n = \zeta$ in Eq. (16a), introduce $\beta_{in} = \omega_i/\omega_n$, and insert Eq. (16a) into Eq. (15) to obtain

$$\rho_{in} = \frac{\zeta^2(1+\beta_{in})^2}{(1-\beta_{in})^2 + 4\zeta^2\beta_{in}} \tag{19}$$

Figure 1 shows Eqs. (18) and (19) for the correlation coefficient ρ_{in} plotted as a function of $\beta_{in} = \omega_i/\omega_n$ for four damping values: ζ = 0.02, 0.05, 0.10, and 0.20. Observe that the two expressions give essentially identical values for ρ_{in}.

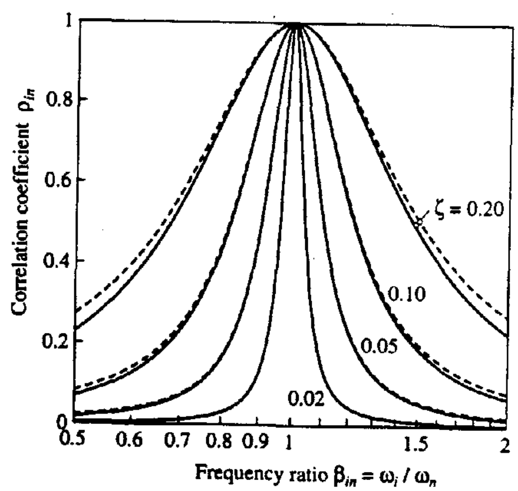

Fig. 1. Variation of correlation coefficient ρ_{in} with modal frequency ratio $\beta_{in} = \omega_i/\omega_n$ for four damping values; abscissa scale is logarithmic; Eqs. (18) and (19) are plotted in solid and dashed lines, respectively.

However, ρ_{in} should depend on the effective duration s of the ground motion, which is neglected in Eqs. (17) and (18). In this sense, Eqs. (15) and (16) have a wider range of applicability.

Figure 1 also provides an understanding of the correlation coefficient. Observe that this coefficient rapidly diminishes as the two natural frequencies ω_i and ω_n move farther apart. This is especially the case at small damping values that are typical of structures. In other words, it is only in a narrow range of β_{in} around $\beta_{in} = 1$ that ρ_{in} has significant values; and this range depends on damping. For structures with well-separated natural frequencies the coefficients ρ_{in} vanish; as a result all cross ($i \neq n$) terms in the CQC rule, Eq. (14), can be neglected and it reduces to the SRSS rule, Eq. (10).

COMBINED EFFECTS OF GROUND MOTION COMPONENTS

Most building codes specify how to combine the effects of various ground motion components. For example, the *Uniform Building Code* states:

> "The requirement. . . may be satisfied by designing such elements for 100 percent of prescribed seismic forces in one direction plus 30 percent of the prescribed forces in the perpendicular direction. The combination requiring the greater component strength shall be used for design."

While such combination rules had been proposed and used in the early 1970's, it appears that the first published work that provides a rational basis for these rules is due to Rosenblueth and Contreras (1977). Their approach assumes that such effects are uncorrelated Gaussian processes or that correlations are taken into account in computing modal responses. A simple approximation was derived under the additional assumption that the failure surfaces are convex.

The authors state that:

> "This approximate procedure is applied as follows:
>
> "1. Compute the responses to gravity loads and to the J components of ground motion regarded as potentially significant. Let these responses be arranged into vectors $\mathbf{r} = \mathbf{r}_g$ and $\mathbf{r}_j$, respectively, with $j = 1, 2, \ldots, J$.
>
> "2. Obtain the vectors
>
> $$\mathbf{r} = \mathbf{r}_g + \sum_{j=1}^{J} \alpha_j \mathbf{r}_j \qquad (20)$$
>
> assigning plus and minus signs to $\alpha_j \mathbf{r}_j$, ordering the $\mathbf{r}_j$ values in all possible combinations, and giving the α_j terms the values in Table 1.
>
> "3. If the problem is one of analysis, find whether all points fall within the failure surface. If the problem is one of design, assign the design parameters such values that the safe domain will contain all the points."

It was shown that $\alpha_1 = 1$ and $\alpha_j = 0.3$ for $j \geq 2$.

The Acknowledgements section includes the following statement:

"The simplified procedure was proposed early in 1975 (with $\alpha_j = 1/3$ for $j \geq 2$) by A. S. Veletsos. Even earlier N. M. Newmark proposed this procedure with $\alpha_j = 0.4$ for $j \geq 2$. The main ideas in the present paper were developed in Ref. 8 [Rosenblueth, 1975]."

RESPONSE ANALYSIS FOR MULTIPLE SUPPORT EXCITATION

The governing equations for MDF systems excited by prescribed motions $\ddot{u}_{gl}(t)$ at the various supports ($l = 1, 2, \ldots, N_g$) of the structure are the same as Eq. (1) with the effective earthquake forces (Chopra, 1995)

$$\mathbf{p}_{\text{eff}}(t) = -\sum_{l=1}^{N_g} \mathbf{m}\boldsymbol{\iota}_l \ddot{u}_{gl}(t) \tag{21}$$

instead of Eq. (2) where $\boldsymbol{\iota}_l$ is the vector of static displacements in the structural DOF due to $u_{gl} = 1$.

The displacement response of the structure contains two parts (Chopra, 1995):

1. The dynamic displacements:

$$\mathbf{u}(t) = \sum_{l=1}^{N_g} \sum_{n=1}^{N} \Gamma_{nl} \boldsymbol{\phi}_n D_{nl}(t) \tag{22}$$

where

$$\Gamma_{nl} = \frac{L_{nl}}{M_n} \qquad L_{nl} = \boldsymbol{\phi}_n^T \mathbf{m}\boldsymbol{\iota}_l \qquad M_n = \boldsymbol{\phi}_n^T \mathbf{m}\boldsymbol{\phi}_n \tag{23}$$

and $D_{nl}(t)$ is the deformation response of the nth-mode SDF system to support acceleration $\ddot{u}_{gl}(t)$.

2. The quasistatic displacements $\mathbf{u}^s$ are given by

$$\mathbf{u}^s = \sum_{l=1}^{N_g} \boldsymbol{\iota}_l u_{gl}(t) \tag{24}$$

Combining the two parts gives the total displacements in the structural DOF's:

$$\mathbf{u}^t(t) = \sum_{l=1}^{N_g} \boldsymbol{\iota}_l u_{gl}(t) + \sum_{l=1}^{N_g} \sum_{n=1}^{N} \Gamma_{nl} \boldsymbol{\phi}_n D_{nl}(t) \tag{25}$$

This well known procedure is now a part of textbooks and engineering practice. This author was first exposed to this treatment in the fall of 1964 when Prof. Rosenblueth presented a graduate course at the University of California, Berkeley and distributed to the class a draft of the early chapters of his book with N. M. Newmark; this procedure appeared in Section 2.4 of the published book. Soon thereafter, we at Berkeley used the procedure to analyze the earthquake response of earth dams (Chopra et al., 1969). Later, it was used in many research publications. However, for many years its practical application was limited for lack of analytical methods and instrumental records to define the spatial variation of ground motion. With advances in these subjects Rosenblueth's analysis procedure is being rediscovered and applied to practical problems, e.g., the seismic retrofit of the Golden Gate Bridge and the San Francisco-Oakland Bay Bridge.

ACKNOWLEDGEMENTS

A draft of this paper was reviewed by Profs. J. Bielak, A. Der Kiureghian, L. Esteva, W. J. Hall, J. Penzien, and R. Villaverde. The author is grateful to them for their comments.

REFERENCES

Chopra, A.K., M. Dibaj, R.W. Clough, J. Penzien, and H.B. Seed (1969). Earthquake analysis of earth dams. *Proceedings*, Fourth World Conference on Earthquake Engineering, Santiago, Chile.

Chopra, A.K. (1995). *Dynamics of Structures: Theory and Applications to Earthquake Engineering*, Prentice Hall, Englewood Cliffs, New Jersey.

Der Kiureghian, A. (1981). A Response Spectrum Method for Random Vibration Analysis of MDF Systems. *Earthquake Engineering and Structural Dynamics*, **9**, 419-435.

Esteva, L. and E. Rosenblueth (1964). Espectros de temblores a distancias moderades y grandes. *Boletin Sociedad Mexicana de Ingenieria Sismica, A.C.*, **2**, 1-18.

Goodman, L.E., E. Rosenblueth, and N.M. Newmark (1953). Aseismic design of firmly founded elastic structures. *Proceedings, Separate No. 349, ASCE*, **79**, 27 pages. Also *Transactions, ASCE*, 120, 782-802.

Kan, C.L. and A.K. Chopra (1977). Effects of Torsional Coupling on Earthquake Forces in Buildings. *Journal of the Structural Division*. ASCE, **103**, 805-819.

Newmark, N.M. and E. Rosenblueth (1971). *Fundamentals of Earthquake Engineering*, Prentice Hall, Englewood Cliffs, New Jersey.

Rosenblueth, E. (1951). *A Basis for aseismic design*, doctoral thesis, University of Illinois, Urbana, Illinois.

Rosenblueth, E. and J. Elorduy (1969). Response of linear systems to certain transient disturbances. *Proceedings, Fourth World Conference on Earthquake Engineering*, Santiago, Chile, **I**, A-1. 185-196.

Rosenblueth, E. (1975). Effectos del Componente Vertical en Edificios Altos. Presented at the Fourth National Conference on Earthquake Engineering, Oaxaca, Mexico, 29.

Rosenblueth, E. and H. Contreras (1977). Approximate Design for Multicomponent Earthquakes. *Journal of the Engineering Mechanics Division*, ASCE, **103**, 881-893.

Villaverde, R. (1984). On Rosenblueth's Rule to Combine the Modes of Systems with Closely Spaced Natural Frequencies. *Bulletin of the Seismological Society of America*, **74**, 325-338.

ACCIDENTAL AND NATURAL TORSION IN EARTHQUAKE RESPONSE AND DESIGN OF BUILDINGS

Anil K. Chopra and Juan C. De la Llera

Department of Civil and Environmental Engineering, 707 Davis Hall,
University of California, Berkeley, CA 94720, U.S.A.

Department of Structural and Geotechnical Engineering
Pontificia Universidad Católica de Chile
Vicuña Mackenna 4860, Casilla 306, Correo 22, Santiago, Chile

ABSTRACT

Considering that a comprehensive review of past work in this field is available, this paper focuses on the description of two recently developed procedures to incorporate the effects of accidental and natural torsion in earthquake analysis and design of asymmetric buildings. The new procedure for accidental torsion consists in specifying an increase in edge displacements due to the most important sources of elastic accidental torsion, such as uncertainty in stiffness, mass, and base rotation, as a function of two building parameters, the ratio between the plan dimension b and the radius of gyration r, and the frequency ratio Ω. This procedure has several advantages over the current code accidental torsion provisions, such as the elimination of the two extra cumbersome analyses in each lateral direction specified by current codes. On the other hand, the new procedure for natural torsion provides a globally applicable framework to understand and evaluate the inelastic behavior of asymmetric structures even prior to any elaborate inelastic analysis. This framework is based on using the story shear and torque surfaces in conjunction with a simplified structural model of a single element per building story. Such a model is tested in this paper using a building with a setback and a strong asymmetry.

KEYWORDS

accidental torsion, accidental eccentricity, design envelope, frequency ratio, natural torsion, single element model, story shear and torque surface, asymmetric structures, inelastic behavior

INTRODUCTION

Buildings subjected to ground shaking undergo lateral as well as torsional motions simultaneously. Such motions are due to *natural torsion* in buildings with asymmetric plan; and *accidental torsion* in all buildings, even those with symmetric plan. Symmetrical buildings undergo torsional motions because no building as built is *perfectly* symmetric, and unrecorded rotational motion at the building base, among other factors, causes torsional motion of the structure.

The coupling between lateral and torsional motions in a building with plan asymmetry inevitably leads to non-uniform displacement demands on the lateral resisting planes of the system. Such displacement demands are of principal interest in the sizing and detailing of structural elements for earthquake resistance. Consequently, many studies have attempted to understand the change in building displacements that arise from building asymmetry; see list of over seventy references in a recent review paper (Rutenberg, 1992). Most of these investigations involve interpretation of parametric studies of the earthquake response of simple idealizations of asymmetric one-story structures. Although these results are important for understanding the inelastic response of asymmetric systems, they have two major limitations. First, because of the inherent complexity of the problem, it has not been possible to glean general trends that apply to structures other than those analyzed. Second, these conclusions do not seem extendable to multistory buildings. The results available for the response of code-designed asymmetric multi-story buildings are even more problem-specific and difficult to generalize. These limitations of past parametric studies of inelastic earthquake response of asymmetric structures are discussed in a review paper (Rutenberg, 1992) which states:

> "The picture emerging from the foregoing review is somewhat confusing. It appears that most of the problems and disagreements among researchers are the result of using different models. This is not surprising considering the large number of parameters involved. . . the lack of a unique system definition by an accepted set of parameters is perhaps the main obstacle to progress in this field."

Considering that a comprehensive review of past work is available, we have adopted an unconventional approach in this state-of-the-art paper. To overcome the limitations of past parametric studies and their sometimes inconsistent conclusions, we will present a simple conceptual framework to enable the designer to understand the performance of different structural configurations prior to any elaborate inelastic analysis. Also included is a simplified method for the analysis and design of asymmetric-plan structures which is suitable for trying alternative structural configurations and seeking the most seismically efficient and cost-effective configuration.

The subject of accidental torsion is not amenable to investigation by traditional analytical approaches because standard dynamic analyses do not predict torsion in symmetric-plan buildings. Perhaps for this reason the work on this subject is meager compared to the substantial body of literature on natural torsion. Summarized herein is a recently developed procedure to estimate accidental torsion in the design of buildings.

PART I: ACCIDENTAL TORSION

Code Predictions of Accidental Torsion

Building codes require consideration of accidental torsion in one of two ways: (1) apply the equivalent static lateral forces at a distance e_d from the center of stiffness (CS), which includes the accidental eccentricity $e_a = \pm\beta b$; and (2) perform dynamic analyses with the center of mass (CM) of each floor shifted a distance equal to the accidental eccentricity $e_a = \pm\beta b$ from its nominal position, where b is the plan dimension of the building perpendicular to the direction of ground motion. For each structural element the e_a value leading to the larger design force is to be used. Implementation of these code provisions requires two three-dimensional (3-D) static or dynamic analyses of the building for each lateral direction. The two types of analyses--static and dynamic--predict a significantly different increase in design forces resulting from accidental eccentricity; the code-static analyses are not consistent with the analytical results (Fig. 2) (De la Llera and Chopra, 1994d).

Analytical Estimates of Accidental Torsion

The increase in building displacements due to individual sources of accidental torsion, such as stiffness and mass uncertainty, base rotational excitation, and other less important sources, is a function of the system parameters p, which are random variables describing the stiffness and mass matrices of the system, and a random base rotational excitation $a_{g\theta}(t)$. The normalized displacement of the building plan at a distance x from the CM is defined as the ratio $\hat{u}_x = u_x^* / u_x$ between the displacement u_x^* considering the effect of all sources of accidental torsion and the displacement u_x neglecting accidental torsion; then, the increase in response is $\hat{u}_x - 1$. Based on the assumption of statistical independence among the system parameters, first-order approximations for the mean and standard deviation of the normalized displacement are given by (De la Llera and Chopra, 1994d):

$$\mu_{\hat{u}_{b/2}} = 1 + \mu_{\hat{u}_{g\theta}} \qquad \sigma_{\hat{u}_{b/2}} = \sqrt{\sum_{i=1}^{N_p} \left(\frac{\partial \hat{u}_{b/2}}{\partial p_i} \right)^2 \sigma_{p_i}^2 + \sigma_{\hat{u}_{g\theta}}^2} \tag{1}$$

where $\mu_{(\cdot)}$ and $\sigma_{(\cdot)}$ denote the mean and standard deviation of $(\cdot)$, $\mu_{\hat{u}_{g\theta}}$ and $\sigma_{\hat{u}_{g\theta}}$ are the mean and standard deviation of $\hat{u}_{b/2}$ resulting from base rotational excitation, N_p is the number of system parameters, σ_{p_i} is the standard deviation of the parameter p_i, and $\partial \hat{u}_{b/2} / \partial p_i$ is the sensitivity of $\hat{u}_{b/2}$ with respect to the parameter p_i.

Determined in earlier investigations (De la Llera and Chopra, 1994b,e,f) are the normalized response and increase in response due to the following sources of accidental torsion: (1) rotational motion of the building foundation, (2) uncertainty in the stiffness of structural elements in both principal directions of analysis, (3) uncertainty in the location of the CM, and (4) uncertainty in stiffness and mass distributions in stories of a building other than the story analyzed. The variation of normalized displacements with $\Omega = \omega_\theta / \omega_y$ (the ratio between the natural frequencies of uncoupled torsional and lateral motions of the building) in Fig. 1 leads to the following observations:

1. The largest increase in building displacements results from uncertainty in the location of the CM orthogonal to the direction of ground motion (Fig. 1a). Somewhat smaller are the effects of uncertainty in the stiffness of structural elements in the direction of ground motion (Fig. 1b). These two sources combined account for over 70% of the total increase in response due to accidental torsion (De la Llera and Chopra, 1994b,f).

2. Stiffness uncertainty and uncertainty in the location of the CM can be modeled as a perturbation of the static eccentricity of the system, an observation that partially justifies the code dynamic analysis procedure.

3. The increase in edge displacement due to base rotational motion, derived from true base rotations of thirty buildings during recent California earthquakes (De la Llera and Chopra, 1994e), is generally less than 8% for systems with uncoupled lateral vibration period T_y over, say, 1/2 sec. and a wide range of Ω (Fig. 1c); it may reach values as large as 40% for short period systems (T_y < 1/2 sec.) that are torsionally flexible (Ω < 2/3).

4. The increase in edge displacement resulting from uncertainty in the stiffness of structural elements in the direction orthogonal to the direction of ground motion and in the location of the CM along the direction of ground motion are in general less than 5% (Fig. 2d) (also, De la Llera and Chopra, 1994f). This increase is zero for nominally symmetric systems and increases with increasing stiffness eccentricity in the system.

5. The increase in edge displacements due to uncertainty in the stiffness and mass distributions in stories other than the one analyzed (Fig. 2e) is between one-third to one-half of the increase due to the uncertainty of these properties in the story considered (Fig. 2b) (also, De la Llera and Chopra, 1994f).

6. Most sources of accidental torsion increase the response of nominally symmetric systems more than they do for unsymmetric systems (De la Llera and Chopra, 1994b,e,f).

7. The increase in edge displacements due to stiffness and mass uncertainty is essentially insensitive to changes in T_y (De la Llera and Chopra, 1994b,f).

8. Buildings with the plan dimension perpendicular to the direction of ground motion much larger than the other dimension (large b/r) show the largest increase in response due to accidental torsion.

9. The increase in response of single-story systems due to accidental torsion is also the exact result for a special class of multistory systems with the following properties: (a) the CM of all floors lie on a vertical line; (b) the resisting planes are arranged such that their principal axes form an orthogonal grid in plan and are connected at each floor by a rigid diaphragm; and (c) the lateral stiffness matrices of all resisting planes are proportional.

Shown in Fig. 2 are the mean and mean-plus-one standard deviation of $\hat{u}_{b/2}$ computed from Eq. (1) considering all sources of accidental torsion (De la Llera and Chopra, 1995a). The mean value of the increase in response, $\hat{u}_{b/2} - 1$, is usually less than 3%. Furthermore, with the exception of systems with $T_y < 0.5$ sec. and $\Omega < 1$, this mean increase in response is insensitive to Ω. The mean-plus-one standard deviation value of the response increase reaches a peak value of 45% for systems with $\Omega = 0.85$ or $\Omega = 1.1$; it decreases steadily for values of Ω larger and smaller than these two values; and it varies rapidly between its peaks at $\Omega = 0.85$ and 1.1 to a minimum at $\Omega = 1$. As shown in the figure this increase in response is larger for nominally symmetric systems ($e_s/b = 0$) than for unsymmetric systems (De la Llera and Chopra, 1994c).

Design Considerations

Compared in Fig. 3 is $\hat{u}_{b/2}$ predicted by code-dynamic analysis with $e_a = \pm 0.05b$ and the "true" value (Fig. 2). The code increase in edge displacements is much larger than the mean value of the "true" increase. However, it is about one-half of the mean-plus-one standard deviation of the "true" value; it corresponds to an exceedance probability of about 30%.

The discrepancy in the design forces due to accidental torsion, as predicted by code-specified static and dynamic analysis procedures, can be overcome by defining a unique design envelope for the edge displacements:

$$\hat{u}_{b/2} = \begin{cases} A & 0 \leq \Omega \leq 1 \\ A - \dfrac{A-1}{\Omega_c - 1}(\Omega - 1) & 1 < \Omega \leq \Omega_c \\ 0 & \Omega > \Omega_c \end{cases} \tag{2}$$

where $\Omega_c = 1.8$ and

$$A = 1 + 0.0475(b/r)^2 \tag{3}$$

Equation (3) is a good approximation to the maximum value of $\hat{u}_{b/2}$ over all Ω (Fig. 4a) determined by code-specified dynamic analysis (Fig. 4b). Furthermore, Eqs. (2) and (3) have been intentionally calibrated to produce values that are conservative, especially for the range $0.9 \leq \Omega \leq 1.1$. There are three reasons for this. First, the estimation of Ω is obviously subject to error; therefore, taking advantage of the dip in the response curve near $\Omega = 1$ is not appropriate for design. Second, this conservatism proves to be useful in preventing resisting planes in the interior of the building plan to be underdesigned by the procedure developed. Third, the "recorded" increase in response for a system with $\Omega \simeq 1$ can be larger than predicted by code-specified dynamic analysis for accidental torsion (De la Llera and Chopra, 1995a).

Simplified Procedure

In order to overcome the limitations of the present code procedures, a procedure has been developed to include accidental torsion in the seismic design of buildings. This procedure is implemented in four steps:

1. Determine $\Omega = \omega_\theta/\omega_y$; ω_θ and ω_y can be estimated by Rayleigh's Method:

$$\omega_y \simeq \sqrt{\frac{\sum_i F_i\delta_i}{\sum_i m_i\delta_i^2}} \qquad \omega_\theta \simeq \sqrt{\frac{\sum_i T_i\theta_i}{\sum_i I_{pi}\theta_i^2}} \tag{4}$$

   where F_i and T_i are any reasonable heightwise distribution of equivalent static forces and torques (e.g., $T_i = F_i e$, where e is an arbitrary eccentricity value), δ_i and θ_i are floor displacements and rotations associated with these forces, and m_i and I_{pi} are the floor masses and moments of inertia.

2. Calculate from Eqs. (2) and (3) the normalized edge displacement $\hat{u}_{b/2}$.

3. Compute the normalized displacement $\hat{u}_x$ at distance x from the CM by

$$\hat{u}(x) = 1 + (\hat{u}_{b/2} - 1) \left| \frac{x}{b/2} \right| \tag{5}$$

   which states that the displacement varies linearly from the CM to the edge.

4. Compute the forces in the structural members of each resisting plane by amplifying the forces without accidental torsion by the normalized displacement determined in Step 3.

This procedure is "exact" for single-story systems and for multistory buildings belonging to the special class defined earlier; it is also a good approximation for other multistory systems. It has several important advantages over the current seismic code procedures. First, it avoids the two additional 3-D static or dynamic analyses of the building in each lateral direction. Second, it includes the effects of all sources of accidental torsion whereas codes include only those that can be represented by a constant accidental eccentricity. Third, it gives a unique value for the increase in a design force due to accidental torsion, whereas current codes give very different results depending on whether the analysis is static or dynamic. Fourth, the procedure defines explicitly the expected increase in design forces due to accidental torsion, in contrast to the use of accidental eccentricity in codes implying an indirect increase in member forces. Fifth, the increase in design forces specified by the new procedure has a well-established probability of exceedance.

Evaluation of Procedure

The key element of the simplified procedure described above are the design displacement envelopes of Fig. 4. These envelopes are evaluated against motions of seven nominally symmetric buildings recorded during the Loma Prieta and Northridge earthquakes (Table 1). At each instrumented floor of these buildings, three channels of acceleration were recorded. First, the recorded accelerations, after they have been appropriately processed, are integrated to determine the corresponding displacements. From these "recorded" displacements the "true" value of the normalized edge displacement is computed assuming the floor diaphragm to be rigid; this is the ratio between the "recorded" value of displacement and the value excluding accidental floor rotation. The ratio between two values of the maximum edge displacement, one including floor rotation and the other excluding it, are presented in Fig. 5 for each building corresponding to its frequency ratio Ω determined from its recorded motions and the b/r value (Table 1). The vertical line for each building shows the range of values for $\hat{u}_{b/2}$ for various floors. Superimposed on these results are the design displacement envelopes for $b/r=1,2$, and 3.

Table 1. Nominally Symmetric Buildings Considered

Buildings	CSMIP	PGA	Material	$(b/r)_x$[1]	$(b/r)_y$	Ω_x	Ω_y
A:Richmond	58506	0.11g	Steel	3.12	1.49	1.36	1.52
B:Pomona	23511	0.13g	RC	2.22	2.67	1.42	1.34
C:San Jose	57562	0.20g	Steel	3.22	1.28	1.00	1.03
D:Sylmar	24514	0.67g	Steel	2.44	2.45	1.10	1.10
E:Burbank	24385	0.29g	RC	2.45	2.45	1.64	1.53
F:Burbank	24370	0.29g	RC	3.28	1.10	0.97	0.80
G:Warehouse	24463	0.26g	RC	2.74	2.12	1.37	1.42

It is apparent from Fig. 5 that buildings with larger frequency ratio Ω present a smaller increase in edge displacements, which is in agreement with theoretical predictions (Fig. 2). Besides, the increase in response for buildings with frequency ratio close to one varies from essentially zero for building F to about 40% for building D. This is precisely the main reason why the proposed envelopes have ignored the dip in the theoretical curves at $\Omega=1$ (Fig. 3). However, Figure 5 must be interpreted with caution since for each frequency ratio Ω, the increase in displacements is a random variable. Thus, the points presented in the figure are just few "true" outcomes of this set of random variables.

[1]In computing (b/r), the subscripts x and y denote selection of the plan dimension b perpendicular to the direction of analysis; in computing Ω, x and y denote the direction of vibration of the structure.

PART II: NATURAL TORSION

Story Shear-Torque (SST) Yield Surface

To develop a conceptual and engineering-practice-oriented strategy to understand the seismic response of asymmetric buildings, the story shear and torque response histories are presented in the force space spanned by the story shears in the two principal directions of the building and by the story torque. At each instant of the response the story shears and torque define one point in this space. These combinations of shears and torques are bounded by the SST yield surface, a polygonal surface defined by a set of story shear and torque combinations corresponding to different collapse mechanisms that can be developed in the story. The parameters that define the SST yield surface are (1) strength of resisting planes; (2) strength of resisting planes in the orthogonal direction; (3) asymmetry in stiffness; (4) asymmetry in strength; (5) planwise distribution of strength; and (6) number of resisting planes. How these parameters affect the earthquake response of a structure can be predicted based on their influence on the yield surface (De la Llera and Chopra, 1995b).

In order to avoid detailed and "exact" calculation of the SST surface for the specific system to be analyzed, a new superelement model (SEM) has been developed to represent the elastic and inelastic properties of each story of the building (Fig. 6). The eight-vertex polygon presented in Fig. 7 is the exact model of a section of the SST yield surface at a constant story shear V_x for a story with three resisting planes along the y-axis, the direction of asymmetry and of ground motion, and two resisting planes in the orthogonal direction. This model can also be used to predict with sufficient accuracy the responses of systems with an arbitrary number of resisting planes. The coordinates $(x_j,\ y_j)$ of the vertices of this surface are given by the following expressions:

$$\begin{aligned}
x_1 &= V_{yo} & y_1 &= V_{yo}x_p + T_\perp(1-\hat{V}_x)\\
x_2 &= V_{yu} + V_{yc} & y_2 &= T_o - T_\perp\hat{V}_x\\
x_3 &= V_{yu} - V_{yc} & y_3 &= T_o - T_\perp\hat{V}_x\\
x_4 &= -V_{yo} & y_4 &= -V_{yo}x_p + T_\perp(1-\hat{V}_x)\\
x_5 = -x_1,\ x_6 = -x_2,\ &x_7 = -x_3,\ x_8 = -x_4; & y_5 = -y_1,\ y_6 = -y_2,\ &y_7 = -y_3,\ y_8 = -y_4
\end{aligned} \tag{6}$$

where,

(1) $\hat{V}_x = V_x / V_{xo}$ is the normalized story shear in the x-direction, $V_{xo}=\sum_{i=1}^{M} f_x^{(i)}$ is the lateral capacity of the story in the x-direction, $f_x^{(i)}$ is the capacity of the i^{th} resisting plane in the x-direction, and M is the number of resisting planes in the x-direction;

(2) $V_{yo} = \sum_{i=1}^{N} f_y^{(i)}$ is the lateral capacity of the story in the y-direction, $f_y^{(i)}$ is the capacity of the i^{th} resisting plane in the y-direction, and N is the number of resisting planes in the y-direction;

(3) V_{yc} is the capacity of the resisting planes in the y-direction passing through the CM of the system (in practical terms it will represent the capacity of all resisting planes "close" to the CM);

(4) $T_o = \sum_{i=1}^{N} |f_y^{(i)}x^{(i)}| + \sum_{i=1}^{M} |f_x^{(i)}y^{(i)}|$ is the torsional capacity of the system;

(5) $T_\perp = \sum_{i=1}^{M} f_x^{(i)}y^{(i)}$ is the torque provided by the resisting planes in the orthogonal direction;

(6) $x_p = \sum_{i=1}^{N} f_y^{(i)}x^{(i)} / V_{yo}$ is the strength eccentricity, or first moment of strength; and

(7) $V_{yu} = \sum_{\substack{i=1\\ i\neq 2}}^{N} f_y^{(i)}x^{(i)} / |x^{(i)}|$ is the "strength unbalance" in the story.

In order to test the accuracy of the SEM, the inelastic response--of a four-story steel frame building (Fig. 8a-b) to the N-S component of 1940 El Centro ground motion amplified by a factor of 2--was computed using the SEM and the exact multi-plane models. This building exhibits coupling of lateral and torsional motions because of asymmetry due to the setback at the second floor level. The SEM for the building is shown in Fig. 8c. Shown in Fig. 9 is the SST surface for the first story and a comparison between the story shears and torque histories computed from the SEM and the exact multiplane models for each building story. Both responses show remarkable similarity in spite of the significant lateral-torsional coupling of the structure. The fact that yielding occurs on branches of the SST surface with negative slope implies that yielding in the first story occurs mainly on the planes to the right of the CM (1995b,c). Figure 10 indicates that the results predicted by the SEM are satisfactory for practical design purposes, although the SEM uses only four superelements instead of the 54-column elements in the "exact" analysis. In the example considered, the peak displacement ductilities for the resisting planes are about 2. This small ductility demand is typical of steel-frame buildings where sizing of the elements is usually controlled by serviceability (stiffness) requirements. More important, this intermediate ductility case constitutes a tough test for the SEM since the model is based on the assumption of an elastic-perfectly-plastic behavior, which ignores the transition between the elastic and plastic states.

Design Aspects

A comprehensive investigation was conducted to understand the effect of the following six characteristics controlling the behavior of multistory asymmetric structures: (1) strength of resisting planes in the orthogonal direction; (2) stiffness asymmetry; (3) strength asymmetry; (4) planwise distribution of strength; (5) number of resisting planes; and (6) bidirectional ground motion (De la Llera and Chopra, 1995b,1996). Computed for five-story buildings with several different plans were the story shear and torque history superimposed on the SST surface, building displacements, and member forces. Interpretation of these results led to the following conceptual guidelines for improving the design of asymmetric structures:

1. The responses of asymmetric-plan single and multistory buildings belonging to the special class considered, i.e., with regular asymmetry in height, show trends that are similar (1995b,1996). This suggests that, at least conceptually, earlier results for single-story systems may be applicable to this class of multistory systems.

2. Stiffness asymmetry of a system influences the story shear and torque combinations inside the SST surface and hence the elastic response of the system. However, changes in the stiffness eccentricity will affect the inelastic response of the system only if they lead to a shift of the inelastic action to a different region (or branch) of the SST surface.

3. Strength asymmetry produces concentration of deformation demand in resisting planes that are farther from the strongest plane in the plan. Furthermore, buildings with strength asymmetry are prone to develop torsional mechanisms and, hence, uneven displacement demands among resisting planes.

4. The two observations above may be combined into an interesting point. Since stiffness asymmetry controls the behavior inside the surface and strength asymmetry controls the shape of the surface, we can, theoretically speaking, adjust both to direct the inelastic behavior to any desired region of the surface.

5. A reduction in the torsional capacity of stiffness-asymmetric systems may produce, at the expense of larger displacements, more uniform displacement demands among resisting planes, implying a dominantly translational response.

6. Equivalent three-plane models of buildings with multiple resisting planes lead to sufficiently accurate estimates of the building displacements, story shears, and story torques. This is the basis for the SEM developed in the preceding section for preliminary analysis and design of buildings.

7. Increased strength in the resisting planes in the direction orthogonal to the ground motion reduces the torsion in an asymmetric structure. Indeed, substantial yielding of the resisting planes in the direction orthogonal to the ground motion implies that desirable lateral mechanisms with uniform displacement demand for all resisting planes are essentially impossible to generate, even in nominally symmetric structures.

Retrofit Design Example

The conceptual guidelines developed in the previous section are applied next to a hypothetical retrofit solution of a building. We seek a retrofit solution for the five-story building in Fig. 11 for the design earthquake equal to twice the E-W and N-S components of the El Centro earthquake in the x- and y-directions, respectively. The stiffnesses of the resisting planes are as shown, and their yield deformations are all assumed to be equal to $v_y = 0.02$ ft. Observe that the system is asymmetric in both directions as a result of the setback in the second story and because, in the second and upper stories, resisting plane 5 is stiffer and stronger than resisting plane 2. Besides, the building has resisting planes with lateral stiffness matrices which are not proportional.

Before proposing different retrofit solutions for this structure, it is necessary to understand its inelastic dynamic behavior (Fig. 12). Response results are presented for the second story of the building; columns (a), (b), and (c) present the floor displacements, force-deformation relations, and story shear and story torque histories, respectively. The floor displacements at the left and right edges of the plan are substantially different; the ratio of the two ranges between 3 and 5 for different floors (e.g. Fig. 12, part a). The peak deformation ductility demand for the most critical resisting plane in the second story is approximately 15 (Fig. 12, part b). The ductility demands on the various resisting planes differ by close to 100% in the first story and 60% in the second story. All the above observations are verified by the base shear and torque response histories superimposed on the SST surfaces. Figure 12, part c shows that yielding in the second story is quite extensive and spreads to the large-torque regions of the constant story shear branches where mechanisms become increasingly torsional. Therefore, there is clear evidence that the system is torsionally unbalanced, and any proposed retrofit solution should aim to correct this unbalance in order to lead to more uniform deformation demands among resisting planes.

First Retrofit Solution. The strength of resisting planes A and C is increased by factors of 2.5 and 2 in the first story and all upper stories, respectively, such that the lateral capacity of each story in the x-direction has been doubled (Fig. 11b). It is apparent by comparing the earthquake response of the modified building (Fig. 13) with the response of the original building (Fig. 12) that, as expected, the torsional unbalance in the system has been partially corrected, i.e., the displacements of different resisting planes become less different (Fig. 13, part a), their deformation ductility demands also become more similar (Fig. 13, part b), and the mechanisms developed at different stories are less torsional (Fig. 13, part c).

Although the benefit of increasing the strength in the orthogonal planes is apparent, some aspects of the behavior of the new system are not completely satisfactory. First, given the large increase in strength of the orthogonal planes, we would have preferred a better agreement between the left and right edge displacement histories. Second, the force-deformation histories in the second story (Fig. 13, part b) show that yielding in the resisting planes occurs asymmetrically about the force axis, indicating a residual drift in the structure. Third, the increase in strength in the orthogonal planes leads to an increase in the story torques developed in the system (Fig. 13, part c). Despite these deficiencies, the retrofit solution proposed accomplishes our goal of reducing differences in demands among resisting planes. However, as shown next, it is possible to achieve a much better performance by adjusting the stiffness and strength of the resisting planes.

Second Retrofit Solution. We first recall from points 2, 3, and 4 in the previous section that, by changing the stiffness and strength distribution in the system, we may concentrate yielding in specific resisting planes of the structure. Thus, the strategy for this solution is to decrease the capacity of those planes that remain essentially elastic in the original system and increase the capacity of planes that yield excessively in that system; however, the overall lateral capacity is kept the same as that of the original system. For this purpose, in the first story the capacity of plane 5 is increased and that of plane 1 is decreased, both by 25%; in the second story the strength of resisting plane 3 is increased by 50% and that of plane 5 is reduced by 25%.

The dynamic response of the modified system (Fig. 14) is remarkable in many respects. First, the displacement histories at different locations of the building plan (Fig. 14, part a) are very similar, especially for the second and upper stories. Second, the force-deformation histories (Fig. 14, part b) show essentially identical peak deformation demands on the different resisting planes, as well as symmetric behavior about the force axis. Further, since all resisting planes are used more effectively, the peak ductility demands have been reduced from 15 in the original system (Fig. 12, part b) to about 8 in the new system (Fig. 14, part b). Third, the second story shear and torque combinations now lie close to the zero torque axis (Fig. 14, part b), implying that the mechanisms developed are mainly translational.

As demonstrated by this example, the conceptual guidelines presented in the previous section concerning the inelastic behavior of asymmetric buildings provide a basis to develop practical solutions to improve the torsional behavior of an existing structure, even if that structure is highly asymmetric. Thereafter, the retrofit solution can be tested further by inelastic dynamic analyses of the system. Such analyses, which are costly if standard methods are used, can be greatly simplified using the SEM presented earlier.

CONCLUSIONS

This investigation has led to two proposals to include the effects of accidental and natural torsion in building design.

First, a new procedure for accidental torsion has been developed. This procedure consists in specifying an increase in edge displacements due to all sources of accidental torsion in the elastic range as a function of two building parameters, the ratio b/r and the frequency ratio Ω.
This procedure has several advantages over the current code accidental torsion provisions. First, it avoids the important discrepancies between the increase in response obtained by static and dynamic analysis procedures to account for accidental torsion. Second, it is simple to use and eliminates the two extra 3D-static or dynamic analyses of the building in each lateral direction. Third, it includes the effect of all sources of accidental torsion whereas codes include only those that can be represented by an accidental eccentricity. Fourth, it defines explicitly the expected increase in design forces due to accidental torsion, in contrast to the use of an accidental eccentricity which implies an indirect increase in member forces. Fifth, the envelopes for the increase in response are associated with a well established probability of exceedance.

This investigation has also led to a new procedure for integrated analysis and design of asymmetric plan structures. The procedure differs from previous work in the sense that it does not develop simple rules based on extensive parametric studies for the effects of natural torsion, but provides a model which enables the engineer to understand, prior to any elaborate inelastic analysis if the planwise earthquake performance of the building is adequate or not. Based on this framework, we developed an explanation for the parameters that control the inelastic behavior of torsionally coupled systems, a tool for simplified inelastic analysis of asymmetric multistory buildings (SEM model), and a set of guidelines to improve their inelastic performance.

ACKNOWLEDGEMENTS

This paper is based on Dr. J. C. De la Llera's Ph.D. dissertation, resulting from research supported by the National Science Foundation under the Grant BCS-8921932. The authors are grateful for this support.

REFERENCES

De la Llera, J.C. and A.K. Chopra (1994a). Evaluation of code accidental-torsion provisions from building records. *Journal of Structural Engineering*, ASCE, **120**, 597-616.

De la Llera, J.C. and A.K. Chopra (1994b). Accidental torsion in buildings due to stiffness uncertainty. *Earthquake Engineering and Structural Dynamics*, **23**, 117-136.

De la Llera, J.C. and A.K. Chopra (1994c). *Accidental and Natural Torsion in Earthquake Response and Design of Buildings*, Report No. UCB/EERC-94/07, Earthquake Engineering Research Center, University of California, Berkeley.

De la Llera, J.C. and A.K. Chopra (1994d). Using accidental eccentricity in code-specified static and dynamic analyses of buildings. *Earthquake Engineering and Structural Dynamics*, **23**, 947-967.

De la Llera, J.C. and A.K. Chopra (1994e). Accidental torsion in buildings due to base rotational excitation. *Earthquake Engineering and Structural Dynamics*, **23**, 1003-1021.

De la Llera, J.C. and A.K. Chopra (1994f). Accidental torsion in buildings. *Proc., 6th U.S. Nat. Conf. in Earthquake Engrg.*, Vol. II, 401-410.

De la Llera, J.C. and A.K. Chopra (1995a). Estimation of accidental torsion effects for seismic design of buildings. *Journal of Structural Engineering*, ASCE, **121**, 102-114.

De la Llera, J.C. and A.K. Chopra (1995b). Understanding the inelastic seismic behavior of asymmetric-plan buildings. *Earthquake Engineering and Structural Dynamics*, **24**, 549-572.

De la Llera, J.C. and A.K. Chopra (1995c). A simplified model for analysis and design of asymmetric-plan buildings. *Earthquake Engineering and Structural Dynamics*, **24**, 573-594.

De la Llera, J.C. and A.K. Chopra. Inelastic behavior of asymmetric multistory buildings (1996). *Journal of Structural Engineering*, ASCE, accepted for publication.

Rutenberg, A. (1992). Nonlinear response of asymmetric buildings and seismic codes: a state-of-the-art review. *European Earthquake Engineering*, **2**, 3-19.

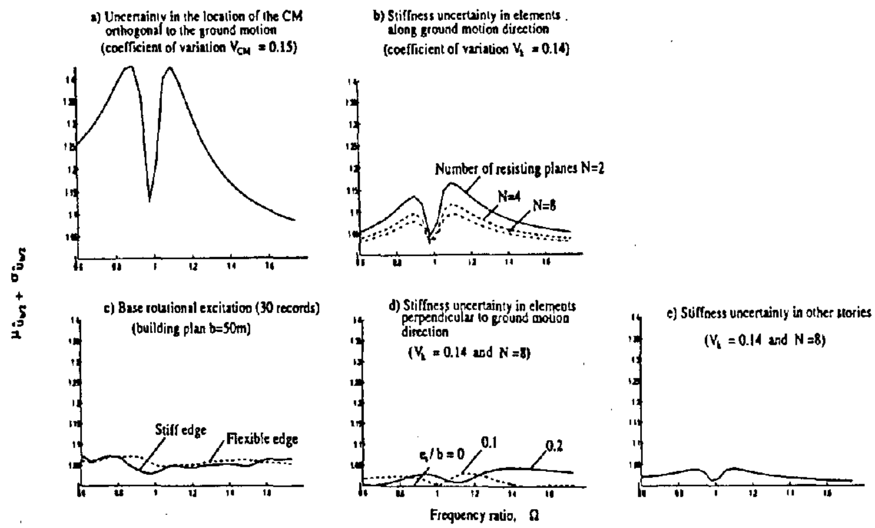

Fig.1 Mean-Plus-One Standard Deviation $\mu_{\hat{u}_{b/2}} + \sigma_{\hat{u}_{b/2}}$ of Normalized Edge Displacement $\hat{u}_{b/2}$ due to different sources of accidental torsion.

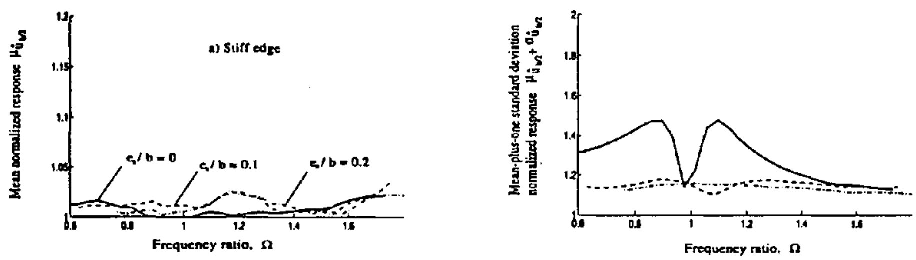

Fig.2 Mean and Mean-Plus-One Standard Deviation of Normalized Edge Displacement $\hat{u}_{b/2}$-Systems with $T_y = 1$ and square plan $b/r = \sqrt{6}$

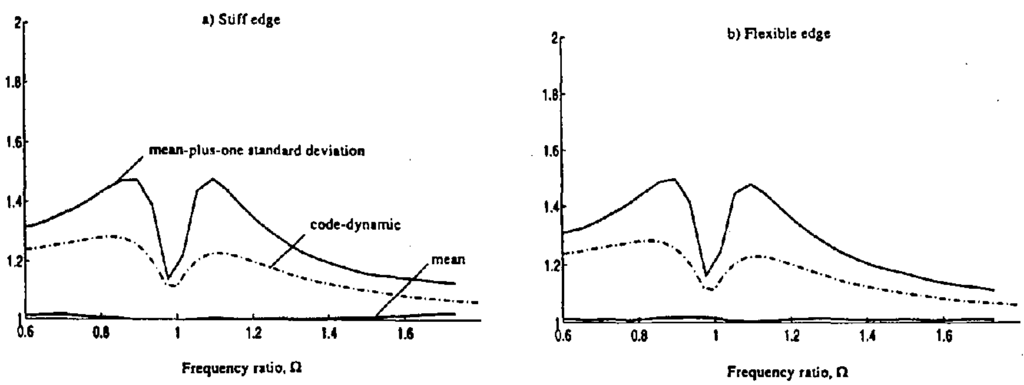

Fig.3 Comparison between $\hat{u}_{b/2}$ Computed from Code-Dynamic Analysis and from Statistical Analysis of Different Sources of Accidental Torsion-Systems with $T_y = 1$ sec and Square Plan $b/r = \sqrt{(6)}$

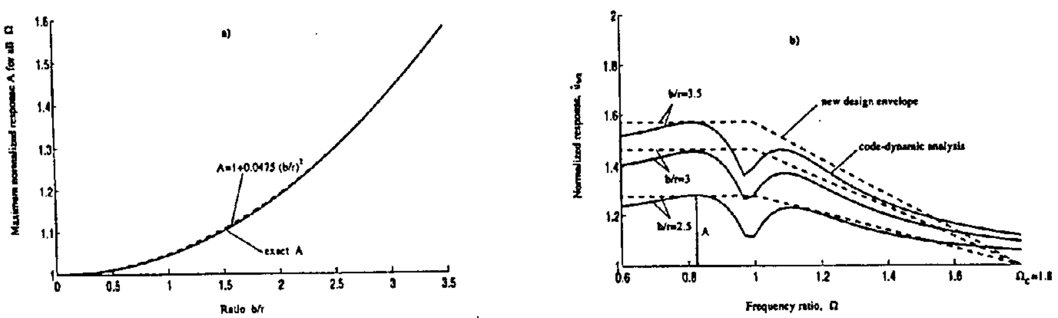

Fig.4 Design Envelopes for Normalized Edge Displacement $\hat{u}_{b/2}$: (a) Variation of A as Function of b/r; and (b) Design Envelopes for $b/r = 1.5, 3$, and 3.5 in Systems with $T_y = 1$ sec

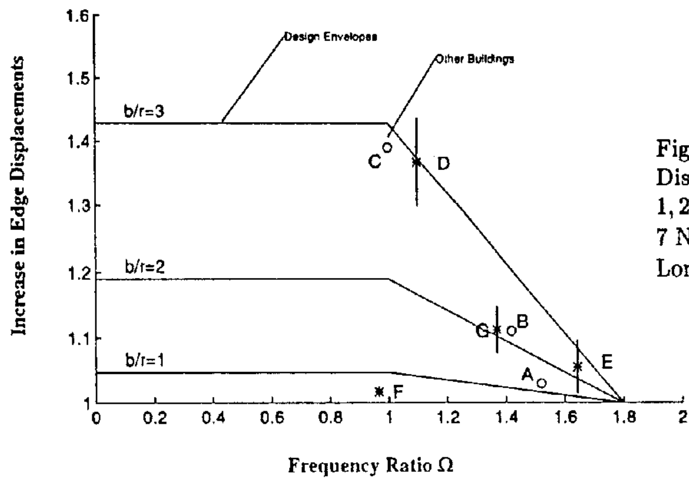

Fig.5 Design Envelopes for Normalized Edge Displacement $\hat{u}_{b/2}$ Corresponding to b/r = 1, 2 and 3, and "True" Results Obtained in 7 Nominally Symmetric Buildings During the Loma Prieta and Northridge Earthquakes

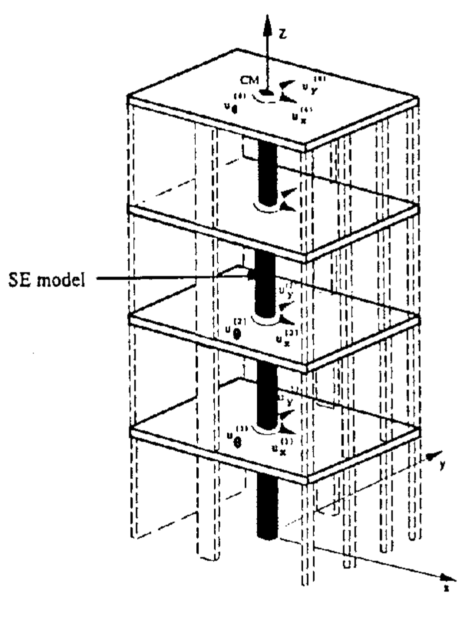

Fig.6 Single Element Model of a Four-Story Building

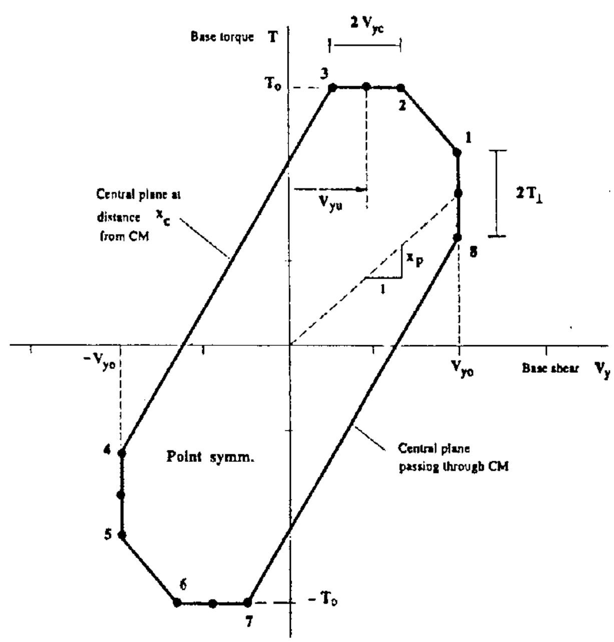

Fig.7 Parametric Representation of the Story-Shear and Torque Surface

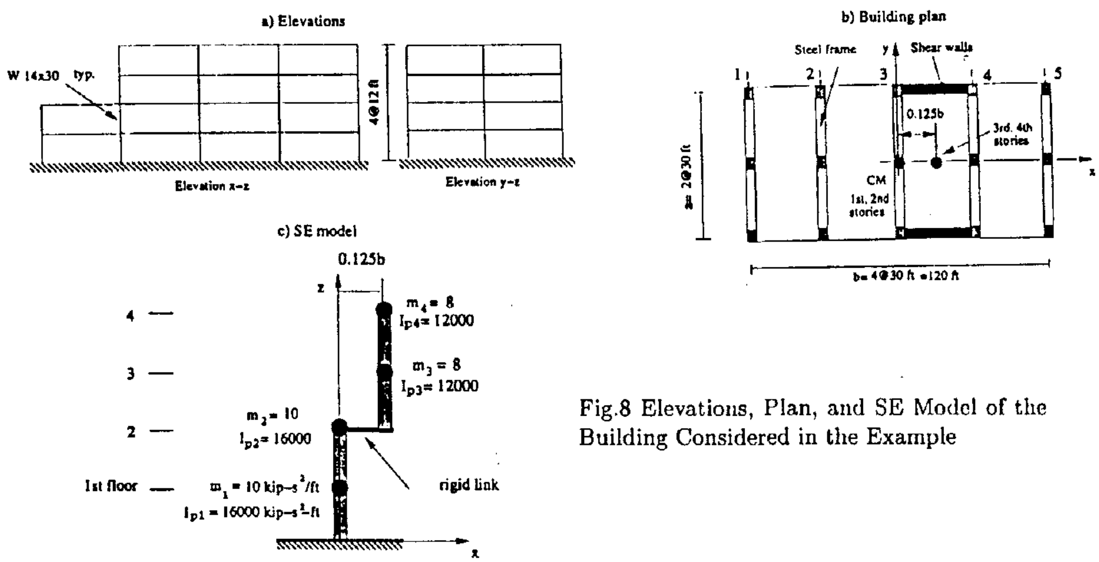

Fig.8 Elevations, Plan, and SE Model of the Building Considered in the Example

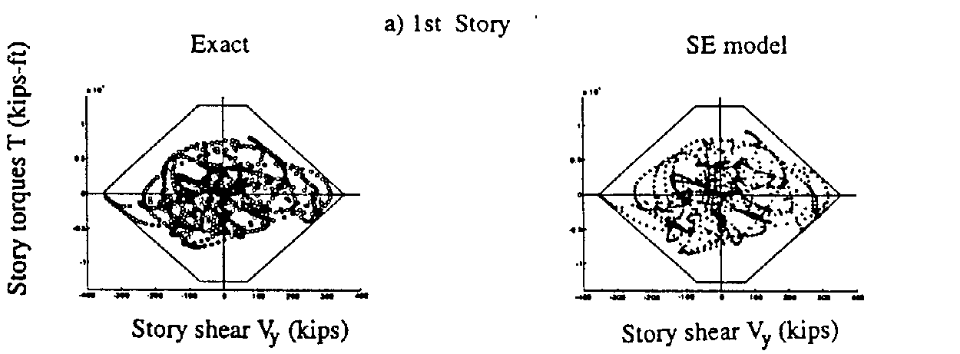

Fig.9 Comparison of Base-Shear and Torque Diagrams Computed from the Exact and SE models

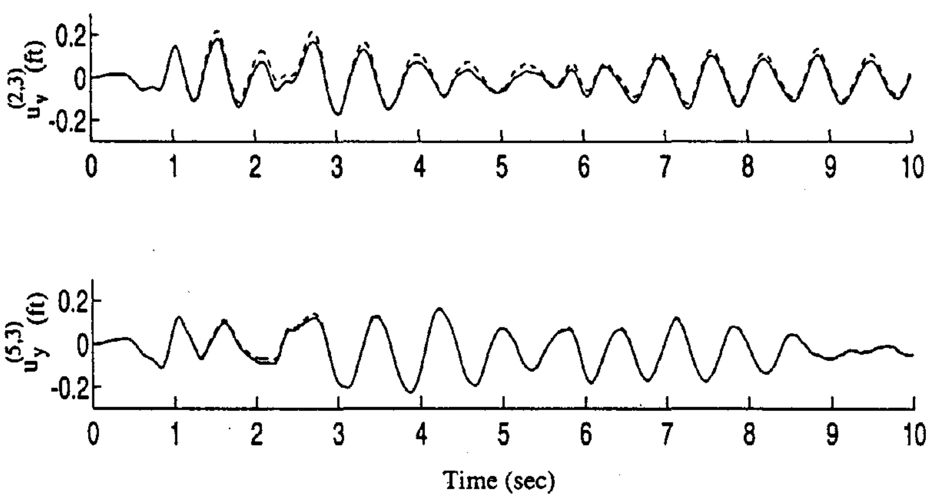

Fig.10 Displacements at Location of Resisting Planes 2 and 5 on the Third Floor

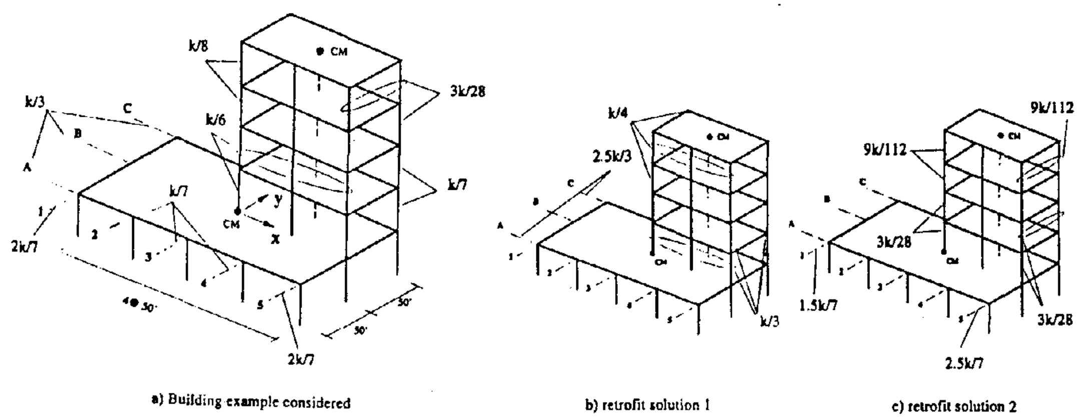

Fig.11 Building with Setback Considered in the Example and Two Possible Retrofit Solutions

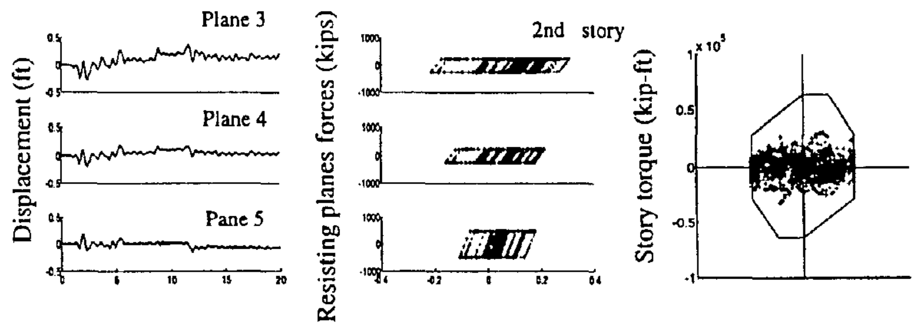

Fig.12 Behavior of the Second Story of the Original Building

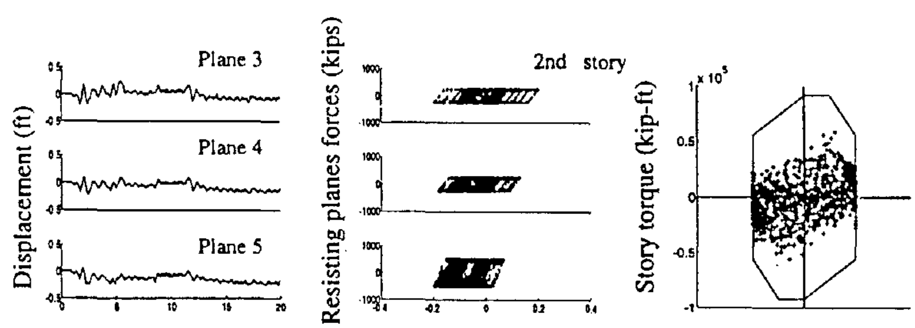

Fig.13 Behavior of Building with Increased Strength in the Orthogonal Resisting Planes

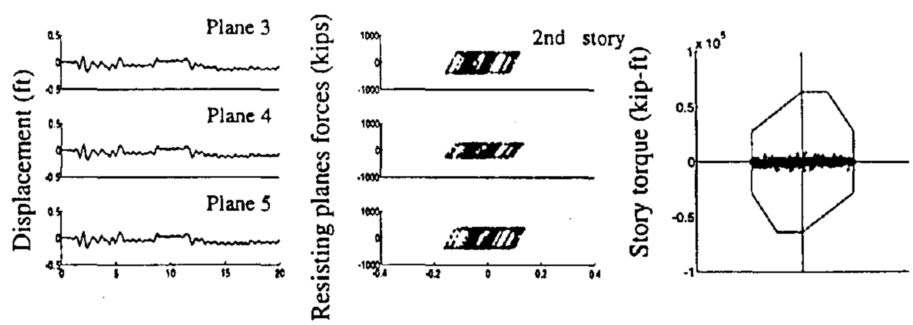

Fig.14 Behavior of Building with Modified Stiffness and Strength in Edge Resisting Planes

ANALYSIS OF THE BEHAVIOR OF BUILDINGS DURING THE 1994, NORTHRIDGE EARTHQUAKE

J. C. De la Llera and A. K. Chopra

Department of Structural Engineering, The Catholic University of Chile,
Casilla 306, Correo 22, Santiago, Chile
Department of Civil and Environmental Engineering, 707 Davis Hall,
University of California, Berkeley, CA 94720, U.S.A.

ABSTRACT

Evaluated in this study is the behavior of eight buildings during the 1994, Northridge, earthquake using recorded building motions. The "recorded" behavior is first compared with theoretical predictions based on nominal, three-dimensional, linear building models. Results show that the predictions based on these models are in most cases inaccurate. Because of this, a recently developed simplified inelastic procedure, which uses ultimate story shear and torque surfaces, is successfully tested and formulated as an alternative to conventional linear models. Finally, instrumentation and building analysis and design issues are discussed in light of the results generated in this research.

KEYWORDS

Building models; building records; model uncertainty; single element model; story shear and torque

INTRODUCTION

The 1994 Northridge earthquake has produced one of the most valuable databases of ground and earthquake building responses in history. A total of 193 stations of the California Strong Motion Instrumentation Program recorded 116 free-field ground motions and 77 structural responses. From the latter, 57 correspond to buildings records obtained for a wide range of structural configurations. The seismic performance of eight of these buildings, the ones most strongly shaken, are studied in this investigation. In particular, the objectives are to: (1) evaluate the uncertainty present in conventional structural linear building models; (2) evaluate the deficiencies in current procedures for earthquake analysis and design, and (3) propose improved analysis and design procedures calibrated using "measured" responses.

BUILDINGS CONSIDERED AND RECORDED MOTIONS

The buildings considered in this study are listed in Table 1. They cover a wide range of structural systems in use today, such as R/C frames, precast R/C walls, R/C column-flat-slab frames, steel bracings, steel walls (uncommon), and mixed R/C and steel frame systems. Notice that for all these structures the peak ground accelerations during Northridge exceeded $0.2g$. Shown in Fig. 1 are the recorded acceleration components at the base of each building in the East-West direction. In this study the buildings are ordered according to distance to the epicenter, A being the closest and H the farthest.

Table 1 Buildings considered

CSMIP Station	Building	Number of Stories	System	PGA x-direction	PGA y-direction
24386	**A**: Van Nuys (hotel)	7	R/C frame	0.44g	0.37g
24514	**B**: Sylmar (hospital)	6	R/C, steel frame,walls	0.52g	0.67g
24231	**C**: UCLA (Math-Science)	7	R/C walls, steel frame	0.25g	0.29g
24332	**D**: LA (commercial)	3/2	Braced frame	0.33g	0.32g
24385	**E**: Burbank (residential)	10	R/C precast walls	0.27g	0.29g
24370	**F**: Burbank (commercial)	6	Steel frame	0.25g	0.29g
24652	**G**: LA (office)	5/1	Braced frame	0.24g	0.20g
24463	**H**: LA (warehouse)	5/1	R/C frame-flat slab	0.20g	0.26g

ANALYSIS OF BUILDING RECORDS

In order to clearly identify the building behavior, recorded motions were subjected to four different analyses: (1) non-parametric identification---used to estimate apparent vibration frequencies and modes of each building, (2) time-frequency analysis---used to identify nonlinearities in a building's response, (3) story shears and torque analysis---used to interpret inelastic behavior of the building and construct the inelastic SEM (single element) model defined later, and (4) story force-deformation analysis.

Shown in Fig. 2 are typical results of this phase of record processing; the results selected in this case are for building A. Non-parametric identification is presented in Fig. 2a, where the frequency response function between ground motion and roof response is presented for the x,y, and θ directions--the top two rows represent transfer functions at the roof and midheight; the bottom row represents just the spectrum of the input. Results of time-frequency analysis of the same building are presented in Fig. 2b; in this case, the analysis was done also for other four motions recorded on the building during previous earthquakes. Such analysis lead us to the conclusion that the building was slightly damaged during the San Fernando earthquake, it was then retrofitted before Whittier, damaged again during Landers, and, finally, severely damaged during Northridge (De la Llera and Chopra, 1996). Using also the recorded accelerations, story shears and torques are computed by assuming the story masses of the building. Such results are presented in Fig. 2c, in which a point, denoted with "+", represents a combination of story shear and torque for a given instant of time. The interpretation of these plots has been studied earlier (De la Llera and Chopra, 1994). Finally, empirical story force-deformation relations are obtained by plotting story shears and story drifts, the latter computed from the integrated acceleration records.

BUILDING MODELS

The main objective of this phase was to estimate the uncertainty present in conventional linear building models used today in practice. For that purpose, a three dimensional finite element model was developed for each building, assuming rigid floor diaphragms and three degrees of freedom located at the center of mass (CM) of each floor, where all the story masses were lumped. A complete description of these models as well as the assumptions considered may be found elsewhere (De la Llera and Chopra, 1996).

Shown in Fig. 3 is a comparison between the predicted and "true" deformations at the roof of five of the buildings considered. It is apparent that the accuracy obtained between the predicted and actual responses is not good. The reasons for that vary from building to building. For instance, in building A, the nonlinear behavior of the structure, evidenced by the damage in the fourth-story columns, is not accounted for in the linear model developed. Note that the estimated traces of the roof deformation are similar to the true deformations during the first few seconds, but become substantially different after the building damages. Leaving aside building A, all other buildings remained elastic during this earthquake and one would expect a much better accuracy in their response predictions. However, as shown in the figure, the accuracy obtained by complex three dimensional linear models in terms of time responses as in peak responses is poor in general.

Although the sources of model uncertainty vary considerably among buildings, it is often true that in the case of linear elastic behavior of buildings, the structure of the model considered would be enough for a good fitting of predicted and "measured" responses if the parameters defining the model were varied. In other words, good predictions would be obtained if the model was adjusted a priori by identification of the building stiffness (principally) and mass properties.

IMPROVED ANALYSIS PROCEDURES

Because of the inaccurate responses predicted by linear models, a new simplified procedure for inelastic building analysis that has been recently proposed by the authors is evaluated and tested using recorded building responses. In this model, each story is represented by a single super-element (SEM) capable of representing the elastic and inelastic properties of the story. The formulation, accuracy, and implementation of this model are described in De la Llera and Chopra (1994). Presented next is the formulation and analysis of building A using a SEM model.

The first step in computing the SEM is to estimate the lateral and torsional capacities of each story. This is done by first computing the lateral capacity of each building column associated with a realistic axial load--assumed in this case equal to the gravity load--on it. Shown in Fig. 4a are the heightwise distribution of lateral capacities of the different columns of the building. In the figure, the values identified with circles and stars represent lateral capacities corresponding to shear and flexural failure mechanisms in each column, respectively. It is apparent that for essentially all columns shear failure mechanisms precede flexural mechanisms between the 2nd and 4th stories; these stories correspond to those most severely damaged during the earthquake.

Once the lateral capacity of columns is known, story shear and torque surfaces (SST) are constructed for each story using simplified rules (De la Llera and Chopra, 1994). Each point on one of these surfaces represents a static combination of story shear and torque that produces collapse of the story. Superimposed in Fig. 4b are the SST surfaces and the story shear and torque histories computed from recorded responses. Several interesting observations are obtained from Fig. 4b. First, it is apparent that all the response shear and torque combinations lie, as it should, inside or on the boundaries of the computed SST surfaces. Second, a close look of the third-story surface (Fig. 4c) shows that there is a number of story shear and torque combinations that approximately describe the SST, implying that the plasticity model implicit in the SST surface occurs in reality. Moreover, interpretation of the SST surface enables us to conclude that the building underwent inelastic torsional behavior in spite of its nominal symmetry---shear and torque combinations on the inclined branches correspond to predominantly torsional mechanisms. Indeed, it can be shown that this will be the case in most buildings with a perimeter frame as the only lateral resisting system.

Finally, by using the SST surface for each story, a SEM can be constructed to predict the inelastic response of the building. Such response is presented in Fig. 4d. Although differences still persist between model and "measured" responses, they are smaller than for the elastic prediction shown earlier in Fig. 3.

BUILDING ANALYSIS AND DESIGN IMPLICATIONS

This investigation has led to the following implications for building analysis and design:

A fundamental aspect in interpreting the building responses in this investigation was the use of recorded motions to the maximum possible extent without introducing strong modeling assumptions. Results based on tools such as story shear and torque histories help to establish inadequate inelastic properties of a building that otherwise would be hard to visualize. For the development and details of this and other useful record processing techniques the reader is referred to De la Llera and Chopra (1996).

The results presented earlier in Fig. 3 pose delicate questions such as: do we need to get as sophisticated as we do today using complex three dimensional linear building models in order to predict meaningful earthquake responses?, or why do our structural models "fail" in providing better predictions?.

In first place, buildings designed according to current codes, with large R factors, are likely to experience substantial inelastic behavior during a strong earthquake. For them, there is little hope that a linear model, as complete as it can be, will be able to predict representative earthquake responses. In that regard it would be better to use a simplified inelastic model, such as the SEM, capable of representing the fundamental inelastic features of the structure during the earthquake. In second place, the reason why our structural models fail in predicting more accurate responses is given through a counter example. Consider the response of base isolated buildings during the Northridge earthquake. Shown in Fig. 5 is a comparison between the predicted and "measured" deformations of the Fire Command and USC hospital buildings. Interestingly, the accuracy of these predictions is substantially better than that of fixed based buildings (Fig. 3). Why?, because the building behavior is controlled by elements with well known properties and behavior. Our sophisticated techniques of structural analysis are in this case extremely useful in providing realistic estimations. Indeed, to improve our earthquake response estimations we should improve our knowledge on the material and behavior of the structural elements used, or, otherwise, introduce in the design structural elements, such as dissipators or isolators, whose properties are well defined and in which the inelastic behavior of the structure is predominantly confined.

Finally, because several of the buildings considered are nominally symmetric, they are especially appropriate to evaluate the increase in response due to accidental torsion. This topic has been studied recently and design envelopes have been proposed to account for this effect (De la Llera and Chopra, 1994). The procedure proposed is based on a statistical study of the different sources of accidental torsion and avoids the cumbersome two extra analyses in each direction with shifted equivalent lateral forces or centers of mass. Shown in Fig. 6 are three design envelopes corresponding to values of $b/r=1,2$, and 3, where r is the radius of gyration of the building plan. Superimposed to these envelopes are the "recorded" increases in edge displacements due to accidental torsion in seven nominally symmetric buildings. First, as results insinuate, the increase in response of buildings with lateral to torsional frequency ratio, Ω, close to 1 is very sensitive to variations in Ω, as it has been predicted theoretically (De la Llera and Chopra, 1994). Moreover, it is apparent that buildings with larger Ω have a smaller increase in response due to accidental torsion as intended by the design envelopes. Because of this, it has been proposed that the effects of accidental torsion be neglected for buildings with $\Omega > 1.8$.

ACKNOWLEDGMENTS

This research has been supported by the Strong Motion Instrumentation Program, California Division of Mines and Geology, and the National Science Research Foundation of Chile, Fondecyt under Grant No. 1950987. The authors are grateful for this support.

REFERENCES

De la Llera, J.C., and Chopra, A.K. (1994). Accidental and Natural Torsion in Earthquake Response and Design of Buildings. UCB/EERC-94/07, University of California, Berkeley.

De la Llera, J.C., and Chopra A.K. (1996). Evaluation of Seismic Code Provisions Using Strong-Motion Building Records from the 1994 Northridge Earthquake. CSMIP report, Sacramento.

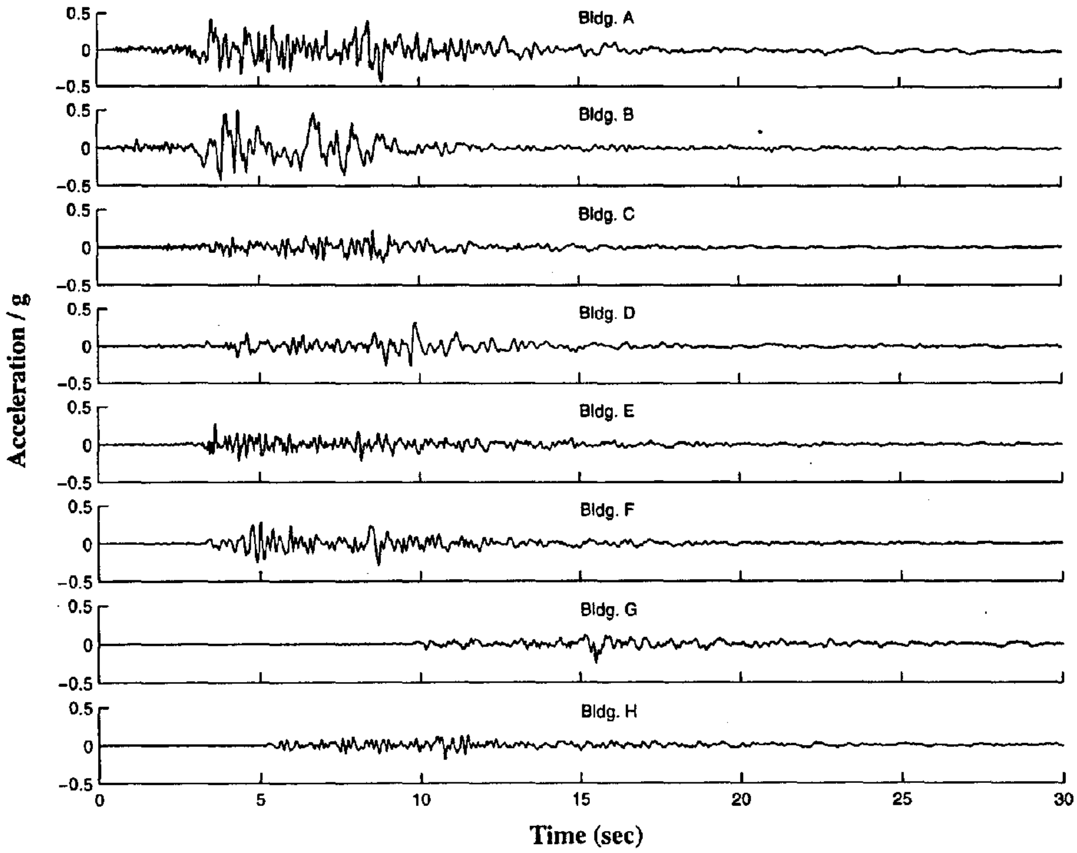

Figure 1: Recorded accelerations in all buildings considered in the East-West direction

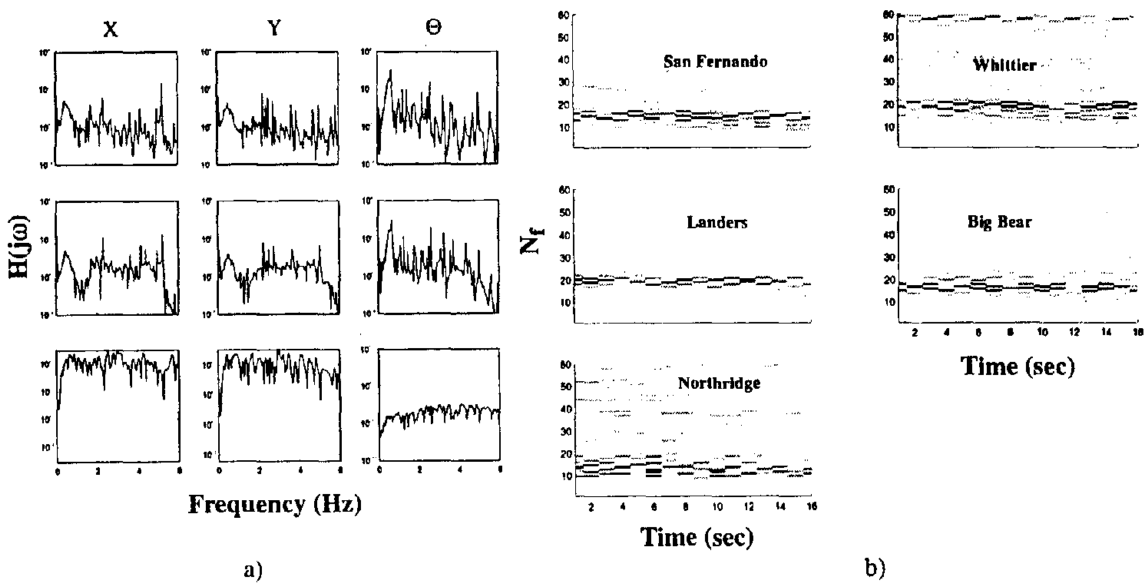

Figure 2: Selected results from record processing using building A as an example: (a) transfer functions at three building levels; (b) time frequency analysis; (cont.)

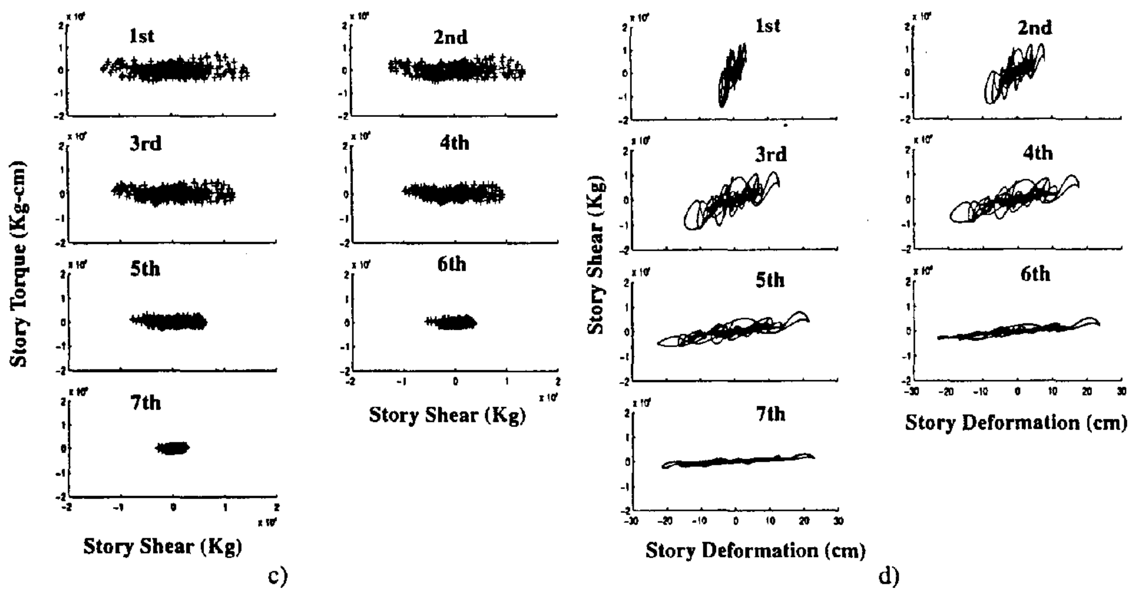

Figure 2 (cont.): c) story shears and torques; d) story shears versus story deformations

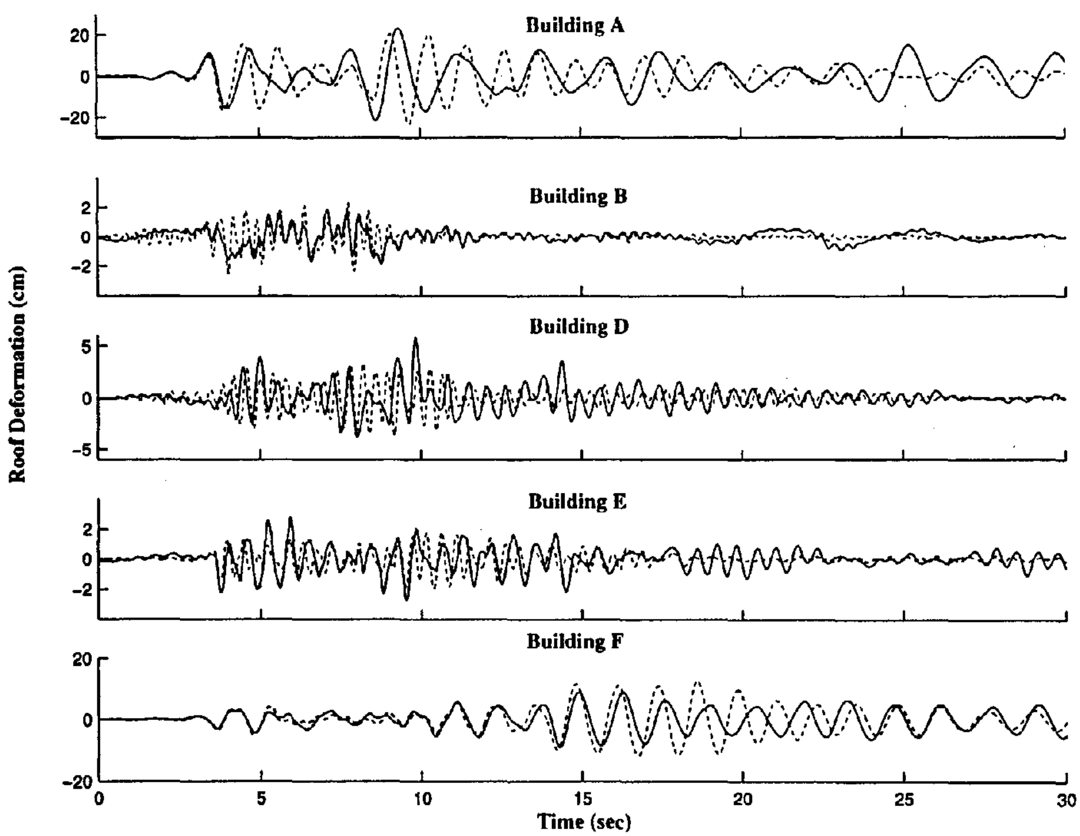

Figure 3: Comparison between predicted deformations at building roof using nominal linear elastic models (dashed line) and building deformations obtained from recorded motions (solid line)

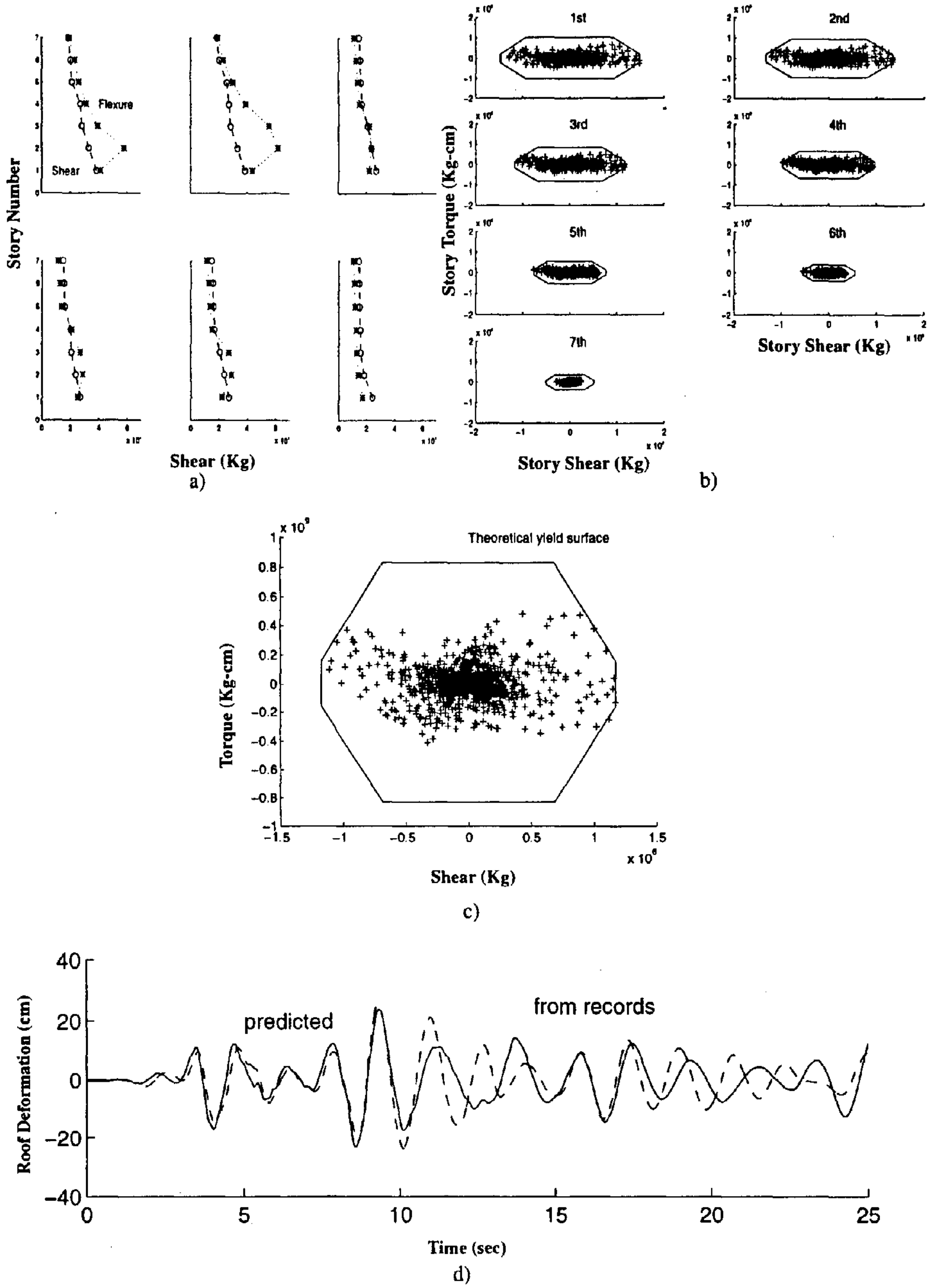

Figure 4: Inelastic analysis of Building A using a SEM model: a) shear capacities of columns; b) story shears and torques and ultimate surfaces; c) third story ultimate surface; and d) comparison between predicted building deformations and deformations computed from building records

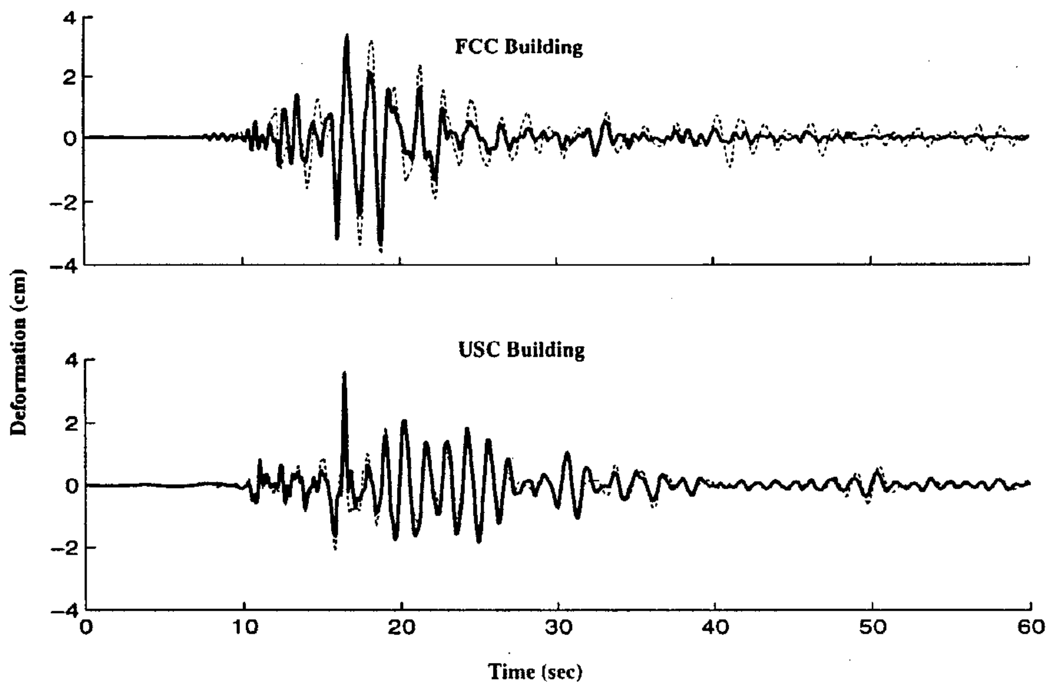

Figure 5: Comparison between predicted deformations on top of the isolators by an equivalent linear model and deformations obtained from recorded building motions

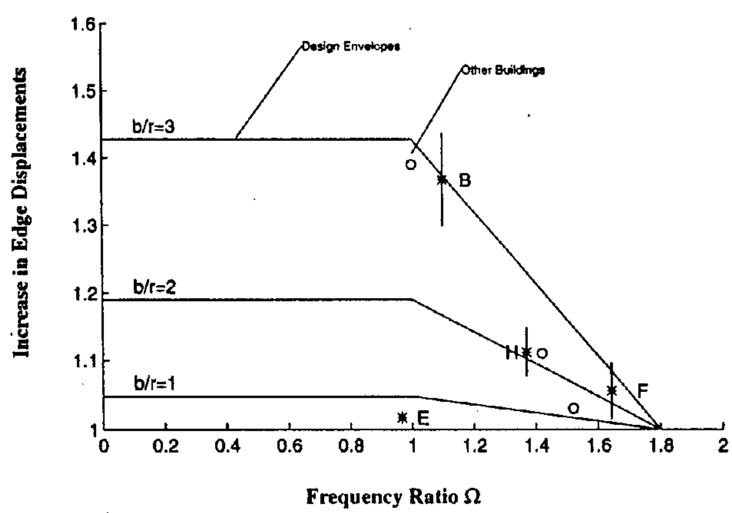

Figure 6: Comparison between design envelopes for the buildings selected and the 'true' increase in edge displacements due to accidental torsion computed from building records

EFFECT OF SITE RESPONSE ON SPATIAL VARIABILITY OF GROUND MOTION

A. DER KIUREGHIAN and P. KESHISHIAN

Department of Civil Engineering, University of California
Berkeley, CA 94720, USA

ABSTRACT

The validity of a recently developed mathematical model for the site-response component of ground motion spatial variability is examined. Use is made of earthquake recordings in two downhole arrays. A procedure is described to compute an equivalent frequency response function to characterize the dynamic properties of the local soil. These functions for each pair of stations completely define the site-response component of the coherency function that characterizes the spatial variability. Predictions with the theoretical model are in close agreement with "exact" results derived from the recorded data, thus validating the model. Results also show that the site-response effect on the coherency of ground motion is most significant at resonant frequencies of each site.

KEYWORDS

Coherency function; frequency response function; ground motions; impulse response function; phase angle; power spectral density; site response; spatial variability.

INTRODUCTION

Spatial variation in earthquake ground motions arises from four sources: (1) loss of coherency of seismic waves due to scattering in the heterogeneous medium of the ground and due to differential superpositioning of the waves arriving from an extended source, collectively denoted as the "incoherence effect"; (2) difference in the arrival times of waves at different stations, commonly known as the "wave-passage effect"; (3) gradual decay of wave amplitudes with distance due to geometric spreading and energy dissipation in the ground medium, denoted the "attenuation effect"; and (4) spatially varying local soil profiles and the manner in which they influence the amplitude and frequency content of the bedrock motion underneath each station as it propagates upward, denoted herein as the "site-response effect". These effects are well characterized by the so called coherency function, which is the normalized cross-power spectral density of the motions at two stations. Use of this function in response spectrum analysis of multiply-supported structures, such as bridges, is described by Der Kiureghian and Neuenhofer (1994).

Past studies have shed considerable light on the effects of incoherence, wave passage and attenuation (e.g., Abrahamson *et al.*, 1991). However, the site response effect has only recently received attention (Somerville, *et al.*, 1988, Schneider *et al.*, 1992, Zerva and Harada, 1994, Der Kiureghian, 1994). In a recent paper(Der Kiureghian 1996), the first author has proposed a new, composite model for the coherency function that incorporates all the four effects mentioned above. This paper aims at validating the site-response component of this model. Use is made of two sets of recorded ground motions from downhole arrays and direct comparisons are made between predictions by the model and by the recorded data. The numerical comparison shows remarkable agreement between theory and observation. The paper also describes a method for characterizing the required parameters and functions for the site-response component of the coherency function. Additionally, the numerical results clearly demonstrate the importance of this component of the ground motion variability.

THE COHERENCY MODEL

The coherency model derived by Der Kiureghian (1996) is based on elementary concepts of random process theory and employs simplifying assumptions for propagation of waves in the ground medium (i.e., plane wave assumption) and through the local soil column (i.e., vertically propagating shear waves, linear stationary response). Neglecting the attenuation effect that is shown to be insignificant, the model has the form

$$\gamma(\omega) = |\gamma(\omega)| \exp\left\{ i[\theta_{wp}(\omega) + \theta(\omega)_{sr}] \right\} \tag{1}$$

where ω denotes the circular frequency, $|\gamma(\omega)|$ denotes the modulus of the coherency function representing the incoherence effect, $i = \sqrt{-1}$, and $\theta_{wp}(\omega)$ and $\theta_{sr}(\omega)$ are phase angles that represent the wave passage and site response effects, respectively, and are given as follows:

$$\theta_{wp}(\omega) = \frac{\omega d_{kl}^{L}}{v_{app}(\omega)} \tag{2}$$

$$\theta_{sr}(\omega) = \tan^{-1} \frac{\mathrm{Im}[H_k(\omega) H_l(-\omega)]}{\mathrm{Re}[H_k(\omega) H_l(-\omega)]} \tag{3}$$

In the above expressions, d_{kl}^{L} denotes the distance between a pair of stations k and l measured in the longitudinal direction of wave propagation, $v_{app}(\omega)$ is the "apparent" wave velocity (expressed as a function of ω in account of dispersion effects), and $H_k(\omega)$ and $H_l(\omega)$ denote frequency response functions of the soil columns at the two stations as defined in the following section. It is noted that the wave passage effect is completely defined by the apparent wave velocity and the geometry of the stations relative to the earthquake source, whereas the site response effect is completely defined in terms of the characteristics of the local soil at each station. The incoherence component usually must be determined by statistical fitting to observed data because of the complex and random nature of the underlying phenomena.

The remainder of this paper describes a method for evaluation of the frequency response function for a soil site with an approximate account of the nonlinearity in the soil behavior, and verifies the site-response component of the coherency model in (3) by comparison with the phase angle generated from recorded data.

DETERMINATION OF THE FREQUENCY RESPONSE FUNCTION

The site-response component of the coherency model in (3) is derived by considering the soil columns at stations k and l as two linear systems. The derivation makes use of elementary concepts of stationary random vibration theory involving the frequency response function $H_k(\omega)$ at each station. By definition, this function is the steady-state response of a linear system to a complex harmonic excitation of the form $\exp(i\omega t)$. Of course soil behavior under strong earthquake motions is not linear. Hence, we need to define this function for some sort of an "equivalent" linear soil system. Three ideas for this purpose are described below.

If one is fortunate enough to have recorded earthquake ground motions at the base rock and surface levels at the site of interest, then, based on stationary random vibration theory, the frequency response function for an equivalent linear soil system can be computed from

$$H_k(\omega) = \frac{\Phi_{\text{base-surface}}(\omega)}{\Phi_{\text{base}}(\omega)} \tag{4}$$

where $\Phi_{\text{base}}(\omega)$ is the power spectral density of the base motion and $\Phi_{\text{base-surface}}(\omega)$ is the cross-power spectral density of the base and surface motions at station k. In practice it is rare that one has such recordings for a selected site. Nevertheless, this approach is valuable as a means to investigate the validity of the analytical methods that are described below.

A simple approach would be to consider the soil column at the site as a single-degree-of-freedom system with viscous damping. The frequency response function then has the well known form

$$H_k(\omega) = \frac{\omega_k^2 + 2\mathrm{i}\zeta_k\,\omega_k\omega}{\omega_k^2 - \omega^2 + 2\mathrm{i}\zeta_k\omega_k\omega} \tag{5}$$

where ω_k and ς_k respectively denote the natural frequency and viscous damping ratio of the equivalent soil system. This, however, is a very crude model for several reasons, including the fact that soil damping is not viscous and deep soil columns usually possess several significant modes of vibration. Additionally, it is not easy to determine the parameters ω_k and ς_k on a rational basis. Nevertheless, this model is a simple alternative when other options are not practical. It is noted that this model is consistent with the well known Kanai-Tajimi model for ground motions on soil sites (Clough and Penzien, 1993). Typical ranges of the parameter values for that model are $\omega_k = 2\pi$ - 5π rad/s and ς_k = 0.2 - 0.6.

For a better representation of the frequency response function, one must model the site itself, not the frequency response function directly. Having such a model, one can use existing time-domain, soil response analysis methods, e.g., the program SHAKE (Idriss *et al.*, 1991), to compute the frequency response function. The analysis would require computing the response of the soil column to a complex harmonic excitation for a long period in order to achieve the steady-state response, as required by the definition of that function. Naturally, such an approach can account for the non-viscous and nonlinear behavior of soils, albeit in an approximate "equivalent" linear sense. This analysis must be repeated for each frequency ω to obtain a complete description of $H_k(\omega)$. A more efficient approach is described below.

It is well known that for a linear system, the frequency response function is the Fourier transform of the unit-impulse response function, denoted $h(t)$. Thus, the frequency response function can be computed from

$$H(\omega) = \int_0^\infty h(t)\exp(-\mathrm{i}\omega t)\,\mathrm{d}t \tag{6}$$

By definition, $h(t)$ is the response of the system to an impulsive load of unit magnitude applied at time $t = 0$. For a given soil model, this can be easily computed by modeling the input excitation as a short duration pulse and scaling the response by the magnitude of the pulse. The advantage here, relative to the method described in the previous paragraph, is that $h(t)$ is computed by a single time-history analysis of the soil model. Furthermore, as $h(t)$ typically decays rapidly with time, it is not necessary to compute the soil response for too long a duration. It is important, however, to properly select the impulse magnitude so as to adequately account for the nonlinearity in the soil response.

The nonlinearity in the soil response depends primarily on the properties of the soil and the intensity of the ground motion, and secondarily on the duration and frequency content of the motion. For a given soil, the nonlinearity inherent in the computed $h(t)$ and, therefore, $H(\omega)$ depends on the magnitude of the impulse used. Naturally, it is desirable to select the impulse magnitude such that the nonlinearity inherent in the frequency response function is equivalent to the nonlinearity present in the soil response to a design earthquake.

To determine the required impulse magnitude, a parametric study with three soil models representing "stiff", "medium" and "soft" sites, shown in Fig. 1, and a large number of earthquake motions recorded on rock is performed. The selected ground motion records represent a wide variety in terms of their intensity, frequency content, and duration. For each site, the surface motion is computed with each of the rock motions as input by use of the SHAKE program and (4) is used to compute the "exact" frequency response function.

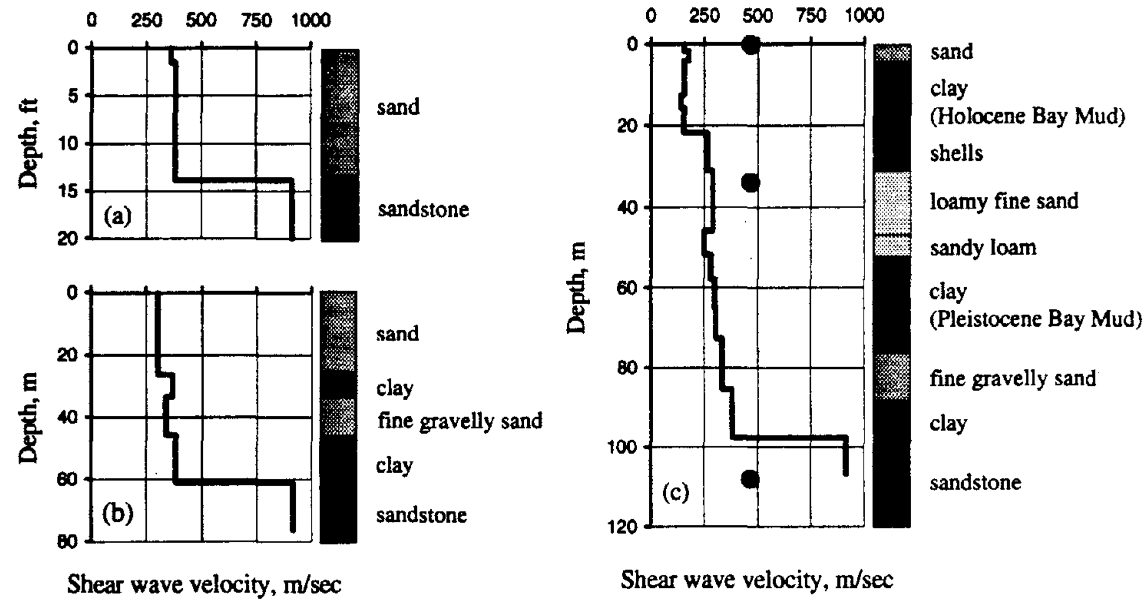

Fig. 1. Soil models for (a) stiff site, (b) medium site, and (c) soft site, Treasure Island

Then (6) is used to compute the theoretical frequency response function with varying impulse magnitude, and the "required" magnitude is determined by minimizing the difference between the two frequency response functions. Figure 2 summarizes the results of the analysis for the three sites where the required impulse magnitude is plotted versus the intensity of the input motion as described by the peak ground acceleration computed by SHAKE on the surface. No appreciable difference between the required impulse magnitudes for the three sites is observed. A least-square fit to the combined data gives the following relation between the required impulse magnitude, I, and the peak ground acceleration, A:

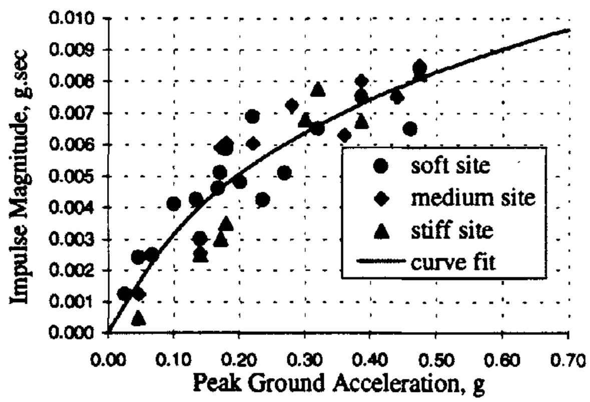

Fig. 2. Required impulse magnitude for equivalent linear system

$$I = -0.00213 + 0.01835A^{0.5} - 0.00512A \tag{7}$$

The procedure described above is clearly an approximate one. Hence, there is need to provide a verification of its accuracy. Given the complexity of the problem and lack of exact analytical solutions, comparison with recorded data is the obvious choice. However, it is necessary to select records that isolate the site-response effect from the effects of ground motion incoherence, wave passage, and attenuation. Downhole array recordings achieve this objective. The following section describes the selected records used in the subsequent analysis.

SELECTED DOWNHOLE ARRAY RECORDINGS

For experimental verification of the models in (3) and (6), two sets of downhole array recordings are used. The first set was recorded at the Treasure Island Geotechnical Downhole Array Station during the Gilroy, California, Earthquake of January 16, 1993 (Darragh *et al.*, 1993). The magnitude of the earthquake was 5.3 and the peak acceleration recorded on the ground surface and at 104m below were 0.0142g and 0.0032g, respectively. This motion obviously is not sufficiently strong to cause a significant amount of nonlinearity in the soil response. On the other hand, a good description of the site geology is available, thus allowing a refined modeling of the site. Figures 1c, the "soft" site model, describes the shear wave velocity and soil types with depth for this site. Figure 3 shows the first 20 seconds of the recorded acceleration time histories at three elevations. Strong amplification of the motion as it propagates upward is observed. For the purpose of this analysis, it is assumed that the bottom of the downhole represents the base rock. The second set of recordings was taken at Chiba Experimental Station during Tokyo area earthquake of November 6, 1985 (Katayama *et al.*, 1990). The magnitude of the earthquake was 5.0 and peak ground accelerations recorded on the surface and at 40m below the surface were 0.077g and 0.0135g, respectively, which again shows a very strong amplification. The recorded acceleration time histories at three elevations are shown in Fig. 4.

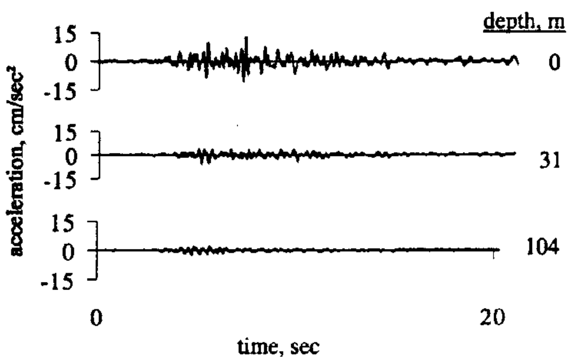

Fig. 3. Recorded accelerations at Treasure Island downhole array for Gilroy earthquake of January 16, 1993

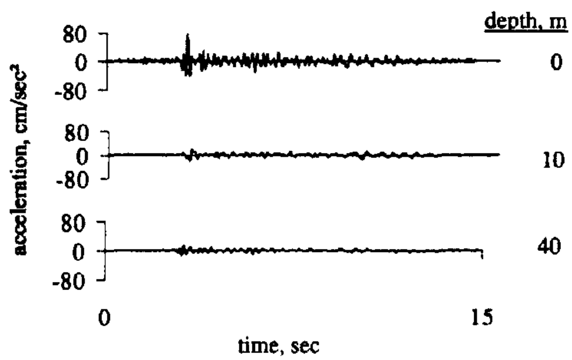

Fig. 4. Recorded accelerations at Chiba downhole array for Tokyo area earthquake of November 6, 1985

Unfortunately geologic information available for this site only allowed a crude modeling of the soil, which is shown in Fig. 5.

It is appropriate at this point to stress the need for downhole recordings at soil sites during strong earthquakes, especially near the source. The significant amplifications observed in the above two sets of recordings highlight the importance of the soil response effect and its influence on the spatial variability of ground motions in regions with rapidly varying local geology.

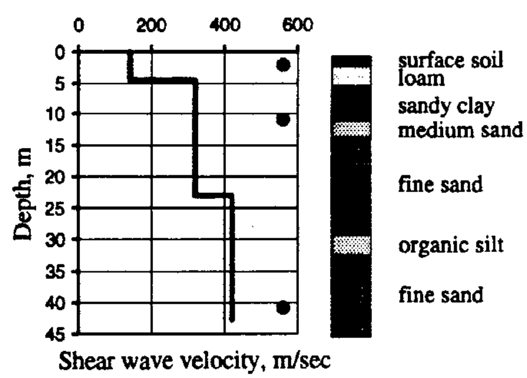

Fig. 5. Soil model for Chiba site

MODEL VERIFICATION

To verify the procedure for determining the site frequency response function, each of the soil models in Figs. 1c and 4 are subjected to a short-duration triangular acceleration impulse at the base level. The required impulse magnitudes (area of the triangle) is obtained from (7) resulting in $I = 0.049$ cm/s for the Treasure Island records and $I = 0.0686$ cm/s for the Chiba records. The program SHAKE (Idriss *et al.*, 1991) is used to compute the soil unit impulse response function $h(t)$ at each site. The Fourier transforms of these functions represent the theoretical predictions of the frequency response function for each site. The moduli of these functions are shown as dashed lines in Figs. 6ab and 7a. The "exact" moduli of the frequency response functions, shown as solid lines in Figs. 6ab and 7a, are computed by use of (4) and the recordings at each site.

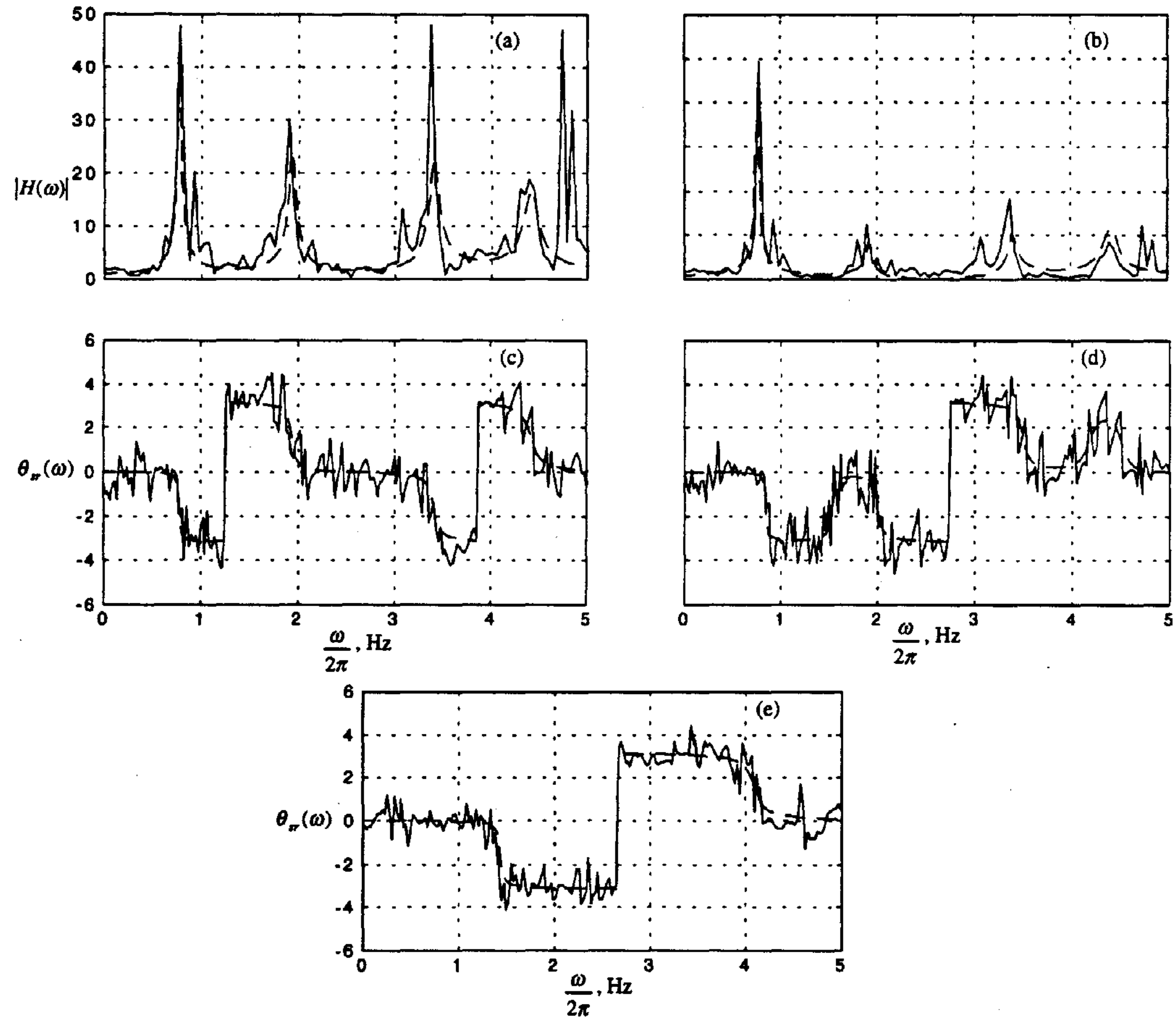

Fig. 6. Comparison of model predictions (dashed lines) with "exact" results (solid lines) for Treasure Island site: (a) frequency response function at surface, (b) frequency response function at depth 31m, (c) phase angle between motions at 0m and depth 104m, (d) phase angle between motions at depths 31m and 104m, (e) phase angle between motions at 0m and depth 31m.

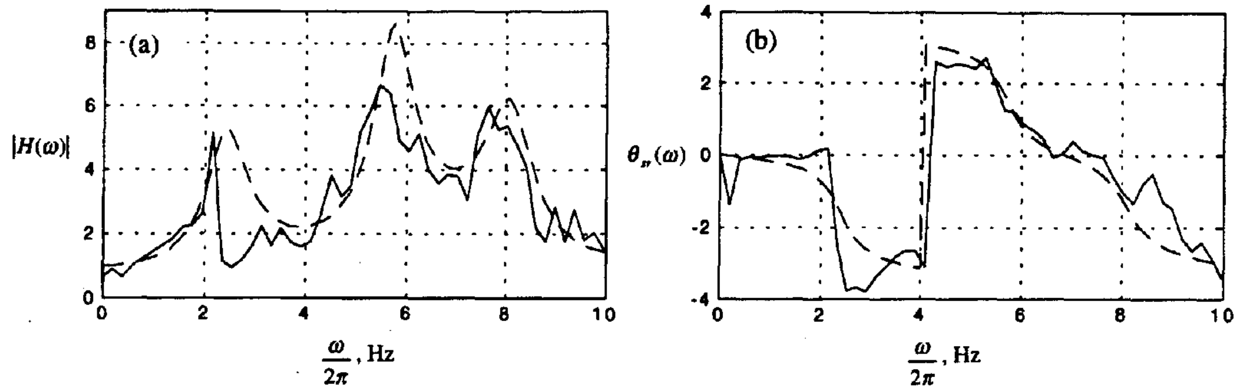

Fig. 7. Comparison of model predictions (dashed lines) with "exact" results (solid lines) for Chiba site: (a) frequency response function at surface, (b) phase angle between motions at 0m and 40m.

For both sites the agreement between the theoretical predictions and "exact" estimates of the frequency response function are remarkable. This is partly due to the low intensity of the motion and hence linearity of the soil response. It is interesting to observe that the two sites have multiple resonant frequencies. Obviously, if a single-degree-of-freedom soil model as in (5) is used, at best one can model one resonant frequency. However, one should not discard this simple model too soon, since there are many structures, e.g., long-span bridges, for which the high-frequency components of ground motion are not significant and even this simple model may be adequate if it captures the first resonant frequency well.

We now turn to the verification of the model in (3) for the coherency phase angle due to the site-response effect. An "exact" estimate of the phase angle is computed for each site by using the formula

$$\theta_{\text{exact}}(\omega) = \tan^{-1}\left(\frac{\operatorname{Im}\Phi_{\text{base-surface}}(\omega)}{\operatorname{Re}\Phi_{\text{base-surface}}(\omega)}\right) \tag{8}$$

where $\Phi_{\text{base-surface}}(\omega)$ is the cross-power spectral density of the recorded motions at the base and surface levels. The predictions of the phase angle based on the proposed model are computed by use of (3) and the frequency response function obtained by the procedure described earlier (i.e., the dashed curves in Figs. 6ab and 7a. The results are shown in Figs. 6c-e and 7b. The agreement between the "exact" and theoretical values is remarkable for both sites. It is worth noting that sharp changes of the phase angle occur at points of resonant frequency for each site, the sharpness being dependent on the bandwidth of the frequency response function. It follows that in predicting the site-response effect, it is essential to accurately predict the resonant frequencies for the site of interest. It is also evident that the site response effect will be most significant for multiply supported structures that have supports situated on sites with different resonant frequencies.

SUMMARY AND CONCLUSIONS

Downhole array recordings are used to verify a theoretical model for the site-response component of the ground motion spatial variability. A procedure is developed and verified for computing the frequency response function of a soil site that is required for the model. Predictions by the theoretical model are in close agreement with "exact" results obtained from the recorded motions at two downhole arrays.

ACKNOWLEDGMENT

This study was supported by the California Department of Transportation Contract No. 59U429, which is gratefully acknowledged.

REFERENCES

Abrahamson, N.A., J.F. Schneider, and J.C. Stepp (1991). Empirical spatial coherency functions for application to soil-structure interaction analysis. *Earthq. Spectra*, **7**, 1-28.

Clough, R.W., and J. Penzien (1993). *Dynamics of structures*, 2nd Ed., McGraw-Hill Book Co., New York, NY.

Der Kiureghian, A. and A. Neuenhofer (1992). Response spectrum method for multiple-support seismic excitation. *Earthq. Eng. Struc. Dyn.*, **21**, 713-740.

Der Kiureghian, A.(1994). Model for coherency function for spatially varying ground motions. *Proc., 5th U.S. National Conf. Earthq. Eng.*, Chicago, IL, July 1994, **I**, 541-550.

Der Kiureghian, A.(1996). A coherency model for spatially varying ground motions. *Earthq. Eng. Struct. Dyn.*, **25**, 99-111.

Darragh, R., M. Huang and A. Shakal (1993). "Processed strong-motion records from the CSMIP/NSF Treasure Island geotechnical array for the Gilroy earthquake of 16 January 1993." *Report No. OSMS 93-09*, California Strong Motion Instrumentation Program, California Department of Conservation, Division of Mines and Geology, Office of Strong Motion Studies.

Idriss, I.M., J. I. Sun and P.B. Schnabel. (1991). "User's manual for SHAKE91: a computer program for conducting equivalent linear seismic response analyses of horizontally layered soil deposits." *Center for Geotechnical Modeling, Department of Civil & Environmental Engineering, University of California at Davis, CA.*

Katayama, T., F. Yamazaki, S. Nagata, L. Lu and T. Turker (1990). "Development of strong motion database for the Chiba seismometer array." *Report No. 90-1 (14)*, Earthquake Disaster Mitigation Engineering, Institute of Industrial Science, University of Tokyo.

Schneider, J.F., J.C. Stepp and N. Abrahamson (1992). The spatial variation of earthquake ground motion and effects of local site conditions. *Proc., 10th World Conf. Earthq. Eng.*, Madrid, Spain, July 1992, **II**, 967-972.

Somerville, P.G., J.P. McLaren, C.K. Saikia, and D.V. Helmberger (1988). Site-specific estimation of spatial incoherence of strong ground motion. *Earthquake Engineering and Soil Dynamics II -- Recent Advances in Ground-Motion Evaluation*, ASCE Geotechnical Specialty Publication No. 20, J.L.Von Thun, Ed., 188-202.

Zerva, A. and T. Harada (1994). A site-specific model for the spatial incoherence of the seismic ground motions. *Proc., 5th U.S. National Conf. Earthq. Eng.*, Chicago, IL, July 1994, **IV**, 931-940.

EVALUATION OF EARTHQUAKE INDUCED SLIDING IN GRAVITY DAMS

GREGORY L. FENVES and JUAN W. CHÁVEZ

Department of Civil and Environmental Engineering, University of California, Berkeley
Berkeley, CA 94720 U.S.A.

ABSTRACT

The stability of a concrete gravity dam against excessive sliding at the dam base must be assured during an earthquake. Sliding refers to concentrated deformation at the interface between the dam and the foundation rock. The objective of a sliding evaluation procedure is to first guarantee stability, and second estimate the deformation at the base. Current evaluation techniques for sliding are either empirical, based on an equivalent static equilibrium model, or involve very simplified assumptions. The present work applies a novel modeling and solution procedure (hybrid frequency-time domain analysis) which accounts for the dynamics of the dam, foundation rock flexibility, compressible water, and a Mohr-Coulomb model for base sliding. The results of an extensive parametric study of gravity dams illustrate the important factors affecting the earthquake induced base sliding displacement. The foremost factor is foundation rock flexibility: estimates of base sliding assuming rigid foundation rock are much larger than when foundation rock flexibility is included. The sliding is also sensitive to the coefficient of friction and cohesion of the interface zone. A framework for evaluation sliding stability is proposed.

KEYWORDS

Dam; gravity dam; concrete; sliding; stability; friction; nonlinear analysis.

INTRODUCTION

The stability of concrete gravity dams with respect to large rigid-body displacements in the downstream direction must be assessed in a seismic safety evaluation. Sliding can occur when the forces on the interface zone between the dam and foundation rock exceed the strength of the zone. The traditional check of sliding stability involves computing a factor of safety (*FS*) against sliding using a Mohr-Coulomb model of the concrete and foundation materials in the interface zone and equivalent static loads on the dam that represent the dynamic effects of an earthquake. The *FS* is defined for a postulated failure surface as:

$$FS = \frac{C + \mu N_{st}}{V + V_{st}} \tag{1}$$

where N_{st} and V_{st} are the gravity normal and tangential forces (self weight, hydrostatic, and uplift) on the interface zone, V is the maximum dynamic tangential force. The properties of the interface zone are represented by the coefficient of friction, μ, and total cohesion force, C. The cohesion force is $C = cA$, where c is the unit cohesion stress of the interface (force/area) and A is the area of the interface zone developing cohesion. The latter is typically assumed to be the portion of the interface plane with compressive normal stresses due to the forces N_{st}, V_{st}, and V. The typical evaluation procedure involves investigating various interface zones to find the lowest FS (according to the upper bound theorem). For extreme loads such as an earthquake an FS greater than unity is considered acceptable.

A consistent definition of the equivalent static loads, recognizing all the dynamic effects in the force, can be used to determine if a dam will slide using Eq. 1. Fenves and Chopra (1987) have presented a simplified analysis procedure that can be used to compute V including the characteristics of the earthquake, and the effects of dam-water interaction, dam-foundation rock interaction, and reservoir bottom absorption.

However, a strength criterion based on equivalent static earthquake forces, such as Eq. 1, cannot give information about the magnitude of the rigid-body displacement once sliding commences. The earthquake induced sliding displacement of a dam can be rationally estimated by a dynamic analysis of the system which accounts for the frequency-dependent effects of dam-water and dam-foundation rock interactions and the nonlinear sliding behavior at the dam-foundation rock interface. Although several investigators have examined the earthquake response of gravity dams including sliding (Leger and Katsouli, 1989; Chopra and Zhang, 1991; Hall, Dowling, and El-Aidi, 1991), the studies were limited by assumptions about the dam system.

Chávez and Fenves (1995a, 1995b) have presented an analysis method based on the hybrid frequency-domain procedure (Darbre and Wolf, 1988) for analysis of gravity dam monoliths including sliding. The analysis rationally accounts for the frequency-dependent characteristics of the system and the nonlinear behavior of a sliding on a possibly sloped interface between the dam and foundation rock.

The objectives of this paper are to summarize the model used for dynamic analysis of gravity dams including sliding, illustrate the important factors affecting the sliding displacement, examine a case study to show the relationship between the static factor of safety and the sliding displacement, and finally propose a framework for evaluating the sliding stability of gravity dams.

DYNAMIC ANALYSIS FOR SLIDING

Modeling

The idealized concrete gravity dam, shown in Fig. 1, is a two-dimensional monolith (height=H_s), with rigid base supported by flexible foundation rock and impounding a reservoir of compressible water (depth=H). The dam may slide along the interface between the dam base and the foundation rock. Rocking of the dam about the base is not represented in the model. The system is subjected to horizontal and vertical components of free-field earthquake ground motion at the base of the dam.

The monolith is modeled using plane stress finite elements with linear elastic material properties. The water impounded in the reservoir is idealized as a two-dimensional domain extending to infinity in the upstream direction. The water is treated as an inviscid and compressible fluid that produces hydrodynamic pressures that are dependent on the excitation frequency. The foundation rock is idealized as a homogeneous, isotropic and viscoelastic half-plane.

The interface between the dam monolith and the foundation rock is assumed to be a straight surface with the resistance to sliding governed by the Mohr-Coulomb law. This friction model allows quantification of the deformation in the interface zone without requiring detailed modeling of the complex region that consists of shear keys, grout curtains, and roughened surfaces. The sliding resistance at the interface depends on a cohesion force, the coefficient of friction, and the time varying normal force. Although degradation of the friction parameters and rate-dependent effects could be included, there is not sufficient experimental data to develop such as refined model. The model assumes that sliding occurs along the entire interface.

Solution Procedure

The equations of motion for the dam-water-foundation rock system include the frequency-dependent hydrodynamic forces acting on the dam, the dam-foundation rock interaction forces, and the nonlinear inertia forces at the base due to sliding of the dam along the interface. A Rayleigh-Ritz transformation reduces the degrees-of-freedom for the dam to a small number of generalized coordinates.

The hybrid-frequency time domain procedure (Darbre and Wolf, 1988) is used to solve the nonlinear and frequency-dependent equations of motion. The detailed solution procedure for dams is described by Chávez and Fenves (1995a). The procedure iterates over segments of time in three major steps:

1. Linearization of the equations of motion. The nonlinear inertia forces due to sliding are estimated using the current sliding acceleration history.
2. Solution of the linearized equations of motion. The linearized equations of motion are solved in the frequency domain to account for the frequency dependency of the interaction forces. The resultant forces due to dynamic loads at the base of the dam, that includes the shear force $V(t)$ and normal force $N(t)$ are computed at this stage.
3. Determination of sliding state in time domain. The dam slides when the the total shear force at the base, according to Mohr-Coulomb law, exceeds the strength at the interface:

$$|V(t) + V_{st}| \geq |C + \mu\,[N(t) + N_{st}]| \qquad (2)$$

Convergence for a segment of time is achieved when the maximum difference between successive iterations of the response quantities is less than a tolerance at every time step in the segment.

The earthquake analyses are performed using the computer program EAGD-SLIDE, which implements the solution procedure (Chávez and Fenves, 1994).

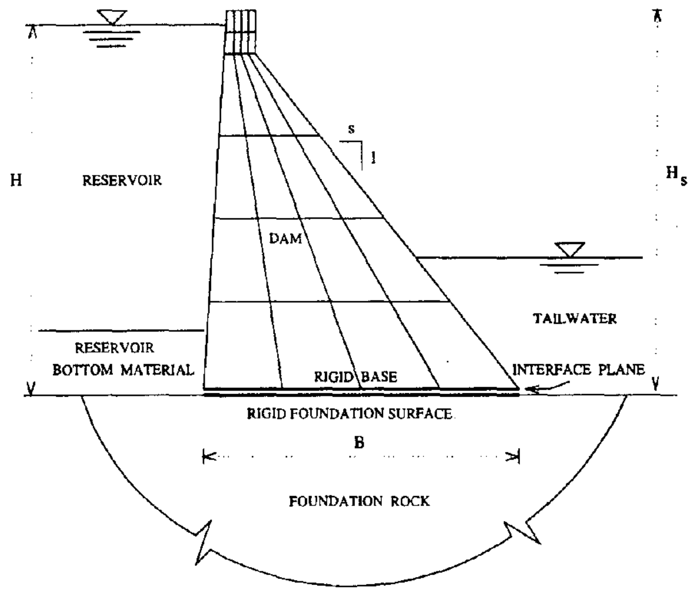

Fig. 1. Dam-reservoir-foundation rock system with interface plane for sliding at the base.

IMPORTANT EFFECTS ON SLIDING

A typical concrete gravity dam monolith with full reservoir is used to investigate the effects peak ground acceleration, foundation rock flexibility, coefficient of friction, and water compressibility on the sliding displacement at the base.

The height of the dam is varied from 25 m (82 ft) to 175 m (574 ft). The modulus of elasticity of concrete, E_{cd}, is 27.6 GPa (4 million psi). The modulus of elasticity of the foundation rock, E_{fr}, varies according to the moduli ratio $E_{fr}/E_{cd} = \infty, 1.0, 0.25$. The first case corresponds to a rigid foundation rock, and the third case corresponds to a very flexible foundation rock. A hysteretic damping coefficient of 0.10 is assumed for the dam and foundation rock. The cohesion force at the base is assumed to be zero and the coefficient of friction varies from 0.8 to 1.2. The monolith is subjected to the S69E horizontal component of the 1952 Taft ground motion, scaled to 0.3g, 0.4g, 0.5g, and 0.6g.

The analysis is simplified by using one generalized coordinate to represent the motion of the dam in its fundamental vibration mode. The sliding displacements computed using the simplified model are a good approximation of the displacements obtained by using a finite element discretization of the dam. An extensive parametric study using this simplified analysis is presented by Chávez and Fenves (1995b).

Influence of Peak Ground Acceleration

The maximum sliding displacement increases substantially with increasing peak ground acceleration, as shown in Fig. 2(a). The sliding increase by a factor of five times when the peak ground acceleration increases from 0.3g (moderate earthquake) to 0.6g (strong earthquake). Dams taller than 50 m (164 ft) subjected to the same peak ground acceleration have more base sliding as the foundation rock becomes more rigid.

Influence of Foundation Rock Flexibility

Foundation rock flexibility affects the value of sliding displacement because the vibration period of the system lengthens and the damping increases. As shown in Fig. 2(a), the peak of the sliding spectrum decreases as the foundation rock flexibility increases. The shorter dams are shifted into the amplified region of the response spectrum for the ground motion, because the period of the system lengthens as the foundation rock flexibility increases.

Another view of how the effects of foundation rock flexibility depend on dam height is shown in Fig. 2(b). For short dams, height less than 50 m (164 ft), the flexible foundation rock has almost no effect on the sliding displacement. For taller dams, height 150 m (492 ft), the sliding displacement decreases as the foundation rock becomes more flexible.

The base sliding displacements computed using the regression equation by Danay and Adeghe (1993) for a dam on rigid foundation rock are also shown in Fig. 2(b). There is a good agreement between the sliding displacements computed using the present model and the regression equation for the mean plus two standard deviations for 50 m (146 ft) dams. For taller dams, the present results fall between the expression for the mean and the mean plus two standard deviations. The regression equation overestimates the sliding displacement when dam-foundation rock interaction effects are important since such effects were not included in the development of the approximate expression.

Influence of Coefficient of Friction

The maximum sliding displacement increases nonlinearly as the coefficient of friction decreases, as shown in Fig. 2(c). For the same value of μ, a dam on rigid foundation rock slides more than a dam on flexible foundation rock. The location of peaks of maximum sliding shift from tall dams, H_s=125 m (410 ft), on rigid foundation rock, to short dams, H_s=75 m (246 ft), on flexible foundation rock with $E_{fr}/E_{cd} = 0.25$, due to the lengthening of the period of the dam system as the dam height increases and the foundation rock flexibility increases.

Influence of Water Compressibility

The sliding displacement for a dam is greater when the water is considered to be compressible compared with the case of incompressible water, as shown in Fig. 2(d). Water compressibility has the largest effect when the dam is on rigid foundation rock, especially for dams less than 150 m (492 ft) tall. In this range of dam heights, the sliding displacement obtained with incompressible water is as much as 40% less than the displacement with compressible water. The effects of compressibility are smaller for dams on flexible foundation rock because the foundation rock damping generally reduces the importance of dam-water interaction.

EVALUATION OF SLIDING

This section examines the earthquake earthquake sliding response of a typical concrete gravity dam. The static procedure using a *FS* and the dynamic analysis to compute the sliding displacement are investigated and the results are compared.

The tallest monolith, 122 m (400 ft) high, of Pine Flat dam is selected for the evaluation. Two cases are considered: dam on rigid foundation rock, and dam on flexible foundation rock with $E_{fr}/E_{cd} = 1$. The impounded compressible water has a depth of 116.2 m (381 ft). The unit cohesion stress at the base varies

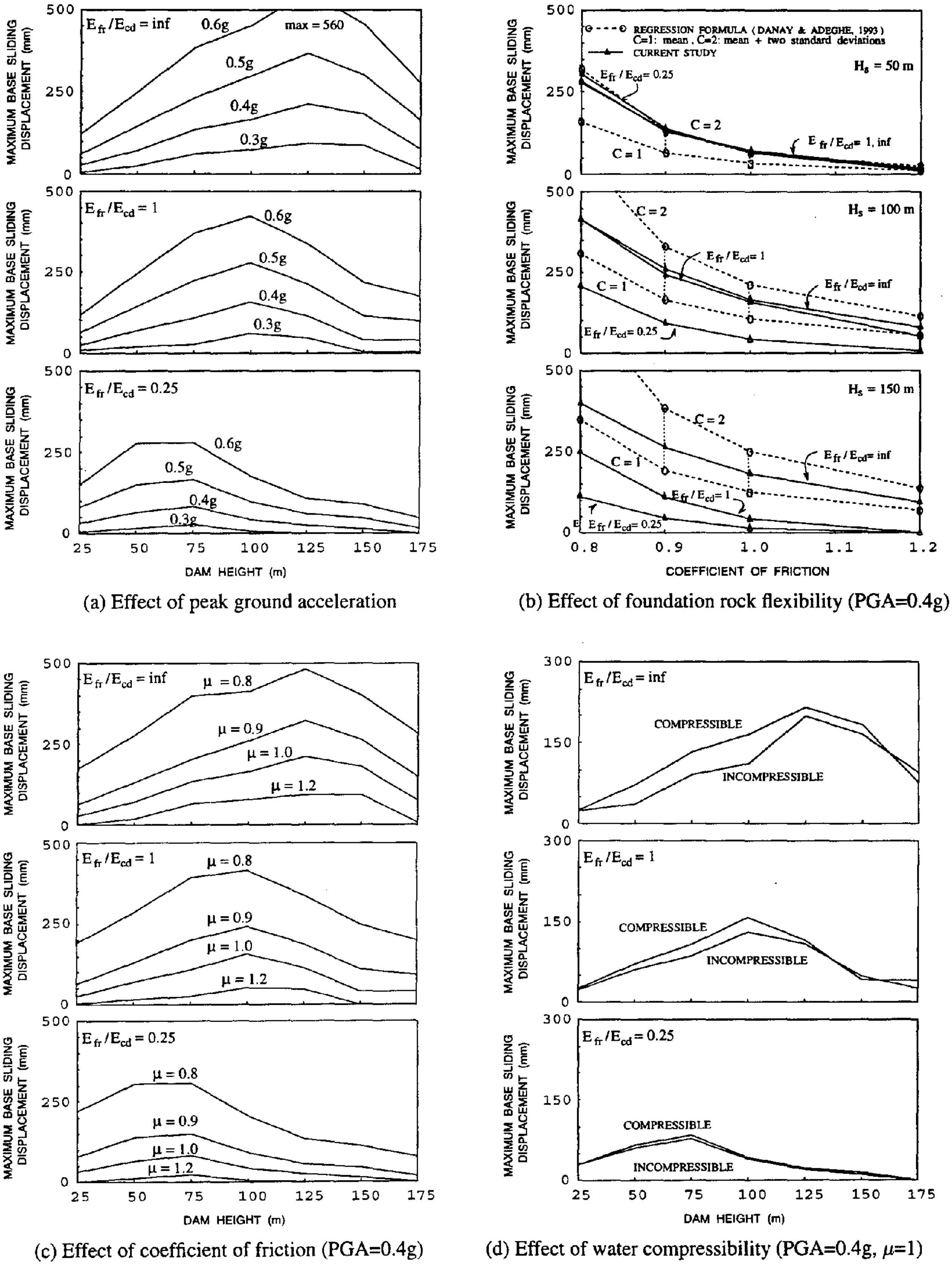

(a) Effect of peak ground acceleration

(b) Effect of foundation rock flexibility (PGA=0.4g)

(c) Effect of coefficient of friction (PGA=0.4g)

(d) Effect of water compressibility (PGA=0.4g, μ=1)

Fig. 2. Important effects on the maximum base sliding displacement of a typical dam with full reservoir, $C = 0$, subjected to the Taft S69E ground motion.

from 0 to 800 kPa, and the coefficient of friction varies from 0.75 to 1.25. The dam is subjected to the S69E horizontal component of the 1952 Taft ground motion, scaled to a peak ground acceleration of 0.6g.

Static Procedure

The equivalent static analysis for stability uses Eq. 1 to compute a factor of safety against sliding. The area developing cohesion is $A = rA_g$, where A_g is the gross section area at the base and r is a reduction factor that accounts for cracking of the concrete at the base (Bureau of Reclamation, 1976). The factor r is 0.66 for the dam on rigid foundation rock, and 0.85 for the dam on flexible foundation rock, using the static and maximum earthquake forces for Pine Flat dam. The equivalent static loads are computed using the simplified analysis procedure by Fenves and Chopra (1987) that includes the characteristics of the earthquake, the effects of the dam-water interaction, dam-foundation rock interaction, and reservoir bottom absorption. Computed values of *FS* are shown in Fig. 3(a) for rigid foundation rock and in Fig. 4(a) for flexible foundation rock. The *FS* for the dam on flexible foundation rock is larger than the *FS* for the dam on flexible foundation rock. For the cases when *FS* is much less than unity, large sliding displacements can be expected.

Dynamic Analysis

The dynamic analysis, using EAGD-SLIDE (Chávez and Fenves, 1994), is performed to compute the base sliding displacements of Pine Flat dam for the cases considered. The results are shown in Fig. 3(b) for rigid foundation rock and in Fig. 4(b) for flexible foundation rock. For both cases the sliding displacement decreases substantially with an increase of the coefficient of friction and unit cohesion stress. The dam on rigid foundation rock slides more than the dam on flexible foundation rock.

Comparison

Figure 5 shows the comparison between *FS* and the sliding displacement for the Pine Flat dam for the different cases of coefficient of friction and unit shear stress. The dam slides when the safety factor is less than unity and sliding increases as the safety factor decreases.

A FRAMEWORK FOR EVALUATING SLIDING STABILITY

The previous results show that the static procedure (Eq. 1) for determining the sliding factor of safety, with a rational definition of the equivalent lateral earthquake load, can be used to determine when sliding is prevented from cases when sliding will occur. If the static procedure shows that sliding will not occur ($FS > 1$), then no further analysis is required.

For cases when *FS* is less than unity, the proper question is not whether the dam is stable, but rather what is the magnitude of the sliding displacement. The dynamic analysis procedure described in this paper can be used to evaluate sliding displacement. An important parameter for the sliding analysis is the value of the cohesion force. Based on the results in the previous section, the cohesion force may be selected as $C = cA$, where A is the area of the interface under compression as determined from the static analysis with the equivalent lateral forces. Of course an upper bound on the sliding displacement can be obtained by assume zero cohesion, $C = 0$. Although it could be argued that zero cohesion is appropriate once sliding commences, it is believed that zero cohesion is overly conservative because the materials do not necessarily lose all cohesive properties under small deformations.

In the current version of the analysis procedure, the cohesion force is a constant (Eq. 2), hence requiring an assumption on the value of A. A future modification of the program would be to determine the time varying value of area under compression and hence the area providing cohesion.

A dynamic analysis accounting for all the factors effecting sliding provides a rational estimate for the sliding displacement. Although there have been attempts to approximate sliding displacements by sliding block analysis or definition of a critical acceleration causing sliding, they can produce substantial errors (Chopra and Zhang, 1991).

The magnitude of the sliding displacement from a dynamic analysis must be compared with a criterion for the maximum allowable displacement. This is a difficult question to answer because sliding may cause damage to joints, grout curtains, and drains, and the possibility of water intrusion into a damaged interface zone must be considered. However, for an extreme earthquake with low probability of occurrence (such as a maximum

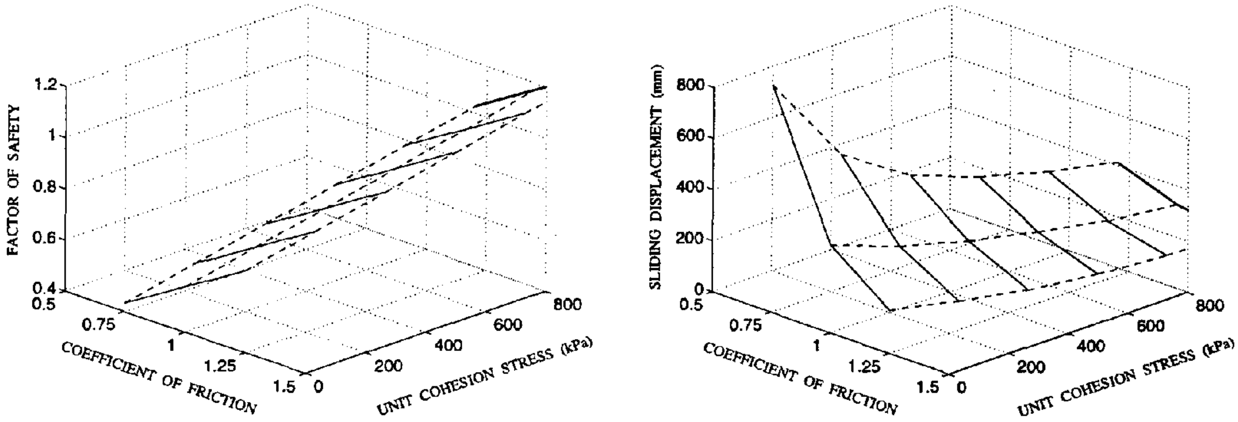

(a) Static procedure

(b) Dynamic analysis

Fig. 3. Static solution and dynamic evaluation of sliding for Pine Flat dam on rigid foundation rock.

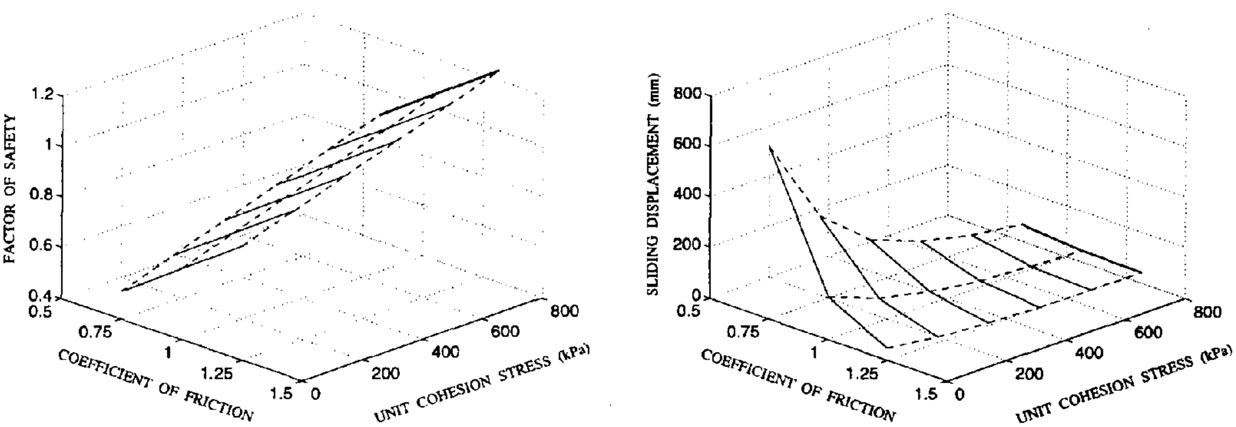

(a) Static procedure

(b) Dynamic analysis

Fig. 4. Static solution and dynamic evaluation of sliding for Pine Flat dam on flexible foundation rock.

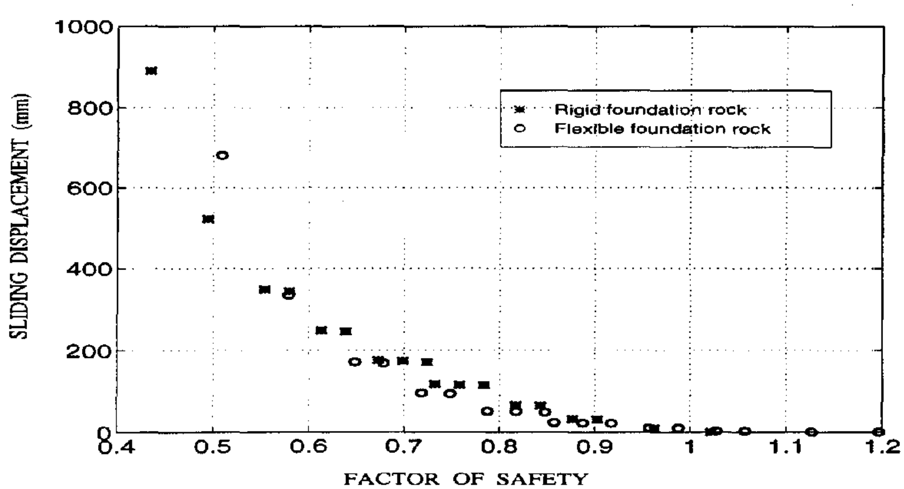

Fig. 5. Comparison between factor of safety and sliding displacement.

credible event), allowing sliding displacements of less than 50 mm appears to be reasonable.

Finally, there may be an intermediate range of the factor of safety near unity, $FS_{cr} < FS < 1$, where it can be expected that sliding displacements are small enough to not require a dynamic analysis. The previous results indicate that an $FS_{cr} = 0.90$, for which the maximum forces exceed the interface strength by only 10% for a short duration, correlates with limited sliding displacement. Again it must emphasized that the factor of safety should be computed using a rational procedure for the earthquake forces, such as by Fenves and Chopra (1987). It is very important that the effects of dam-foundation rock interaction be included in the static evaluation procedure. Otherwise, the sliding determination will be based on unrealistically small factors of safety or large sliding displacements.

ACKNOWLEDGMENTS

The research described in this paper was support by the National Science Foundation under Grant No. BCS-8896121. The authors thank the Program Director, Dr. S. C. Liu for his support.

REFERENCES

Bureau of Reclamation (1976). "Design of Gravity Dams," A Water Resources Technical Publication.

Chávez, J. and Fenves, G. (1994). "EAGD-SLIDE: A Computer Program for the Earthquake Analysis of Concrete Gravity Dams Including Base Sliding," *Report No. UCB/SEMM-94/02*, Department of Civil Engineering, University of California, Berkeley, California.

Chávez, J. and Fenves, G. (1995a). "Earthquake Analysis of Concrete Gravity Dams," *Earthquake Engineering and Structural Dynamics*, Vol. 24, No. 5, pp. 673-686.

Chávez, J. and Fenves, G. (1995b). "Earthquake Response of Concrete Gravity Dams Including Base Sliding," *Journal of Structural Engineering, ASCE*, Vol. 121, No. 5, pp. 865-875.

Chopra, A. K. and Zhang, L. (1991). "Base Sliding Response of Concrete Gravity Dams to Earthquakes," *Report No. UCB/EERC-91/05*, Earthquake Engineering Research Center, University of California, Berkeley, California.

Danay, A. and Adeghe, L. N. (1993). "Seismic Induced Slip of Concrete Gravity Dams," *Journal of Structural Engineering, ASCE*, Vol. 119, No. 1, pp. 108-129.

Darbre, G. R. and Wolf, J. P. (1988). "Criterion of Stability and Implementation Issues of Hybrid Frequency-Time Domain Procedure for Non-Linear Dynamic Analysis," *Earthquake Engineering and Structural Dynamics*, Vol. 16, No. 4, pp. 569-581.

Fenves, G. and Chopra, A. K., (1987). "Simplified Analysis of Concrete Dams," *Journal of Structural Engineering, ASCE*, Vol. 113, No. 8, pp. 1688-1708.

Hall, J. F., Dowling, M. J. and El-Aidi, B. (1991). "Defensive Design of Concrete Gravity Dams," *Report No. EERL 91-02*, California Institute of Technology, Pasadena, California.

Leger, P., and Katsouli, M. (1989). "Seismic Stability of Concrete Gravity Dams," *Earthquake Engineering and Structural Dynamics*, Vol. 18, No. 6, pp. 889-902.

EARTHQUAKE INFORMATION SOURCES ON THE INTERNET

KATHERINE A. FROHMBERG

Earthquake Engineering Research Center
University of California at Berkeley
1301 S. 46th St, Richmond, CA 94804-4698 USA

ABSTRACT

As a service to members of the international earthquake community, the author has compiled this directory of earthquake sources on the Internet. It is a selected world-wide list, providing e-mail, telnet, finger, anonymous ftp, gopher, or world-wide web listings for organizations considered most relevant to the earthquake engineering community. Due to limitations of space, organizations with a more seismological orientation have been omitted, however, most of the sites listed below provide links to seismological sites. This list is accurate as of January 1, 1996.

This paper does not attempt to provide technical information on how to access the Internet or use the various utilities such as finger or telnet. Access is very dependent on local conditions, and there are many books available which describe the use of these utilities. Since internet addresses can change without warning, an e-mail address is provided wherever possible. The user should know that Internet utilities are upwardly compatible, thus from the World Wide Web one can access anonymous ftp sites, finger sites, and gopher sites without any special knowledge or information. Most of the Web sites listed provide transparent links to gopher, ftp, and finger sites.

Many earthquake organizations do not yet have World Wide Web or gopher sites, but routinely do business by electronic mail. Those organizations are listed at the end with their e-mail addresses.

KEYWORDS

Internet, World Wide Web, Telnet, Gopher, Information Sources, finger, ftp.

GATEWAY SYSTEMS

The Internet in its current state is analogous to the United States highway system without any roadmaps. Gateway systems are springing up which either impose a hierarchical organization on Internet sites (Yahoo) or which search words or terms within Internet sites (Inktomi).

Yahoo

web site: *http://www.yahoo.com/Science/Earth_Sciences/Geology_and_Geophysics/Seismology*
Yahoo provides hierarchical subject access to the Internet world. It is well organized and updated continuously. The following alternate path in Yahoo provides access to the same directory of earthquake information as is found under Geology & Geophysics:
http://www.yahoo.com/environment_and_nature/disasters

Inktomi
web site: *http://inktomi.berkeley.edu*
e-mail: *brewer@cs.berkeley.edu*
Inktomi provides keyword access to the World Wide Web. Inktomi ranks results by relevance. However, a non-specific search on a word like "earthquake" will result in thousands of hits, most of them not useful. Inktomi is best used if searching for a particular organization or person. It is not useful to search for a specific engineering term on Inktomi (such as "shear walls").

Surfing the InterNet for Earthquake Data
web site: *http://www.geophys.washington.edu/seismosurfing.html*
e-mail: *steve@geophys.washington.edu*
Steve Malone, seismologist at the University of Washington, maintains an up-to-date listing (with links) to organizations with earthquake data. This is the most complete site for links to earthquake and seismological organizations in various parts of the world.

HazardNet
web site: *http://hoshi.cic.sfu.ca:80/~hazard/IMFORMAT/quake.html*
e-mail: *anderson@sfu.ca*
HazardNet is a prototype natural and technological hazard information sharing network under development as a collaborative demonstration project of the International Decade for Natural Disaster Reduction. It is based at the Centre for Policy Research on Science and Technology, Simon Fraser University, Vancouver, Canada. The earthquake section provides access to many international sites and organizations.

DISCUSSION LISTS

Bigquake
Send e-mail to: *bigquake-request@neis.cr.usgs.gov.* In the body of your message, type *subscribe bigquake.* The National Earthquake Information Center (NEIC) is mandated to put out news releases on all earthquakes larger than 6.5 worldwide, thus, all such quakes should appear on Bigquake fairly quickly. NEIC tries to include as many 5.5 or greater earthquakes as possible worldwide. NEIC does not attempt to release the smaller California earthquakes due to their frequency and because USGS offices in Menlo Park and Pasadena have better capabilities for locating and computing their magnitudes. With the exception of those occurring in California and Alaska, the vast majority of quakes generating felt reports in the U.S. are included on Bigquake.

Qedpost
Send e-mail to: *qedpost-request@neis.cr.usgs.gov.* In the body of your message, type *subscribe qedpost.* Qedpost stands for Quick Epicenter Determinations from the National Earthquake Information Center. This list provides notification of all earthquakes processed by the National Earthquake Information Center.

Disaster Research Electronic Newsletter
Send e-mail to: *listproc@lists.colorado.edu.* In the message body type, *subscribe Hazards yourname*
This moderated newsletter is issued approximately twice a month by the Natural Hazards Research and Applications Information Center at the University of Colorado, Boulder, and covers all hazards. Back

issues of Disaster Research are archived at the NHRAIC home page (*http://adder.colorado.edu/~hazctr/intro.html*). Disaster Research serves as an informal communication tool among persons interested in hazards research and disaster management.

NEWSGROUPS

The newsgroup *sci.geo.earthquakes* contains serious technical discussion of recent earthquakes from the geological point of view. Other newsgroups such as *ca.earthquakes*, *alt.disasters.earthquake*, and *fj.misc.earthquake* tend to be less technical.

TELNET SITES

Earthquake Engineering Abstracts
Telnet to: *melvyl.berkeley.edu*
Earthquake Engineering Abstracts is a bibliographic database produced by the National Information Service for Earthquake Engineering, Earthquake Engineering Research Center, University of California at Berkeley. Enter your terminal type (usually vt100). Once in Melvyl, type *use eea* to enter the Earthquake Engineering Abstracts database. Help screens are available.

Quakeline®
Telnet to: *bison.cc.buffalo.edu*
Quakeline® is a bibliographic database produced by the National Center for Earthquake Engineering Research/Information Center at the State University of New York, Buffalo. When asked for terminal emulation, press the <enter> key to get a listing of choices, and enter your response (usually vt100). At the blank screen, press <enter>. Once connected to the DATABASE SELECTION MENU, choose the "INDX" menu option by typing *INDX <enter>* and then type *QKLN <enter>*. Follow screen instructions for searching. To exit, type *STOP <enter>* at any screen.

Quick Epicenter Determinations
Telnet to: *neis.cr.usgs.gov.* Username: QED
The Quick Epicenter Determinations (QED) provides a listing of earthquakes which have occurred during the last three weeks. Events within seven days of real-time are still being revised and republished for the QED as new data are received from contributing observatories. Events older than seven days are no longer revised, but are retained in the database. The event list is revised every morning. In addition to the daily update, any earthquake for which the NEIC has issued a press release is added to the QED list within about one hour of the time of release. Events in the QED database may be searched by date range, magnitude, or geographic location. The Earthquake Lists option provides choices for viewing seven lists: significant earthquakes of the world, significant earthquakes of the United States, most destructive earthquakes in the world, worldwide earthquakes causing 1000 or more deaths, the ten largest earthquakes in the United States, earthquake facts and statistics, and the number of occurrences of magnitude 7 or greater earthquakes each year from 1900 through 1989.

ANONYMOUS FTP SITES

National Center for Earthquake Engineering Research Anonymous ftp
Ftp to: *clark.eng.buffalo.edu*
This anonymous ftp site provides access to over 612 computer search reprints as well as other data files such as the *Information Service News*, the NCEER technical report list, topical bibliographies, and guides. These files can be downloaded and printed freely with no intermediary required.

California Division of Mines and Geology, California Strong Motion Instrumentation Program
Ftp to: *ftp.consrv.ca.gov.pub/dmg/csmip*
This site contains newly processed strong motion data from very recent earthquakes. The data is also available through their Web page (see below).

FINGER

Many seismological stations provide quick access to recent earthquake information via the *finger* utility. By issuing the *finger* command to a particular internet address, a list of recent earthquakes recorded by that particular station is returned. The gateway system Surfing the InterNet for Earthquake Data (see above) provides a directory and automatic links to these finger sites plus many, many others.

finger quake@andreas.wr.usgs.gov
This site provides a quick listing of magnitude 2 or greater earthquakes recorded by the Northern California Seismic Network in Central and Northern California during the last three days.

finger quake@gldfs.cr.usgs.gov
This is a listing of Near-Real-Time Worldwide Earthquake Locations. This site provides a quick listing of reviewed locations for earthquakes worldwide from the U.S. National Seismic Network and corresponding agencies. Within 24 hours, most earthquakes of magnitude 3.5 or greater in the contiguous United States, 4.0 or greater in Alaska, 4.5 or greater in Hawaii, 5.0 or greater in the Aleutian Islands, and 5.5 or greater for the rest of the world will be posted to this list.

GOPHER SITES

Earthquake Information Gopher
gopher to *nisee.ce.berkeley.edu*
Operated by the National Information Service for Earthquake Engineering, this site provides mission statement, publications lists, and other information to organizations active in earthquake studies.

Emergency Preparedness Information Exchange (EPIX)
gopher to *hoshi.cic.sfu.ca:80*
EPIX is the gopher companion to HazardNet, providing gopher access to emergency management, disaster, and earthquake sites around the world.

Federal Emergency Management Agency Gopher
gopher to *www.fema.gov*
Information about FEMA plus an historical list of press releases are provided.

NCEER Gopher
gopher to *nceer.eng.buffalo.edu*
Included in the Gopher menu selections are the NCEER Anonymous FTP site, access to the QUAKELINE® database, NCEER-produced software programs, and other resources.

WORLD WIDE WEB SITES

Applied Technology Council (ATC)
web site: *http://www.atcouncil.org*
e-mail: *atc@atcouncil.org*
ATC is a nonprofit corporation involved in earthquake hazard preparedness, response, and mitigation research related to the design and engineering of structures.

Association of Bay Area Governments (ABAG)
web site: *http://www.abag.ca.gov*
e-mail: *jeannep@abag.ca.gov*
ABAG is the regional planning agency for the San Francisco Bay Area. It offers a number of publications related to earthquake planning, as well as training classes and technical assistance to local government and businesses. A key feature of this site are earthquake hazard maps for scenario earthquakes in the San Francisco Bay Area.

California Division of Mines & Geology, Strong Motion Instrumentation Program
web site: *http://www.consrv.ca.gov/dmg*
e-mail: *bkondo@www.consrv.ca.gov*
In addition to recently processed strong motion records from California earthquakes, the Division of Mines & Geology publishes seismic hazard zone maps and the Alquist-Priolo earthquake fault zone maps, providing very detailed fault information for the State of California. The maps are not on the web site, but information about them is.

California Office of Emergency Services, Earthquake Program
web site: *http://www.oes.ca.gov:8001*
e-mail: *sdm@oes.ca.gov*
The goal of the OES Earthquake Program is to support and assist local and state government and the private sector in integrating hazard identification, risk assessment, risk management, and prevention into a comprehensive approach to hazard mitigation, and to maximize the effective use of available public and private sector resources devoted to hazard mitigation.

Center for Earthquake Research and Information (CERI), University of Memphis
web site: *http://www.ceri.memphis.edu*
e-mail: *stevens@ceri.memphis.edu*
The Center for Earthquake Research and Information (CERI), a research institute of the University of Memphis, provides accurate, immediate reports and information on the occurrence of regional and worldwide earthquakes; research related to the causes and effects of earthquakes originating in the New Madrid seismic zone and the Southern Appalachian seismic zone; studies related to the need for earthquake resistant construction; and advice on the methods, means, and feasibility of reducing

earthquake damage.

Earthquake Engineering Research Center/ National Information Service for Earthquake Engineering/ University of California at Berkeley
web site: *http://nisee.ce.berkeley.edu*
e-mail: *eerclib@eerc.berkeley.edu*
EERC is dedicated to research, education, and dissemination of technical information in earthquake engineering. The information program supports technology transfer activities in software distribution, bibliographic databases, the EERC Library, and technical reports. A key feature of this site is the Earthquake Image Information System (EqIIS), which has 7000 digitized images of earthquakes and earthquake damage from 1868 to the present. The images can be searched by earthquake name, by photographer, and by keyword/subject.

Earthquake Research Institute, University of Tokyo
web site: *http://www.eri.u-tokyo.ac.jp*
e-mail: *webmaster@eri.u-tokyo.ac.jp*
Information about the Earthquake Prediction Research Center and the Division of Disaster Mitigation Science is provided.

Earthquake Engineering Research Library, California Institute of Technology
National Information Service for Earthquake Engineering (NISEE/Caltech)
web site: *http//:www.cadre.caltech.edu/eerl/eerl.html*
e-mail: *eerllib@caltech.edu*
This site provides strong-motion accelerogram data, technical reports, slides, and videotapes of earthquake damage and structural engineering topics, as well as conference proceedings and technical serials.

Federal Emergency Management Agency (FEMA)
web site: *http://www.fema.gov*
e-mail: *eipa@fema.gov*
The primary mission of FEMA is to protect lives and reduce property loss from natural disasters and other emergencies. To accomplish this, FEMA acts as the focal point for all levels of government to develop a national emergency management capability that can deal effectively with any emergency.

Instituto de Ingenieria, Universidad Nacional Autonoma de Mexico
web site: *http://pumas.iingen.unam.mx*
e-mail: *mosaic@pumas.iingen.unam.mx*
By selecting Actividades del Instituto, announcements and information about the Eleventh World Conference on Earthquake Engineering will be found.

International Center for Disaster-Mitigation Engineering, University of Tokyo
web site: *http://incede.iis.u-tokyo.ac.jp/Incede.html*
e-mail: *webmaster@incede.iis.u-tokyo.ac.jp*
The INCEDE home page includes general information about this Japanese center, abstracts of all INCEDE reports, back issues of their newsletters, and summaries of INCEDE research. A special feature is KobeNet, providing information and links about the Great Hanshin earthquake.

National Center for Earthquake Engineering Research (NCEER) Information Service, State University of New York at Buffalo
web site: *http://nceer.eng.buffalo.edu*
e-mail: *nernceer@ubvms.cc.buffalo.edu*
The NCEER Information Service was established to disseminate earthquake engineering and hazard information to researchers, practitioners, and the general public. This site includes information about NCEER produced software programs, the NCEER anonymous ftp site (previously described), and the Quakeline database.

National Geophysical Data Center
web site: *http://www.ngdc.noaa.gov*
e-mail: *info@mail.ngdc.noaa.gov*
The National Geophysical Data Center acquires, processes, and analyzes technical data on earthquake hazards and disseminates it to federal agencies, private industry, academia, and the public. Operating as both a national and a world data center, NGDC holds global data for terrestrial and marine environments. In addition, NGDC and the World Data Center-A for Solid Earth Geophysics help to compile, catalog, and synthesize available information on tsunami sources and effects to support modeling, engineering, planning, and educational purposes.

National Institute of Standards and Technology (NIST), Structures Division
web site: *http://www.nist.gov*
e-mail: *hsl@enh.nist.gov*
NIST is one of four program agencies of the National Earthquake Hazards Reduction Program (NEHRP). In the enabling legislation, Congress assigns NIST the responsibility for "carrying out research and development to improve building codes and standards and practices for structures and lifelines." NIST conducts applied analytical and experimental research in-house and collaboratively with private sector organizations and universities.

Natural Hazards Research and Applications Information Center, University of Colorado, Boulder
web site: *http://adder.colorado.edu/~hazactr/Home.html*
e-mail: *hazctr@colorado.edu*
The Natural Hazards Research and Applications Information Center is a national clearinghouse for data relating to the economic loss, social disruption, and human response associated with natural disasters and related technological risks. The main goal of the Center is to strengthen communication between researchers and the individuals, organizations, and agencies responsible for reducing losses from disasters.

Seismographic Station, University of California at Berkeley
web site: *http://www.seismo.berkeley.edu*
e-mail: *www.seismo.berkeley.edu*
The Seismographic Station has monitored and studied earthquakes in California and the world since 1887. The Northern California Earthquake Data Center (NCEDC) and Rapid Earthquake Data Integration (REDI) Projects are projects of the Seismographic Station.

Southern California Earthquake Center (SCEC), University of Southern California
web site: *http://www.usc.edu/dept/earth/quake*
e-mail: *SceclInfo@usc.edu*
SCEC's Data Center (SCEC-DC) is the principal archive of seismological and geodetic data associated with seismicity in Southern California. The mission of the Center is to promote earthquake hazard reduction by estimating when and where future damaging earthquakes will occur, calculating the expected ground motion, and disseminating information to the public.

U.S. Geological Survey, National Earthquake Information Center
web site: *http://gldfs.cr.usgs.gov*
e-mail: *sedas@gldfs.cr.usgs.gov*
See the entry under Telnet: Quick Epicenter Determinations, as this provides Web access to the same information. Also provided are current seismicity maps for the world, definitions of earthquake terms, information about the Center, and **finger** access to other sites.

U.S. Geological Survey, Office of Earthquakes and Volcanoes
web site: *http://quake.wr.usgs.gov* and *http://info.er.usgs.gov*
e-mail: *webmaster@www.usgs.gov*
The first web address provides basic information about the Menlo Park, California office of the U.S. Geological Survey. The second address provides broader coverage for the entire Office of Earthquakes and Volcanoes within USGS.

Western States Seismic Policy Council (WSSPC)
web site: *http://vishnu.glg.nau.edu/wsspc.html*
e-mail: *wsspc@vishnu.glg.nau.edu*
WSSPC is a broad regional forum for technology transfer, multi-disciplinary membership, and enhanced emergency management/geoscience partnerships toward earthquake hazard mitigation. The primary aims of the organization have been to improve public understanding of seismic risk, to improve earthquake preparedness, and to provide a cooperative forum to enhance transfer of mitigation technologies at the local, state, interstate, and national levels.

OTHER ORGANIZATIONS

These organizations have e-mail access and are actively developing other Internet services. Contact them by e-mail for further information on their Internet plans.

Building Seismic Safety Council. e-mail: *cheider@nibs.org*
Central U.S. Earthquake Consortium. e-mail: *cusec@ceri.memphis.edu*
California Seismic Safety Commission. e-mail: *sscbase@aol.com*
Earthquake Engineering Research Institute. e-mail: *susant@eerc.berkeley.edu*
Imperial College, London, Engineering Seismology & Earthquake Engineering Section.
e-mail: *d.ryan@ic.ac.uk*
Interagency Committee on Seismic Safety in Construction. e-mail: *dtodd@enh.nist.gov*
Seismological Society of America. e-mail: *info@seismoc.org*
Tohoku University, Japan, Faculty of Engineering, Disaster Control Research Center.
e-mail: *shibata@struct.archi.tohoku.ac.jp*

EVALUATION OF CODE FORMULAS FOR FUNDAMENTAL PERIOD OF BUILDINGS

RAKESH K. GOEL
Department of Civil and Environmental Engineering
Syracuse University, Syracuse, NY 13244-1190.
and
ANIL K. CHOPRA
Department of Civil Engineering
University of California, Berkeley, CA 94720.

ABSTRACT

The formulas specified in US building codes to estimate the fundamental vibration period are based largely on motions of buildings recorded during the 1971 San Fernando earthquake. These formulas should be re-evaluated in light of the new data that has become available from recent earthquakes. For this purpose, a comprehensive database has been developed on periods of buildings identified (or measured) from their motions recorded during the 1971 and subsequent earthquakes. From this database, measured periods of three categories of buildings were extracted and compared with those obtained from the code formulas. This comparison showed that the code formulas for concrete and steel moment resisting frame buildings generally lead to periods that are shorter than measured periods, and periods estimated from these formulas almost always lead to higher values of seismic coefficients compared to the values based on measured periods. The comparison for shear wall buildings showed that the formula based on a coefficient independent of the shear wall area leads to periods much longer than the measured periods which in turn results in unconservative design forces. The formula based on shear wall area, on the other hand, results in periods much shorter than measured periods and hence overly conservative design forces.

KEYWORDS

Building codes; building period; dynamic analysis; earthquake analysis; earthquake design; fundamental period; period database; seismic codes; system identification; vibration period.

INTRODUCTION

The fundamental vibration period is needed to calculate the design base shear and lateral forces according to building codes. Because this building property can not be computed for a structure that is yet to be designed, building codes provide empirical formulas that depend on the building material (steel, concrete, etc.), building type (frame, shear wall, etc.), and overall dimensions. The empirical formula specified in US building codes -- UBC-94 (*Uniform Building Code*, 1994), ATC3-06 (*Tentative Provisions*, 1978), SEAOC-90 (*Recommended Lateral Force Requirements*, 1990), and NEHRP-91 (*NEHRP*, 1991) -- is of the form:

$$T = C_t (h_n)^{3/4} \tag{1}$$

where h_n is the height of the building in feet above the base and C_t is a numerical coefficient related to the lateral-force-resisting system. The values of C_t specified in these codes are summarized in Table 1.

Table 1. Code-specified values of numerical coefficient C_t.

Code	Values of C_t			
	Steel Moment Resisting Frames	Concrete Moment Resisting Frames	Eccentrically Braced Steel Frames	Others
UBC-94, SEAOC-90, NEHRP-91	0.035	0.030	0.030	0.02
ATC3-06	0.035	0.025	--	--

For concrete or masonry shear wall buildings, UBC-94 and SEAOC-90 provide an alternative value of the coefficient:

$$C_t = 0.1/\sqrt{A_c} \tag{2}$$

where

$$A_c = \sum A_e\left[0.2 + (D_e/h_n)^2\right]; \qquad D_e/h_n \le 0.9 \tag{3}$$

in which A_e = the effective horizontal cross-sectional area, in square feet, of a shear wall in the first story of the structure, and D_e = the length, in feet, of a shear wall element in the first story in the direction under consideration. ATC3-06 specifies that the fundamental period of all other buildings, including building with shear walls and eccentric braced frames, be calculated by the formula:

$$T = \frac{0.05\,h_n}{\sqrt{L}} \tag{4}$$

where L = overall length, in feet, of the building at the base in the direction under consideration.

For preliminary design of a building, it is desirable to use a conservative estimate of the base shear. As described later, such a conservative estimate would be obtained if estimated period of the building is smaller than its true period. Therefore, the code formulas for fundamental period (Eqs. 1, 3, and 4) were intentionally calibrated to underestimate the period (*Tentative Provisions*, 1978).

The codes also recommend that whenever feasible the fundamental period should be calculated using the structural properties and deformation characteristics of the resisting elements in a properly substantiated analysis. This requirement may be satisfied by using the following formula based on Rayleigh's method:

$$T = 2\pi\sqrt{\left(\sum_{i=1}^{n} w_i\,\delta_i^2\right) \div \left(g\sum_{i=1}^{n} f_i\,\delta_i\right)} \tag{5}$$

where w_i is the seismic dead load at level i, g is the acceleration due to gravity, and f_i (i = 1,2, ...N) are a set of selected lateral forces with reasonable height-wise distribution and δ_i are the resulting deflections.

The codes specify that the period calculated from rational analysis (Eq. 5) should not be longer than that estimated from empirical formulas (Eqs. 1 and 3) by a certain factor. The factors specified in various US codes are: 1.2 in ATC3-06, 1.3 for high seismic region (Zone 4) and 1.4 for other regions (Zones 3, 2, and 1) in UBC-94; and a range of values with 1.2 for regions of high seismicity to 1.7 for regions of very low seismicity in NEHRP-91. SEAOC-90 specifies that the base shear calculated using the period from the rational analysis shall not be less than 80 percent of the value obtained by using the period from the empirical formulas, which corresponds to a value of 1.4 (Cole et al., 1992).

As mentioned previously, the codes recognize that the true period of a building may be longer than its period estimated from code specified empirical formulas (Eqs. 1 and 3). Therefore, the codes permit the period computed from rational analysis (Eq. 5) to be longer than that from empirical equations (Eqs. 1 and 3). However, in order to safeguard against unreasonable assumptions in the rational analysis, which may lead to uncoservatively long period, codes impose the aforementioned restrictions on the period computed from Eq. (5). These limiting values are indicative of by how much the codes expect the true period of a building to be longer than its period estimated from the empirical formulas.

The US seismic codes, for example UBC-94 and SEAOC-90, specify the base shear as:

$$V = \frac{ZIC}{R_w} W \tag{6}$$

where Z is the seismic zone factor, I is the importance factor, C is the elastic seismic coefficient, W is the total seismic dead load, and R_w is the reduction factor to account for energy dissipation capacity of the building. The elastic seismic coefficient C is a function of the fundamental period T and is given as:

$$C = \frac{1.25S}{T^{2/3}} \leq 2.75 \tag{7}$$

in which S is the site coefficient depending on the soil characteristics. The formulas specified in NEHRP-91 and ATC3-06 are similar in nature to that given by Eqs. (6) and (7) but differ slightly in details.

The empirical formula for fundamental period (Eqs. 1 and 3) in US building codes is based largely on motions of buildings recorded during the 1971 San Fernando earthquake (*Tentative Provisions*, 1978). These formulas should be re-evaluated in light of the wealth of data that has become available from recent earthquakes. This research investigation is aimed towards filling this need. For this purpose, a comprehensive database has been developed on periods of buildings identified (measured) from their strong motions recorded during the 1971 and subsequent earthquakes. This database is then used to evaluate the code formulas for estimating the fundamental period of buildings with steel and concrete moment resisting frames, and concrete shear walls.

DATABASE FOR BUILDING PERIODS

The vibration periods and modal damping ratios of about twenty buildings have been identified from their recorded motions during the 1994 Northridge earthquake using parametric system identification techniques (Beck, 1978; Li and Mau, 1990; Safak, 1988). These results are combined with similar data available from the 1971 San Fernando earthquake and other recent California earthquakes to form a comprehensive set of data. These data are compiled on an electronic database that can be easily updated after every major earthquake.

Contents of this database are arranged into the following five broad categories: (1) General information, (2) structure characteristics, (3) excitation characteristics, (4) recorded motions, and (5) vibration properties. For each of these general categories, several individual parameters are defined. The general information includes building location, identification number, occupancy, name, address, and reference that reported the data. The structural characteristics include height, plan dimensions, number of stories above and below the ground, material, and longitudinal and transverse resisting systems. The excitation is characterized by the earthquake name and date. The recorded motion data include peak values of roof and base accelerations, roof displacement relative to the base, and drift ratio in each of the two building directions. Vibration properties considered include period and damping ratio for up to two longitudinal, transverse, and torsional modes. A separate set of data (or record) is established for each building. In addition, a separate record is created for data obtained for the same building but for different earthquakes or by different investigators for the same earthquake.

From this comprehensive database, the information on fundamental vibration period has been extracted for three categories of buildings: (1) Concrete moment resisting frame buildings, (2) steel moment resisting frame buildings, and (3) concrete shear wall buildings. The extracted information included 37 data points for 27 concrete moment resisting frame buildings, 53 data points for 42 steel moment resisting frame buildings, and 27 data points for 16 concrete shear wall buildings. The number of data points exceed the number of buildings because some buildings yielded data for more than one earthquake or because data were reported by more than one investigator for the same earthquake. This information is then used to evaluate the code formulas for fundamental period. Although, the database contains information on buildings with other types of material and structural system, this information is not presented in this paper for brevity.

EVALUATION OF CODE PERIOD FORMULAS

In order to evaluate the code period formulas, we compare for each of the aforementioned categories of buildings:

- The measured building periods identified from their strong motion records with those obtained from the empirical code formulas (Eqs. 1 and 3), and
- The seismic coefficients calculated according to UBC-94 (Eq. 7) using the measured and code periods.

The measured and code periods are compared in Figures 1, 3, and 5 where they are plotted against the building height. The measured periods in two orthogonal directions are shown by solid circles connected by a vertical line, whereas code periods are shown by the curve denoted as T. Note that the code formula (Eq. 1) would lead to same period in the two directions as long as the lateral resisting systems in these directions are identical. Also included are curves for $1.2T$ and $1.4T$ representing restrictions on the period from rational analysis (Eq. 5) imposed by various US codes for high seismic regions like California. The former corresponds to the limit specified in ATC3-06 and NEHRP-91, whereas the latter is obtained from SEAOC-90 provisions; the limiting value of $1.3T$ specified in UBC-94 falls between these two extremes.

The seismic coefficients calculated according to UBC-94 (Eq. 7) using measured and code periods are compared in Figures 2, 4, and 6. These values are calculated for rock sites (S = 1 in Eq. 7). The seismic coefficients calculated using measured periods in the two orthogonal directions are shown by solid circles connected by a vertical line whereas those calculated using code periods are shown by a solid line. In order to calculate the seismic coefficient as a function of the building height, Eqs. (1) and (7) were utilized to get:

$$C = \frac{1.25S}{\left(C_t h_n^{3/4}\right)^{2/3}} \leq 2.75 \tag{8}$$

Concrete Moment Resisting Frame Buildings

The following trends can be gleaned from the results presented in Figures 1 and 2 for 27 concrete moment resisting frame (MRF) buildings:

- As intended by the code writers, the code formula leads to periods that are generally shorter than measured periods (Figure 1).
- The code formula leads to periods that form the lower bound of measured periods for building up to 160 ft tall.
- The lower bound of measured periods for buildings taller than 160 ft is about twenty percent higher, that is, the lower bound for such buildings is $1.2T$ rather than T. However, this conclusion is based on limited data as there are few concrete MRF buildings taller than 225 ft in the database.
- In general, measured periods of concrete MRF buildings fall between the curves for $1.2T$ and $1.4T$ indicating that the code imposed limits on the period from the rational analysis (Eq. 5) are reasonable.

- The code formula for estimating the building periods almost always leads to higher values of seismic coefficient compared to the values based on the measured period (Figure 2).

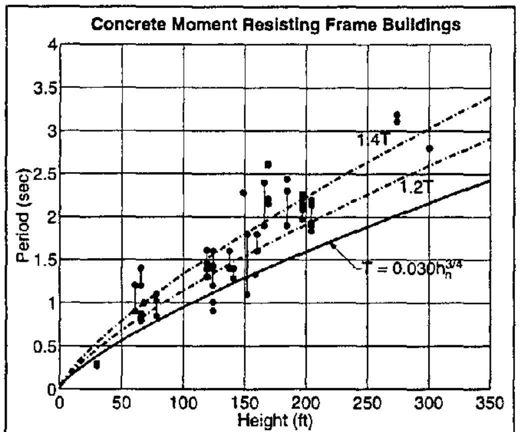

Figure 1. Measured and code periods for concrete moment resisting frame buildings.

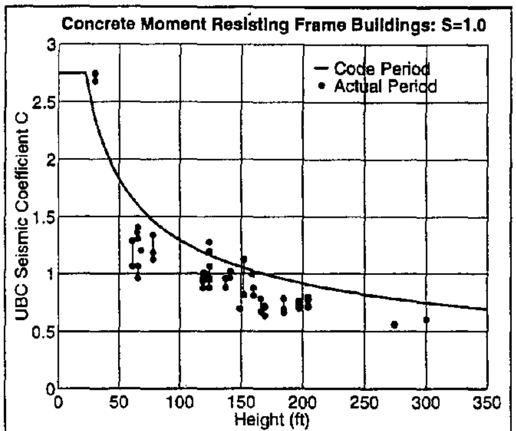

Figure 2. UBC-94 seismic coefficients for concrete moment resisting frame buildings.

Steel Moment Resisting Frame Buildings

The results presented in Figures 3 and 4 for 42 steel MRF buildings lead to the following conclusions:

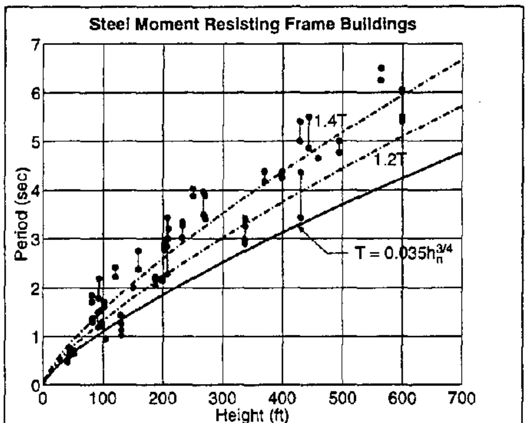

Figure 3. Measured and code periods for steel moment resisting frame buildings.

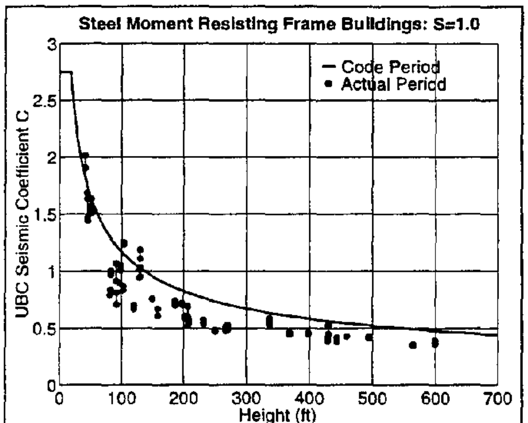

Figure 4. UBC-94 seismic coefficients for steel moment frame buildings.

- As noted previously for concrete MRF buildings, the code formula leads to periods that are generally shorter than measured periods (Figure 3). However, the margin between the code and measured periods is much larger for steel MRF buildings.
- The code formula leads to periods close to the lower bound of measured periods for buildings up to about 120 ft tall.
- With a few exceptions, the lower bound of measured periods for steel MRF buildings taller than 120 ft is twenty to thirty percent higher. Unlike concrete MRF buildings, many more data points support this conclusion for steel MRF buildings.
- Many measured period values exceed $1.2T$ and even $1.4T$ indicating that these limits are unrealistically restrictive for steel MRF buildings.

- As noted for concrete MRF buildings, the code formula for estimating periods of steel MRF buildings leads to seismic coefficients that are almost always higher than those from measured periods (Figure 4).

Concrete Shear Wall Buildings

The trends observed for concrete shear wall buildings (Figures 5 and 6) are quite different compared to those noted previously for concrete and steel MRF buildings. The trends gleaned from results presented for 16 concrete shear wall buildings are:

- The scatter in the plotted data is significantly larger (Figure 5) compared to both concrete and steel MRF buildings (Figures 1 and 3). This indicates that building height alone may not be a good parameter for estimating the periods of shear wall buildings and other parameters should be investigated.
- Unlike MRF buildings, the code formula based on $C_t = 0.02$ may lead to periods of shear wall buildings that are longer than measured periods (Figure 5).
- Obviously, the limiting values of $1.2T$ and $1.4T$ imposed by the codes on the period from rational analysis are unreasonable for shear wall buildings.
- The code formula based on $C_t = 0.02$ also leads to seismic coefficients that are smaller and hence unconservative compared to those from measured periods (Figure 6).

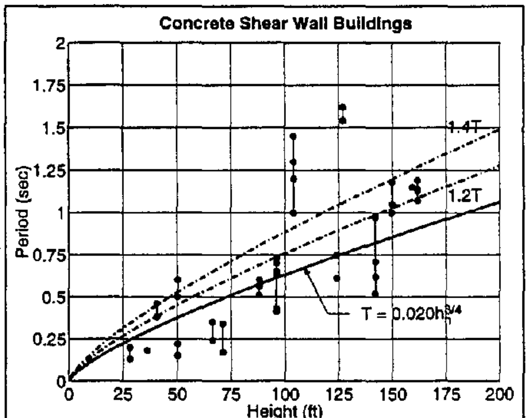

Figure 5. Measured and code periods for concrete shear wall buildings: $C_t = 0.02$.

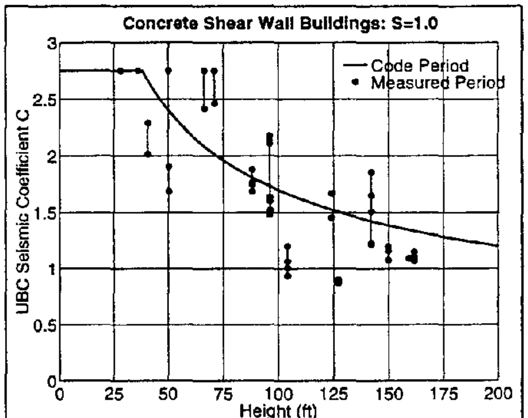

Figure 6. UBC-94 seismic coefficients for concrete shear wall buildings.

As mentioned previously, US seismic codes permit use of an alternative value of C_t (Eq. 2), that involves area of shear walls, to estimate the periods of concrete shear wall buildings. In order to evaluate this formula, measured and code periods are compared in Figure 7 for 10 selected buildings for which information on area of shear walls is available. The measured periods are shown by circles whereas code periods are shown by squares; the period values in the two orthogonal directions are connected by a vertical line. Since, areas of shear walls in the two orthogonal directions can be different, the code formula may lead to different periods in these directions. Also compared in Figure 8 are seismic coefficients calculated according to UBC-94 using the measured and code periods. The following trends emerge from these comparisons:

- Code Eq. (2) predicts periods that are generally much shorter than measured periods (Figure 7).
- The periods based on Eq. (2) also lead to seismic coefficients that may be significantly larger than calculated from measured periods (Figure 8). To reduce this resulting conservatism, Eq. (2) should be modified.

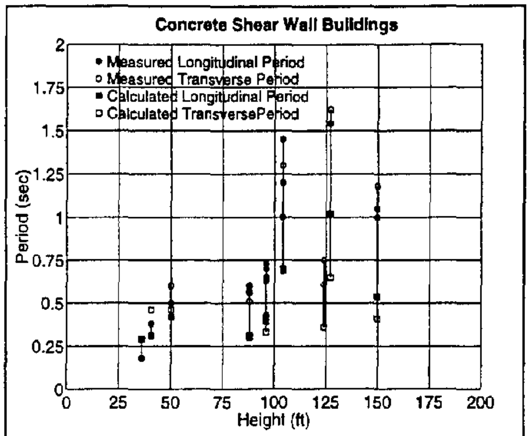

Figure 7. Measured and code periods for concrete shear wall buildings: $C_t = 0.1/\sqrt{A_c}$.

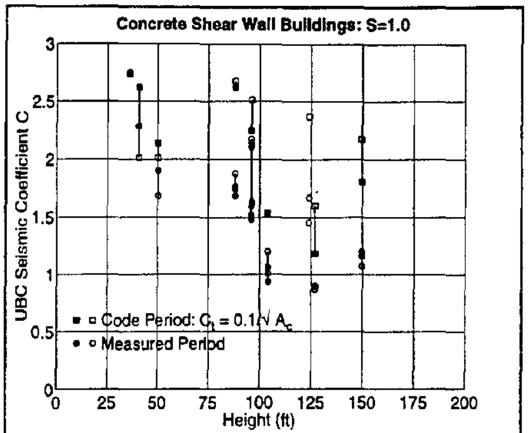

Figure 8. UBC-94 seismic coefficients for concrete shear wall buildings.

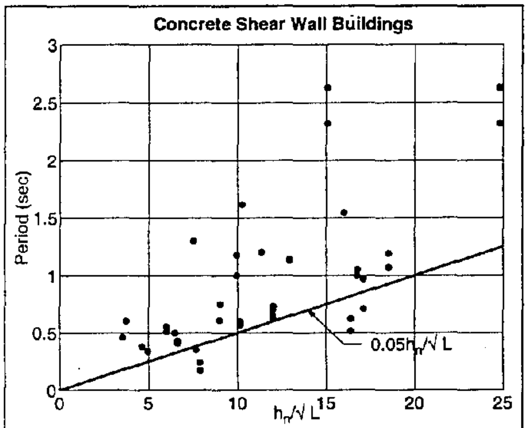

Figure 9. Measured and code periods for concrete shear wall buildings: Code period from Eq. (4).

ATC3-06 specifies that the period of a shear wall building be calculated from Eq. (4) that involves not only the building height but also the building base dimension. In Figure 9, the measured periods of 14 selected buildings are compared with the values calculated from Eq. (4). Comparison of the two sets of data indicates that:

- There is significant scatter in the plotted data indicating that $h_n/\sqrt{L}$ may not be a good parameter to estimate periods of shear wall buildings.
- Eq. (4) underestimates significantly the periods of buildings and leads to unnecessarily large seismic coefficients.

CONCLUSIONS

This investigation on evaluation of code formulas for fundamental period of buildings has led to the following conclusions:

- Code formulas for concrete and steel MRF buildings lead to periods that are generally shorter than periods measured from strong motion records of buildings. The difference between the code and measured periods, however, is much larger for taller buildings.
- The code formulas for estimating the periods of steel and concrete MRF buildings almost always lead to higher values of seismic coefficients compared to the values based on measured periods.
- The code imposed limits on the period from rational analysis are reasonable for concrete MRF buildings, but they are unrealistically restrictive for steel MRF buildings.
- For shear wall buildings, code formula based on $C_t = 0.02$ leads to periods much longer than measured periods which in turn results in unconservative design forces. The code formula based on $C_t = 0.1/\sqrt{A_c}$, on the other hand, results in much shorter periods and hence overly conservative design forces.

- The height, or height along with the base dimension, of a shear wall building alone may not be good parameter(s) to estimate its fundamental period.
- Based on this data and observations, the period formulas in US seismic codes should be revised.

ACKNOWLEDGMENTS

This research investigation is supported by the National Science Foundation under Grant CMS-9416265. The authors are grateful for this support. The authors also acknowledge the assistance provided by Anthony Shakal, Moh Huang, Bob Darragh, Gustavo Maldonado, and Praveen Malhotra of California Strong Motion Instrumentation Program in obtaining recorded motions and structural plans; and by Prof. S. T. Mau, Prof. J. L. Beck, and Dr. M. Celebi in implementing the system identification procedures.

REFERENCES

Tentative Provisions for the Development of Seismic Regulations for Buildings. (1978). ATC3-06, Applied Technological Council, Palo Alto, CA.

Beck, J. L. (1978). *Determining Models of Structures from Earthquake records*, Report No. EERL 78-01, Earthquake Engineering Research Laboratory, California Institute of Technology, Pasadena, CA, June.

Cole, E., Tokas, C. V. and Meehan, J. F. (1992). "Analysis of Recorded Building Data to Verify or Improve 1991 Uniform Building Code (UBC) Period of Vibration Formulas," Proceedings of SMIP92, Strong Motion Instrumentation Program, Division of Mines and Geology, California Department of Conservation, Sacramento, CA.

NEHRP Recommended Provisions for the Development of Seismic Regulations for New Buildings. (1991). Building Seismic Safety Council, Washington, D. C.

Li, Y. and Mau, S. T. (1990). "A Computer Program for Multiple Input-Multiple Output System Identification Using Building Seismic Records," *Report UHCEE 90-07*, University of Houston, TX.

Recommended Lateral Force Requirements and Commentary. (1990). Seismology Committee, Structural Engineers Association of California, CA.

Safak, E. (1988). *Analysis of Recordings in Structural Engineering: Adaptive Filtering, Prediction, and Control*, Open-file Report 88-647, US Geological Survey, Menlo Park, CA.

Uniform Building Code. (1994). International Conference of Building Officials, Whittier, CA.

HEAT GENERATION EFFECTS ON VISCOELASTIC DAMPERS IN STRUCTURES

J. A. INAUDI, M. BLONDET, J. M. KELLY
Earthquake Engineering Research Center, CA 94804
University of California at Berkeley

A. APRILE
Engineering Institute, University of Ferrara
Via G. Saragat, 1, 44100 Ferrara, Italy

ABSTRACT

The first part of this paper is concerned with the response of viscoelastic dampers subjected to transient temperature conditions caused by heat generation during cyclic deformation. Simple tools for modeling viscoelastic materials are discussed and verified using experimental data obtained in a test program on shear dampers using the polymer Scotchdamp 109 of The 3M Company conducted at the Laboratory of the Civil Engineering Department of the University of California at Berkeley. The second part of this study is a numerical investigation of the effects of heat generation on the response of structures with supplemental viscoelastic dampers with the aim of defining design guidelines for structures incorporating this type of dissipater.

KEYWORDS

Damping, energy dissipation, nonlinear viscoelasticity, damper design, experimental research.

INTRODUCTION

Application of acrylic-polymer dampers in retrofit and new construction has been accompanied by extensive experimental research on their mechanical behavior (Mahmoodi, 1969; Aiken and Kelly, 1990; Soong and Lai, 1991; Chang *et al.*, 1992; Kasai *et al.*, 1993; Blondet, 1993; Nielsen *et al.*, 1994). Due to the high sensitivity of the mechanical properties of this type of material to variations in temperature, modeling this dependence and assessing its effects on the dynamic response of structures with supplemental viscoelastic (VE) dampers is of significant relevance in developing design guidelines for this type of energy dissipater.

Consider the following linear model of the shear force in a VE damper

$$F(\varpi) = \frac{A}{h}(G_s(\varpi) + jG_l(\varpi))V(\varpi) \tag{1}$$

where A = shear area of the damper, h = thickness of the VE pad, $G_s(\varpi)$ = storage *modulus* of the VE material, $G_l(\varpi)$ = loss *modulus*, j = imaginary unit, and $V(\varpi)$ = Fourier transform of the damper deformation, $v(t)$. At constant temperature and subjected to sinusoidal deformation of amplitude γ_o, the dissipation of energy per cycle per unit volume is $\pi|G_l(\varpi)|\gamma_o^2$. This energy, in the form of heat, causes a rise in the temperature of the material proportional to the square of the deformation amplitude.

For an arbitrary deformation signal, the total dissipated energy per unit volume is

$$W = \frac{1}{2\pi}\int_{-\infty}^{\infty} G_l(\varpi)\varpi|\Gamma(\varpi)|^2\, d\varpi \tag{2}$$

where $\Gamma(\varpi)$ is the Fourier transform of the shear deformation $\gamma(t) = v(t)/h$. Designs of VE dampers with variations in h, maintaining constant the ratio A/h, lead to lower or higher strains levels in the VE material and, consequently, lower or higher dissipation per volume of material. This implies that h plays an important role in the temperature problem because h controls the strain demand on the damper.

The design of VE dampers requires then the definition of design strain levels that guarantee appropriate behavior of the dampers during operation. These strain levels will depend on the mechanical properties of the VE material, the damper geometry, the frequency content of the deformation signals, the duration of the excitation process, and the thermal conductivity and radiation properties of the damper.

This work describes an experimental program conducted at the University of California at Berkeley to obtain data on the response of VE dampers during transient temperature conditions so that the merits of modeling tools could be assessed. A second purpose of this investigation is to determine the effects of temperature on the response of structures incorporating VE dampers so as to draw recommendations and guidelines for the design of this type of dissipater.

EXPERIMENTAL PROGRAM

Experimental Setup

Six small dampers manufactured by The 3M Company using the Scotchdamp™ Polymer 109 were used in the experimental program. They had identical nominal geometry with two $0.5in$ thick layers, and cross sectional areas of $1.5in \times 1.5in$.

The dampers were tested in a Universal Testing Machine built by MTS Systems Corporation. The actuator, commanded by a 5 GPM servovalve, had a capacity of $35kips$ and a stroke of $6in$. The servolvalve was commanded by an MTS 436 Control Unit which in turn, was digitally controlled using a personal computer with data acquisition and control software. The load in the damper was measured using a tension and compression load cell (Model 3174 Lebow, EATON Corp.) with a nominal capacity of $10kips$. An electrical oven with a digital temperature controller was used to heat the specimens to the desired initial temperatures. An LVDT was used to measure the deformation of the damper; this signal was used as feedback in the controller. Thermocouples (TC) were installed in the specimens tested and temperature readings were accurate to $\pm 0.1^\circ C$. The TC junction diameter was 0.003 in; this especially thin junction was used to reduce the time constant (thermal inertia) of the TC. Room temperature was measured with a thermometer.

The tests conducted in the dampers consisted in imposed deformation signals at various initial temperatures. The command signals utilized were sine signals of frequencies between $0.1Hz$ and $4Hz$, sine sweeps, steps, and broad-band signals. During the tests, deformation, force, material temperature and ambient temperature were recorded. In addition, several tests were conducted to characterize the cooling process of the damper with the damper undeformed. This was aimed at obtaining a simple first-order differential model for the temperature of the damper to be used in the analytical phase of this research. Only a small fraction of the data analyzed is presented herein. A detailed analysis of the data is presented elsewhere (Inaudi *et al.*, 1996).

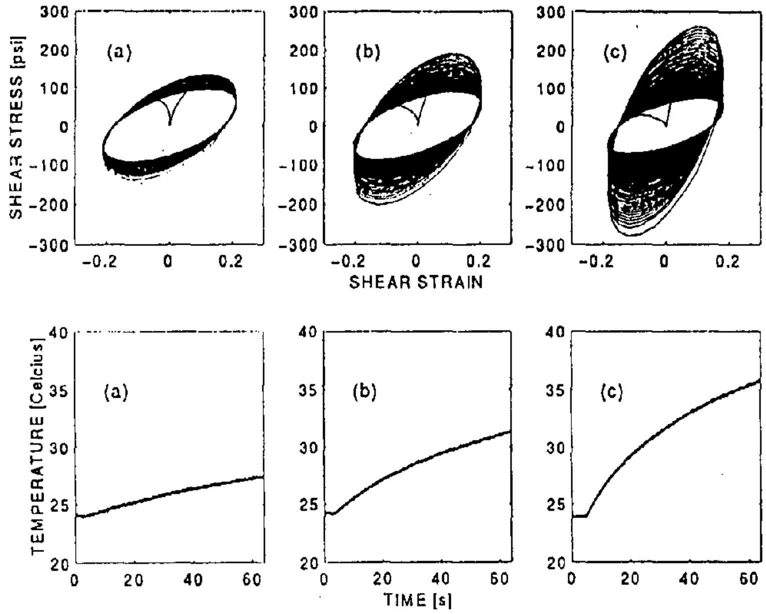

Fig. 1. Hysteresis loops and material-temperature histories obtained in tests of sinusoidal deformation: (a) $0.5Hz$, (b) $1Hz$, (c) $2Hz$.

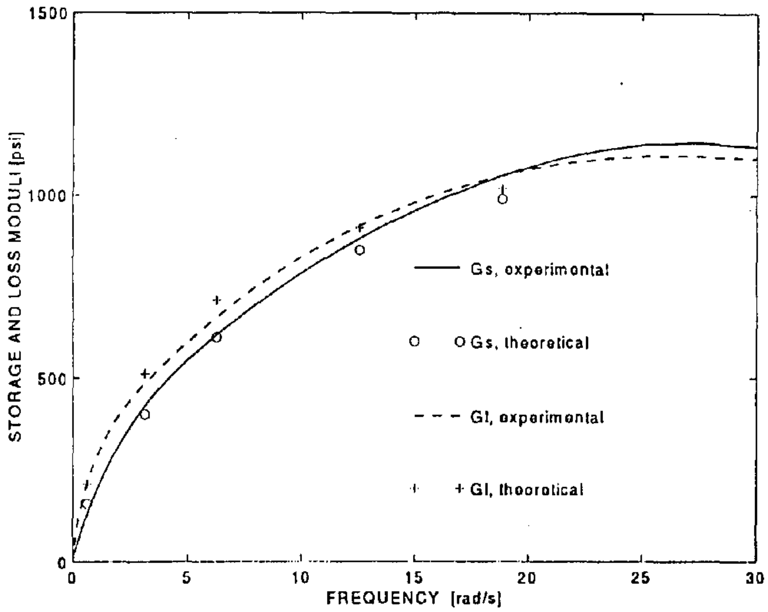

Fig. 2. Experimental and theoretical storage and loss *moduli* for polymer Scotchdamp 109 at a reference temperature of $21\,^{\circ}C$.

Results

Figure 1 shows stress-strain curves measured during three sinusoidal-deformation tests of equal amplitude and different frequencies ($0.5Hz, 1Hz$, and $2Hz$) and their corresponding temperature histories $\theta(t)$ during the sixty seconds of testing. As illustrated in the figures, the higher the deformation frequency, the higher the temperature increase in the VE material and, the higher the deterioration of the mechanical properties for the same test duration. While a temperature increase of $3^\circ C$ causes only a minor decrease in the energy dissipation per cycle (Fig. 1a), an increase of $12^\circ C$ causes a very significant reduction in the energy dissipation per cycle (Fig. 1c).

The cooling process of the VE material during periods with no deformation after heating produced by cyclic deformation of the damper was investigated during the tests. Data of the material-temperature decay from various initial temperatures were obtained. It was observed that the rate of the temperature decay depends on the initial temperature of the VE material and, modeled as a simple exponential decay

$$\dot{\theta}(t) = -\frac{1}{\gamma_\theta}(\theta(t) - \theta_{amb}), \tag{3}$$

where θ_{amb} = ambient temperature, yields cooling times γ_θ of about $2000s$ for $\theta(t) - \theta_{amb} \approx 1^\circ C$, $1000s$ for $\theta(t) - \theta_{amb} \approx 10^\circ C$, and $700s$ for $\theta(t) - \theta_{amb} \approx 20^\circ C$, for the dampers tested. In general, the rate of cooling of a VE damper will depend on its geometry, and is a complex process because it depends on the initial temperature distribution which in turn depends on the stress history. An important aspect verified during testing is that the time constant of this process is significantly longer than the duration of earthquake signals.

MODEL OF VISCOELASTIC MATERIAL INCORPORATING TEMPERATURE

A model using a chain of Maxwell elements in parallel with temperature-dependent properties is described in this section. The dynamics of the material temperature is modeled using a first-order differential equation which accounts for heat generation in the VE material and energy losses due to conductivity and radiation. The model of the damper is implemented numerically to assess the effects of temperature variations on the performance of structures incorporating VE dampers.

Models Considered in the Literature

A widely used concept in linear viscoelasticity is the time-temperature superposition principle, which states that the following relationship holds for the complex *modulus* $G(\varpi,\theta) = G(\varpi\alpha(\theta),\theta_{ref})$, where θ is the temperature of the material, θ_{ref} = a reference temperature, and $\alpha(\theta)$ = shift factor. In the time domain, these relationships imply $E(t,\theta) = E(t/\alpha(\theta),\theta_{ref})$, where E is the relaxation function of the material and $t/\alpha(\theta)$ is called the reduced time. Materials exhibiting this property are called thermorheologically simple.

For transient temperature conditions, Morland and Lee (1960) proposed the use of an integral expression of the reduced time. More recently, a Kasai *et al.* (1993) and Aprile (1995) have proposed evolutionary models in which the shear stress is expressed as:

$$\sigma(t) = \frac{1}{2\pi}\int_{-\infty}^{\infty} G(\varpi,\theta(t))\Gamma(\varpi)e^{j\varpi t}d\varpi \tag{4}$$

where the evolutionary complex *modulus* $G(\varpi,\theta(t))$ is modeled using fractional derivative operators and the temperature dynamics is modeled neglecting heat losses due to radiation and conduction in the damper and approximating the energy dissipation rate by the instantaneous power, which leads to

$$\theta(t) - \theta(t_o) \approx \frac{1}{c_\theta}\int_{t_o}^{t}\sigma(t')\dot{\gamma}(t')dt' \tag{5}$$

where c_θ = thermal inertia of the VE material, and t_o = initial time.

A model of this kind incorporates the dependence of the mechanical properties of the VE material on temperature, but makes an approximation in the dynamics of the material temperature because of the difference between the energy dissipation rate and the input energy rate (Inaudi and Kelly, 1996) and the neglect of conduction and radiation heat losses of the material. In addition, these models use fractional derivatives which require step-by-step solutions in the frequency domain (Aprile, 1995) or memory variables to approximate the integro-differential equations in the time domain (Kasai *et al.*, 1993) in the case of transient temperature.

Maxwell Chains with Temperature-Dependent Parameters

A Maxwell chain with temperature-dependent relaxation times is used to model VE materials in this section. In an attempt to improve the temperature model shown in Eq. (5), and still keeping a simple model for the temperature dynamics without accounting for strain localization and variations of the temperature field in the VE pad, yet at the same time, accounting for radiation and conduction heat losses from the damper, a simple one dimensional differential model for the temperature of the VE material is proposed. The main motivations behind this approach are computational advantages over fractional-derivative models, simpler parameter identification procedure for the model parameters (a linear least-square problem), and exact estimation of the energy dissipation rate.

The force $f(t)$ in the proposed model for the damper satisfies

$$f(t) = A\sum_{1}^{N_e} z_i(t) + k_o v(t) \tag{6}$$

where A = shear area of the damper, k_o = static stiffness, and the N_e state variables $z_i(t)$ satisfy

$$\dot{z}_i(t) = -\frac{1}{\tau_i(\theta)} z_i(t) + \beta_i \dot{\gamma}(t) \tag{7}$$

where $\tau_i(\theta)$ = relaxation time of the i-th Maxwell element, β_i = elastic *modulus* of the i-th Maxwell element, and $\dot{\gamma}(t) = \dot{v}(t)/h$. Utilizing a thermorheologically-simple model for the Maxwell chain, we have

$$\tau_i(\theta) = \tau_i(\theta_{ref})\alpha(\theta) \tag{8}$$

In this work, we use the following expression for the shift factor (Kasai *et al.*, 1993)

$$\alpha(\theta) = (\theta_{ref}/\theta)^p \tag{9}$$

Using the database of polymer Scotchdamp 109 and for a reference temperature of $21^\circ C$, the shift factor is curve fitted to the experimental data to obtain $p = 5.61$. The model parameters β_i are obtained using least squares by selecting a set of $\tau_i(\theta_{ref})$ and minimizing the square differences in the storage and loss *moduli* between the model and the experimental values.

The temperature dynamics is modeled as

$$\dot{x}(t) = -\frac{1}{\gamma_\theta} x(t) + \frac{1}{c_\theta}\dot{W}(t) \tag{10}$$

where $x(t) = \theta(t) - \theta_{amb}$, γ_θ = cooling time constant due to conduction and radiation losses, c_θ = thermal inertia of the VE material, and $\dot{W}(t)$ = energy dissipation rate per unit mass which for this model, can be written as

$$\dot{W}(t) = \sum_{i=1}^{N_e} \frac{z_i^2(t)}{\tau_i(\theta(t))\beta_i} \tag{11}$$

Equations (7) and (10) are coupled differential equations that model the stress and temperature dynamics in a model with $N_e + 1$ internal variables, $z_i(t)$ and $x(t)$.

Comparison with Experimental Data

Comparisons were made between the recorded experimental data and the model predictions. This was done using deformation signals recorded during tests and simulating the proposed model subjected to these deformation signals. The numerical integration scheme utilized used a predictor-corrector scheme on a partition of the differential equations based on the fact that the temperature dynamics has a large time constant. Analytical predictions with and without temperature transients were compared with recorded responses and very satisfactory correlation was obtained incorporating Maxwell chains with 5 to 10 elements in parallel.

Figure 2 shows the model prediction of the storage and loss *moduli* at $21^\circ C$ obtained using 10 Maxwell elements with relaxation times at the reference temperature between $0.001s$ and $1000s$. Better fit to the experimental data can be obtained using a larger number of Maxwell elements in parallel at the cost of increasing the order of the model.

Figure 3 shows a comparison of experimental and simulated damper force in the case of a sweep deformation signal of $40s$ in duration obtained using the Maxwell model shown in Fig. 2. The ambient temperature of this test was $24^\circ C$, $\gamma_\theta = 1000s$, and $c_0 = 0.0051^\circ Cin^2 / lb$. As shown in Figs. 3a and 3b very satisfactory correlation is obtained in the estimation of the damper force. Figure 3c shows the material temperature recorded in the tests and that obtained in the simulation; again very good correlation is obtained.

EFFECTS OF TEMPERATURE IN DEFORMATION SPECTRA

A study of the effects of temperature variations on the response of single-degree-of-freedom (SDOF) oscillators incorporating VE dampers was carried out using numerical simulation. The model studied was

$$m\ddot{y}(t) + m\omega^2 y(t) + f(t) = -m\ddot{u}_g(t) \qquad (12)$$

where $m =$ mass, $\omega =$ undamped natural frequency, $\ddot{u}_g(t) =$ ground acceleration, and $f(t) =$ force in the VE damper modeled according to Eq. (6). The parameters A and h of the damper were selected such that the model had a specified equivalent damping $\xi = (AG_l(\omega)/h)/2(AG_s(\omega)/h + m\omega^2)$ at the ambient temperature, and a specified estimated maximum shear strain $\hat{\gamma}_{max} = D(\omega,\xi)/h$ for the ground motion considered, where $D(\omega,\xi) =$ displacement response spectra of a Kelvin SDOF oscillator with parameters ω and ξ, for the ground motion considered.

Figure 4 shows deformation spectra and material temperature spectra for SDOF oscillators with equivalent damping $\xi = 0.05, 0.10, 0.15, 0.20$ and estimated maximum shear strains of $\hat{\gamma}_{max} = 0.20$ in figures (a) and $\hat{\gamma}_{max} = 0.50$ in figures (b). The initial temperature and ambient temperature were assumed as $21^\circ C$. As shown in the bottom figures, the temperature increase in the VE material decreases with an increase in the equivalent damping constant (Inaudi *et al.*, 1993; Inaudi and Kelly, 1996), and does not exceed $4^\circ C$ in the case of $\hat{\gamma}_{max} = 0.20$ (low design shear-strain values), while it reaches almost $30^\circ C$ in the case of $\hat{\gamma}_{max} = 0.50$ and $\xi = 0.05$. As shown in the top figures, these temperature variations have a detrimental effect on the deformation of the oscillator which increases as the temperature rise in the damper increases. It is observed that the temperature increase decreases with the undamped natural period of the structure because, although the estimated strain levels are the same for the complete period range, the number of deformation cycles increases with the natural frequency of the structure and, consequently, higher total energy dissipation should be expected in the case of structures with larger frequencies. Similar conclusions can be reached analyzing other earthquake signals (Inaudi and Kelly, 1996).

These type of response spectra can be utilized to recommend allowable design shear strain values for VE dampers and are being currently studied by the writers.

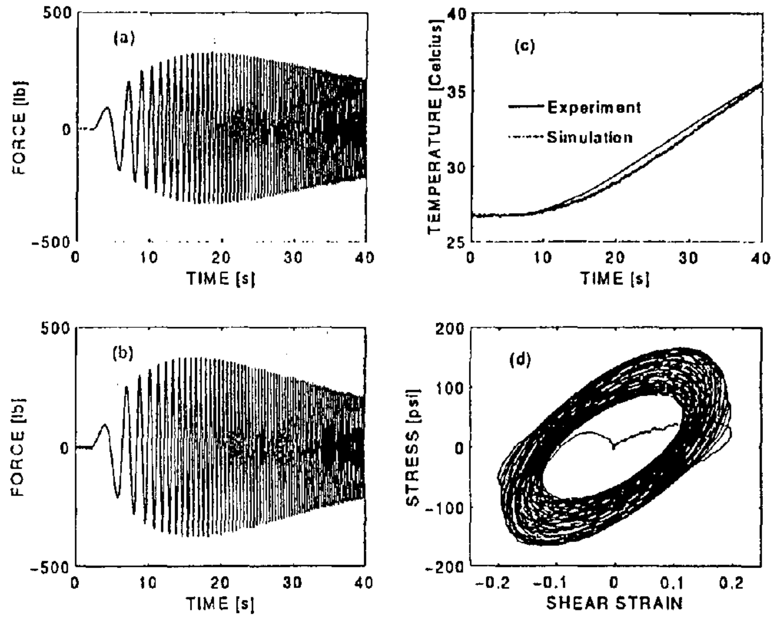

Fig. 3. Comparison of experimental and simulation results during a sweep deformation test (ambient temperature = 24°C): (a) Force recorded during experiment, (b) Force obtained by simulation, (c) Material temperature in experiment and simulation, (d) Hysteresis loops obtained in the simulation.

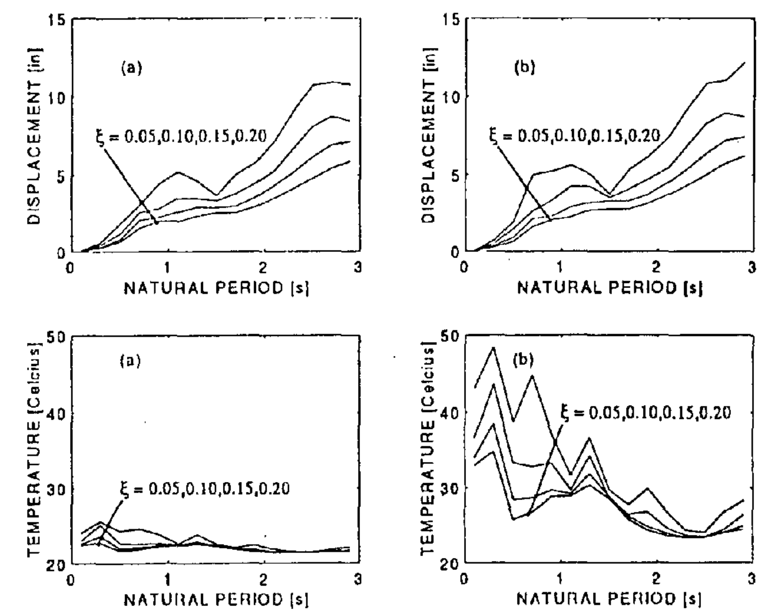

Fig. 4. Displacement spectra and material temperature spectra: (a) Design shear strain = 0.20, (b) Design shear strain = 0.50.

CONCLUSIONS

A simple and efficient model for VE dampers in structures subjected to earthquake or wind-type excitations which accounts for temperature variations due to heat generation in the material and radiation and conductivity losses was presented. Good correlation was obtained when comparing analytical predictions and experimental data. The effects of heat generation on the response of SDOF structures with supplemental VE dampers were evaluated using numerical simulation. Based on these results, design recommendations regarding design strain levels for VE dampers can be developed. On the basis of results obtained in this research, a maximum value of $\hat{\gamma}_{max} = 0.15$ is recommended when linear analysis is to be used in the estimation of the response of the structure, that is if transient temperature effects are to be neglected. Nonlinear analysis is recommended for cases in which $\hat{\gamma}_{max} > 0.15$, that is when temperature can have significant effect on the structural response.

ACKNOWLEDGMENTS

This test program was carried out with the financial support of The 3M Company. This support is greatly appreciated. The experiments were conducted at the Laboratory of the Civil Engineering Department of the University of California at Berkeley. Mark Troxell was in charge of the specimen setup and Todd Merport verified all electronic components, and programmed and operated the data acquisition and control system.

REFERENCES

Aiken, I.D., and Kelly, J.M., (1990). Earthquake simulator testing and analytical studies of two energy-absorbing systems for multistory buildings, *Report No. UCB/EERC-90/03*, Earthquake Engineering Research Center, University of California at Berkeley.

Aprile, A., (1995). Evolutionary constitutive model for viscoelastic dissipaters (In Italian), *Ph. D. Thesis*, Universita degli Study di Bologna, Bologna, Italy.

Blondet, M., (1993). Dynamic response of two viscoelastic dampers, *Report to County of Santa Clara Construction Service Division*, University of California at Berkeley, Department of Civil Engineering.

Chang, K.C., Soong, T.T., Oh, S-T., and Lai, M.L., (1992). Effect of ambient temperature on viscoelastically damped structures, *Journal of Structural Engineering, Vol. 118, No. 7*, pp. 1955-1973.

Inaudi, J.A., Zambrano, A. and Kelly, J.M., (1993). On the analysis of structures with viscoelastic dampers", *Report No. UCB/EERC-93/06*, University of California at Berkeley.

Inaudi, J.A., and Kelly, J.M., (1996). Nonlinear models for viscoelastic dampers subjected to transient temperature conditions, *Report UCB/EERC* (to be published).

Kasai, K., Munshi, J.A., Lai, M. L., and Maison, B.F., (1993). Viscoelastic damper hysteretic model: theory, experiment and application, *Proc. of ATC 17-1 Seminar on Seismic Isolation, Passive Energy Dissipation, and Active Control, Vol. 2*, pp. 521-532, Applied Technology Council, Redwood City, California.

Mahmoodi, P., (1969). Structural dampers, *Journal of Structural Division, Vol. 95, No. ST8*, pp. 1661-1672.

Morland, L.W. and Lee, E.H., (1960). Stress analysis for linear viscoelastic materials with temperature variation, *Trans. Soc. Rheology, Vol 4.* No. 4. pp. 223.

Nielsen, E.J., Lai, M.L., Soong, T.T., and Kelly, J.M., (1994). Viscoelastic damper overview for seismic and wind appliactions, *Proc. First World Conference on Structural Control, Vol. 3*, pp. FP3/42-FP3/51.

Sackman, J. L, Kelly, J.M., and Javid, A.E., (1991). Constitutive modeling of nonlinear damping materials, *Proc. of Damping'91, Vol. II*, pp. EBC/1-EBC/15, Wright-Patterson Air Force Base, Ohio.

Soong, T.T., and Lai, M.L., (1991). Correlation of experimental results with predictions of viscoelastic damping of a model structure, *Proc. of Damping'91, Vol. II*, pp. FCB/1-FCB/8. Wright-Patterson Air Force Base, Ohio.

EVALUATION METHODS FOR REINFORCED CONCRETE COLUMNS AND CONNECTIONS

D.E. LEHMAN[1], A.C. LYNN[1], M.A. ASCHHEIM[2] AND J.P. MOEHLE[1]

[1] Earthquake Engineering Research Center
University of California at Berkeley
1301 S. 46th St. Richmond CA 94804-4698

[2] Department of Civil Engineering, University of Illinois
2118 Newmark Civil Engineering Laboratory MC-250
205 North Mathews Urbana IL 61801

Abstract

Damage to reinforced concrete frames not meeting current seismic code regulations has been prevalent in recent earthquakes. Performance of reinforced concrete frame buildings in past earthquakes reveals common failure modes: shear failure and/or splice failure of columns, shear failure of beam-column joints or pullout of reinforcement embedded in beam-column joints. The following paper presents methods to evaluate the strength of reinforced concrete columns and connections with deficient details. Recent experimental and analytical research efforts at the University of California at Berkeley have focused on methods to evaluate concrete frames vulnerable to damage in an earthquake. Evaluation methods to assess the strength of reinforced concrete columns and connections are validated using experimental research results.

Keywords

Reinforced concrete, columns, beam-column joints, retrofit, evaluation, rehabilitation, splices, shear strength

Introduction

Reinforced concrete buildings designed according to older code provisions have been found to be especially vulnerable to earthquake damage. Where current code regulations have stringent detailing requirements to ensure ductile behavior, previous regulations have been primarily strength based. Although new design permits economical construction of well-detailed components, the construction cost of upgrading schemes may be prohibitive. An accurate assessment of the system capacity may be required for economical reasons.

The paper presents methods to evaluate the strength of columns and beam-column connections found in older reinforced concrete building construction. The methods included were verified using results from recent experimental efforts at U.C. Berkeley as well as other research institutions. Methods to evaluate the shear strength and lap splice capacity of reinforced concrete building columns are presented in light of recent column tests. Strength of connections is evaluated considering bar pullout and joint shear.

Details

In existing, pre-1970's construction, it is common to find column longitudinal reinforcement spliced just above the joint where maximum moments develop. Splice lengths and transverse reinforcement along the splice were often calculated assuming the splice acted only in compression; the resulting splice tensile strength and ductility are commonly inadequate for expected loadings. Column longitudinal reinforcement may be poorly distributed around the perimeter of the column core. Transverse reinforcement was often sized to resist code-specified shear forces and may be inadequate to resist the shear corresponding to development of column or beam flexural plastic hinges. It is not uncommon for beams bottom longitudinal reinforcement to terminate a short distance into the joint, creating the possibility of bar slip (or pullout) under moment reversals. Column bars may be poorly distributed around the joint perimeter, and may be spliced just above the joint. Finally, there may be minimal transverse reinforcement in the joint, or none at all. Other potential problems such as eccentric joints may also be found.

Materials

Evaluating the behavior of existing reinforced concrete construction requires evaluation of *in situ* material strengths. Assumed material strength values should be realistic yet conservative estimates of expected values. Longitudinal reinforcement yield strength commonly may be as low as the specified yield strength; however, yield strengths exceeding the minimum specified strength by as much as 20 percent of the nominal value also are not uncommon. For members subjected to inelastic moment reversals, high yield strength combined with strain hardening may result in stresses as high as $1.5f_y$ (f_y is defined as the specified or nominal yield strength). Concrete material strengths vary widely relative to design values. With well-compacted, well-cured concrete, compressive strengths usually exceed design values at early ages and continue to increase with time. In other cases, substandard concrete will be found.

Columns

Response and failure of a reinforced concrete column in a building frame under reversed cyclic loading may be controlled by combined axial load and flexure, shear, splice failure, or a combination of these. An experimental program at the University of California at Berkeley has studied these aspects for deficient building columns (Lynn and Moehle). Eight columns were constructed at full scale with an 18-in. (46-cm) square cross-section and 10-ft (3-m) clear height. The columns were reinforced with Grade 40 (275 MPa) steel, either eight # 8 bars (25-mm) or eight # 10 (32-mm) bars longitudinally with #3 (1-mm) Grade 40 (275 MPa) perimeter hoops. Ties used in the first six specimens were square hoops with an 18-in. spacing. Specimens 7 and 8 were detailed with diamond ties spaced at 12 inches. Lap splices, used in three of the eight columns, have a length of 20 longitudinal bar diameters. The loading included axial load plus reversed cyclic lateral load with zero imposed rotation at the column ends. Details of all columns in the test series are provided in Table 1.

Flexural-axial strength of column sections with light transverse reinforcement can be calculated using standard ACI methods with expected material strengths, with direct consideration of material overstrength, strain hardening, or understrength is sufficient. Table 1 presents flexural strengths for the columns tested by Lynn and Moehle computed according to ACI 318-95.

Figure 2 displays results for specimen 2 (Lynn and Moehle). The column was detailed with lapped longitudinal bars. For Grade 40 bars, 20-bar diameter laps, and widely-spaced ties, the bars are barely able to develop yield, and rapidly lose capacity following yield. When the lap fails, moment capacity at the lap reduces to a value corresponding approximately to the product of the axial load and half the section depth. This failure may transform an otherwise strong-column/weak-beam connection into a weak-column/strong-beam connection.

For columns with short, unconfined lap splice lengths, the cover concrete controls the splice capacity. The stress capacity of the splice may be computed according to equation proposed by Orangun *et al.*, as follows:

$$f_s = \frac{4ul_s}{d_b} \leq f_y \;. \tag{1}$$

where the bond strength, u, is determined using Equation 2.

$$u = (1.22 + 3.23C/d_b + 53d_b/l_s)\sqrt{f_c'} \text{ with } C/d_b \le 1.5, \text{ with } f_c' \text{ in psi.} \qquad (2)$$

This formulation has been verified for nominal steel strengths of 60 ksi (400 MPa) or less, and specified concrete strengths not exceeding 5 ksi (30 MPa).

Post-yield behavior of a lap splice is strongly dependent on the amount and arrangement of the transverse reinforcement. According to Sivakumar, *et al.* a well-confined lap splice has transverse steel at a spacing not exceeding s_{max}, with s_{max} defined as follows:

$$s_{max} = \frac{25l_s\sqrt{A_{tr}}}{f_y d_b^2} * \frac{m}{n} \qquad (3)$$

where the ratio m/n is 1 for circular sections. When Equation (3) is not satisfied, it is likely that the stress capacity will degrade with continued cycling. When Equation (3) is satisfied, the post-yield behavior may allow excursion into the inelastic range without rapid degradation.

Experimental details for five specimens with inadequate lapped splices are shown in Table 2. For all columns, failure corresponded to loss of lap splice capacity. Results for the five specimens using Equations 1, 2 and 3 is also included in the table. Using Equation 2 for a typical building column, represented by Specimen 2 by Lynn and Moehle, results in a bond strength of $10\sqrt{f_c'}$, psi .

Shear strength of a reinforced concrete column varies with concrete strength, transverse reinforcement, axial load, load history and flexural ductility demand. Shear strength expressions used for the design of new building columns tend to be unnecessarily conservative for existing construction where the engineer does not have the opportunity to place copious amounts of transverse reinforcement at a reasonable cost. Alternative expressions may be desirable for existing construction.

Figure 3 compares the observed variation of shear strength as a function of displacement ductility demand using experimental results from Lynn and Moehle. All columns failed in an apparent shear mode (as indicated by crack patterns) following flexural yield. The plot shows the normalized shear as a function of the displacement ductility, both at time of failure. The displacement ductility is defined as the ratio of the displacement corresponding to a 20% reduction in strength to the displacement corresponding to first yield of the longitudinal bars. The data indicate that shear strength is reduced for increased displacement ductility demand. On the basis of the data shown in Figure 3, as well as other data, the following model for shear strength is proposed. The equation is appropriate for building columns with an aspect ratio exceeding 2.5.

$$V_n = 3.5\left(q + \frac{N_u}{f_c' A_g}\right)\sqrt{f_c'}A_e, \text{(psi) with } 1 \ge q = (4 - \mu_\delta)/3 \ge (1/3.5) \qquad (4)$$

Typical tie spacings in existing buildings column exceed d/2, rendering the shear strength normally associated with transverse confinement (ACI-318) negligible. Equation 4 is appropriate for columns with widely-spaced ties. For columns with a larger amount of transverse reinforcement, the following expression from Aschheim and Moehle (1992) may be more appropriate.

$$V_n = V_c + V_s,\ V_c = 3.5\left(k + \frac{N_u}{2000A_g}\right)\sqrt{f_c'}A_e, \text{(psi)},\ V_s = \frac{mA_{tr}f_y d}{s\tan 30} \qquad (5)$$

$$\text{with } 1 \ge k = (4 - \mu_\delta)/3 \ge 0$$

Values given by the previous expressions should be interpreted with caution. The displacement ductility term, μ_δ, is difficult to assess, in the laboratory and more so in existing buildings. Furthermore, the slope of the line representing the relationship between column shear strength and displacement ductility demand is dependent on the load history; a larger number of cycles at the same displacement ductility demand is likely to result in a steeper slope and vice versa. Both issues should be considered when evaluating column shear strength.

The preceding expressions have been developed for slender columns. Studies show these expressions are unnecessarily conservative for columns with an aspect ratio of less than 2.5. The following expressions from Umehara and Jirsa give reasonable correlation with observed shear strengths for columns with aspect ratio less than 2.5.

$$V_n = \left(11 - 3\frac{a}{d}\right)A_c\sqrt{f_c'} + \frac{0.2N_u}{a/d}, \text{psi} \; ; \; \frac{0.2N_u}{a/d} \le \frac{160A_g}{a/d}, \; 1 \le a/d \le 2.5 \qquad (6)$$

Beam-Column Connections

Embedded Bar Strength

Strength of a beam-column connection may be limited by pullout of discontinuous bottom beam reinforcement. To determine if the bar embedment length is adequate, a procedure adopting guidelines developed by Eligehausen *et al.* is used. In the adaptation, the stress in the column longitudinal reinforcement is used as an indicator of the transverse stress field acting on the embedded bar. For zero column reinforcement tensile stress, the maximum pullout strength is obtained corresponding to shearing failure of the concrete surrounding the bar. For high column reinforcement stresses, a minimum pullout strength is obtained. The procedure is as follows:

1. Following the recommendations of Eligehausen *et al.*, the maximum and minimum strengths for normal strength concrete and for bars that are #10 or less are:

$$F_{min} = 5\sqrt{f_c' \text{ psi}}(\pi d_b l_s) \; ; \; F_{max} = 30\sqrt{f_c' \text{ psi}}(\pi d_b l_s)$$
$$\text{with } F_{min} < F_{max} \le F_y \qquad (7)$$

   where F_{max} is less than or equal to the expected yield strength.
2. The flexural strengths of the beam, M_{bmin} and M_{bmax}, corresponding to development of F_{min} and F_{max}, are determined.
3. The column flexural demands, M_{co} and M_{c1},, are computed. Using the Eligehausen *et al.* recommendations, development of M_{bmax} in the beam corresponds to no tensile stress in the column longitudinal bars. Development of M_{bmin} in the beam corresponds to a tensile stress of 43 ksi in the column longitudinal bars. Therefore, M_{co} corresponds to $f_{sc} = 0$ ksi and M_{c1} corresponds to $f_{sc} = 43$ ksi.
4. Assuming the flexural demand is distributed according to the relative stiffnesses of the columns adjacent to the connection, the maximum and minimum flexural demands in the column, M_{cmin} corresponding to M_{bmin} and M_{cmax} corresponding to M_{bmax}, are determined.
5. The following table can be constructed and the two series plotted (Figure 4):

X axis	Series 1	Series 2
M_{bmin}	M_{c1} (43 ksi)	M_{cmin}
M_{bmax}	M_{co} (0 ksi)	M_{cmax}

The intersection point of the two series is the beam flexural strength, M_b, corresponding to bond failure of the embedded bar.

Table 3 presents experimental data for joints with embedded bars. The embedment length, material strength and experimental results are presented. The flexural strength, M_b, computed using the above procedure gives reasonable correlation with the experimental values.

Shear Strength

Several researchers have reported behavior of interior and exterior connections representative of those found in pre-1970's concrete construction. A commonly reported index is the nominal joint shear stress before onset of joint failure. This measure of joint capacity must be viewed cautiously. Joint shear strength appears to depend not only on joint size, geometry, materials, and reinforcement quantity, but also on bond conditions within the joint and flexural ductility levels of the adjacent framing members. For example, a joint shear strength measured in a test in which the framing members did not yield may not be applicable for an identical joint in which the framing members are yielding. More general relations between joint shear strength and component ductility levels are desirable but not yet available for existing construction details. Modern beam-column connections in ductile moment resisting frames are required to remain intact even after flexural yielding of adjacent members. Since most upgrading schemes require ductile retrofit of adjacent members, joint shear strength values reported herein are for joints failing in shear following flexural yielding only.

Figure 5 presents data on interior joints gathered by Otani. These data suggest that interior joint shear strength is sensitive to small changes in transverse reinforcement, but strength does not increase significantly for transverse reinforcement ratios above about 0.003 (relevant data labeled with triangles). Similar results were reported by Kurose *et al.* as shown in Figure 6 (relevant data labeled with squares) (The mechanical joint lateral reinforcement ratio of 3 is approximately equivalent to a reinforcement ratio of 0.003 for typical material strengths found in existing construction). Figure 7 presents data on exterior joints reported by Kurose *et al.* (relevant data labeled with squares). Note that for exterior joints, ACI 318-95 prescribes a joint shear strength of $12\sqrt{f_c'}A_j$. All exterior joints (without transverse beams) failing at a joint shear demand less than that prescribed by ACI had a deficient amount of transverse steel.

On the basis of the preceding information, nominal joint shear strength can be expressed as:

$$V_n = \lambda\gamma\sqrt{f_c'}A_j, \text{psi} \tag{8}$$

in which λ= 0.75 for LWC or 1 for NWC, and γ and A_j are as defined below.

Value of γ	Interior joint		Exterior joint		Knee joint
ρ''	With transverse beams	Without transverse beams	With transverse beams	Without transverse beams	
<0.003	12	10	8	6	4
≥0.003	20	15	15	12	8

Effective joint area A_j is defined according to ACI 318-95 for concentric joints. Joint shear strength values for exterior joints without transverse beams may overestimate the joint shear strength capacity of joints with high flexural ductility demand. Use of joint shear strength values without further experimental verification should be done so with caution.

Acknowledgments

The experimental research program focusing on the evaluation of building columns was funded by the National Science Foundation. In addition, the authors would like to acknowledge the California Seismic Safety Commission and the Applied Technology Council for their support of this research. Opinions, findings and conclusions expressed in this paper are those of the authors, not necessarily those of the sponsors.

References

ACI-318 (1995), Building Code Requirements for Reinforced Concrete, American Concrete Institute

Aboutaha, R.S.; Engelhardt, M.D.; Jirsa, J.O.; Kreger, M.E. (1993), Seismic Strengthening of R/C Columns Using Steel Jackets, ASCE Structures Congress 1993, Irvine CA

Aschheim, M.A. and Moehle, J.P. (1992), Shear Strength of Deformability of R/C Bridge Columns Subjected to Inelastic Cyclic Displacements, U.C. Berkeley, Report No. UCB/EERC-92/04, April 1992

Beres, A.; El-Borgi, S.; White, R.N.; Gergely, P. (1992), Experimental Results of Repaired and Retrofitted Beam-Column Joint Tests in Lightly Reinforced Concrete Frame Buildings, NCEER-92-0025

Chai, Y. H.; Priestley, M.J.N.; Seible, F. (1991) Seismic Retrofit of Circular Bridge Columns for Circular Flexural Performance, *ACI Structural Journal*, Vol. 88 no. 5, Sept. 1991

Eligehausen, R.; Popov, E.P.; Bertero, V.V. (1983) Local Bond Stress-slip Relationships of Deformed Bars under General Excitations, U.C. Berkeley, Report No. UCB/EERC-83/23, Oct. 1983

Kurose, Y.; Guimaraes, G.N.; Liu, Z.; Kreger, M.E.; Jirsa, J.O. (1988), Study of R/C Beam-Column Joints under Uniaxial and Biaxial Loading, University of Texas at Austin, PMFSEL Report 88-2

Lowes, L.N.; Moehle, J.P. (1995), Seismic Behavior and Retrofit of Older Reinforced Concrete T-Joints, U.C. Berkeley, UCB/EERC - 95/09, Sept. 1995

Lynn, A.C.; Moehle, J.P. (1996) Evaluation of Existing Reinforced Concrete Building Columns, U.C. Berkeley, Internal Document

Orangun, C.O.; Jirsa, J.O.; Breen, J.E. (1977) A Reevaluation of Test Data on Development Length and Splices, *ACI Structural Journal*, March 1977, pp. 114-122

Otani, S. The AIJ Proposal of Ultimate Strength Design Requirements for R/C Buildings with Emphasis on Beam-Column Joints, Design of Beam Column Joints for Seismic Resistance, ACI SP-123

Pessiki, S.P.; Conley, C.H.; Gergely, P.; White, R.N. (1990), Seismic Behavior of Lightly Reinforced Concrete Column and Beam-Column Joint Details, NCEER-90-0014

Priestley, M.J.N.; Seible, F.; Chai, Y.H.; Wong, R. (1992), Santa Monica Viaduct Retrofit - Full-Scale Test on Column Lap Splice with #11 [35mm] Reinforcement, UCSD Report No. SSRP-92/08, Sept. 1992

Sivakumar, B.; Gergely, P.; R.N. White (1983), Suggestions for the Design of R/C Lapped Spliced for Seismic Loading, *Concrete International*, February 1983, pp. 46-50

Soyer, C.; Moehle, J.P. (1992), Behavior of R/C Cap Beam-Column Exterior Bridge Joints, U.C Berkeley, 299 Report, April 1992

Umehara, H.; and Jirsa, J. (1984), Short Rectangular R/C Columns Under Bidirectional Loadings, *Journal of Structural Engineering*, Vol. 110, no. 3, March 1984

Valluvan, R.; Kreger, M.E.; Jirsa, J.O. (1993) Strengthening of Column Splices for Seismic Retrofit of Nonductile Reinforced Concrete Frames, *ACI Structural Journal*, Vol. 90, no. 4, July 1993

List of Symbols

a/d - column aspect ratio
A_c - area of core cross-section
A_e - area of effective cross-section
A_g - area of gross cross-section
A_j - effective joint area (ACI-318)
A_{tr} - area of transverse reinforcing bar
C - concrete cover
d_b - bar diameter
f'_c - concrete compressive strength
f_s - lap splice strength
f_{sc} - tensile stress in column longitudinal bars
f_y - yield strength of longitudinal steel
l_s - lap splice length
m - number of transverse reinforcing bars
M_{exp} - experimental flexural strength
μ_δ - displacement ductility
n - number of spliced longitudinal bars
n_s - number of cycles sustained
N_u - axial load
ρ'' - transverse reinforcement ratio
s - actual tie spacing
s_{max} - maximum tie spacing
u - bond stress
V_c - shear strength attributed to concrete
V_n - shear strength of concrete section
V_s - shear strength attributed to steel
V_u - experimental shear strength

Tables and Figures

I.D.	f'_c	d_b	s	l_s	N_u	V_u	Δ_u	μ_δ	M_{exp}	M_{ACI}
1	3.71	1.25	12	no splice	113.4	61	1.91	1.60	3539	3604
2	3.71	1.25	12	25 in.	113.4	60	2.03	1.44	3481	3604
3	4.80	1.00	12	no splice	113.4	54	2.03	3.75	3133	2718
4	4.80	1.00	12	20 in.	113.4	52	2.16	4.94	3017	2718
5	3.70	1.00	12	no splice	340.0	71	1.27	1.20	4119	3364
6	4.00	1.25	12	no splice	340.0	76	1.07	1.43	4410	4258
7	4.00	1.25	18	no splice	340.0	80	1.91	1.20	4642	4258
8	3.70	1.25	18	25 in.	340.0	85	1.91	1.20	4932	4134

Table 1 Specimens Tested by Lynn and Moehle

Reference (I.D.)	f'_c	f_y	d_b	s	l_s	f_s actual	f_s Eqn. 2	f_{sact}/f_{scomp}	s_{max}	n_s
Lynn (2)	4.70	50	1.00	18	20	50	50	1.00	2	2
Aboutaha (1)	2.85	70	0.98	16	24	53	52	1.01	2	1
Priestley (1)	4.06	45	1.38	3.5	30	45	45	1.00	4	5
Chai (1)	5.54	46	0.75	5	15	46	46	1.00	3	
Valluvan (1)	3.50	70	0.75	12	18	42	44	0.96	3	1

Table 2 Splice Strength

Reference	f'_c	f_y	d_b	l_{de}	M_{exp}	M_b	M_{exp}/M_b
Pessiki (7)	3.37	69.4	1.00	6.0	1121	841	1.33
Pessiki (8)	3.37	69.4	0.75	6.0	1121	1104	1.01
Beres (4)	3.37	69.4	1.00	6.0	752	671	1.12
Lowes (1)	5.10	48	0.88	17.5	1472	1488	0.99
Soyer (1)	6.16	46	0.75	15.0	M_p	M_p	1.00

Table 3 Embedded Bar Strength

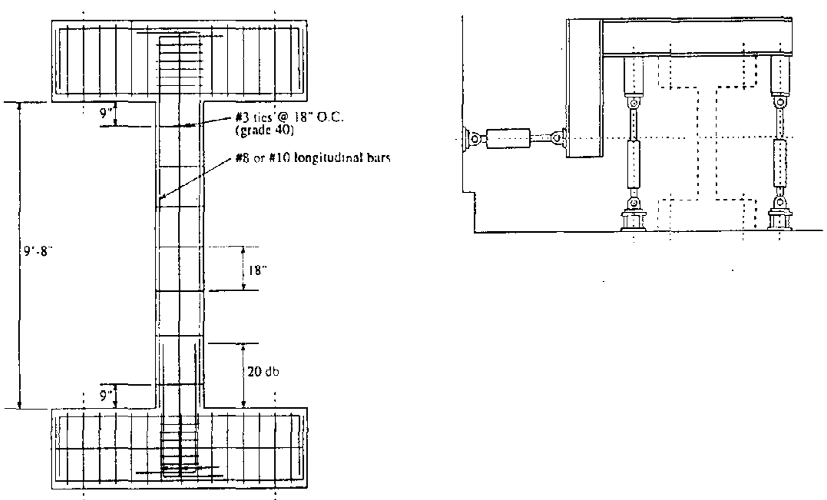

Figure 1 Columns Tested by Lynn and Moehle

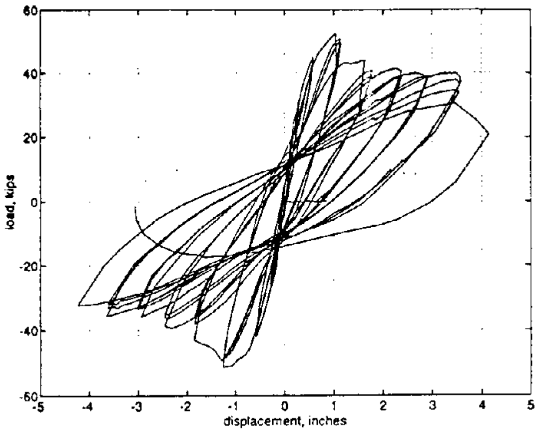

Figure 2 Response of Column with Spliced Bars

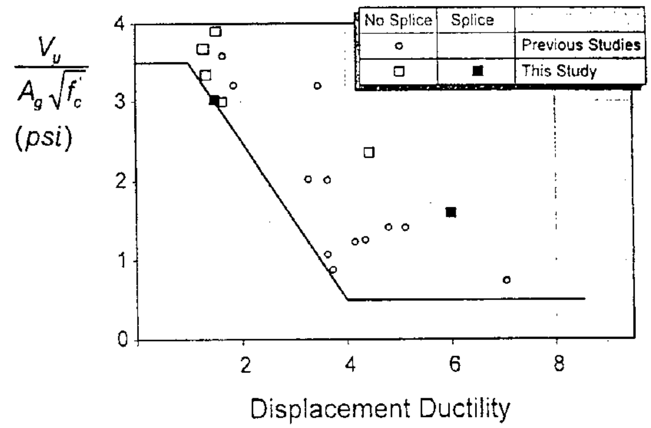

Figure 3 Experimental Column Shear Strength

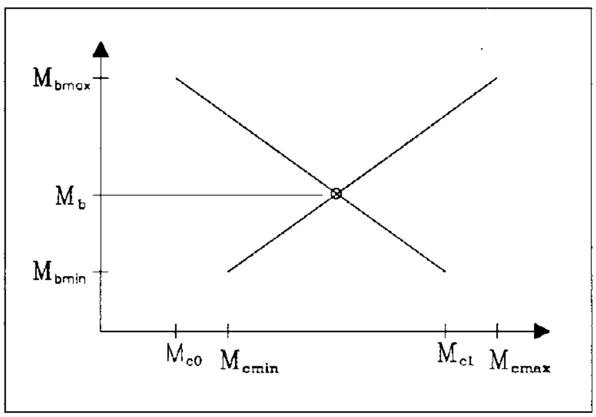

Figure 4 Graphical Computation of M$_b$

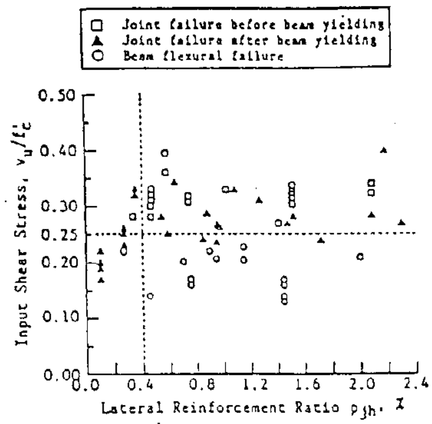

Figure 5 Interior Joint Shear Strength (Otani)

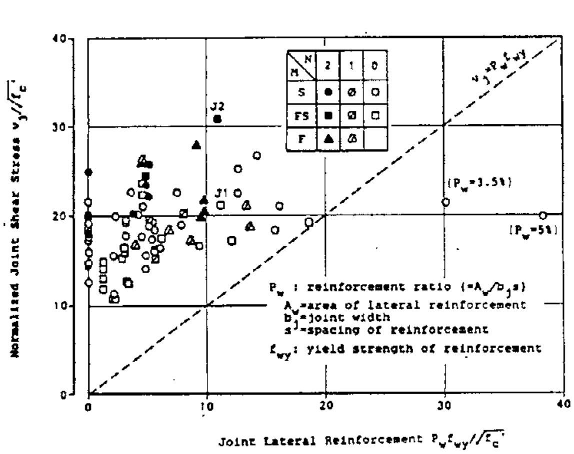

Figure 7 Interior Joint Shear Strength Kurose *et al.*

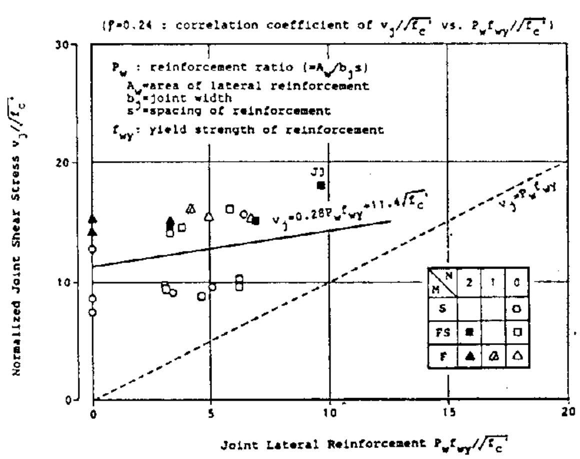

Figure 8 Exterior Joint Shear Strength Kurose *et al.*

BEHAVIOR AND REHABILITATION OF BEAM-COLUMN T-JOINTS IN OLDER REINFORCED CONCRETE BRIDGE STRUCTURES

LAURA N. LOWES,
Graduate Student Researcher, Department of Civil Engineering,
721 Davis Hall, University of California, Berkeley, California 94720.
and
JACK P. MOEHLE,
Professor of Civil Engineering and Director, Earthquake Engineering Research Center,
EERC, 1301 South 46th Street, Richmond, California 94804.

ABSTRACT

A series of experimental tests investigating the seismic behavior of reinforced concrete beam-column T-joints was recently completed at the University of California, Berkeley. The evaluated connection was representative of interior beam-column joints in multi-column bridge frames constructed in the 1950's and 1960's. Three one-third scale models, representing the as-built joint and two retrofit joints, were tested. The results of this research project are an improved understanding of the seismic behavior of lightly reinforced bridge T-joints, as well as verification of a design procedure for retrofitting this type of connection.

KEYWORDS

reinforced concrete; earthquake loading; retrofit; bridge design; seismic design; beam-column joint; t-joint; experimental testing; cyclic loading; bond.

INTRODUCTION

Recent earthquakes have exposed the weaknesses of older reinforced concrete beam-column bridge joints. The collapse of the upper deck of the Cypress Street Viaduct in Oakland, California during the Loma Prieta earthquake was attributed to the failure of exterior beam-column joints (Bollo, 1990). The Viaduct was constructed in the late 1950's when standard practice for bridge design did not specifically address joint design. At that time, design details for longitudinal reinforcement passing through or terminating in the joint were commonly based solely on anchorage requirements under gravity loading. Additionally, for ease of construction, transverse reinforcement was frequently discontinued in the joint region.

Researchers began a dedicated investigation of the design of beam-column joints for earthquake loading in the 1960's. Since then, the majority of this research has focused on new design of building joints and has not addressed the issues critical to retrofit design for existing bridge joints. Based on this research, current standard practice for the design of new building joints requires that transverse reinforcement be provided in the joint to transfer load and to confine the joint core concrete. However, it is often impractical to retrofit older, lightly reinforced joints with the volume of transverse reinforcement and reinforcement details recommended for design of new joints. Additionally, with older, lightly reinforced bridge joints, there are the concerns of deterioration of load transfer mechanisms due to the yielding of the members that frame into the joint, as well as development of adequate bar anchorage for member longitudinal steel passing through or terminating in the joint.

In California there is a significant number of older reinforced concrete bridges. Many of these bridges require retrofit of beam-column connections in order to ensure a ductile response to earthquake loading. With the goal of verifying a design procedure for retrofitting these joints, scaled models of an as-built beam-column T-joint (Model One) and two retrofit T-joints (Model Two and Model Three) were tested.

EXPERIMENTAL TEST MODELS AND TEST PROCEDURE

Engineering drawings of single level, multi-column reinforced concrete bridge frames designed and constructed in California in the late 1950's and early 1960's were reviewed to determine typical dimensions and reinforcement details. Based on this review, a prototype frame was designed (Figures 1 and 2). This frame included the following typical reinforcing details that were considered to be critical to the behavior of interior beam-column joints:

- Grade 40 (f_y = 317 MPa) column longitudinal reinforcing bars were anchored in the joint with straight development lengths of 20 d_b.
- Neither beam nor column transverse reinforcement was continuous through the joint region.
- The majority of beam bottom longitudinal reinforcement was not continuous through the joint.
- Column axial load was approximately three percent of nominal concrete capacity.
- Beams were designed so that maximum flexural reinforcement strain under gravity loads was approximately 25 percent of the yield strain.

During the 1950's and 1960's common practice did not dictate consideration of the relative flexural capacity of beams and columns framing into the joint, consideration of the force transfer through the joint region, or consideration of member shear capacity as a function of member flexural capacity. For this test program, the flexural reinforcement ratios of the prototype frame were adjusted to result in a frame that included the following target design features:

- The sum of the cap beam nominal flexural strengths exceeded the column nominal flexural strength (both projected to the joint center), although yield of the beam in positive flexure was expected prior to flexural yielding of the column. This target yield path was expected to result in particularly critical anchorage conditions for the column reinforcement.
- The maximum nominal joint shear stress was expected to be $22\sqrt{f_c}$ kPa, with f_c equal to the concrete compressive strength in kPa ($8.5\sqrt{f_c}$ psi, f_c in psi).
- To prevent shear failure of either the beams or the column, transverse reinforcement for both the beams and the column was designed to support the shear force corresponding to the member ultimate flexural strength. This resulted in the use of significantly more transverse reinforcement than is usually found in existing bridges from this time period.

Because of the size and strength of actual bridges it was not feasible to experimentally test in the laboratory an entire bridge frame. Therefore scaled sub-assemblages from the prototype frame were tested (Figures 1 and 2). By using a scaling factor of one-third, the test specimens were sufficiently large that it was possible to use the same construction materials in the models as were found in the actual structures. Sub-assemblages consisted of a single interior column, the beam-column joint and a portion of the cap-beam extending on either side of the joint. To model the internal force distribution, determined from an analytical model of the prototype frame, appropriate boundary conditions included the following (Figures 1 and 2):

- The moment and shear distribution at the beam-joint interface due to gravity loading was simulated by point loads acting on the top of beam. Gravity loads were reacted at the base of the column.
- Simulated earthquake loads were applied to the base of the column through an idealized pin. This loading was equilibrated by concentrated reactions acting perpendicular to the beam at the ends of the beam and by a compressive reaction acting along the axis of the beam at one end of the beam.

ANALYSIS OF EXPERIMENTAL DATA

To ensure that the results of this study could be compared with the results of previous research, nominal joint shear stress was computed as a measure of joint load. The ACI-ASCE Committee 352 (ACI-ASCE 352, 1985) procedures for calculation of joint shear force are based on the assumption that beams develop flexural strength at the joint face and that columns remain essentially elastic. The nominal joint shear stress calculated by this procedure acts on a horizontal plane at the mid-height of the joint. In bridge construction, where column yielding often is the desired mode of inelastic response, revised procedures for calculating the nominal joint shear stress are required, as described below.

To determine a nominal joint shear, the actions from the members framing into the joint were assumed to comprise member shear and tension and compression forces, with tension and compression forces representing the member moment and axial load, see Figure 3. Tension and compression forces at both the beam and column critical sections were assumed to act at the centroid of the extreme longitudinal reinforcement in the member (see Figure 3). The effective depth of the joint was defined to be equal to the depth of the member tension-compression couple (see Figure 3). Effective joint width was taken equal to the width of the beam, including retrofit if present. It is also noted that the member critical sections were located at the perimeter of the effective joint. Nominal horizontal joint shear was computed at mid-height of the joint and nominal vertical joint shear was computed at mid-span of the joint. Nominal joint shear stresses were computed as the nominal joint shear force divided by the appropriate effective joint area. Because in this study joint forces and joint areas were computed in a consistent manner, the resulting nominal vertical and horizontal joint shear stresses were equal (see Figure 3).

The effect on the joint of cyclic loading was evaluated through analysis of the load-displacement and nominal joint shear stress-strain relationships. The experimental load-displacement relationship was compared with that computed from a simple analytical model. Applied load corresponded to the simulated earthquake load applied transverse to the column axis by the actuator at the column base. Model displacement was defined as the displacement of the base of the column parallel to the beam axis. Analytical model strength was computed based on the flexural strength of the members. Member nominal flexural strengths were computed in accordance with ACI Committee 318 (ACI 318, 1989), with the exception that for Model One, beam positive nominal flexural strength was computed based on beam bottom longitudinal reinforcement being at the yield point. For Model One it was expected that beams would develop nominal positive flexural strength prior to the column; beam post-yield strength was computed based on the assumption that the beam bottom reinforcement carried the maximum measured tensile strength. Analytical model stiffness was computed assuming a rigid joint zone and constant stiffness for each member cross-section. For all members, with the exception of Model Three beams, cross-section stiffness was computed as the secant stiffness to the cross-section moment-curvature relationship at 75 percent of the nominal flexural strength. For Model Three beams, the cross-sectional stiffness was taken as the secant stiffness to the moment-curvature relationship at 75 percent of the maximum flexural load carried by the beams.

Nominal joint shear stress-strain relationships were also evaluated through comparison of the experimental and computed relationships. Nominal joint shear stress was computed from the measured load as previously discussed and joint shear strain was computed from deformation at the surface of the joint as measured by direct current differential transformers (DCDT's) and from deformation as measured by concrete strain gages embedded in the joint core. The experimental nominal joint shear stress-strain relationships were compared with that computed from the material constitutive relation.

Slip of column longitudinal reinforcement was measured as a means of evaluating the anchorage of this reinforcement in the joint. PVC tubing was used to leave a hole in the concrete extending from the top of the joint to the end of two column longitudinal bars anchored in the joint. DCDT's were used to measure the movement of the bar ends with respect to the top of the joint.

EXPERIMENTAL TEST MODEL ONE

Model One was the as-built model previously discussed (see Figure 2). When subjected to the simulated earthquake loading, the model did not perform in a ductile manner. Although the model carried the simulated gravity forces throughout the test, peak simulated earthquake load was only 66 percent of the nominal strength. The model exhibited a large reduction in stiffness and load capacity when cycled to relatively small maximum displacements and this degradation continued as testing progressed. Also during small displacement cycles, diagonal cracks formed in the cover concrete in the joint area; these cracks appeared to initiate in the concrete over the anchored column reinforcement and propagate towards the column compression zone. At the peak load, significant cracking occurred in the joint. These cracks appeared to delineate the anchorage zone of the column longitudinal reinforcement. During subsequent displacement cycles, damage continued to accumulate in the joint and the model began to lose simulated earthquake load carrying capacity. Testing of Model One was concluded when the model exhibited only minimal earthquake load capacity.

Figure 4 shows the experimental and computed load-displacement relationships for Model One, Figure 5 shows the experimental and computed nominal joint shear stress-strain relationships and Figure 6 and Figure 7 show the relationship between model displacement and slip of column longitudinal reinforcement. Model One carried a peak nominal joint shear stress of $14\sqrt{f_c}$ kPa, f_c in kPa ($5.4\sqrt{f_c}$ psi, f_c in psi). At the maximum load, column bar slip of 1.5 mm (0.06 inches) was measured. Bar slip accumulated as testing continued and the instrumentation maximum of 31 mm (1.2 inches) was measured prior to the final displacement cycles.

EXPERIMENTAL TEST MODEL TWO

Model Two was a retrofit as-built connection. The retrofit was designed following the testing of Model One and consisted of casting reinforced concrete bolsters on both sides of the existing as-built cap beam (see Figure 2). Bolsters were designed to increase beam flexural capacity so that under earthquake loading the column would develop nominal flexural strength while beams would remain essentially elastic. It was expected that the additional concrete volume in the joint region would result in a maximum joint shear stress comparable to the maximum stress developed in Model One and that additional concrete cover would increase bond stress capacity in the joint for the column reinforcement.

When subjected to simulated earthquake and gravity loads, Model Two maintained gravity load throughout the test and earthquake load carrying capacity to a nominal ductility of four. Model Two carried a peak nominal joint shear stress of $13.7\sqrt{f_c}$ kPa, f_c in kPa ($5.2\sqrt{f_c}$ psi, f_c in psi). However, damage accumulated in the joint. Also, measured maximum column bar slip was equal to the instrumentation maximum of 31 mm (1.2 inches).

EXPERIMENTAL TEST MODEL THREE

Following the testing of Models One and Two, a second retrofit design was implemented in Model Three. This retrofit consisted of the addition of post-tensioned concrete bolsters on both sides of the as-built beam (see Figure 2). As was the case for Model Two, the addition of bolsters was anticipated to increase beam flexural strength so that under simulated earthquake loading, inelastic deformation would be isolated in the column. The bolsters and post-tension force were designed to reduce the maximum nominal joint tensile stress to below the nominal concrete tensile strength. Additionally, it was expected that the addition of the post-tension force would improve anchorage of column longitudinal reinforcement in the joint by widening the zone of compression in the joint. Qualitative evaluation of the joint load transfer mechanism for Model One indicated that very little of the column reinforcement was anchored in the joint compression zone. Addition of the post-tension force in Model Three increased the zone of compression in the joint, thereby increasing the length of column longitudinal reinforcement developed in this zone and improving anchorage of this reinforcement.

Only the retrofit bolsters were post-tensioned, and force transfer between the existing beam section and the bolsters was achieved through shear friction at the concrete interface. Steel reinforcing dowels were epoxied into holes drilled in the existing beam, the reinforcing steel in the retrofit bolsters was placed around these dowels and the bolster concrete was cast. At the ends of the beam segments, these dowels were designed to ensure that the post-tension force would be evenly distributed between the bolsters and the existing beam at a distance of 1.25 times the beam depth from the beam-joint interface. Elsewhere along the length of the beam, these dowel bars were placed at a nominal spacing of 102 mm (4 inches) for the one-third scale model.

With the added post-tension force, a consistent method for calculating nominal joint shear stress was not entirely obvious. It was decided that at the beam critical section the post-tension force would be modeled as a single point force acting at the mid-height of the member. Based on this model, the nominal joint shear stress did not depend on the post-tension force. Nominal joint principal stresses were computed from the nominal joint shear stress and the nominal joint compressive stress, that was considered to be equal to the post-tension force distributed across the entire beam area.

Model Three behaved in a ductile manner when subjected to simulated earthquake and gravity loading. Throughout the laboratory test, the joint remained essentially elastic and flexural yielding was isolated in the column. The model carried a maximum simulated earthquake load of approximately 1.1 times the calculated strength at a displacement of approximately nine times the nominal yield displacement. Figure 8 shows the computed and experimental load-displacement relationships, Figure 9 shows the computed and experimental nominal joint shear stress-strain relationships and
Figure 10 and Figure 11 show the relationship between model displacement and slip of column longitudinal reinforcement. For this model, the maximum load corresponded to a nominal joint shear stress of $13\sqrt{f_c}$ kPa and a maximum nominal joint tensile stress of $7.9\sqrt{f_c}$ kPa, f_c in kPa ($4.8\sqrt{f_c}$ psi and $3.0\sqrt{f_c}$ psi, f_c in psi). For this model, maximum column bar slip was less than 0.5 mm (0.02 in.).

CONCLUSIONS

Consideration of nominal joint shear stress is not sufficient for evaluation or retrofit of beam-column T-joints in older reinforced concrete bridge frames. Evaluation and retrofit must include appraisal of load transfer mechanisms and anchorage of member longitudinal reinforcement in the joint. Nominal joint shear stress can be used in evaluation and retrofit design; however, because older reinforced concrete bridge joints are usually only very lightly confined by joint transverse reinforcement and by members framing into the joint, the nominal joint shear strength of these joints is relatively low. For post-tensioned joints, evaluation of nominal joint principal tensile stress provides a useful criterion for design. The distribution of stresses within the joint should be evaluated qualitatively to verify that yielding of members framing into the joint does not deteriorate joint load transfer mechanism and to verify that member longitudinal reinforcement terminating in the joint is anchored in compression zones. Retrofit design should focus on reducing bond stress demand, increasing bond stress capacity and reducing concrete nominal principal tensile stress in the joint as well as development of desirable frame yield mechanisms.

REFERENCES

ACI-ASCE Committee 352 (1985). Recommendations for Design of Beam-Column Joints in Monolithic Reinforced Concrete Structures. *ACI Structural Journal.*

ACI Committee 318 (1989). *Building Code Requirements for Reinforced Concrete (ACI 318-89) and Commentary - ACI 318R-89.* American Concrete Institute, Detroit, 1989.

Bollo, M.E., Mahin, S.A., Moehle, J.P., Stephen, R.M., and Qi, X. (1990). *Observations and Implications of Tests on the Cypress Street Viaduct Test Structure.* Report No. UCB/EERC-90/21. Earthquake Engineering Research Center, University of California, Berkeley.

ACKNOWLEDGEMENT

The views expressed in this paper were developed in part through research activities sponsored by the California Department of Transportation (Caltrans), but do not necessrily represent the views of the sponsor. The authors would like to recognize the participation of Li-Hong Sheng, Caltrans, Division of Structures, as well as fomer and current UC Berkeley graduate students Abe Lynn, Mark Aschheim, Graham Archer, Scott Campbell, Stephen Jirsa, Dawn Lehman, Silvia Mazzoni, Boza Stojadinovic and Wendy Taniwangsa.

FIGURES

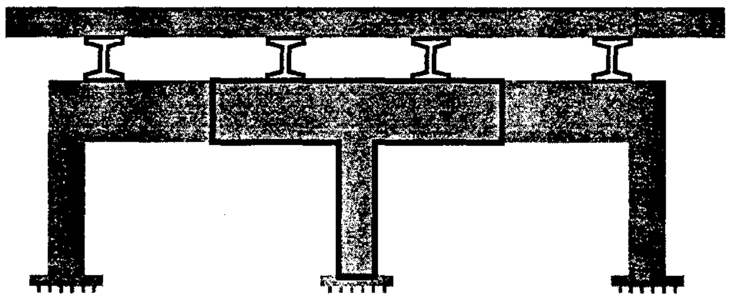

Figure 1: Prototype As-Built Bridge Frame and Experimental Test Sub-Assemblage

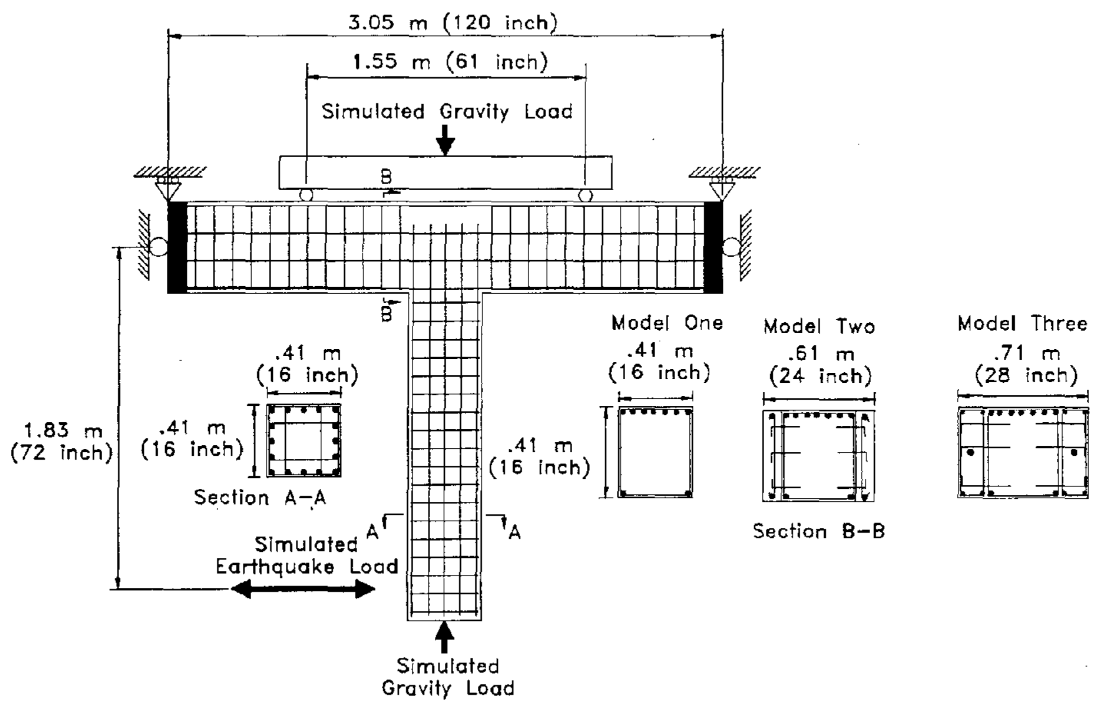

Figure 2: Idealized Loading of Experimental Test Models One, Two and Three

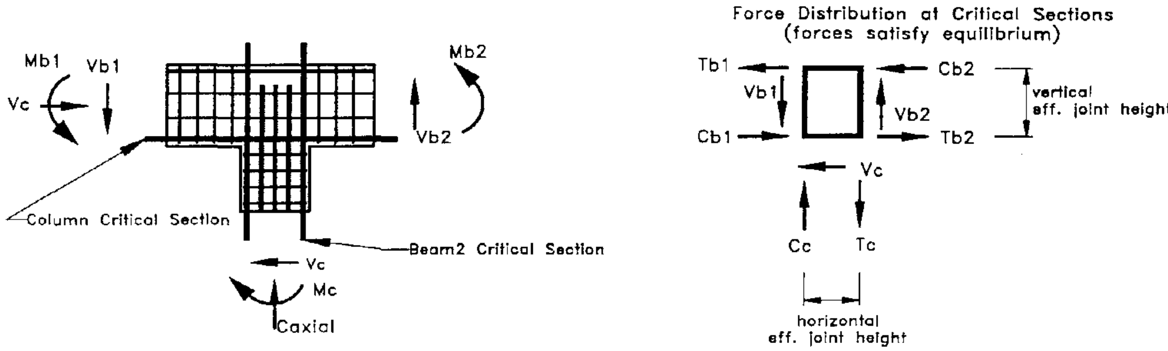

$$\text{nominal joint shear stress} = \frac{Tb1 + Cb2}{\text{horz. height} * \text{width}} = \frac{Cc - Vb1}{\text{vert. height} * \text{width}}$$

Figure 3: Idealization of Joint Loads and Area Used in Computation of Nominal Joint Shear Stress

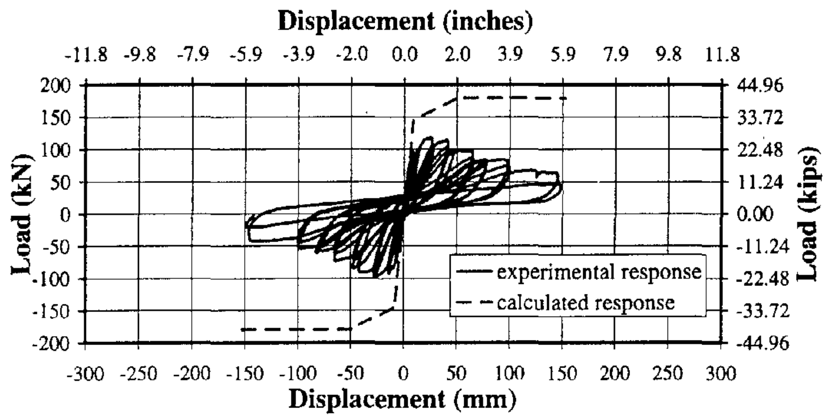

Figure 4: Model One Load-Displacement Relationship

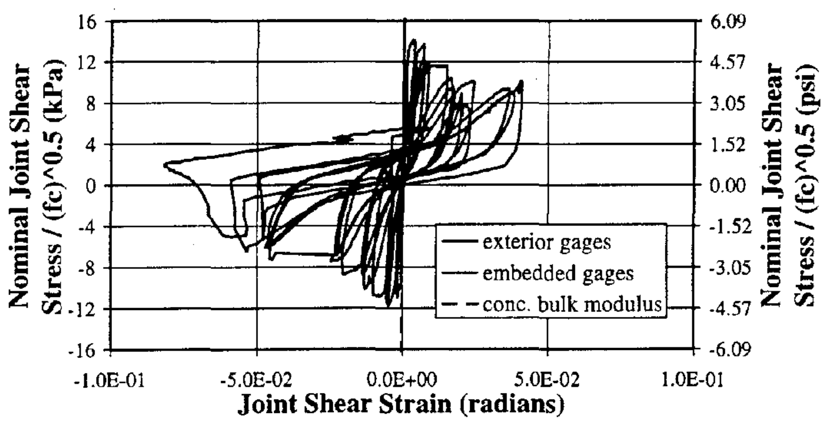

Figure 5: Model One Nominal Joint Shear Stress-Strain Relationship

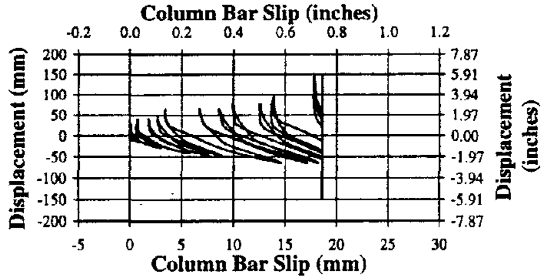

Figure 6: Model One Displacement Versus Column Bar Slip (Top Bar)

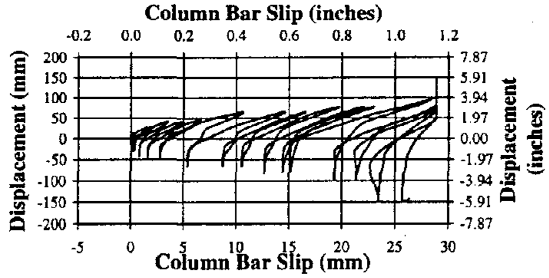

Figure 7: Model One Displacement Versus Column Bar Slip (Bottom Bar

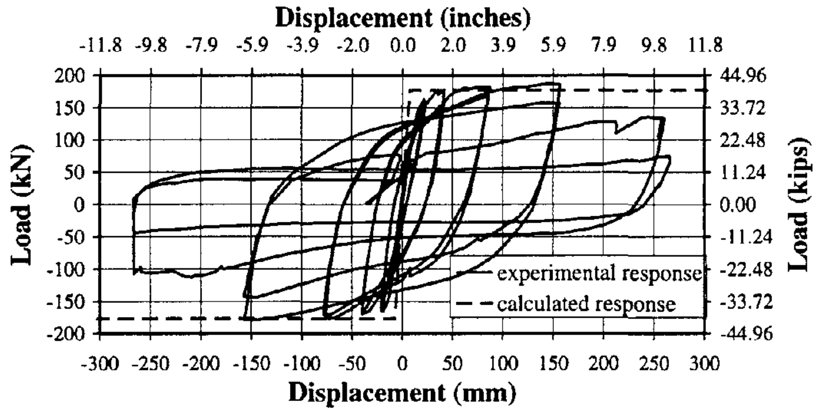

Figure 8: Model Three Load-Displacement Relationship

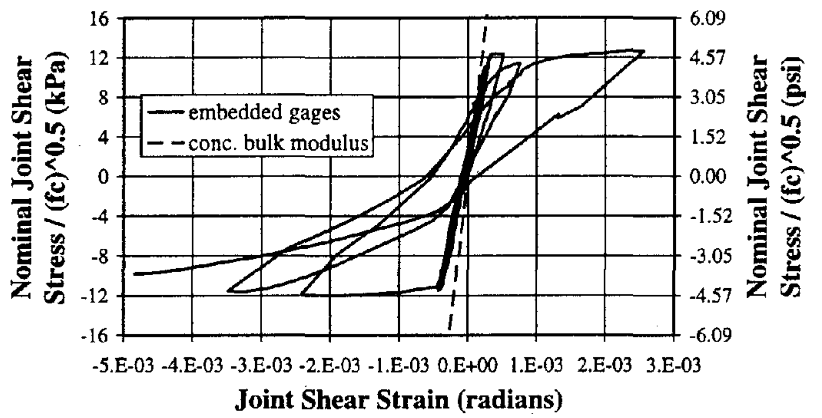

Figure 9: Model Three Nominal Joint Shear Stress-Strain Relationship

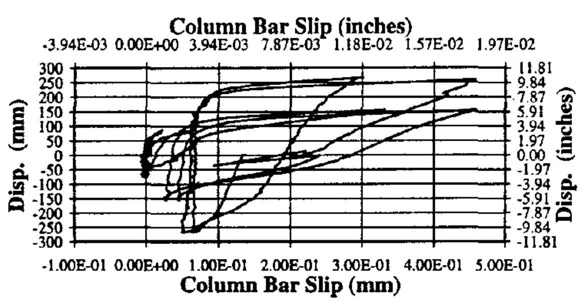

Figure 10: Model Three Displacement Versus Column Bar Slip (Top Bar)

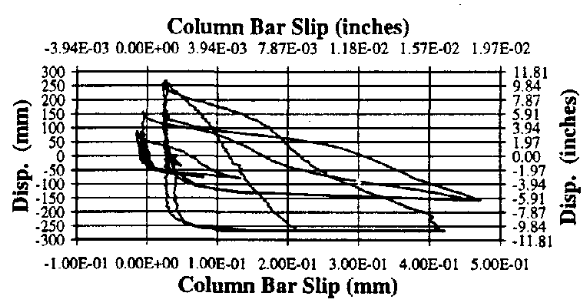

Figure 11: Model Three Displacement Versus Column Bar Slip (Bottom Bar)

EXPERIMENTAL OBSERVATIONS ON THE SEISMIC RESPONSE OF BEAM-COLUMN JOINTS IN REINFORCED CONCRETE DOUBLE-DECK BRIDGE STRUCTURES

SILVIA MAZZONI

Graduate Research Assistant, SEMM, Department of Civil and Environmental Engineering,
Earthquake Engineering Research Center, University of California, Berkeley, CA 94708

ABSTRACT

A research program to study the mechanisms controlling the seismic response of reinforced concrete beam-column joints in ductile double-deck bridge structures is being conducted at the University of California at Berkeley. Two one-third scale beam-column joint test specimens were built according to current design criteria and tested in the laboratory. The two test specimens differed in the capacity of the members framing into the joints. This difference in capacity resulted in a difference in maximum demands on the beam-column joint at the member interfaces. The scope of the tests was to determine the response of the joints when subjected to uni- and bidirectional loading cycles and compare the response to different levels of maximum joint shear stress demand. The test specimens were able to sustain the design forces and deformations without significant distress in the joint. Most of the plastic deformation and damage concentrated at the column ends. Analysis of the response of the two specimens will be used in the development of joint force transfer mechanisms.

KEY WORDS

seismic design, beam-column joints, compression strut mechanism, truss mechanism, joint shear stress

INTRODUCTION

The principal mechanisms that are widely accepted to model joint behavior in the design of building structures are the compression strut mechanism and the truss mechanism. In the compression strut mechanism, the concrete transfers the compression forces across the joint while member longitudinal reinforcement in tension is anchored in this compression force field, as shown in Fig. 1. In the truss mechanism, the tension and compression forces are transferred by the interplay of joint reinforcement and core concrete, as shown in Fig. 2. In joints where yielding occurs at the beam ends and the columns remain elastic, both models require additional horizontal joint reinforcement to confine the concrete or resist joint shear. The distributed column reinforcement, being elastic, is usually relied on to act as vertical joint reinforcement. In bridge construction it is more common to design a structural system where yielding is anticipated in the columns rather than the beams. In this case it is unclear whether the distributed column reinforcement can be relied on to act as vertical joint reinforcement. The objective of the test program described in this paper is to investigate this issue.

Two one-third scale beam-column joints with different levels of joint shear stress demands were built according to current design criteria and tested in the laboratory. The difference between the two specimen lies in the difference in capacity of the members framing into the joint. The nominal strength of the columns and beams of the second specimen are greater than those of the first. This results in a higher joint shear stress demand imposed on the beam-column joint of the second specimen.

The joint design was according to the recommendations of the 1985 report of ACI-ASCE Committee 352 [ACI-ASCE, 85]. These recommendations are given for the design of beam-column joints in building frames, where yielding is expected at the beam ends. Because yielding is expected at the column ends in the test specimens, the applicability of these design recommendations is assessed in the test program. The joint shear stress demand imposed on the beam-column joint of the first test specimen equals the capacity prescribed by the ACI-ASCE Committee 352 recommendations for this type of joint. The demand imposed on the beam-column joint of the second specimen exceeds the prescribed capacity. The tested beam-column joints, reinforced only with a horizontal spiral and no vertical ties, were able to carry the imposed shear demands without significant distress.

The specimen design, instrumentation system, testing set-up, and test results for the first test specimen have been discussed in more detail elsewhere in the literature by Mazzoni [Mazzoni *et al.* 1995].

ACI-ASCE COMMITTEE 352 RECOMMENDATIONS

ACI-ASCE Committee 352 recommendations provide guidelines on the design of member proportions and reinforcement details in the beam-column joints of reinforced concrete moment resisting building frames. The design criteria for the joint specify the amount of transverse reinforcement necessary to confine the joint core so it can resist the design shear stresses. The recommendations published in 1985 hypothesize that joint shear is carried primarily by a diagonal compression strut from one corner of the joint to the opposite corner. Joint transverse reinforcement serves the purpose of confining the diagonal compression strut so that it can retain strength to target inelastic deformation levels.

For joints with anticipated large inelastic deformation demands in adjacent beam components, the nominal joint shear strength, V_n, is expressed as:

$$V_v = \gamma \sqrt{f_c'}\,(psi)\, b_j h \tag{1}$$

where f'_c is the specified compressive strength of the concrete in the joint; b_j is the effective joint width; and h is the thickness of the column in the direction of load being considered. Because it does not have horizontal structural members framing into all four sides, the lower level beam-column joint in a double-deck bridge structure is considered an exterior joint. For this case, γ=15. The committee report recommends that the design should ensure flexural hinging in the beams rather than in the columns, as is typical in the design of moment resisting building frames.

The joint reinforcement prescribed by the committee consists of a horizontal spiral, or horizontal rectangular hoops and cross-ties. In consideration of vertical joint shear stresses, the committee report specifies that column reinforcement shall be distributed uniformly around the joint. It is assumed that the column longitudinal reinforcement, expected to remain elastic, will provide any needed restraint against vertical dilation of concrete in the joint.

DESIGN OF TEST SET-UP

In a typical double-deck bridge structure, the lower deck is rigidly framed into the columns, whereas the upper deck and footing are pin-connected to the columns. During seismic excitation, the longitudinal inertial forces are resisted by framing action between the lower deck and the columns. A longitudinal edge beam stiffens the deck at this level to improve this framing action. Transverse inertial forces are resisted by framing action between the lower deck bent cap and the column.

In the laboratory, the two lateral load resisting systems, longitudinal and transverse, are studied both independently and simultaneously. The model tested in the laboratory is shown in Fig. 3. The lateral loads are applied by actuators attached to the top column. Even though the inertial loads in the prototype are distributed between both levels, the specimen in the laboratory is subjected to lateral loads at the top level only so that both columns are subjected to similar loads. The loading actuators are shown in Fig. 4. The actuators are installed perpendicular to each other and at an angle to the specimen so that bidirectional loads can be imposed from a single reaction frame. Displacement cycles of increasing amplitude are imposed by these actuators.

The dead load of the structure is simulated by an unbonded prestressing rod passing through the column center. The prestressing load is the same for both columns.

DESIGN OF TEST SPECIMEN

The experimental program involves testing of two physical models of a joint of a double-deck bridge structure. The joint configuration is depicted in Fig. 3. The specimens are designated Specimen-1 and Specimen-2.

As described previously, the design approach for bridge structures commonly strives to have flexural plastic hinges in the column, with effectively elastic response in all other components. For Specimen-1, the objective is to achieve a relatively high nominal joint shear stress of 15 $\sqrt{f'_c}$ (psi). The quantity of column longitudinal reinforcement is set so as to achieve this target joint shear stress when the column reaches its plastic moment strength. The columns are designed to have the same strength so that the worst loading conditions are imposed on the joint.

The objective in the design of Specimen-2 was to achieve a higher nominal joint shear stress of 20 $\sqrt{f'_c}$ (psi). The same design procedure as that used for Specimen-1 was used for Specimen-2. The joint configuration and member dimensions were kept the same as those of Specimen-1. The reinforcement details for the two specimens were also kept the same by replacing the #5 bars used for the longitudinal reinforcement of Specimen-1 with #6 bars in Specimen-2. The amount of transverse reinforcement in the joint is identical for the two specimens since it is based on the recommendations of ACI-ASCE Committee 352. The amount of transverse reinforcement was changed only in the transverse cap beam due to the increased shear demand. Reinforcement details are shown in Fig. 5-7.

TEST PROGRAM AND RESULTS

Loading History

The test specimen was subjected to both unidirectional and bidirectional loading. The loading scheme is shown in Fig. 8. The last two unidirectional loading cycles are performed to determine the damaging effects of bidirectional loading on the specimen response. This loading scheme is applied to each specimen at cycles of displacement amplitudes increasing from 0.1 inch to 12 inch.

Observed Behavior -- Specimen-1

The first hairline cracks appeared at the bottom column-joint interface at displacements of 0.1 inch. The number and size of the cracks increased with increasing displacement amplitudes. Typical bending cracks were distributed along the column height near the joint.

At displacement cycles of 3 inch it was visually noticeable that most of the deformation concentrated in the top story. As the displacement amplitude increased, the damage concentrated in the top column plastic hinge where significant increase in distress was evident. Even though the cover concrete had previously spalled over a significant length, no further distress was noticed in the bottom column plastic hinge zone.

At displacement cycles of 5 inches, diagonal cracks began to appear in the beams near the beam-joint interface. As the displacement amplitude increased, the cracks began to fan out toward the mid-depth, as shown in Fig. 9. At a displacement amplitude of 8 inches, during the longitudinal and transverse cycles after the bidirectional loading, the first signs of buckling of the top column longitudinal reinforcement were noticed.

During the first longitudinal cycle at a displacement of 12 inch, the top column longitudinal reinforcement buckled on the compression side. Some bars buckled in the plane of the spiral, some inward, and some outward. In the second longitudinal cycle at this displacement, one of the bars that buckled in the previous cycle, the one at the extreme tension fiber, fractured. Additional bars buckled and fractured during the excursion in the transverse direction at this displacement level. All of the buckled and fractured bars were in the top column plastic hinge zone.

Observed Behavior -- Specimen-2

The first cracks began to appear at the column-joint interface at displacements of 0.25 inch. At a displacement amplitude of 0.5 inch, additional bending cracks were evident along the column height.

At displacement cycles of 3 inches most of the damage began to concentrate in the bottom column plastic hinge zone. At this displacement amplitude shear cracks appeared in both the columns and the beams -- the amount of shear reinforcement in all the members but the transverse cap beam is the same for both Specimen-1 and Specimen-2.

The diagonal cracks that were seen at the vertical beam-joint interfaces of Specimen-1 were also observed at the same locations in Specimen-2 at displacement amplitudes of 3 inches. At a displacement level of 8 inches inclined cracks began to appear on the face of the stub. At higher displacement levels these cracks were evenly distributed on the stub face. Similar cracks were not observed in Specimen-1.

Because of clearance limitations in the test apparatus, it was necessary at this stage of the test to offset the specimen by 2 inches in the east direction and before beginning the 10 inch cycles. During longitudinal loading at this amplitude, a number of bars in the bottom column buckled. The test was terminated before any bars were able to fracture due to the limited capacity of the gravity loading system.

Hysteretic Response -- Specimen-1

The response of the two stories of Specimen-1 to the different loading conditions is depicted in Fig. 10-13. These figures display the relations between shear and drift of each story during unidirectional loading in the transverse and longitudinal directions. As seen from the response curves, nonlinear structural response of both stories resulting from yield of column longitudinal reinforcement started at a story drift of approximately 1.5%. The maximum drifts reached are characteristic of the loading direction and the story under consideration. However, all stories were capable of reaching lateral drifts of 5% without loss of strength.

Comparison of the hysteretic response curves shows that most of the deformation was concentrated in the top story. This concentration of deformation led to a concentration of damage in the top column plastic hinge. Failure of the specimen was due to buckling and fracturing of the column longitudinal reinforcement in this section. This behavior is most evident in the response curves of the transverse loading: 80% of the deformation in the last excursion occurred in the top story. Even though it did not sustain any damage beyond spalling of the cover concrete, the critical section of the bottom column did reach its nominal capacity and was capable of dissipating hysteretic energy, as seen in Fig. 12 & 13.

The specimen was subjected to three unidirectional loading cycles in each direction. The third cycle occurred after the specimen was subjected to two cycles of bidirectional loading. The response curves show that the capacity reached during this third cycle was lower than that reached during the first two cycles. This behavior apparently is a result of the significant damage incurred on the specimen by bidirectional loading.

Hysteretic Response -- Specimen-2

The hysteretic response curves for Specimen-2 are shown if Fig. 14-17. The increase in column capacity due to the increase in bar size from the first specimen to the second is evident in the resulting increase in the maximum lateral load resisted. This increase in lateral load capacity, however, does not result in a significant change in the ultimate displacement capacity. Even though the column longitudinal reinforcement did not fracture at this maximum displacement, imminent failure can be attributed to the significant reduction in strength at the higher displacement levels.

While it is evident in the curves that most of the inelastic deformation of Specimen-1 was concentrated in the top story, the deformation distribution between the two stories of Specimen-2 varies depending on the loading condition. In the longitudinal direction, the deformation is evenly distributed between the two stories, with a slightly larger deformation in the bottom story. The axial load variation in the bottom column, due to overturing effects during transverse loading, determines whether the nominal capacity of this column is higher or lower than that of the top column. When the bottom column is weaker than the top column, most of the deformation concentrates in the bottom story. When the bottom column is stronger than the top one, the deformation concentrates in the top story.

CONCLUSIONS

Test results have shown that a joint with moderate quantity of reinforcement has the capacity to sustain large joint shear stress demands without significant distress. The second test has shown that a beam-column joint in the configuration considered in this case is able to sustain demands greater than the capacity prescribed in the past.

ACKNOWLEDGEMENTS

The research project was sponsored by the California Department of Transportation and by the National Science Foundation. The author would like to acknowledge the valuable assistance of Professors Jack P. Moehle and Steve A. Mahin as research and academic advisors. The author would also like to acknowledge the participation of Craig Whitten from the Division of Structures at CalTrans.

REFERENCES

ACI-ASCE Committee 352 (1985), "Recommendations for Design of Beam-Column Joints in Monolithic Reinforced Concrete Structures," ACI Journal, Proceedings, May-June 1985, pp. 266-283.

Mazzoni, S., J.P. Moehle and S.A. Mahin (1995). Seismic Response of Beam-Column Joints in Reinforced Concrete Double-Deck Bridge Structures. Proceedings, National Seismic conference on Bridges and Highways. San Diego, California. December 1995.

State of California, Department of Transportation (1990). Bridge Design Specification Manual. 1990.

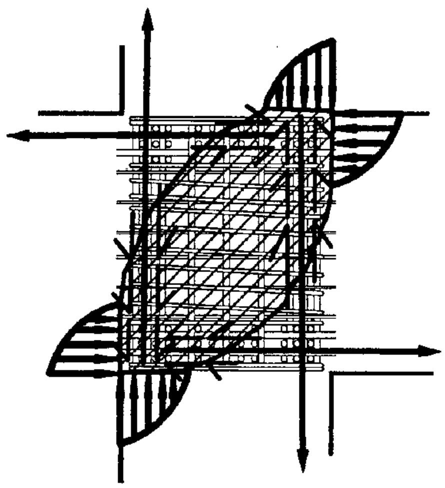

Fig. 1 Compression Strut Mechanism

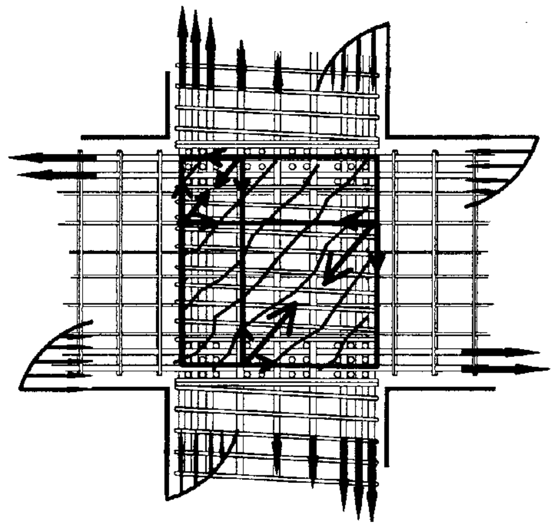

Fig. 2 Truss Mechanism

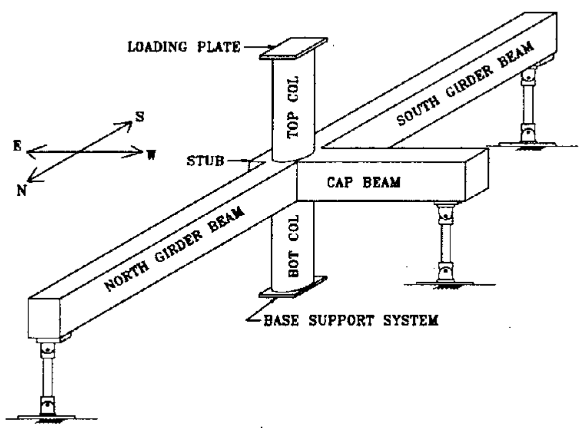

Fig. 3 Test Setup

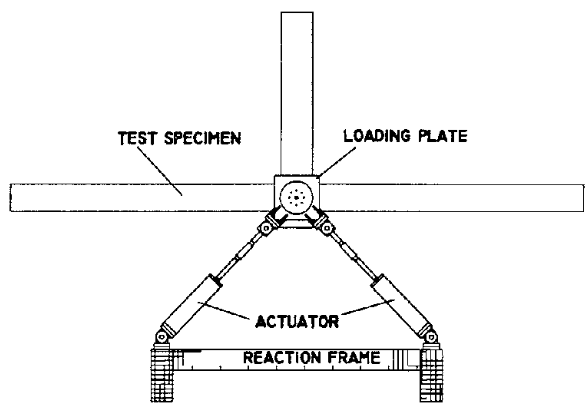

Fig. 4 Lateral Load System

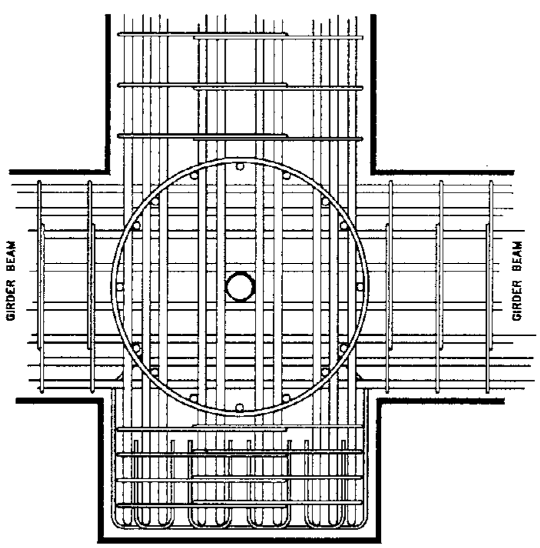

Fig. 5 Joint Detail -- Plan View

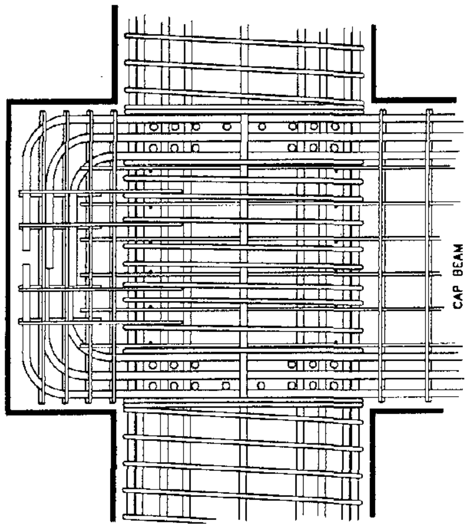

Fig. 6 Joint Detail -- South Elevation

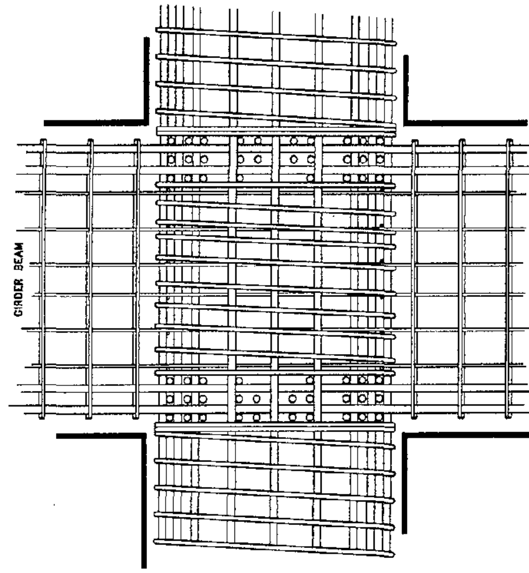

Fig. 7 Joint Detail -- East Elevation

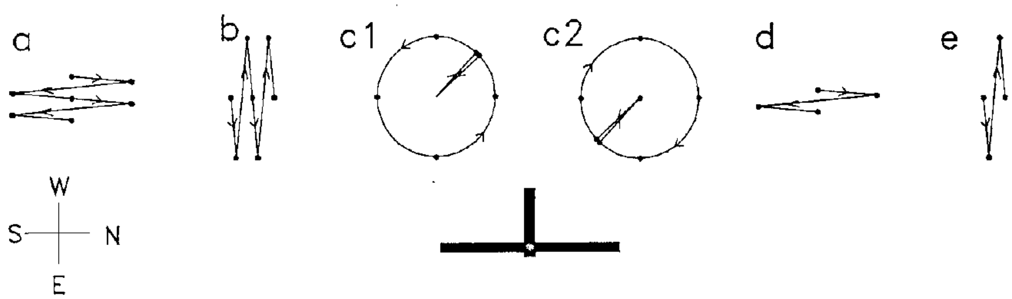

Fig. 8 Loading Scheme

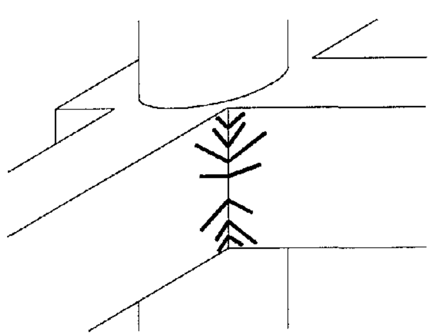

Fig. 9 Beam-End Cracks

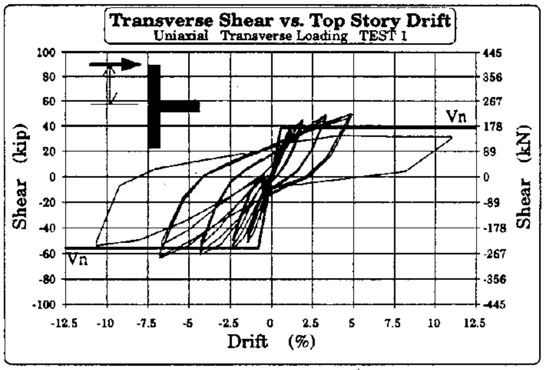

Fig. 10 Transverse Shear versus Top Story Drift TEST-1

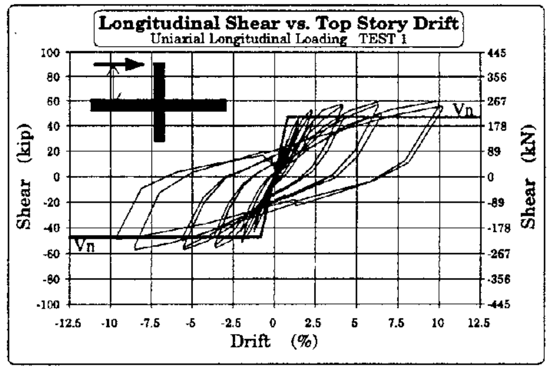

Fig. 11 Longitudinal Shear versus Top Story Drift TEST-1

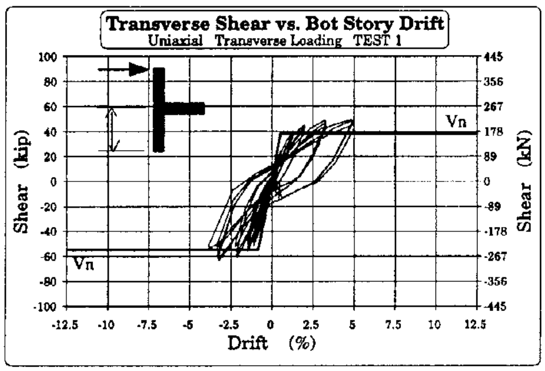

Fig. 12 Transverse Shear versus Bottom Story Drift TEST-1

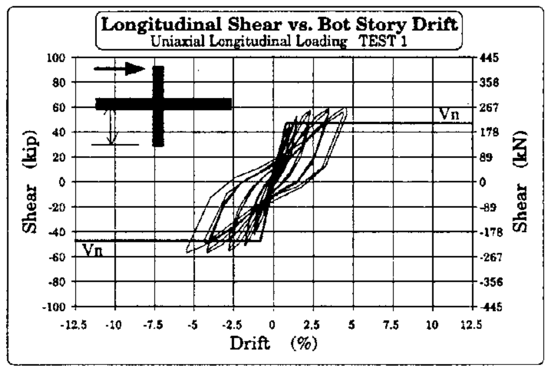

Fig. 13 Longitudinal Shear versus Bottom Story Drift TEST-1

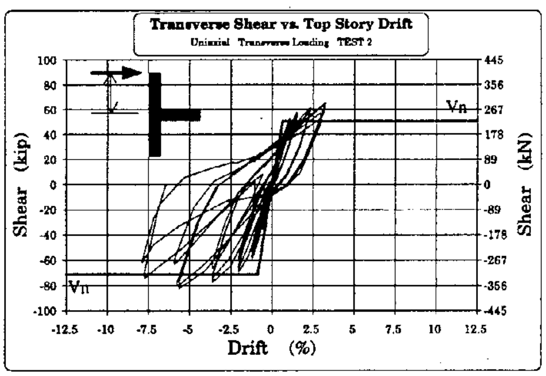

Fig. 17 Transverse Shear versus Top Story Drift TEST-2

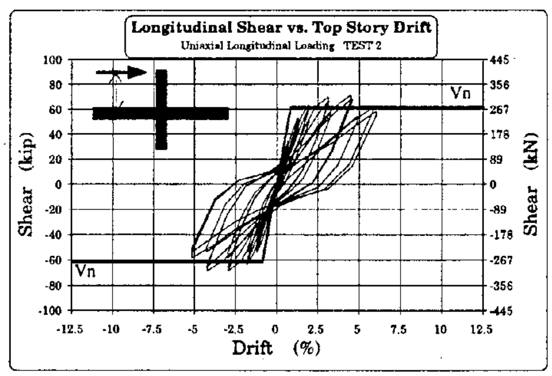

Fig. 14 Longitudinal Shear versus Top Story Drift TEST-2

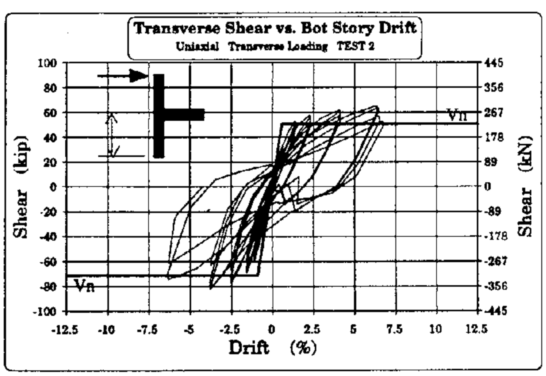

Fig. 15 Transverse Shear versus Bottom Story Drift TEST-2

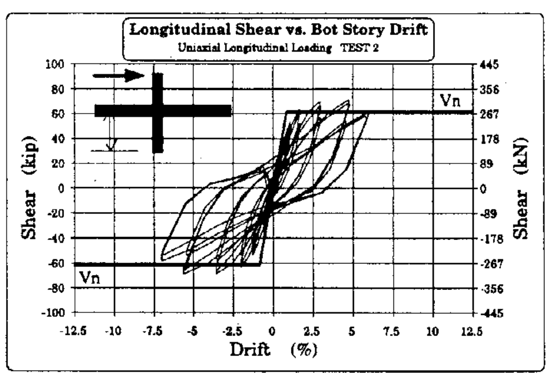

Fig. 16 Longitudinal Shear versus Bottom Story Drift TEST-2

DISPLACEMENT-BASED SEISMIC DESIGN CRITERIA

JACK P. MOEHLE

Earthquake Engineering Research Center, University of California at Berkeley,
1301 S. 46th St., Richmond, CA 94804, USA

ABSTRACT

Performance-based seismic design criteria, intended to produce structures that satisfy specific performance objectives, are under development by various individuals and organizations. Many of these are evolving around displacement-based design concepts, which use expected displacement response of a structure to gauge performance. Displacement-based seismic design criteria possess the benefit of being relatively simple and direct in their application in the design process. Limitations of these criteria should be recognized. Probabilistic approaches should be developed and applied to deal with the uncertainties in estimating demands and capacities.

KEYWORDS

displacement-based design, earthquake-resistant design, experimental data, performance-based seismic design, seismic response, reinforced concrete construction

INTRODUCTION

There are no simple, reliable, and fool-proof rules that will produce safe and economical structures all the time. Earthquakes, and earthquake responses, are complex phenomena depending on uncertain physical conditions, and gauged by social needs and expectations for which there is no universal standard. Earthquake occurrence, earthquake characteristics, and structural response characteristics are not deterministic, and need to be viewed as probabilistic or even chaotic phenomena. Designs are implemented by mere humans, and the design product may be altered by natural or human influences throughout the life of the structure. In the face of these formidable impediments, why, then, displacement-based seismic design?

There are, in fact, simple reasons why displacement-based seismic design is in many cases a useful and preferable approach to seismic design. Perhaps most importantly, displacement-based design is an intelligible tool for achieving a measure of performance in structures constructed at sites prone to earthquake shaking. Its concepts apply to a range of structure types, from single-story, single-element systems to multi-story, mixed-element systems. Of equal importance, displacement-based design can be viewed as a naked tool, one that is so simple and direct that its user can see all its beauties and its flaws.

The object of this paper is to define displacement-based seismic design, to illustrate how it relates to performance, and to describe its current limitations. Some examples of applications in current codes and design guidelines are described.

DEFINITION OF DISPLACEMENT-BASED DESIGN

Displacement-based seismic design means simply that the design takes into account the anticipated earthquake-induced displacements for the design event(s). Whereas conventional code design approaches focus on design forces, the focus of displacement-based design approaches is displacements. Furthermore, an emphasis is directed to achieving a realistic, and realistically-conservative, estimate of the displacements. Several interpretations of the approach have been put forward.

By one interpretation [Sozen; 1981], displacement-based seismic design recognizes that displacement amplitude, and especially interstory drift amplitude, relates directly to structural and non-structural damage in yielding systems. Therefore, the designer should use displacement information to select the structural system that economically will produce reduced displacements by comparison with other competing systems. This version of displacement-based design does not presume to provide adequately accurate information to enable the designer to directly relate the calculated displacements and the structural details. In light of the uncertainties involved, this limited version of displacement-based design may actually be the most realistic.

By another interpretation [Moehle; 1992], displacements are used first as an aid in selecting the basic structural system, and then the anticipated displacements are used directly as an aid in proportioning the structure and selecting details. Wallace and Moehle [1992] show one application of this approach to wall building design, where it is found that requirements for confined boundary elements relate directly to the quantity of walls provided in the structural system. In these approaches, the engineering either selects the details given the expected structural displacements, or selects the structural system to limit the required details. Priestley [1993] suggests that the engineer first select a target displacement and corresponding details, and then back-calculate structural characteristics required to achieve the target displacement. Obviously, these approaches are limited by the quality of information on ground motion and structural response.

The fact that displacements are the focal point of the design process does not excuse the designer from considering other aspects. For example, the design should attempt to control the yielding mechanism in a yielding structure, so amplitudes of local demands can be controlled, and so details can be apportioned to the critical regions. Therefore, elements of capacity are directly applicable in a displacement-based design approach.

DISPLACEMENTS AND PERFORMANCE

Performance of a structure following an earthquake typically is gauged by whether it posed a significant life-safety threat, and if it did not, by how much it will cost and how long it will take to return it to service. Because these parameters generally relate to specific levels of damage, a damage indicator is a critical component of performance based design. For seismic design, implemented by engineers with limited resources, the indicator should be simply defined. Obvious choices are force or displacement amplitude.

Damage in a yielding structure usually can be related more directly to displacement (distortion) than to force or stress. An obvious example on the material level is a steel coupon subjected to direct tension. During a tension test, fracture occurs when the engineering tension strain reaches a characteristic value. Although there exists a corresponding engineering stress level to which failure can be related, the fact that the material is yielding means that strain is a more discerning measure. Similar relations exist for structural components. Practical examples relating damage to deformation include failure of confined concrete at large strain limits, cracking of masonry panels under in-plane loading, and damage to non-structural components under in-plane racking.

Degradation of component strength, and consequent failure modes, also may be related to deformations. An example is provided by the relations in Figure 1 [ATC-6-2; 1983], where it is suggested that shear strength of a reinforced concrete column is directly related to the component deformation demand. Lehman, et al. [1996] present experimental data in support of the relation shown in Figure 1.

Design approaches based on anticipated ductility demands, rather than actual deformations, have been proposed [e.g., Park; 1986]. These approaches have many advantages. However, they ail in some important aspects. Importantly, it has been reported that displacement at first yield cannot be accurately determined for actual structural components, with typical errors being on the order of plus or minus 50% [e.g., Sozen, et al.; 1992]. It follows that deformation ductility capacity (equal to the ratio of deformation capacity to yield deformation) as a measure of performance is problematic.

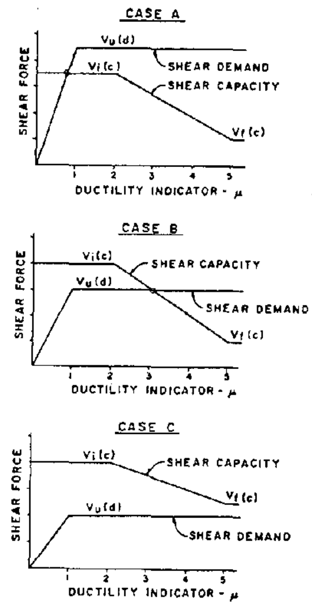

Figure 1 - Relation between shear strength and displacement ductility demand. Case A indicates shear failure without flexural ductility. Case B indicates shear failure after flexural ductility. Case C indicates flexural ductility without shear failure.

Displacement-based approaches hold some distinct advantages for seismic evaluation and rehabilitation of older existing construction where there may exist a mixture of old and new components having widely different stiffness, strength, and deformation capacity. Figure 2 illustrates an idealized problem, where it is determined that an existing structure (Figure 2a) has inadequate deformation capacity (Figure 2c) for the design deformation demands (Figure 2d). By introducing a new bracing system of high stiffness and deformation capacity (Figure 2b), it is possible to improve the overall performance of the system (see Figures 2c and 2d). By viewing the problem through a displacement perspective, the solution is plainly visible. If a traditional strength based approach was used, the designer would be faced with the circuitous path of determining the required strength to limit ductility demands in a mixed system, and deformation compatibility would have to be checked to ensure that the existing components were not deformed beyond their capacities. In cases such as these, a displacement-based approach is more simple, more direct, and more effective.

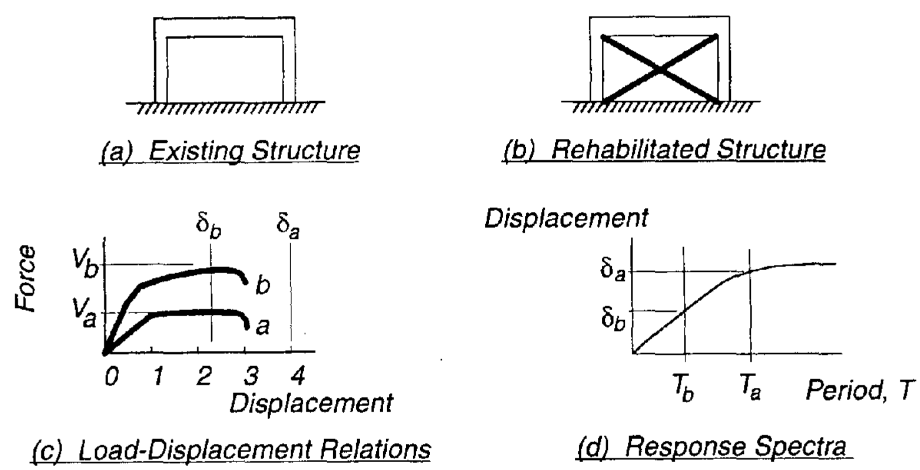

Figure 2 - Illustration of displacement concepts applied to seismic rehabilitation of an existing frame

In promoting displacement-based design, one must not deny its limitations. For some components, including building contents, damage can be more directly related to inertial forces (that is, the products of mass and acceleration). In design for low-intensity earthquakes, it may be more practical to keep a structure essentially elastic, in which case strength becomes a more discerning parameter for design. In any structure, it is well-established that damage is a cumulative process; therefore, a structure that sustains a given maximum drift is likely to be more damaged by a long duration event than by a short one. Some of these basic limitations are characterized in the following section.

LIMITATIONS OF DISPLACEMENT-BASED DESIGN

Performance-based seismic design has as one of its goals to produce structures of more predictable performance. The approach can be organized around the theme of performance objectives, which can be defined as the combination of a performance level (e.g., immediate occupancy, life safety, collapse prevention) and an earthquake demand with a specified probability of exceedance (or return period) [ATC-33; 1995]. Limitations exist with regard to estimating earthquake displacement demands (including ground motions and displacement estimations) and performance levels.

Displacement Demand Estimation

To estimate displacement demands, one must define the design ground motion(s) and the effects on the subject structure.

Design Ground Motion. Design motions should be consistent with the expected performance levels. For new building design, it may well be inappropriate to pair a ground motion having 10 percent probability of exceedance in 50 years with a deformation measure corresponding to structural collapse. Similarly, it may be uneconomical to pair a 2%-in-50-yr ground motion with a deformation measure corresponding to partition cracking.

It is easy to lose sight of the conspicuous statements of the preceding paragraph when attempting to implement displacement-based design concepts in existing design codes. A tangible example is found in the provisions for shear wall confined boundary elements of the 1994 Uniform Building Code [UBC; 1994]. According to these provisions, confined boundary elements are required only if compression strains, calculated for the code loading, exceed the strain corresponding to crushing strain of concrete. For many sites in California, the event represented by this code loading has a probability of exceedance of around 10% in 50 years. Other reasonably credible events have spectral ordinates significantly larger than this code loading. For example, response spectra for the 1994 Northridge earthquake, a moderate event by most measures, exceeded the UBC code loading by a considerable margin (Figure 3) [EERI; 1995]. Because loss of a confined boundary element may represent a serious threat to life safety, a lower probability event than that represented by the code loading might be more appropriate.

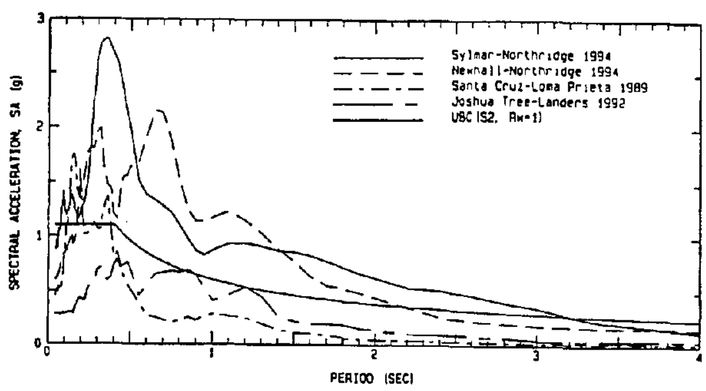

Figure 3 - Spectral acceleration (5% damped) for the UBC design spectrum and various California earthquakes.

An alternate approach to dealing with uncertainty in the seismic loading has recently been adopted in provisions of the 1995 ACI Building Code [ACI; 1995]. According to these provisions, gravity columns (those columns not considered in design to be part of the lateral force resisting system) are to be checked to determine if they are likely to develop strength for the design response spectrum (which may be assumed to be equivalent of the UBC loading). Those that are calculated to reach strength are recognized as requiring significant ductility capacity, and are required to be detailed as if they were part of a ductile moment resisting frame. Those that according to calculations do not reach strength for the code loading are allowed to contain less stringent details, but the details still must allow for some ductility capacity (e.g., shear failure must be avoided for loads corresponding to flexural plastic hinging). Implicit in this provision is the understanding that life-threatening demands well in excess of the code loading are reasonably credible.

Other proposals are available. For example, the ATC-32 report [1996] recommends to use mean response spectra for ordinary structures, and 1.5 times the mean spectra (effectively mean-plus-one-standard-deviation spectra) for important structures, and for all structures an implicit margin is provided between calculated demands and expected capacities. As another example, the draft ATC-33 report [1995] recommends to use 10%-in-50-yrs ground motions for the life safety performance objective, and 2%-in-50-yrs ground motions for the collapse prevention objective (some aspects of near-field effects in western California are as yet unresolved). These procedures provide simple ways of dealing with the general uncertainty surrounding future ground motions.

Estimation of SDOF Displacements. Numerical procedures are required that estimate structural response amplitude to ground motions. For design, simplified procedures usually are appropriate. Since the 1950's, effects have been made to relate response of structures responding non-linearly to that of structures responding linearly. For example, the equal displacement rule, which states that maximum displacement amplitudes are equal for nonlinear and linear response of an oscillator with given damping and initial stiffness, was the product of analog and digital computer studies of the 1960's [Moehle; 1992]. This expedient has formed the basis of many design procedures.

Later studies demonstrated that the equal displacement rule was not valid for a range of structural systems. For example, Sozen and Shimazaki [1984] and others noted that the relation between displacement amplitude for nonlinear and linear response depended on characteristics of the ground motion, initial period of the oscillator, strength of the oscillator, and hysteretic characteristics of the load resistance function. Statistical studies by Miranda [1996] of bilinear oscillators have clarified the significant scatter associated with relations between nonlinear and linear response amplitude. These results, coupled with the basic uncertainty in the loading function, emphasize the need to consider uncertainty as a part of the overall analysis problem.

These studies do not consider the effects of gravity loads acting through lateral displacements. P-delta effects can induce extreme results in otherwise stable systems.

Few codes or design guidelines take full advantage of the available technical information on nonlinear response. For example, the Uniform Building Code [1994] continues to define the design displacement as three-eighths of the displacement calculated for elastic response. On the other hand, recommendations from the ATC-32 project for bridge design [ATC; 1996] and from the draft ATC-33 project for building rehabilitation [ATC; 1995] contain a more realistic representation of expected displacement response; Figure 4 is based on recommendations from the ATC-32 report.

Estimation of Local Displacements. Beyond estimation of SDOF displacement amplitude, as described previously, it is important to obtain a good estimate of the local displacements within the structure. For structures responding nonlinearly, it in general is not adequate to estimate internal displacements using a linear model. As an example, consider a simple, soil-supported, single-column bridge pier, where inelastic action is restricted to column flexure near the base. The total lateral displacement is equal to the sum of the contributions from the foundation, δ_f, elastic deformations of the column, δ_{ce}, and inelastic deformations of the column, δ_{ci}. If we assume that the elastic displacement contributions from all three components are equal, and if we assume that the maximum displacement is equal to twice the yield displacement, then the total displacement of the yielding plastic hinge must be $\delta_y/3 + \delta_y = 4/3\delta_y$, where δ_y = the yield displacement. Therefore, the flexural hinge must accommodate two-thirds of the total displacement, rather than one-third as would be determined from elastic analysis. (Note that the flexural hinge displacement ductility is equal to 4 whereas the system displacement ductility is equal to 2.)

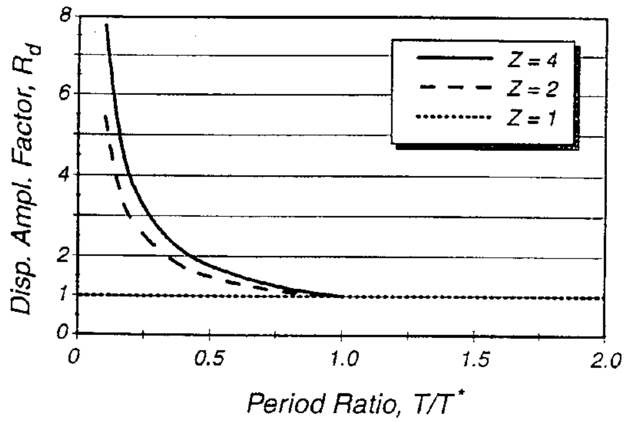

Figure 4 - Displacement amplification factors to account for nonlinear response. T/T is the ratio of structure period to characteristic ground motion period. Z is a strength reduction factor.*

The result of the preceding paragraph is well known, but is not always applied in displacement-based design methods because of uncertainties in how inelastic deformations are distributed. Nonlinear static analysis has been recommended in some design methodologies [ATC-32, 1996; ATC-33, 1995]. However, even these do not adequately address multi-degree-of-freedom structures where apparent higher mode contributions add to the uncertainties. General and rigorous procedures for taking these effects into account are not currently available. Some discussion is provided in [Krawinkler; 1996].

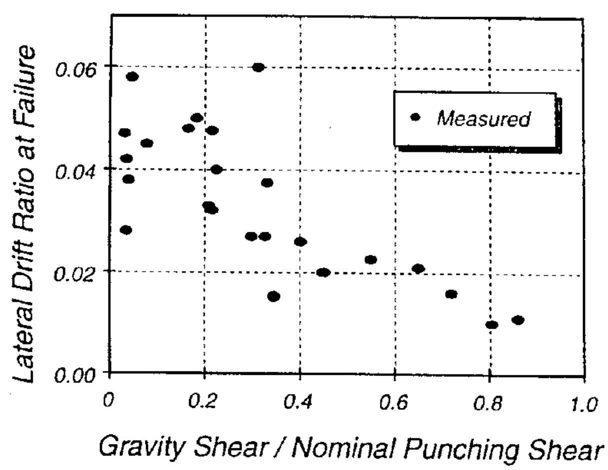

Figure 5 - Displacement capacity of flat-plate construction as a function of the intensity of the gravity shear loading.

Displacement Capacity Estimation

Experimental and analytical research continue to add to our understanding of the deformation capacities of structural components. Still, the available knowledge is incomplete. The user of displacement-based design concepts should understand the limitations imposed by our incomplete knowledge of displacement capacity.

Direct observation of deformation capacities is one common means of establishing design criteria. An example is provided by data for deformation capacity of slab-column connections, as shown in Figure 5 [Moehle; 1996]. Although a basic relation between deformation capacity and shear (acting transverse to the plane of the slab) is identified, no fundamental mechanical model is inferred. To be of general use, relations of this type must report results for representative connections subjected to representative loading histories.

More general, but still limited, approaches are available for some structural components. For example, for flexurally-dominated reinforced concrete construction one may invoke empirical models based on cross-sectional analysis to obtain curvature capacities, combined with procedures for distributing curvature along the component length. Figure 6 shows the familiar plastic hinge model for a reinforced concrete beam, column, or wall. This model enables the engineer to calculate deformation capacity for a range of geometries. Figure 7 compares measured and calculated deformation capacities for spirally-reinforced bridge columns, satisfying modern design provisions, tested at the University of California at San Diego [ATC 32; 1996]. Even though the test specimens satisfied basic conditions for which the predictive model

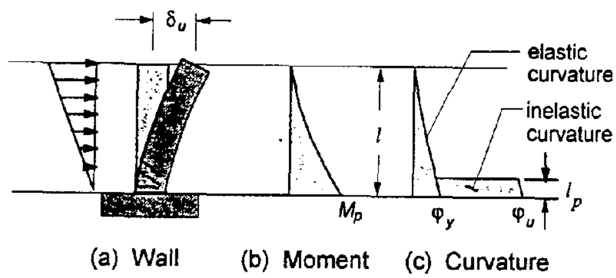

Figure 6 - Plastic hinge model for a flexural member.

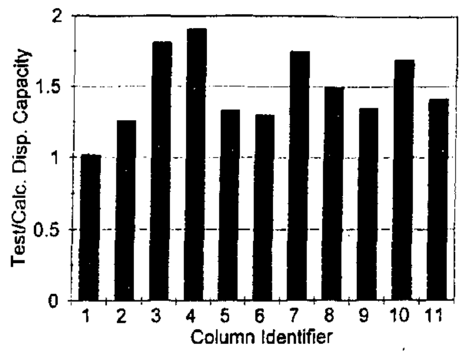

Figure 7 - Comparison of measured and calculated column displacement capacities

was designed, and even though the loading histories all followed a standard routine, there is considerable scatter in the comparison between theory and test. Variations from this testing theme would certainly introduce more scatter. Probabilistic approaches seem unavoidable if reasonable measures of performance are to be obtained.

CONCLUSION

Displacement-based seismic design criteria are simple and direct in representing design parameters that relate to performance. Approaches are available to estimate both displacement demands and capacities, although additional developments are needed. The inherent uncertainty in the design problem is apparent. Therefore, whereas a stated goal of performance-based seismic design is to produce structures of predictable performance, only the probabilities associated with achieving a given performance can be stated.

ACKNOWLEDGMENT

Ideas related to performance-based seismic design have been developed within projects funded by the U.S. Federal Emergency Management Agency and National Science Foundation, the California Seismic Safety Commission and California Department of Transportation, and the Applied Technology Council.

REFERENCES

ACI (1995) *Building code requirements for structural concrete*, American Concrete Institute, Detroit.

ATC-6-2 (1983) *Seismic retrofitting guidelines for highway bridges*, Applied Technology Council, Redwood City, CA, 220 pp.

ATC-32 (1996) *Recommended bridge design specifications*, and *Resource document*, Applied Technology Council, Redwood City, California.

ATC-33 (1995) *Guidelines and commentary for the seismic rehabilitation of buildings (75% Draft)*, Applied Technology Council, Redwood City, CA.

EERI (1995) "Northridge earthquake reconnaissance report - Vol. 1," Earthquake Engineering Research Institute, pp. 40.

Krawinkler, H. (1996) "Modifications of seismic demands for mdof systems," 11 World Conf. on Earthquake Engr., Acapulco.

Lehman, D. E., A. C. Lynn, M. A. Aschheim, and J. P. Moehle (1996) "Evaluation methods for reinforced concrete columns and connections," *Proceedings*, 11 World Conf. on Earthquake Engr., Acapulco.

Miranda, E. (1996) "Site dependent seismic demands for sdof systems," 11 World Conf. on Earthquake Engr., Acapulco.

Moehle, J. P. (1992) "Displacement-based design of rc structures subjected to earthquakes," *Earthquake Spectra*, EERI, V3, N3.

Moehle, J. P. (1996) "Seismic design considerations for flat-plate construction, or Drift happens," ACI SP, Mete A. Sozen Symposium, Tarpon Springs, Florida.

Park, R. (1986) "Ductile design approach for reinforced concrete frames," *Earthquake Spectra*, EERI, V2, N3, pp. 565-619.

Priestley, M. J. N. (1993) "Myths and fallacies in earthquake engineering - conflicts between design and reality," *ACI SP 157*, pp. 231-254.

Shimazaki, K and M. A. Sozen (1984) "Seismic drift of reinforced concrete structures," special research paper, Hazama-Gumi, Ltd, Tokyo.

Sozen, M.A. (1981) "Review of earthquake response of reinforced concrete buildings with a view to drift control," *State of the Art in Earthquake Engineering - 1981*, Ankara, pp. 383-418.

Sozen, M. A., P. Monteiro, J. P. Moehle, and H. T. Tang (1992) "Effects of cracking and age on stiffness of reinforced concrete walls resisting in-plane shear," *Proceedings*, 4th Symp. on Current Issues Related to Nuclear Power Plant Structures, Equipment, and Piping, Orlando, Florida.

UBC (1994) *Uniform building code*, International Conference of Building Officials, Whittier, California.

Wallace, J. W. and J. P. Moehle (1992) "Ductility and detailing requirements of bearing wall buildings," *J. Structural Engineering*, ASCE, V118, N6, pp. 1625-1644.

RESPONSE OF A CONCRETE ARCH DAM IN THE 1994 NORTHRIDGE, CALIFORNIA EARTHQUAKE

SOHEIL MOJTAHEDI and GREGORY L. FENVES

Department of Civil and Environmental Engineering, University of California, Berkeley
Berkeley, CA 94720 U.S.A.

ABSTRACT

The response of Pacoima dam, a 365 ft high arch dam located near Los Angeles, California, to the 1994 Northridge earthquake is studied using the accelerograms recorded in the canyon and on the dam body. The nonlinear effects due to opening of the contraction joints, lift joints and the dam–foundation interface are represented in the model. The effects from the spatial variation of the free–field motion in the canyon are also included. Although a simple assumption is made concerning the spatial distribution of free–field motion, because of lack of recorded data, the computed response is in reasonable agreement with the accelerations recorded on the dam body. The concrete stresses in the model are substantially different from those which are typically computed from an analysis assuming a monolithic dam and uniform free–field canyon motion. The opening of the joints reduces the arch and cantilever stresses, whereas the non–uniform motion of the canyon significantly increases these stresses. The pseudo–static response to the non–uniform input motion is the major cause of large concrete stresses, particularly near the abutments.

KEYWORDS

Dam; arch dam; concrete; joints; finite element; nonlinear analysis; non–uniform ground motion.

INTRODUCTION

Concrete arch dams are constructed as cantilever monoliths separated by contraction joints. The joints cannot transfer substantial tensile arch stresses, so they may open and close as the dam vibrates in response to earthquake ground motion. The opening of contraction joints and the transfer of loads from arch action to cantilever action may result in the opening of lift joints or horizontal cracking of the concrete. For seismic safety evaluation, however, an arch dam is often analyzed as a linear monolithic structure and resort is made to *ad hoc* interpretation of the tensile arch and cantilever stresses predicted by a linear analysis.

The earthquake response of an arch dam is further complicated by dam–water and dam–foundation interaction effects, which are included in an analysis using procedures of varying accuracy. Generally, the free–field motion along the dam–foundation interface is assumed to be uniform. The spatial variation of the free–field motion is disregarded due to lack of data on the actual free–field motion of canyons. A theoretical study of plane wave cases was performed by Nowak and Hall (1990).

Analytical as well as experimental studies on the effects of contraction joint opening have been conducted in recent years. However, there has been no evidence of contraction joint opening in a dam during an earthquake until January 1994 when Pacoima dam was subjected to the Northridge earthquake. The vertical contraction joints in the dam opened during the earthquake, as evidenced by their subsequent clean appearance. After the earthquake, they closed under static loads, except for the left–most joint which had a permanent opening of up to two inches because the thrust block slid downstream. Minor cracking of concrete and block offsets in horizontal and vertical directions also occurred in parts of the dam body.

The response of Pacoima dam in the Northridge earthquake was recorded by a network of California Division of Mines and Geology (CDMG) accelerometers (CSMIP, 1994). The peak accelerations of 1.6 g and 1.2 g, at the left abutment in the horizontal and vertical directions, respectively, are among the largest ever measured during an earthquake. The strong motion accelerograms provide a unique opportunity to examine the contraction joint behavior in an arch dam subjected to a large earthquake. In addition, the limited processed records from the canyon can be used to study the effects of spatial variation of the input motion on the dam response. This paper presents the results of earthquake analyses of Pacoima dam to investigate the effects of opening of the vertical and horizontal joints and the spatial variation of the input motion.

RESPONSE OF PACOIMA DAM TO NORTHRIDGE EARTHQUAKE

Pacoima dam, with a 365 ft height and 589 ft crest length, is a flood control arch dam located 4.5 miles northeast of San Fernando, California. The thickness of the crown section varies from 10.4 ft at the crest to 99 ft at the base (Fig. 1). Uniformly spaced contraction joints with 12 in. deep beveled keys divide the dam into eleven cantilevers. The left abutment is supported by a concrete thrust block through a 60 ft tall joint. The dam was subjected to severe shaking by the M_S=6.8 magnitude 1994 Northridge earthquake, with the epicenter 11 miles from the dam. The reservoir level was 233 ft above the base (about two–thirds full).

Over–stressing of the dam occurred during the earthquake, as indicated by cracks and permanent movements of the concrete blocks. Most of the damage, however, can be attributed to the movement of the thrust block due to a failure in the supporting foundation rock. The contraction joint between the dam and the thrust block opened and remained open after the earthquake: about 2 in. at the crest and 1/4 in. at the bottom. Some permanent differential movement in the vertical direction also occurred at the joint, with the thrust block lower with respect to the dam. A large diagonal crack occurred in the thrust block near the bottom of the thrust block joint. The dam body suffered less damage. A fine diagonal crack opened near the base of the thrust block. A permanent horizontal offset of 3/8 in. to 1/2 in. occurred along the horizontal joint at 48 ft below the crest, with the top block shifting downstream relative to the bottom block. Permanent vertical offsets occurred along most of the joints, with the right block remaining lower relative to the left block. Opening of the contraction joints during the earthquake was indicated by their clean appearance after the earthquake.

The accelerations of the dam and the canyon were recorded by a network of CDMG strong motion accelerometers. The locations of the accelerometers on the dam are shown in Fig. 1. CDMG could not digitize and process all the records because large acceleration peaks, which exceeded the range of instruments, were intertwined on the film. Processed records are available for two locations in the canyon, one at the downstream and the other 50 ft above the left abutment, and channels 8 to 11 on the dam.

The peak accelerations recorded in the canyon were 0.43 g and 1.58 g for the downstream and the upper left abutment (ULA) instruments, respectively, indicating the amplification of ground motion by the canyon topography. The stream component of these motions are shown in Fig. 2. with the radial acceleration recorded at base. Channel 8 recorded the radial acceleration, with a peak of 1.31 g, at the left quarter point at 80% height of the dam. Figure 3 shows the radial accelerations of the dam at three different elevations, the base, 80% height and the crest. The partially digitized but unprocessed acceleration records from the crest of crown section are plotted in Fig. 4.

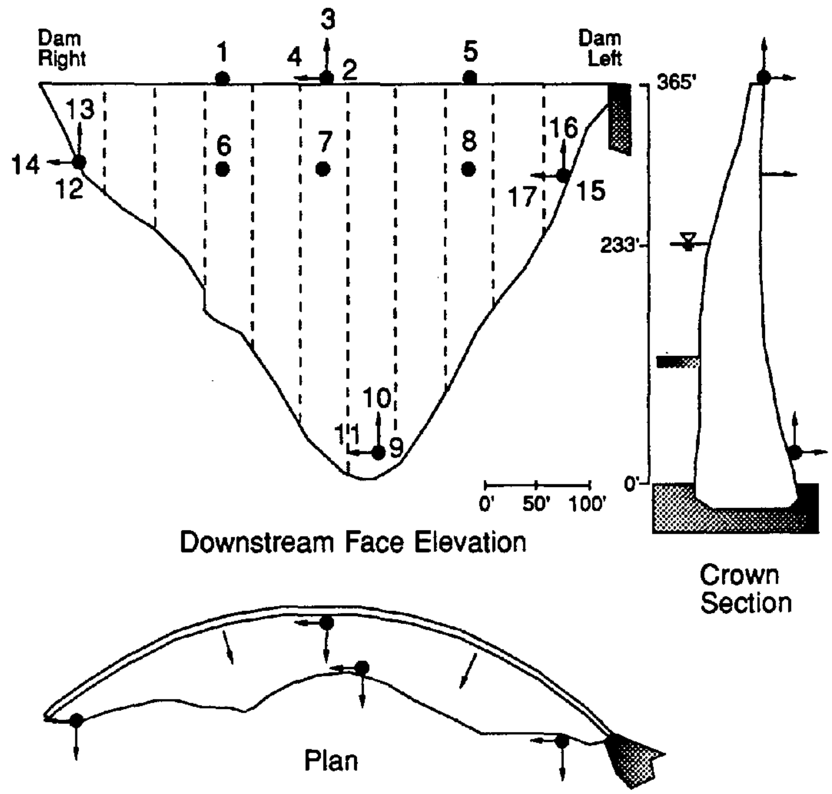

Fig. 1 Pacoima dam showing channels of accelerometers.

FINITE ELEMENT MODEL, INPUT, AND ANALYSIS

The finite element computer program ADAP–88, developed at the University of California, Berkeley, (Fenves, Mojtahedi *et al.*, 1989; Fenves, Mojtahedi *et al., 1992*) was used for the earthquake analysis of Pacoima dam. The program has been verified by a shaking table test of a 1:300 scale model of an arch dam (Chen and Li, 1994). Standard 3–D solid elements are used to model the concrete arch and the foundation rock. Nonlinear joint elements simulate opening–closing of the contraction joints, lift joints, and the dam–foundation interface. Spatially non–uniform seismic input, can be specified through displacement histories at the dam–foundation interface (Mojtahedi and Tseng, 1994).

Input Motion

Two types of earthquake analysis were performed which differed in the specification of the free–field motion at the dam–foundation interface. The first type used a uniform free–field motion, whereas non–uniform free–field motion was considered in the second type. The free–field motions for both cases were derived from the motions recorded in the canyon during the Northridge earthquake. For determining the non–uniform free–field motion, it was not possible to separate dam–foundation interaction effects from the spatial variation of the canyon motion. Hence, those dam–foundation effects were neglected and the recorded motion at the interface was assumed to be the free–field motion.

Due to the profound difficulties in determining the motion of canyon and also lack of sufficient acceleration records form the earthquake, a simple approach was adopted for specification of the non–uniform free–field motion. The same motion was specified for the right and the left abutments. The ULA and the dam base records were specified for the crest and the base of the dam, respectively. The motion at intermediate elevations was computed by linear interpolation from these records. The acceleration histories corresponding to the assumed input motion variation are shown in Fig. 5 for different elevations of the model.

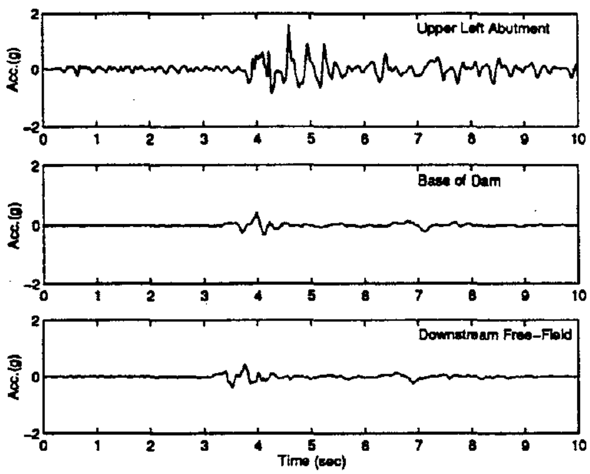

Fig. 2 Recorded acceleration histories for the canyon.

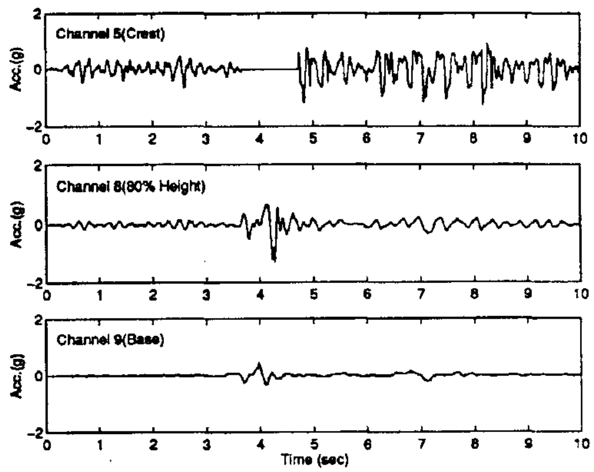

Fig. 3 Recorded radial acceleration history of dam. Zero acceleration is given for gaps in digitization of Channel 5.

Model

A total of 588 eight-node 3-D elements model the dam body. Three joint elements and 3-D solid elements were used through the thickness. Slippage of the joints was not allowed in the model. This assumption is valid for the keyed contraction joints, but may not be true for the horizontal joints, as discussed later. Zero tensile strength was assumed for the joints.

The number of contraction joints and lift joints in the dam model was selected from trial analyses. Of the twelve vertical joints in the dam, only five were included in the model. In addition, five horizontal joints, at 50, 97, 135, 202, and 282 ft above the base, were included to represent lift joints. Each horizontal joint spans an entire horizontal section between the right and left abutments. The material properties used for concrete were obtained from a previous study of the dam: modulus of elasticity = 2400 ksi, Poisson's ratio=0.20, based on testing of core samples of concrete.

A foundation rock region with a depth approximately equal to the height of the dam was included in the model to account for dam-foundation interaction effects. Although the foundation rock geometry and material properties are complicated, a prismatic shape was assumed for the canyon using a coarse mesh of the foundation rock region with 220 3-D solid elements. The material properties for the foundation rock were obtained from the previous studies: modulus of elasticity=2000 ksi, Poisson's ratio=0.20. To suppress the propagation of seismic waves, the foundation rock was assumed to be massless. For analysis with uniform free-field motion, the acceleration was specified at the rigid base of the foundation model. For analyses with non-uniform free-field motion, the displacement was specified at the nodes on the dam-foundation interface.

The first natural frequency computed for the dam using these properties, with the 233 ft reservoir level, was 4.3 Hz with an essentially anti-symmetric mode shape. To confirm the selected properties, the transmissibility function was computed for the radial motions recorded at the base and channel 8. The fundamental frequency of the dam from the peaks of transmissibility function was 4.0 Hz which, considering the limited processed data, is in reasonable agreement with the model frequency.

Rayleigh damping was assumed for the dam-foundation system with parameters selected to produce 10% damping at 5 Hz and 20 Hz. The assumed damping is relatively high, but is justified considering that radiation damping in the massless foundation is not explicitly included in the model.

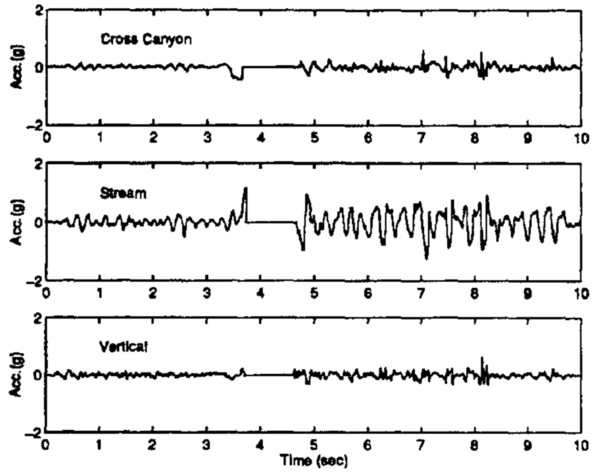

Fig. 4 Unprocessed acceleration histories at crest (channels 2–4). Zero acceleration given for gaps in digitizing.

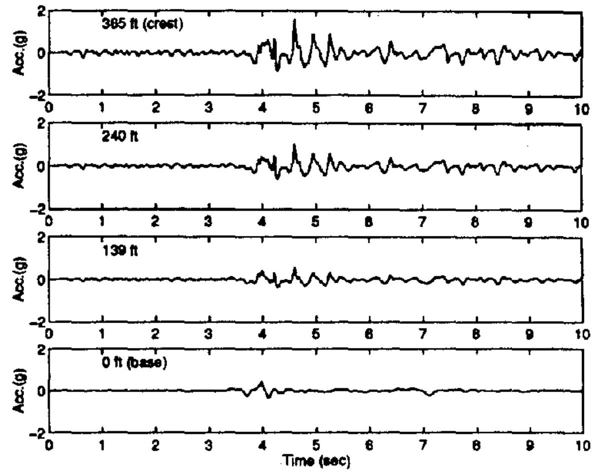

Fig. 5 Assumed non–uniform acceleration histories at the dam–canyon interface in stream direction.

The solution procedure in ADAP–88 is based on a time integration of the nonlinear equations of motion. The hydrodynamic pressures acting on the dam is represented by an added mass matrix neglecting compressibility of water (Kuo, 1982). For computing the added mass, the reservoir is assumed to be bounded by a cylindrical surface obtained by translating the dam–reservoir interface in the upstream direction.

To account for effects of static stresses on opening of the joints, the seismic analysis was preceded by the static analyses for hydrostatic and gravity loads. The vertical joint elements were omitted in the gravity load analysis to account for the independent behavior of the cantilever monoliths. The hydrostatic load was applied to the entire model, including all of the joint elements.

SEISMIC RESPONSE OF PACOIMA DAM

Amplification Effects of Canyon Topography

The amplification of seismic waves in the canyon was indicated by variation in the acceleration amplitudes recorded at the downstream, base, and upper left abutment (Fig. 2). To assess the effects of the ground motion input on the response of the dam, two cases were analyzed with all joints closed. Following previous studies of the dam (Dowling and Hall, 1989), two–thirds of the ULA motion was considered as the average motion of the canyon and was specified as uniform input motion for the first case. The previously described non–uniform free–field motion was used for the second case.

The recorded and computed accelerations for channel 8 are shown in Fig. 6. The accelerations computed for the two closed joint cases differ in amplitude and phase. The case with non–uniform input agrees better with the recorded acceleration than does the uniform input case. However, the response computed for both cases contain a large amplitude cycle which is not present in the recorded motion. The overestimation of the vibration is most likely caused by the lack of radiation damping in the model. The sliding of the foundation rock mass near the left abutment, not accounted for in the model, may also be responsible for the discrepancy.

Figure 7 shows the envelopes of the maximum tensile arch and cantilever stresses at the downstream face, viewed looking downstream. (Observations for upstream face stresses are similar.) The contours are different in distribution and magnitude for the two closed joint cases. For uniform input motion, the peak arch and cantilever stresses are 900 psi and 400 psi, respectively. The peak stress for the non–uniform case are more than three times larger.

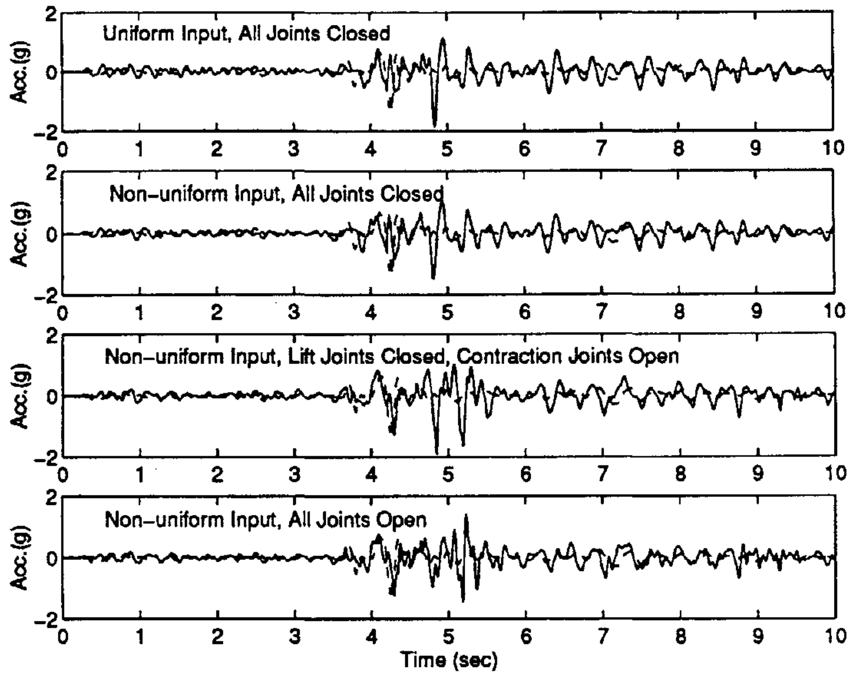

Fig. 6 Comparison of recorded acceleration for channel 8 (dashed line) with computed acceleration (solid line) at the same location.

Opening of Contraction Joints

To examine the effects of contraction joints, as well as opening at the dam–foundation interface due to tensile stresses, the analysis with non–uniform input motion was repeated with these joints allowed to open. From the channel 8 acceleration comparison in Fig. 6, the agreement between computed and recorded acceleration improves significantly when the joints are allowed to open. However, the computed response again contains spikes not present in the recorded motion for the reasons mentioned previously.

When contraction joints are allowed to open, the peak downstream arch stress reduces to 1000 psi from 3400 psi and the peak cantilever stress increases to 1800 psi from 1400 psi. The maximum opening of the contraction joints is 4 in. Significant opening, however, occurs at the base of joint, in contrast with the case of uniform input. The upstream and downstream openings are in–phase for each joint indicating complete separation of the vertical joint. The opening of the right–most joint is almost entirely due to the pseudo–static response caused by the relative displacement along the foundation interface.

Effects of Lift Joints

The cantilever stresses computed for the case with contraction joint opening exceed the tensile strength of concrete and the lift joints. To account for the opening of lift joints, the dam was analyzed with all vertical, horizontal and abutment joints allowed to open, and considering the non–uniform input motion. In view of the permanent opening of the thrust block joint, tangential stiffness of the joint was omitted. The last history in Fig. 6 for non–uniform input and all joints open shows the best comparison between the computed and recorded acceleration at channel 8.

The opening of lift joints releases the cantilever stresses, as seen from contours in Fig. 7. The maximum cantilever stress of downstream face reduces to 1000 psi from 1800 psi for lift joints assumed closed. Significant opening occurs at the top lift joint with a maximum value of 2.6 in. at the base of thrust block on downstream face. The opening for all other locations is less than 0.5 in. Complete separation through the thickness occurs at a number of locations.

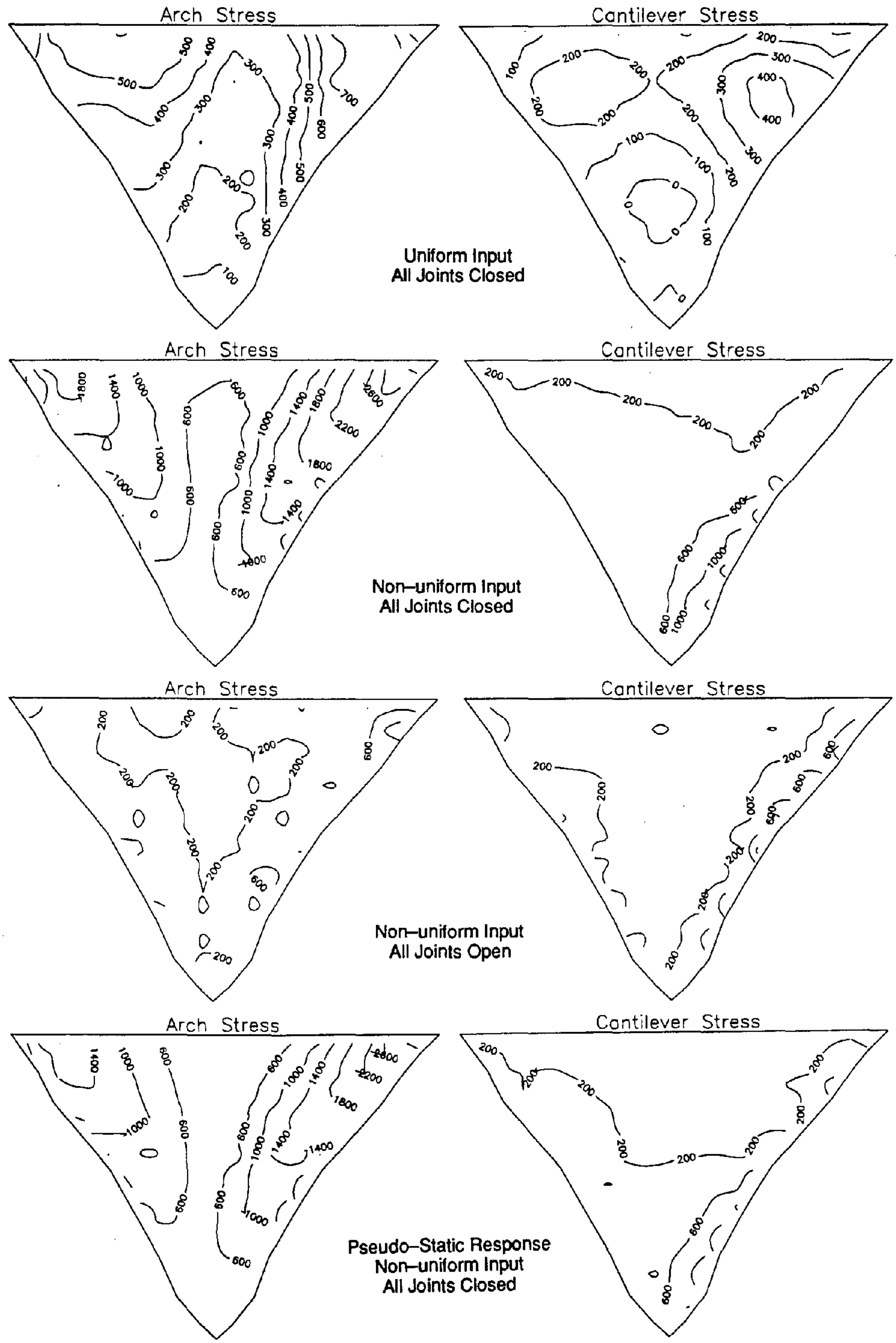

Fig. 7 Envelopes of maximum tensile stress on downstream face (in psi).

Pseudo-static Response

For a better understanding of the response to non-uniform input motion, the seismic response to the non-uniform input motion was computed with all joints prevented from opening and the inertial effects omitted, to compute the pseudo-static response of the monolithic model. From contour plots of the maximum stress in Fig. 7, the peak stresses associated with the pseudo-static response are largest near the abutments with relatively small stresses in the central portion of the dam. The peak stresses near the abutments are similar to the corresponding stresses which are shown in the same figure for the total dynamic response computed with all joints assumed closed. For the assumed non-uniform input motion the pseudo-static response is significant and the contribution from the vibration in total response is limited to the upper center of the dam.

CONCLUSIONS

Seismic analysis of Pacoima dam using the processed strong motion records from the 1994 Northridge earthquake shows that amplification of seismic waves due to canyon topography has important effects on the response of the dam. An analysis with uniform input motion underestimates the stresses, particularly near the abutments. The stresses are dominated by the pseudo-static response caused by relative displacements of the non-uniform free-field motion. The contribution of dam vibration to the stresses is smaller.

A finite element procedure incorporating discrete joint elements for representation of the discontinuities of the dam can simulate the actual response of the dam. According to the model, the maximum joint opening is 4 in. for the contraction joints and 2.6 in. for the lift joints. In view of the opening of the lift joints, the seismic analysis procedure can be improved by including slippage of the open joints. The dam response is over-estimated unless the loss of energy due to the radiation damping is accounted for.

ACKNOWLEDGMENTS

The contents of this paper were developed under Contract No. 1093–558 from the California Department of Conservation, Division of Mines and Geology, Strong Motion Instrumentation Program. The version of ADAP–88 used in this study was developed with partial support from I.C.E.C., Berkeley, CA, with advise from Dr. W.S. Tseng.

REFERENCES

Chen, H. and D. Li (1994). "Model Test and Program Verification on Dynamic Behavior of Arch Dam with Contraction Joints," *Report No. SVL–94/02*, Institute of Water Conservancy and Hydroelectric Power Research, Beijing, China.

CSMIP (1994). "Strong Motion Records from the Northridge, California Earthquake of January 17, 1994," *Report No. OSMS 94–07*, California Department of Conservation, Strong Motion Instrumentation Program.

Dowling, M. J. and J. F. Hall (1989). "Nonlinear Seismic Analysis of Arch Dams," *Journal of Engineering Mechanics*, ASCE, Vol. 115, No. 4, pp. 768–789.

Fenves, G. L., S. Mojtahedi, et al. (1989). "ADAP–88: A Computer Program for Nonlinear Earthquake Analysis of Concrete Arch Dams," *Report No. UCB/EERC–89/12*, Earthquake Engineering Research Center, University of California, Berkeley.

Fenves, G. L., S. Mojtahedi, R. B. Reimer (1992). "Effect of Contraction Joints on Earthquake Response of an Arch Dam," *Journal of Structural Engineering*, ASCE, Vol. 118, No. No. 4, pp. 1039–1055.

Kuo, J. (1982). "Fluid–Structure Interactions: Added Mass Computations for Incompressible Fluid," *Report No. UCB/EERC–82/09*, Earthquake Engineering Research Center, University of California, Berkeley.

Mojtahedi, S. and W. S. Tseng (1994). "ADAP–NF, A Computer Program for Nonlinear Analysis of Arch Dams Considering Nonuniform Seismic Input," International Civil Engineering Consultants, Inc., Berkeley, CA.

Nowak, P. S. and J. F. Hall (1990). "Arch Dam Response to Nonuniform Seismic Input," *Journal of Engineering Mechanics*, ASCE, Vol. 116, No. 1, pp. 125–139.

BEHAVIOR OF LARGE STEEL BEAM-COLUMN CONNECTIONS

Egor P. POPOV and Marcial BLONDET

University of California at Berkeley
Department of Civil and Environmental Engineering
760 Davis Hall, Berkeley, California 94720-1710, USA

ABSTRACT

A surprisingly large number of beam-to-column connections in steel frame buildings suffered brittle failure during the 1994 Northridge earthquake. A large scale testing program was initiated by the SAC Joint Venture to evaluate the seismic worthiness and propose repairs for existing connections, and to establish design guidelines for new steel construction. Three full-scale beam-column connections were tested at the University of California at Berkeley within the SAC Joint Venture. The specimens were nominally identical models of typical exterior beam-column connections found in modern steel moment resisting frame buildings. All specimens were detailed according to the industry standards and procedures in use before the Northridge earthquake, and manufactured simulating field conditions.

Testing consisted of subjecting the specimens to cyclic quasi-static loading. All three connections fractured suddenly. Serious fractures of the column entire flange, sometimes observed during Northridge, were reproduced in two specimens. The third specimen failed due to the weld fracture on the beam bottom flange. The three specimens were repaired according to current repair procedures, and tested again using an identical loading protocol. All three repaired connections showed a somewhat improved behavior compared with the original specimens. Their mode of failure, however, was also a non-ductile, sudden fracture.

KEYWORDS

Steel connections, steel moment frames, seismic behavior, welded connections, structural repair.

INTRODUCTION

Before the Northridge earthquake of January 17, 1994, steel moment-resisting frames were considered to be the reliable systems for seismic resistant construction. After observing extensive fractures in beam-to-column connections during this earthquake, their relaibility is now questioned. In responce to this concern, the SAC Joint Venture (Structural Engineers Association of California, Applied Technology Council, and the California Universities for Research in Earthquake Engineering) implemented a comprehensive program to develop improved professional practices and recommend standards for the repair, design and retrofit of the moment resisting frame buildings so that they would provide reliable, cost-effective seismic performance in future earthquakes.

As part of the experimental research effort of the SAC Steel Program, a set of large-scale external beam-to-column connections, constructed following the pre-Northridge practice, was tested at the Department of Civil and Environmental Engineering of the University of California at Berkeley. The main goals of these tests were to study the seismic response of the standard connections, and to verify the adequacy of current repair methods. This paper briefly presents the main findings of this experimental program. Detailed results are given in the final SAC report (Popov et al., 1996).

SPECIMENS, TEST SETUP & INSTRUMENTATION

Three nominally identical full scale models of a typical beam-to-column connection, labeled as PN1, PN2, and PN3 (for Pre-Northridge), were manufactured by a local fabricating company. The details of the connection, the weld specifications, and the erection procedures closely resembled the industry standards in use before the Northridge earthquake. Figure 1 shows specimen geometry and connection details. All columns were fabricated with A572-Gr. 50 steel. Although it was specified that all beams should be fabricated with A36 steel, the beams of PN1 and PN2 were built from A572-Gr. 50 steel; only PN3 had a beam made of A36 steel. This construction error caused the geometrically identical specimens to have different strength characteristics, since the beams of PN1 and PN2 were considerably stronger than the beam of PN3.

Table 1. Material Properties

		Yield Strength F_y (ksi)			Ultimate Strength F_u (ksi)		
Specimen	Shape & Steel	AISC	Mill	Coupon	AISC	Mill	Coupon
All Columns	W14x257, A572-Gr 50	50.0	53.5	48.3	65.0	72.5	67.8
PN1 & PN2 Beam	W36x150, A572-Gr 50	50.0	62.6	60.6	65.0	74.7	68.6
PN3 Beam	W36x150, A36	36.0	56.8	40.3	50.0	40.3	57.4

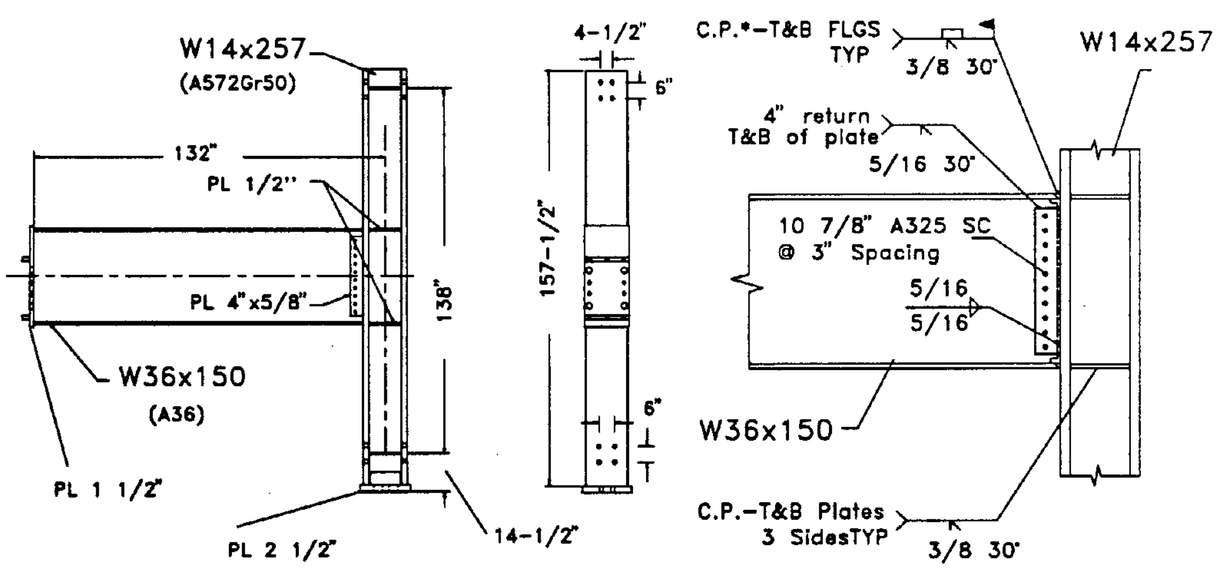

Fig. 1. Specimen dimensions and connection details

The tests were conducted in the Structural Engineering Laboratory of the University of California at Berkeley. The test setup, shown in Fig. 2, was designed to test the specimens in a horizontal position. The support system consisted of three reinforced concrete reaction blocks fixed to the test floor with high strength rods. Both ends of the columns were tightened against the reaction blocks by prestressed steel rods. Load was applied to the cantilever beam end by a servo-hydraulic actuator through a clevis bolted to the beam end plate. To prevent out of plane motion of the beam, a horizontal bracing system was provided near the beam end.

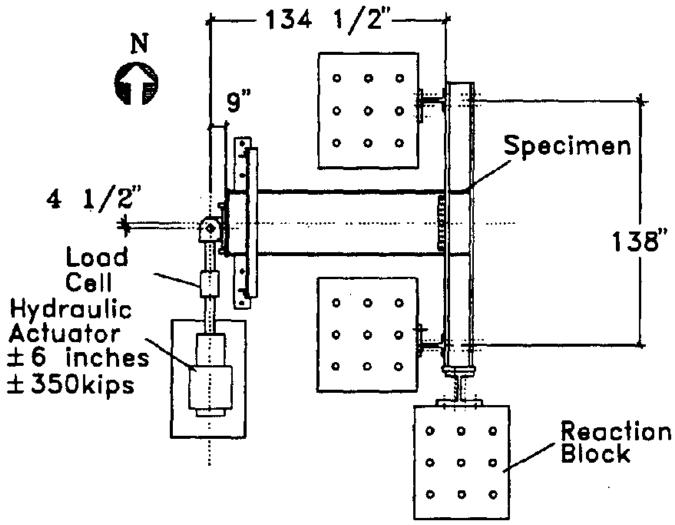

Fig. 2. Test setup

Linear potentiometers were used to measure global behavior: beam end deflection, joint rotation, and panel zone shear deformation. Strain gages and rosettes were glued at critical locations to measure the local response. The applied load was monitored with a load cell attached to the actuator. All instruments were connected to a computer-based data acquisition and control system used to send the displacement command signal to the servohydraulic actuator and to acquire the instrumental readings at programmed times.

All testing was performed under displacement control, following a protocol based on ATC-24 (ATC, 1994). The actuator displacement loading history consisted of a series of cyclic displacements with increasing amplitude, as shown in Fig. 3. The reference displacement of 1 inch corresponds to the estimated beam end yield deflection. Specimens were painted with white-wash prior to testing, to be able to observe yielding in the areas where the mill scale flakes off.

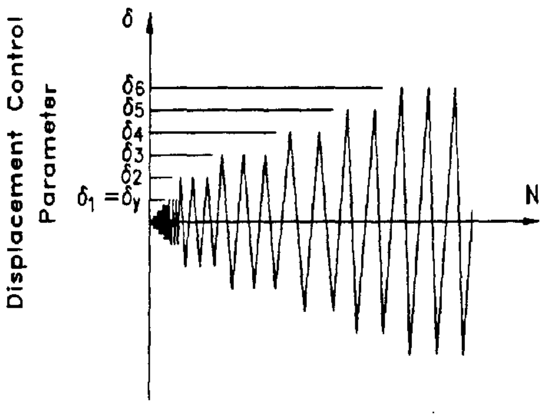

Load Step	Peak Displacement [inch]	Number of Cycles
1	0.10	2
2	0.25	3
3	0.50	3
4	0.75	3
5	1.00	3
6	2.00	3
7	3.00	3
8	4.00	2
9	5.00	2
10	6.00	n

Fig. 3. Loading History

SPECIMEN 1 TEST

PN1 behaved elastically up to and during the 1-inch cycles. During the 2-inch cycles the white-wash spalled due to yielding in both beam flanges, in the column flanges and in the panel zone. PN1 sustained the first 3-inch load cycle, with a maximum force of 223 kips, and a peak displacement of 2.57 inches. This discrepancy with the target displacement of 3 inches, observed consistently throughout the testing of all specimens, was due to slippage of the clevis connection.. The specimen failed suddenly (and very loudly) during the first leg of the second 3-inch load cycle. The failure load and displacement were 206 kips and 1.62 inches, respectively. One of the column flanges fractured completely, and the crack propagated into the column web, as illustrated in Fig. 4a. This mode of failure was unexpected; analysis predicted failure in the A36 steel beam. Some investigation revealed that the beam was built from Grade 50 steel instead of A36. This error was, in a way, fortunate, because this was the first test where this type of column failure, observed during the Northridge earthquake, was reproduced in the laboratory.

The repair procedure consisted of removing the cracked portions of the column flange and web, and welding a new piece made of a Gr. 50, W14 x 257 section. A beam flange splice plate was used to reconnect the beam bottom flange to the repaired column flange and new continuity plates were provided. A beam web doubler plate was welded to the column flange and beam web on the side opposite to the shear tab. Fig. 4b shows a sketch of the repair scheme.

The specimen, now labeled RN1, was retested. Nonlinear response started with the 2-inch cycles. During the 3-inch sequence, significant spalling of the white-wash was observed at the top beam flange and bottom splice plate, at the back column flange, and in the panel zone. RN1 sustained the positive excursion of the first 4-inch cycle with a peak load of 260 kips and 3.54 inch displacement. The specimen failed during the negative excursion of that cycle with a complete fracture of the top flange weld, as shown in Fig. 4c.

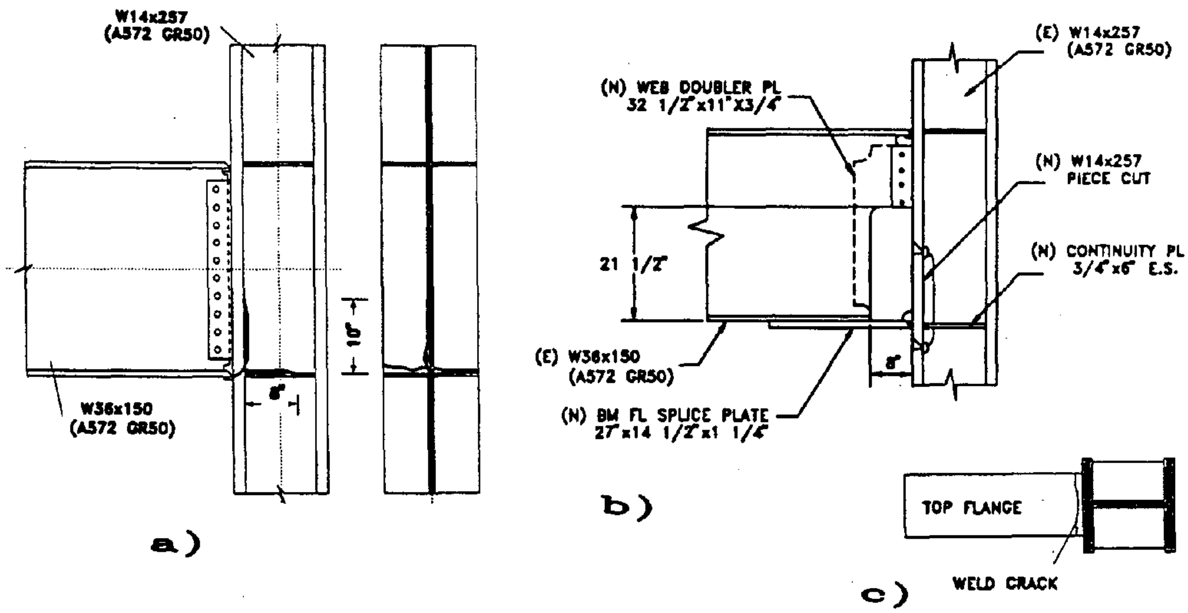

Fig 4. Specimen 1 -- Damage, repair, and damage of repaired connection

SPECIMEN 2 TEST

As with PN1, nonlinear response started during the 2-inch cycles. Spalling of the white-wash indicated significant yielding in the panel zone. PN2 failed suddenly during the first leg of the second 2-inch load cycle at 195 kips load and 1.57 inch displacement. The cracking pattern is sketched in Fig. 5a. Cracking started in the beam bottom flange weld, continued diagonally through the column flange, and entered the panel zone, where it extended upwards along the column flange. This column failure was also due to having the beam mistakenly constructed with Grade 50 steel instead of the specified A36 steel.

Since PN1 and PN2 had similar column failure modes, it was decided to incorporate an improved retrofit scheme by adding a haunch. Damaged portions of the beam and column were removed and replaced with new Grade 50 material. A new A36 plate was used to reconnect the beam bottom flange, and a beam web doubler plate was welded to the column and beam. A tapered haunch made of Grade 50 plate was placed underneath the beam bottom flange. Stiffeners were added to the beam and the column. Figure 5b summarizes the repair procedure. The haunch and stiffeners were initially fabricated and installed with wrong dimensions and it was necessary to remove them and fabricate and install new material.

The repaired and retrofitted specimen, RN2, was able to sustain load up to the 4-inch cycles. First spalling of the white-wash was noted on the bottom beam flange, near the haunch, at the beginning of the 2-inch cycles. Yielding occurred later in the beam top flange, in the column back flange, and in the panel zone. The specimen failed during the first excursion of the first 5-inch cycle. A crack started at the edge of the beam bottom flange between the haunch end and beam stiffener and propagated along the haunch edge up to the beam web, where it branched in two, as shown in Fig. 5c.

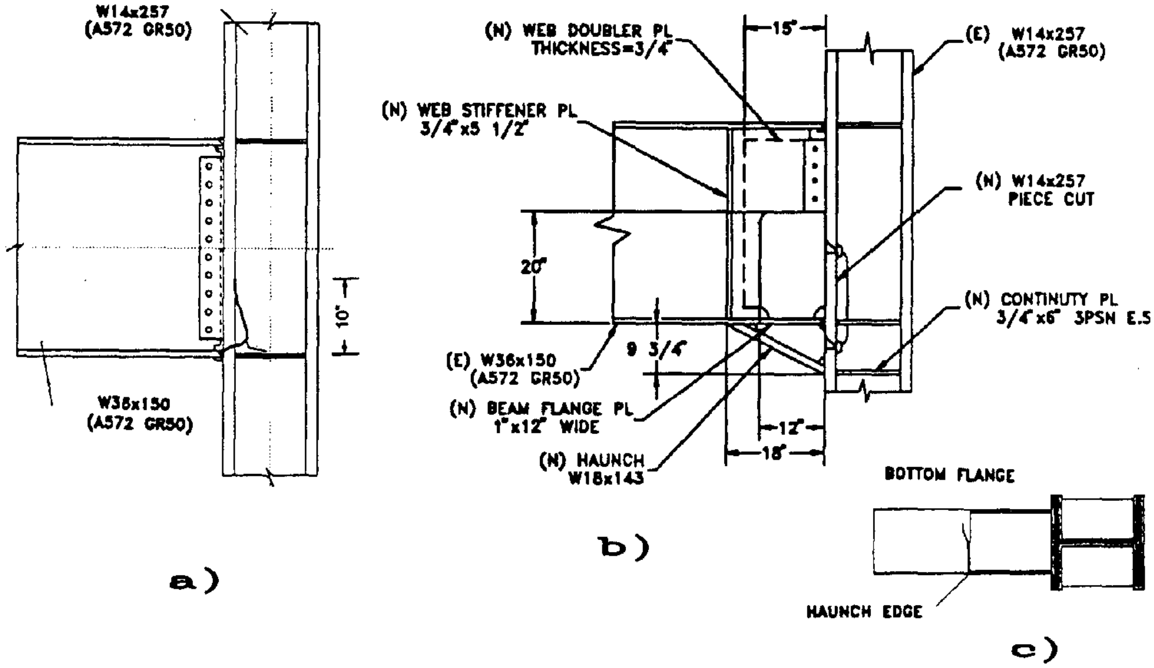

Fig. 5. Specimen 2 -- Damage, repair, and damage of repaired connection

SPECIMEN 3 TEST

PN3 held up to the first 3-inch cycle. Yielding was significant on the beam flanges. The maximum force was equal to 190 kips and the beam end displacement reached during this cycle was 2.67 inches. The specimen failed during the first leg of the second 3-inch load cycle. The bottom beam flange cracked through the weld. Later, some bolts sheared off and the shear tab broke. Loading was continued to finish the cycle. During the negative excursion of the cycle, the beam top flange cracked through approximately 3/4 of its width. This type of beam fracture was expected for all three PN specimens, and occurred only with PN3 which beam was constructed from the correct material, A36 steel. The failure of the specimen is illustrated in Fig. 6a.

The repair of PN3 was achived by gouging out the cracked welds and placing new complete penetration welds at both flanges. All remaining bolts and the cracked shear plate were removed. A new shear plate was welded on the opposite side from the removed old one. Figure 6b shows the repair details.

The repaired specimen, RN3, withstood up to he first 4-inch cycle. Yielding started during the first 2-inch cycle on the beam flanges and on the beam web. After completion of the first 4-inch cycle considerable white-wash spalling could be observed on both beam flanges and beam web and in the panel zone area. The maximum force was equal to 225 kips at the beam end displacement of 3.60 inches.. The specimen failed during the first excursion of the second 4-inch cycle at 196 kips load and 1.48 inch beam end displacement. First crack started at the edge of the beam bottom flange and propagated through the entire flange with a short branch near the flange axis, as shown in Fig. 6c.

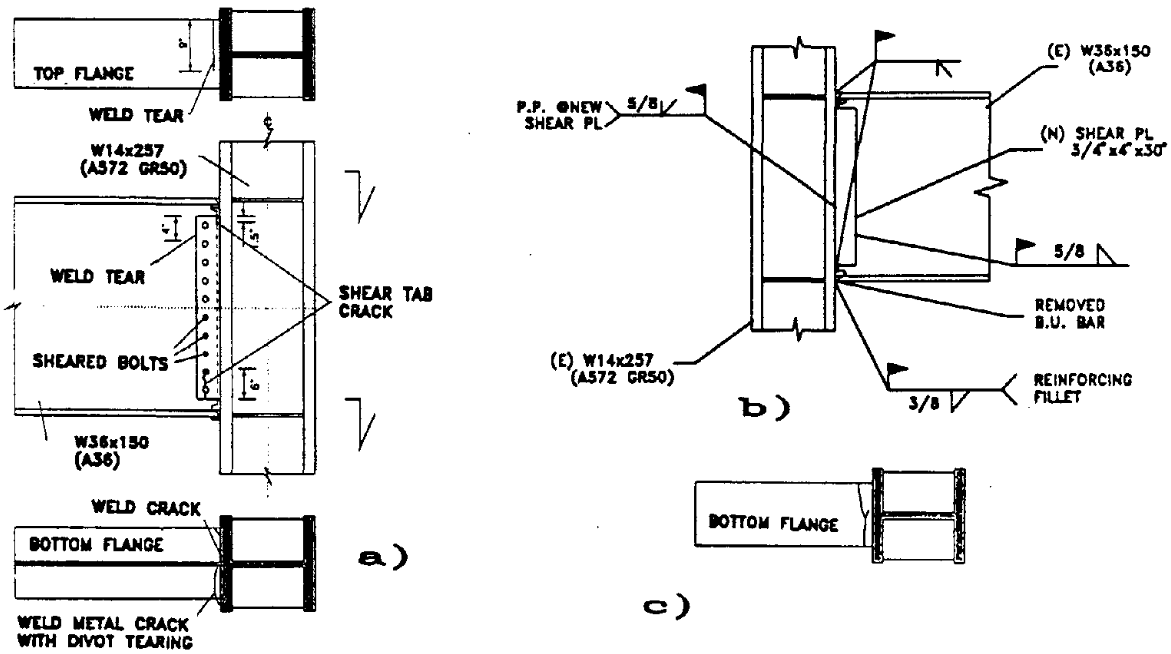

Fig 6. Specimen 3 -- Damage, repair, and damage of repaired connection

EVALUATION OF EXPERIMENTAL RESPONSE

Table 2 shows peak values of various response quantities obtained for Pre-Northridge and repair specimens in this test program. Stiffness values correspond to the applied load versus the beam end displacement. Yield values correspond to the event where there is a sudden increase of energy dissipation through plastic work (Popov et al., 1996). Connection rotation was defined as beam end displacement divided by beam clear length. Energy refers to the total plastic work developed by the specimen up to failure.

Table 2. Summary of Experimental Response

Specimen	PN1	RN1	Δ%	PN2	RN2	Δ%	PN3	RN3	Δ%
Elastic Stiff. (k/in)	151	166	10%	152	183	20%	146	136	-7%
Yield Load (kip)	136	179	32%	130	159	22%	137	136	-1%
Yield Displ. (in)	0.90	1.08	20%	0.86	0.87	1%	0.94	1.00	6%
Max. Load (kip)	223	260	17%	195	319	64%	198	225	14%
Peak. Displ. (in)	2.57	3.54	38%	1.62	4.02	148%	2.67	3.60	35%
Plastic Rot. (%)	0.88	1.55	76%	0.34	1.77	420%	1.07	1.61	50%
Energy (k-ft)	140	370	164%	40	620	1450%	200	420	110%

The hysteretic response of the specimens can be visualized in Figs. 7 and 8, which provide force versus beam end displacement plots and moment at column face versus plastic rotation plots, respectively. The response of the repaired specimens is shown in the second row.

Clearly, the repair techniques evaluated were successful, in the sense that the repaired specimens were stronger and had significantly better energy dissipation characteristics than the Pre-Northridge connections. The most dramatic improvement was obtained for specimen PN2, which was retrofitted with a haunch. RN1 and RN2 were also stiffer than PN1 and PN2 due to the beam/column joint repair. The reweld repair used for PN3 produced a somewhat softer specimen, with improved strength and ductility. It is important to note, however, that the failure mode of all three repaired specimens was abrupt and without previous warning.

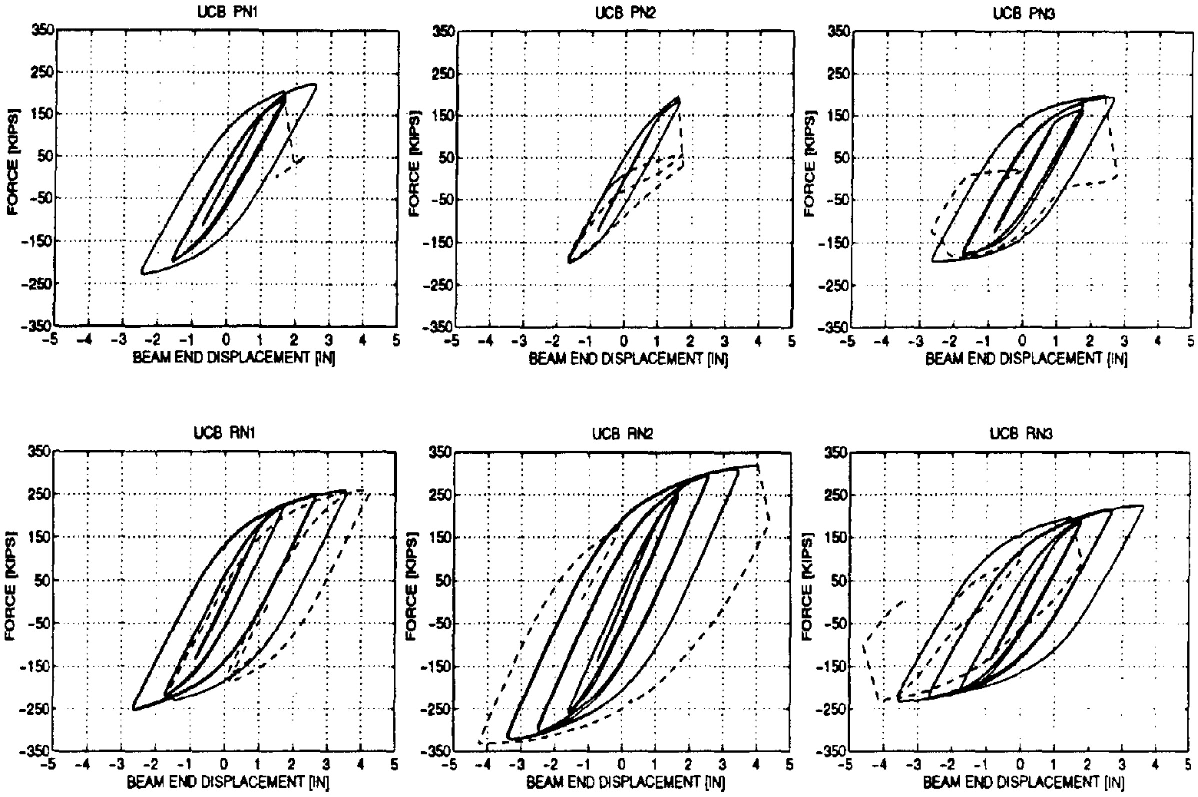

Fig. 7. Applied Load vs. Beam End Displacement

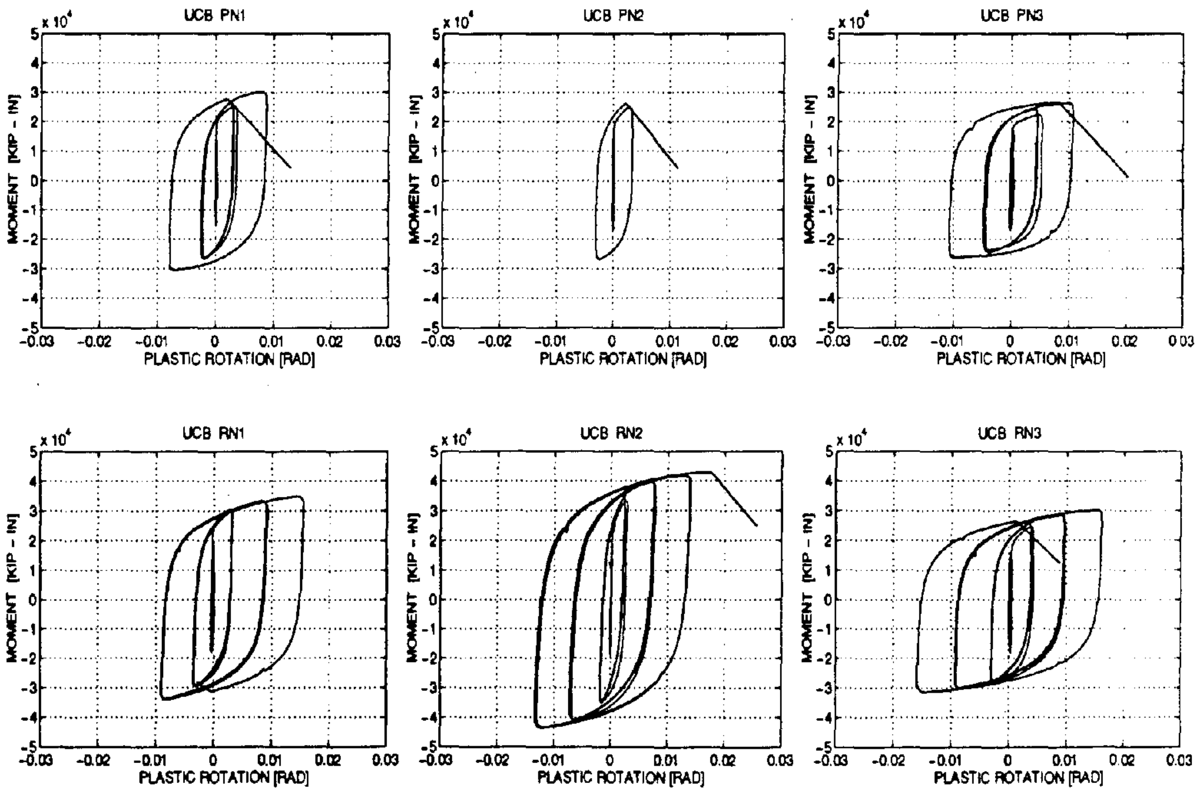

Fig. 8. Moment @Column Face vs. Plastic Rotation

CONCLUSIONS

From the behavior observed during the tests and the results presented above, the following conclusions can be drawn:

1. The pre-Northridge connections showed a very poor response to cyclic loads. They had low capacity for energy dissipation and failed in a brittle, abrupt mode, without warning.
2. The repaired schemes studied here were moderately successful. The repaired specimens were stronger, more ductile, and had better energy dissipation characteristics than the original ones.
3. The failures of the repaired specimens were, however, sudden resulting in brittle fractures. This is a highly objectionable characteristic for structures in seismic zones.

REFERENCES

Popov, E. P., M. Blondet, L. Stepanov and B. Stojadinovic (1996). Full-Scale Steel Beam-Column Tests. SAC Report 1-1, 1996.

Applied Technology Council (ATC). Guidelines for Cyclic Seismic Testing of Components of Steel Structures. ATC-24, 1992.

ACKNOWLEDGMENTS

Many people made this project possible. Prof. Steve Mahin and Mr. James Malley of SAC provided continuous support and valuable technical comments. Barry Shindler of SAC designed the repair schemes. Dr. Lev Stepanov and Dr. Bozidar Stojadinovic of the laboratory staff actively participated in the planning and execution of the tests, data processing, and the preparation of the final report. The following staff of the Department of Civil and Environmental Engineering provided high quality technical assistance: Larry Baker, Jeff Higginbotham, Dick Parsons, Mark Troxler, and Doug Zulaica (Machine Shop); Todd Merport and Chris Moy (Electronics Services Support Group); Jon Asselanis (Materials Testing Lab); and Bill MacCracken (Video). Many students worked extremely hard to perform the tests on schedule: Dr. Tzong-Shuoh Yang, Dr. Chiao-Tung Chang, Brent Blackmann, Hana Mori, and Shi-Poh Chang.

EARTHQUAKE RESPONSE OF TWO-LEVEL VIADUCT BRIDGES

SATINDER P. SINGH* and GREGORY L. FENVES

Department of Civil and Environmental Engineering
University of California, Berkeley, CA 94720

ABSTRACT

The nonlinear effects in the earthquake response of two-level viaduct type bridges are investigated. The nonlinear response is due to the hinge opening and pounding between adjacent frames, tension only cable restrainers, compression only abutments, and plastic hinge formation in the columns. The linear and nonlinear dynamic analyses of typical multiple-frame viaducts are performed using "stick" models for a range of parameters for a typical viaduct. The study shows that it may be necessary to perform nonlinear analysis to determine the effects of hinge opening and closing on the ductility demands. Large hinge openings increase the displacement of interior frames of the viaduct with abutments compared with the case of closed hinges. Considering variable site response effects along a bridge, there can be significant amplification of the frame on stiff soil because of the pounding from an adjacent frame on soft soil. The non-uniform ground motion generally increases the out-of-phase response between the adjacent frames. A large number of restrainers is needed to limit the hinge opening between frames to the yield displacement of the restrainers.

KEYWORDS

Viaduct; bridge; restrainers; hinge opening; nonlinear response.

INTRODUCTION

The damage and collapse of two-level viaducts in the 1989 Loma Prieta earthquake have prompted intensive examination of the seismic response and performance of these important components of the transportation system. These type of long structures are particularly vulnerable to ground motion in the longitudinal direction because of the problematic longitudinal framing system, although the response due to transverse motion is also important. The opening and closing of hinges during an earthquake produces discontinuities which change the load paths in the structure, and hence change the system response. Cable restrainers are provided to restore some continuity between adjacent frames, but they exhibit nonlinear behavior because they can only resist tension and may yield. The abutments are only effective in resisting compression. The yielding of structural members in a viaduct changes the kinematics and internal force distribution, assuming non-ductile failure modes such as shear and joint failure are prevented by proper design. This study examines all these effects to provide the insight for performing earthquake evaluation of two-level viaducts. The study also presents the earthquake response due to the effects of varying site ground motions for a long viaduct.

---

* SOH & Associates, San Francisco, CA 94107.

Three–dimensional elastic and two–dimensional inelastic models are used to understand the system response due to the ground motion in the longitudinal direction. One of the goals of the study is to compare the nonlinear response of the viaducts with the approximate elastic response.

MODELS OF VIADUCT AND ANALYSIS METHODS

The structure selected for this study is representative of a typical pre–1970 construction for a two–level reinforced concrete viaduct with two–column bents. The viaduct has four 270 ft long frames of three bents each. These frames are separated by hinges at the upper and the lower levels. More recent viaducts have hinges further apart. The hinges in this viaduct are connected by cable restrainers 3/4 in. diameter, 20 ft long. The viaduct with abutments used in this study has stiff abutments at the lower level and soft abutments at the upper level. The stiff abutment is representative of the typical construction and soil conditions and the soft abutment is representative of the stiffness of a single–level frame of three spans.

The models used in the study have beam elements for bent caps and box girders and beam–column elements for the columns. The shear capacity of the column is assumed to be greater than the shear demands for the purpose of investigating flexural ductility demands. The models do not account for the failure mode due to large torques in the short outriggers and the strength degradation due to cyclic loading.

The SADSAP computer program (Wilson, 1991) is used in this study for the earthquake analyses of elastic models of the viaduct. A three–dimensional stick model with linear frame elements, shown in Fig. 1, includes local nonlinearities due to the opening and closing of hinges and seats at the abutments. The gross moments of inertia and torsional moment of inertia are multiplied by a factor of 0.60 to approximate the cracked section properties. Corresponding to the gravity axial load of 1,350 kips per column, the moment capacity of the column is 13,300 kip–ft. Based on this flexural strength, the columns at the lower–level yield when the shear force is 700 kips. Each hinge in the box–girder is modeled by two gap elements. The abutments and restrainers are modeled as compression–only and tension–only elements, respectively but these elements remain elastic. The slack in the restrainers is accounted for in the model. The total longitudinal stiffness of the stiff abutment, obtained using the method described in Chapter 14 of *Bridge Design Aids* (Caltrans, 1990), is 62,400 k/ft. Based on the stiffness of a single–level frame of three spans, the soft abutment has the longitudinal stiffness of 20,000 k/ft.

The DRAIN–2DX computer program (Prakash, Powell, and Filippou, 1992) is used to perform the inelastic analyses. The two–dimensional model takes advantage of the symmetry of the viaduct along the longitudinal axis and uses one–half the section properties. The columns are modeled as inelastic elements with concentrated plastic hinges at the ends. The second order P–Δ effects are included in the analyses. The ductility ratios are defined for displacement and section curvature. The ductility ratio for each quantity is defined as the ratio of its maximum value normalized by the yield value. A static pushover analysis gives yield displacement of 2.2 in. for a single frame of the viaduct. The moment–curvature relationship for the columns for static axial load gives the yield curvature of the column as 0.000072 rad/in. The maximum curvature is determined by dividing the maximum plastic rotation at the top of the lower–level column by the plastic hinge length, which is assumed to be one–half the column depth (36 in.). The secant stiffness of moment–curvature curve gives an estimated cracked section modulus approximately 60 percent of the gross section modulus. The nonlinear model accounts for the capacities of the abutments and restrainer yielding.

EARTHQUAKE GROUND MOTION

A ground motion record derived for the location at pier E3 of the San Francisco–Oakland Bay bridge due to a San Andreas fault event (Bolt, 1992) is used as the stiff soil site motion. This record has peak ground acceleration of 0.48g. The base motion derived for rock soil site record is filtered through the SHAKE program to give the ground acceleration for a typical San Francisco soft soil site. This ground motion has a peak acceleration of 0.54g. The spectra for both the soil site ground motions, shown in Fig. 2, have spectral accelerations of the order of 2g for a broad range of periods. The vertical component of the ground motion is not considered as it is expected to have small effect on the response of the viaducts with short outriggers.

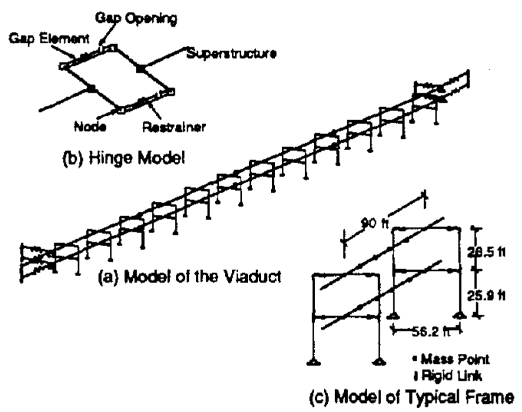

Fig. 1 Three–dimensional model of two–level viaduct.

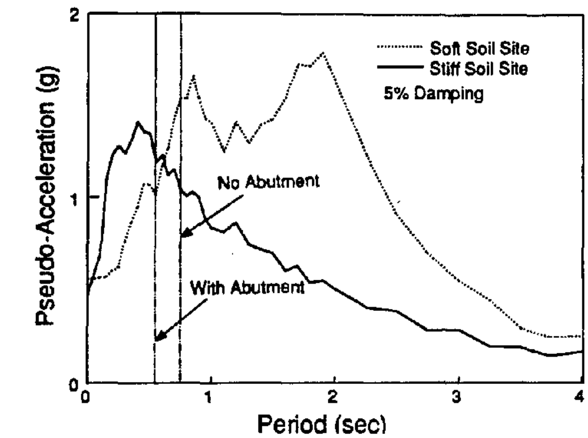

Fig. 2 Response spectra for the ground motion at stiff and soft soil sites.

RESPONSE OF VIADUCT SUBJECTED TO UNIFORM GROUND MOTION

The viaduct models analyzed for uniform ground motion are shown in Table 1. As shown in Table 2, the common assumption of equal elastic and inelastic displacements is true for the viaducts without abutments. It must be recognized, however, that the displacement histories are substantially different. The inelastic displacements are greater than the elastic displacements for Cases 2A and 2B of the viaduct with abutments because the abutments yield, reducing the restraint of the end frames assumed in the elastic model. The large compression displacements in the abutments and the force demand–to–capacity ratios of up to 5 observed for Case 2B indicate that the abutments would experience substantial damage and that the elastic abutment model overestimates the restraint of the abutments. It should be noted, however, that if an iterative procedure for the linearized abutment stiffness is used for the elastic analysis, the inelastic to elastic displacement ratios would not be as large.

Table 1. Viaduct models for uniform ground motion.

Case	1A	1B	2A	2B	3A	3B
Abutment	No	No	Yes	Yes	Yes	Yes
Hinge Opening (in.)	0.75	0.75	0	0	1.5	1.5
Seat Opening (in.)	—	—	0	0	1.4	1.4
Ground Motion for Soil Site	Stiff	Soft	Stiff	Soft	Stiff	Soft

The initial hinge opening does not affect the response of the viaducts without abutments subjected to uniform ground motion as all the frames move in phase. However, the response of a viaduct with abutments is sensitive to the initial hinge opening because it affects the amount of restraint that develops between the adjacent frames. The restrainers have little effect on the response of the viaducts with frames of similar stiffness and subjected to uniform ground motion because the out–of–phase displacement between the adjacent frames is small even without restrainers.

The ductility demands from the inelastic analyses and the moment overstrength ratios from the elastic analyses are listed in Table 2. Although the displacement ductilities are moderate, the curvature ductilities for the plastic hinging at the top of the lower–level columns are large. This is a characteristic of the inelastic response of the two–level viaducts because the plastic hinges form in the lower–level columns. Comparing the displacement ductility demands with the elastic overstrength ratios, it is clear that the displacement ductility demands of 2.3 to 4.5 for the viaducts without abutments exceed the moment overstrength ratios of 1.3 to 3.4. The plastic hinges formed at the top of the lower–level columns produce a soft story mechanism in the lower–

level. Therefore, substantially larger ductility capacities must be provided in the columns than indicated by the moment overstrength ratios. The comparison of Cases 2B and 3B indicates that initial hinge opening can substantially increase the moment overstrength ratios and the ductility demands in the viaduct with abutments.

Table 2. Elastic and inelastic response of viaducts subjected to uniform ground motion.

Case	1A	1B	2A	2B	3A	3B
Ratio of Max. Inelastic to Elastic Displacement	1.06	1.06	1.19	1.76	0.82	1.23
Moment Overstrength Ratio in Lower–Level Column	2.43	3.43	1.46	1.25	2.25	2.49
Displacement Ductility	3.27	4.54	2.30	2.90	2.29	3.82
Curvature Ductility	12.8	17.7	7.1	12.5	7.5	17.9

The earthquake response of a long viaduct with frames of approximately similar stiffness can be bounded by two simple models, so that a nonlinear analysis is not necessary to obtain an approximate response of the viaduct subjected to uniform ground motion. A model of a typical single frame in the viaduct gives a reasonable upper bound of the displacement response, as shown in Fig. 3(a). The lower bound of the displacement response can be obtained by analyzing a complete viaduct in which the hinges are represented by rotational releases to allow the rotation about the vertical and the transverse axis of the viaduct. In this model, the abutments are modeled as linear springs with one half the stiffness of the compression only abutment. Figure 3(b) shows the comparison of elastic displacement for Case 2B with the lower bound model.

RESPONSE OF VIADUCT SUBJECTED TO NON–UNIFORM GROUND MOTION

The large number of bents in a long viaduct provide multiple points of input for the earthquake ground motion. The cases presented in this paper examine the effects of non–uniform ground motion from non–uniform soil sites. The effects of a non–uniform soil site are incorporated in the model by applying two different longitudinal ground motions for the four–frame viaduct model. The first two frames are subjected to the soft soil ground motion and the remaining two frames are subjected to the stiff soil ground motion. The non–uniform ground motions used in the study may be considered limiting cases for the type of motions experienced at an actual site.

The non–uniform ground motion is applied to the two–dimensional model of the viaduct as specified ground displacement histories at the supports. The abutments are assumed to be monolithic. The abutment is modeled for the elastic analysis by a spring with one–half the compression stiffness. The abutment is modeled similarly for the inelastic model but it is allowed to yield at its estimated compressive strength.

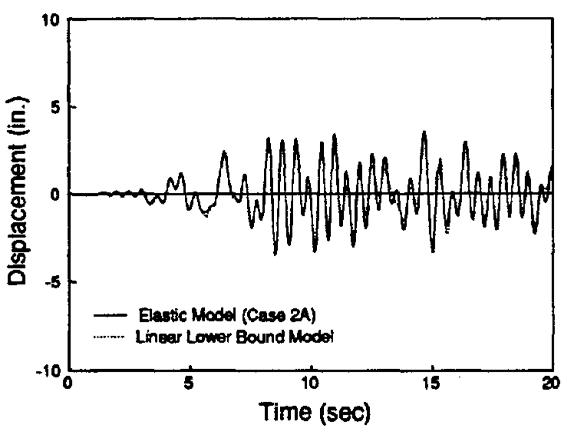

Fig. 3(a) Longitudinal displacements of viaduct with abutments and lower bound model.

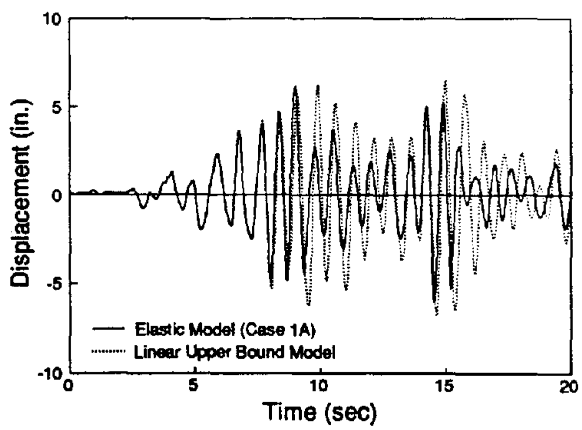

Fig. 3(b) Longitudinal displacements of viaduct without abutments and upper bound model.

The cases analyzed for viaducts on non–uniform soil site are shown in Table 3. The non–uniform ground motion causes pounding between adjacent frames due to the out–of–phase response between these frames. Figure 4 illustrates the relative displacements of the interior frames on the soft and stiff soils according to the elastic and inelastic models for Case 4B. The displacement of the stiff soil frame relative to ground is greater than the soft soil frame because the latter pushes (through pounding at the hinge) on the former. The pounding results in a significant yielding, with residual displacement, of the stiff soil frame. Clearly, the restraint of the soft soil frame and the effect of pounding on the stiff soil frame are more significant for the inelastic model than for the elastic model. The pull from adjacent frames through restrainers may increase the displacement of the frames after the columns yield and, therefore, further increases the offsets in displacement of the yielded columns in a typical frame. The residual displacements due to plastic hinging are also exacerbated by the P–Δ effects. The effects of non–uniform ground motion on the response of viaduct with abutments are similar to that for the viaduct without abutments.

As shown in Table 4, the displacement ductility demand for a viaduct subjected to non–uniform ground motion is as much as 6.1 for the stiff soil frames (Case 4A) compared with the ductility demand of only 3.3 for a viaduct subjected to the uniform stiff soil site ground motion (Case 1A). The displacement ductility reduces as the number of restrainers increases. A comparison of Cases 4A and 4D indicates that the initially open hinges reduce the pounding between the interior frame and the end frame, thereby reducing the ductility demand on the stiff soil frame and increasing the ductility demand on soft soil frame. In the limit with large hinge opening, the response of a frame is approximately equal to its independent response

Table 3. Viaduct models for non–uniform soil site ground motion.

Case	4A	4B	4C	4D	5A	5C
Abutments	No	No	No	No	Yes	Yes
Hinge Opening (in.)	0	0	0	1.5	0	0
Restrainers at Upper Level	0	60	120	60	0	120
Restrainers at Lower Level	0	50	100	0	0	100

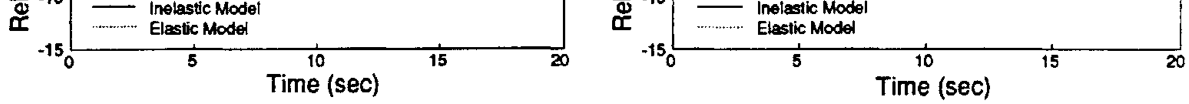

Fig. 4 Longitudinal displacement relative to ground for interior frames on soft and stiff soil sites (Case 4B).

When the number of restrainers is increased from zero (Case 4A) to twice the nominal number (Case 4C), the moment overstrength ratio decreases by less than 5 percent in an interior frame on soft soil site. In contrast, the inelastic response indicates that the ductility demand decreases by about 50 percent for this frame in Case 4C compared with Case 4A. The inelastic response generally shows larger displacement ductility demands for frames on stiff soil site compared with frames on soft soil site for all the cases studied. However, the moment overstrength ratios are not significantly different for frames on stiff or soft soil site in the elastic model. In summary, the elastic model does not accurately predict the inelastic response of the viaduct.

Table 4. Elastic and inelastic response of viaduct subject to non–uniform site ground motion

Case	4A	4B	4C	4D	5A	5C
Max. Inel. Displ. to Elastic Displ.						
Interior Frame on Soft Soil	1.04	0.55	0.53	0.58	0.86	0.71
Interior Frame on Stiff Soil	1.18	1.06	0.99	0.79	1.39	1.11
Moment Overstrength Ratio						
Interior Frame on Soft Soil	4.17	3.96	4.03	3.61	3.11	3.08
Interior Frame on Stiff Soil	4.16	4.11	4.28	3.84	3.56	3.63
Displacement ductility						
Interior frame on Soft Soil	5.4	2.8	2.6	3.3	3.5	3.0
Interior frame on Stiff Soil	6.1	5.5	4.9	4.4	6.2	5.2

Table 5 shows the maximum hinge opening between the two interior frames on different soils from the inelastic and elastic models. The inelastic model gives substantially larger hinge openings compared with the elastic model. Since the inelastic model gives more out–of–phase motion between adjacent frames compared with the elastic model, the restrainers appear to be more useful. As the restrainers yield, however, they become less effective in limiting the out–of–phase response compared with the elastic model. Figure 5 shows that a large number of restrainers is required to limit the maximum hinge opening to less than the yield displacement of the restrainers.

Table 5. Maximum hinge openings at upper level between adjacent interior frames on soft and stiff soil sites. Ductility demand on restrainers is shown in parentheses.

Case	4A	4B	4C	4D	5A	5C
Max. Hinge Opening (in.)						
Elastic Model	17.8	7.8	6.0	7.1	16.7	6.2
Inelastic Model	30.2 —	21.1 (5.0)	9.9 (2.3)	20.4 (4.8)	27.1 —	8.5 (2.0)

The restrainers between two frames on the same soil site tie the frames together. As the adjacent interior frames on different soil sites move out–of–phase, the restrainers between these frames have to pull more than one frame on each side. The current design criteria for calculating the number of restrainers between two adjacent frames do not account for the pull these frames may experience from other frames. Also, the current criteria do not consider the dynamic effects which can significantly increase the forces in restrainers. Whereas older viaducts with 6 in. seat widths at the hinges and no seat extenders would unseat (and collapse) for the cases presented here, new viaducts with seat widths of at least 30 in. are adequate for the cases considered.

RECOMMENDATIONS FOR DESIGN

Linear elastic models can estimate the upper and lower bounds of the earthquake response of straight viaducts subjected to uniform ground motion. The restrainers do not significantly affect the response of the straight two–level viaducts subjected to uniform ground motion. Instead, the large initial hinge openings significantly increase the response of viaducts with abutments. The viaducts with frames of different stiffness show pounding between adjacent frames due to out–of–phase response.

The design provisions should ensure that the plastic hinging would occur in the columns prior to reaching a less desirable, nondductile failure state. The displacement ductility demands, though large, may be acceptable for most viaducts subjected to uniform ground motion. However, the displacement ductility demands indicated in the present analyses for viaducts subjected to non–uniform ground motion are difficult to achieve. The inelastic analyses indicate that abutments do not provide significant restraint in long viaducts.

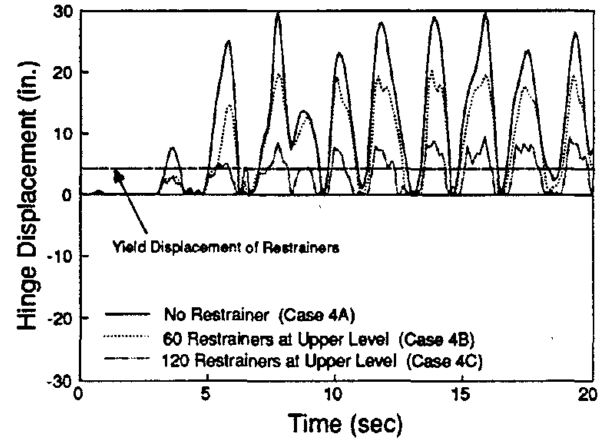

Fig. 5 Effect of restrainers on hinge displacement between adjacent frames on stiff and soft soil site in viaduct without abutments.

The response of a viaduct subjected to non–uniform site ground motion shows that the frames subjected to the amplified soft soil ground motion are restrained by the frames subjected to the stiff soil ground motion. The pounding between adjacent frames due to the out–of–phase motion can substantially increase the response of frames on stiff soils. An unrealistically large number of restrainers are needed to limit the hinge openings to less than the yield displacements of the restrainers. The large maximum hinge opening between adjacent frames of viaducts subjected to non–uniform ground motion indicates that the viaducts should be designed with seat lengths of 30 in., as is the current practice.

Nonlinear analysis should be considered for the design evaluations because of the following reasons: (i) the common practice to correlate the moment overstrength ratio from elastic analysis with the displacement ductility from inelastic analysis invariably underestimates the local demands in multi–column two–level viaducts as the inelastic action is concentrated in lower–level columns; (ii) the effects of restrainers and the abutment restraints are overestimated in the linear analysis; and (iii) the nonlinear analysis is particularly important for analyzing viaducts subjected to non–uniform ground motion to capture the effects of pounding and the interaction between adjacent frames.

ACKNOWLEDGMENT

The research presented in this paper was sponsored by the California Department of Transportation under Grant RTA–59M848 to the University of California, Berkeley.

REFERENCES

Bolt, B. A. (1992). "Seismic Strong Motion Synthesis", *Seminar Proceedings, Seismic Design and Retrofit of Bridges*, University of California, Berkeley, June 8 and 9, 1992.

Caltrans (1990). "Bridge Design Aids," Section 14, California Department of Transportation, Sacramento, CA.

Prakash, V., Powell, G. H., and Filippou, F.C. (1992). "DRAIN–2DX", *Report No. UCB/SEMM–92/29*, Department of Civil Engineering, University of California at Berkeley, Berkeley, CA.

Wilson, E. L. (1991). "SADSAP, A Series of Computer Programs for Static and Dynamic Finite Element Analysis of Structures," Structural Analysis Program, El Cerrito, CA.

ENERGY BALANCED HYSTERESIS MODELS

B. STOJADINOVIĆ
Dept. of Civil and Env. Eng., 2380 G. G. Brown Bldg.,
University of Michigan, Ann Arbor, MI 48100-2125, USA

C. R. THEWALT
Dept. of Civil and Env. Eng., 721 Davis Hall,
University of California, Berkeley, CA 94720, USA

ABSTRACT

Hysteresis models are derived to reproduce the essential characteristics of experimentally observed flexural behavior for reinforced concrete elements. They are computationally inexpensive and versatile. As such, hysteresis models are often used to model the behavior of reinforced concrete structural elements for global nonlinear analysis of structures.

A pair of of new piecewise linear Energy Balanced models are proposed. The new models are based on controlling the amount of dissipated hysteretic energy and the rate of stiffness degradation observed in experiments. The Energy Balanced models are compared to six well-known piecewise linear hysteresis models to examine the differences in the shapes of hysteresis loops, the stiffnesses of loop segments and the amount of dissipated hysteretic energy. The comparison shows that the new Energy Balanced models are capable of accurately reproducing the energy dissipation and stiffness degradation observed in experiments.

KEYWORDS

Hysteresis model, Reinforced concrete, Energy dissipation, Stiffness degradation, Computer implementation

INTRODUCTION

Many computational models have been developed to capture the nonlinear behavior of reinforced concrete beam-column elements. The models can be classified into three classes: (1) models is based on two-dimensional or three-dimensional finite element discretization; (2) models derived from the fiber discretization of the cross section and element assembly using the filament or the variable stiffness formulation; (3) hysteresis models.

The reinforced concrete hysteresis models are empirically based. The goal of the modeling process is to represent the most essential properties of the behavior observed in the experiments on beams and columns under quasi-static cyclic loading. Hysteresis models prescribe a set of rules governing the behavior of the model under all possible cyclic loading histories.

An efficient analysis of large reinforced concrete frame structures requires a computationally inexpensive and acceptably accurate model for the most common structural elements or sub-systems. The hysteresis models are good candidates to fulfill this role. Therefore, in order to facilitate a seismic analysis of the elevated freeway structure [Stojadinović 95], a set of reinforced concrete hysteresis models was used to represent the experimentally observed behavior of upgraded bridge outrigger knee joints.

Six existing reinforced concrete hysteresis models are reviewed. A pair of new hysteresis models, based on controlling the amount of dissipated hysteretic energy and the rate of stiffness degradation, are proposed and implemented. All eight models are evaluated by comparing the shape of the hysteresis loops, the degradation of characteristic loop stiffnesses and the energy dissipation rates to the measurements obtained from the experiments on upgraded outrigger knee joints [Thewalt 92]. The evaluation shows that simple hysteresis models can be enhanced, at the expense of little computational effort, to accurately reproduce the measured stiffness degradation and energy dissipation of reinforced concrete structural elements.

HYSTERESIS MODELS

A reinforced concrete hysteresis model defines a monotonic force/deformation response envelope and a set of rules for constructing the hysteresis loops. The monotonic response envelope is usually symmetric about the origin. The hysteresis loop rules define the behavior of the model in the event of unloading from the response envelope, cycling within the hysteresis loop and reloading to the response envelope. Depending on the types of functions used in the rules, the hysteresis models can be curvilinear or piecewise linear.

Six well-know piecewise linear hysteresis models are considered (Figure 1). The simplest model is the bi-linear (elastic-plastic) hysteresis model. Clough hysteresis model [Clough 66] improves on the bi-linear model by considering the degradation of the hysteresis loop stiffness. Takeda model [Takeda 70, Otani 74] improves on the Clough model in two ways. The monotonic response envelope is tri-linear, accounting for the event of cracking. The unloading stiffness K_u is a fraction of the elastic stiffness K_y that degrades exponentially with increasing deformation ductility μ:

$$K_u = K_y \, \mu^{-0.5}. \tag{1}$$

The Q-hyst model [Saiidi 82] merges the simplicity of the Clough model with the unloading stiffness degradation feature of the Takeda model. Another modification of the Takeda model was implemented in IDARC [Kunnath 92]. Degradation of the unloading stiffness was modeled by adopting a common focal point for all unloading segments of the hysteresis loops. The sixth hysteresis model, developed in [Mander 84], generalizes upon the previous models. It features a tri-linear response envelope and a hysteresis loop composed of two tri-linear halves. By varying two model parameters, Mander hysteresis model is capable of simulating all of the previous mentioned models except the IDARC model.

PROPOSED ENERGY BALANCED MODELS

The proposed reinforced concrete hysteresis models are based on empirical observations and are piecewise linear. Both models have a symmetric multi-segment response envelope. The segments are defined by the first-crack, yield, ultimate-resistance and failure events to match the experimentally observed response envelope. Both models have hysteresis loops consisting of two halves, symmetric about the origin of the coordinate system. The proposed models differ in the hysteresis loop construction rules: the hysteresis loops of the Bi-Linear Energy and Tri-Linear Energy Balanced models are made up of bi-linear and tri-linear symmetric halves, respectively (Figure 2). The length and stiffness of the loop segments are determined to match the observed stiffness degradation rates as well as the measured energy dissipation.

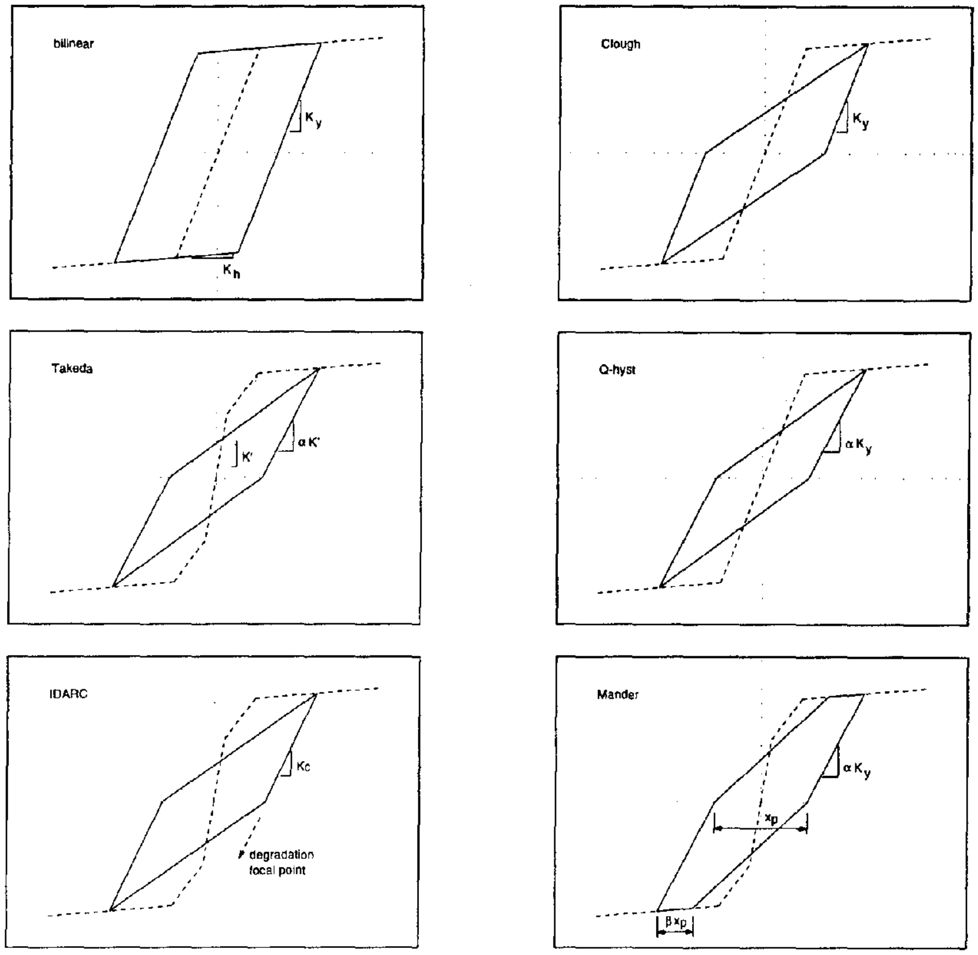

Figure 1: Well-known piecewise linear hysteresis models.

Definition of the Energy Balanced Model

The experimental data used to calibrate the Energy Balanced models in this study was obtained from a series of tests conducted on upgraded outrigger knee joint sub-systems [Thewalt 95]. The upgraded specimens were designed to develop a plastic hinge in the column. Therefore, the measured force/displacement response of the specimen is representative of a reinforced concrete element responding predominantly in flexure.

The force/displacement response of an upgraded specimen is shown in Figure 3. The events of first cracking, yielding of longitudinal reinforcement, ultimate capacity and failure are easy to identify on the specimen response envelope. First yielding of column longitudinal reinforcement occurred at a displacement of 1.25 cm. The force/displacement hysteresis loops are well-rounded, providing significant energy dissipation and showing no pinching up to a displacement of 10 cm, corresponding to a tip displacement ductility of 8. The measured loops are roughly symmetric about the coordinate system origin.

The shape of a hysteresis loops can be quantified by the slopes measured at several characteristic points of the loop Figure 3). The unloading segment can be defined by the tangent unloading stiffness K_u or the average unloading stiffness $\overline{K}_u$ [Krawinkler 92]. The reloading segment of the loop is best described by the slope at the point of zero displacement, the tangent zero-displacement stiffness K_z. The loop ends at a slope similar to the hardening stiffness of the response envelope K_h. The three characteristic

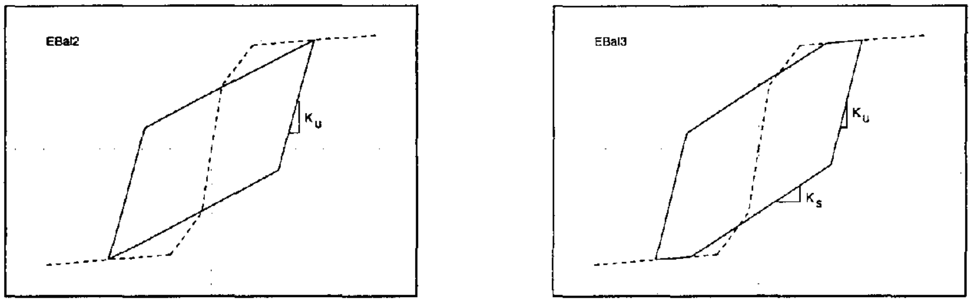

Figure 2: Energy Balanced models.

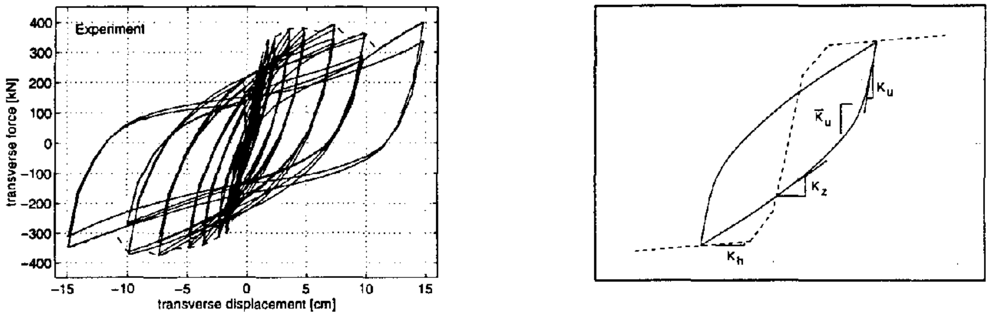

Figure 3: (a) Force/displacement response. (b) Characteristic stiffnesses of a hysteresis loop.

stiffnesses were measured during each load cycle applied to the three outrigger knee joint specimens. The stiffness values, normalized with respect to the specimen yield stiffness, are plotted as a function of the tip displacement ductility in Figure 4. The stiffnesses degrade considerably with increasing ductility. The measured values were interpolated as:

$$K_u = 1.6\, K_y \mu^{-0.35} \tag{2}$$

$$\overline{K}_u = 1.0\, K_y \mu^{-0.3} \tag{3}$$

$$K_z = 0.5\, K_y \mu^{-0.6}. \tag{4}$$

The values of the coefficients are representative of a well-confined square column responding in flexure. Further study is needed to establish a range of coefficient values appropriate for different structural systems.

Another important measure of the hysteresis response is the dissipated hysteretic energy, quantified using an equivalent viscous damping ratio δ. The change of the equivalent viscous damping ratios observed during the tests of three knee joint specimens is shown in Figure 4. The damping ratios remain at approximately 5% during the pre-yield load cycles. After yielding, the ratios grow to peak values of approximately 25% at a displacement level where the specimens reach their ultimate capacity. The measured damping values were interpolated in the least squares sense using a parabola:

$$\delta = \begin{cases} 0.047 & \text{if } \mu < 1 \\ -0.004\mu^2 + 0.071\mu - 0.02 & \text{otherwise.} \end{cases} \tag{5}$$

The use of the interpolation formulas in the Energy Balanced models is illustrated using the Bi-Linear model. The stiffness of the unloading segment is set equal to the average unloading stiffness $\overline{K}_u$ (Equation 3). The end-point of the reloading segment is computed to preserve the central symmetry of the hysteresis loop with respect to the coordinate system origin. The end-point of the unloading segment and, implicitly, the stiffness of the reloading segment, are computed to insure that the area of the hysteresis loop conforms to the energy dissipation model defined by Equation 5. The area of the triangle in

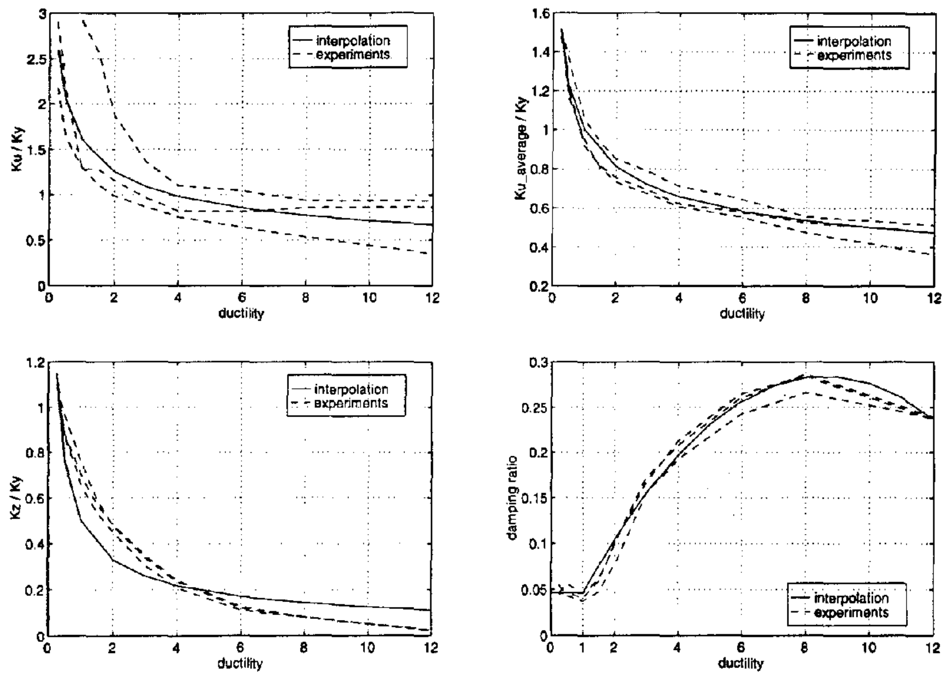

Figure 4: Interpolation of the measured stiffness degradation rates and equivalent viscous damping.

Figure 5 is equal to one half of the area of the hysteresis loop A_h, computed from the equivalent viscous damping interpolation. The following angles are then calculated:

$$\alpha = \arctan(K_u); \qquad \tau = \arctan(K_{pp}). \tag{6}$$

Given the length of the peak-to-peak diagonal D_{pp} and the angle $(\alpha - \tau)$, the length of the projection of the unloading segment on the displacement axis is

$$\Delta = \frac{A_h}{D_{pp}\,\sin(\alpha - \tau)}\,\cos\alpha. \tag{7}$$

The end-point of the unloading segment is defined by the coordinates

$$d_1 = d - \Delta \tag{8}$$
$$F_1 = F - K_u\Delta. \tag{9}$$

COMPARISON OF HYSTERESIS MODELS

The measured force/displacement responses of the upgraded outrigger specimens are used as a benchmark to compare the performance of the hysteresis models (Figure 7). The envelopes of the models were computed to give the best possible estimate of the measured response envelope. The models are subjected to a displacement history that mimics the displacement history imposed on the specimen.

The Bi-linear model poorly represent the hysteresis behavior of a reinforced concrete elements. The importance of stiffness degradation, introduced in the Clough model, to closely model the reinforced concrete hysteresis response is evident from the response graphs. Degradation of unloading stiffness with increasing ductility, introduced in the Takeda model, gives an even more realistic model response. The model with three-segment half-loops, the Mander and the Tri-Linear Energy Balanced models, reproduce the measured response hysteresis loops very closely at all ductility levels.

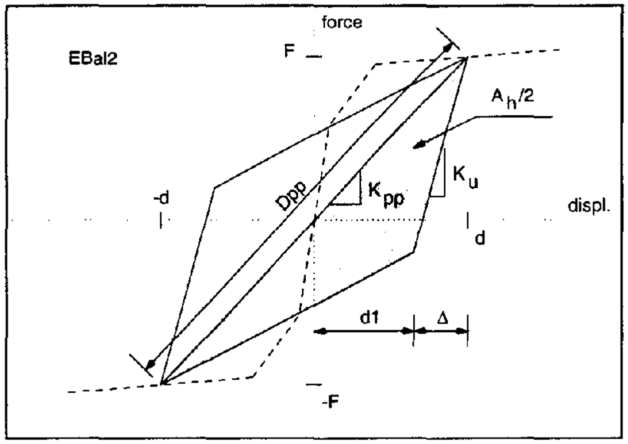

Figure 5: Construction of the hysteresis loop for the Bilinear Energy Balanced model.

Unloading stiffnesses of the hysteresis loop models are compared to the test measurements on the three upgraded knee joint specimens in Figure 6. The Bi-linear and the Clough model have a constant unloading stiffness, equal to the model yield stiffness. All other models incorporate exponential unloading stiffness degradation. The difference in degradation rates is caused by the different ductility exponent values used in the models.

The energy dissipation characteristics of the models are compared by plotting the equivalent viscous damping ratios with respect to the displacement ductility (Figure 6) and comparing them to the measured damping ratios. The Bi-linear model grossly overestimates the energy dissipated in the specimens. The IDARC model has a constant damping ratio of approximately 20% for all ductility levels. Energy dissipated in loops generated by the remaining models increases with increasing ductility, following the basic trend observed in the experiments. The Clough model slightly overestimates damping, while Takeda, Q-hyst and Mander models underestimate damping throughout the range of ductilities. Damping does not decrease in the post-ultimate ductility range for these four models. On the other hand, both Energy Balanced models are designed to closely follow the experimental data.

The Energy Balanced models require more computational effort than the other hysteresis models. The Bi-Linear and the Tri-Linear Energy Balanced models were 1.9 and 3.1 times slower than the Clough model, while Mander's model was only 1.5 times slower. However, if some parameters are pre-calculated the cost of using the Energy Balanced models becomes acceptable. For example, the simplified Bi-Linear Energy Balanced model was only 19% slower than the Clough model.

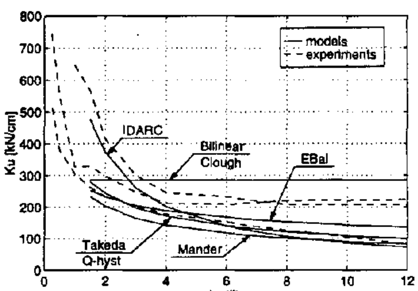

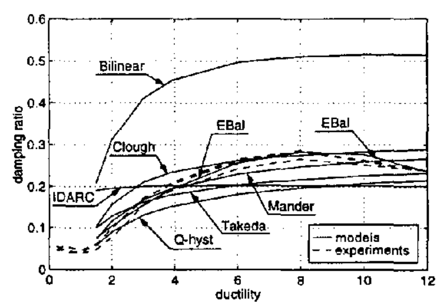

Figure 6: Comparison of model unloading stiffness degradation rates and energy dissipation.

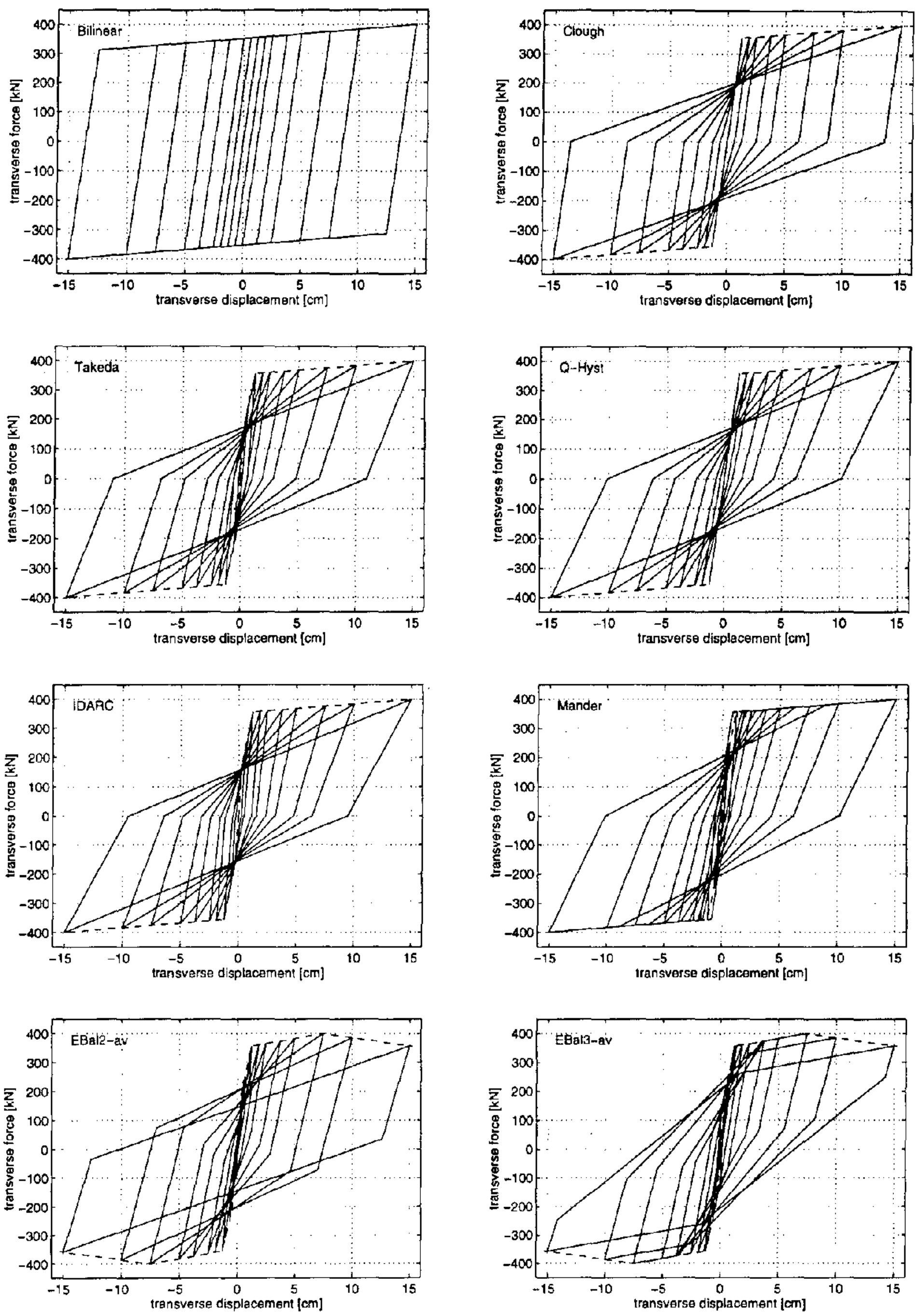

Figure 7: Force/displacement response of the models.

CONCLUSION

Two Energy Balanced hysteresis models, based on quantifying the amount of dissipated hysteretic energy and the rate of stiffness degradation, were proposed and implemented. The comparison of these models to the experimentally obtained data shows that the new models match the observed response. The evaluation of the hysteresis models demonstrates the subtle differences among the models.

The Energy Balanced models are designed to be general tools for global analysis of structures. The parameters of the model envelope, the stiffness degradation rates and the energy dissipation function can be determined using a wider sample of experimental data or from data computed by more sophisticated analytical models. Once the model parameters are established, the Energy Balanced models are good candidates for use in performance based earthquake-resistant design procedures.

REFERENCES

[Clough 66] R. W. Clough. "Effect of stiffness degradation on earthquake ductility requirements." Technical Report SESM 66-16, Department of Civil Engineering, University of California, Berkeley CA 94720, 1966.

[Krawinkler 92] H. Krawinkler. "Guidelines for cyclic seismic testing of components of steel structures." Technical Report ATC-24, Applied Technology Council, 1992.

[Kunnath 92] S. K. Kunnath, A. M. Reinhorn, and R. F. Lobo. "A program for the inelastic damage analysis of reinforced concrete structures." Technical Report NCEER-92-0022, NCEER, SUNY, Buffalo, NY 14261, 1992.

[Mander 84] J. B. Mander, M. J. N. Priestley, and R. Park. "Seismic design of bridge piers." Technical Report 84-2, Department of Civil Engineering, University of Canterbury, Christchurch, New Zealand, 1984.

[Otani 74] S. Otani. "SAKE: A computer program for inelastic response of R/C frames to earthquakes." Technical Report SRS/413, University of Illinois at Urbana-Champaign, 1974.

[Saiidi 82] M. Saiidi. "Hysteresis models for reinforced concrete." *Journal of ASCE, Structural Engineering Division*, 108(ST5):1077–1087, 1982.

[Stojadinović 95] B. Stojadinović and C. R. Thewalt. "Upgrading bridge outrigger knee joint systems." Technical Report UCB/EERC-95/03, Earthquake Engineering Research Center, University of California, Berkeley CA 94720, 1995.

[Takeda 70] T. Takeda, M. A. Sozen, and N. N. Nielsen. "Reinforced concrete response to simulated earthquakes." *Journal of ASCE, Structural Engineering Division*, 96(ST12):2557–2573, 1970.

[Thewalt 92] C. R. Thewalt and B. Stojadinović. "Behavior and retrofit of bridge outrigger beams." In *Proceedings, 10th WCEE*, pages 5291–5296, Madrid, Spain, 1992.

[Thewalt 95] C. R. Thewalt and B. Stojadinović. "Behavior of bridge outrigger knee joint systems." *Earthquake Spectra*, 11(3):477–509, 1995.

STUDIES ON SEISMIC ISOLATION FOR HOUSING IN DEVELOPING REGIONS

W. TANIWANGSA and J. M. KELLY

University of California at Berkeley
Earthquake Engineering Research Center
1301 South 46th Street, Richmond, CA 94804, U.S.A

ABSTRACT

This paper summarizes a time-history analysis of a base-isolated demonstration building that was built in 1994 at Pasir Badak, Indonesia. The building is a four-story reinforced concrete frame with masonry infill walls and is supported on high-damping natural rubber (HDNR) bearings. The modeling of the isolation bearings and the superstructure were based on the experimental studies carried out at the Earthquake Engineering Research Center (EERC), University of California at Berkeley, Berkeley, California.

The superstructure of the demonstration building was modeled as a three-dimensional frame with linear elastic behavior. Beam-column elements were used to model the structural members. The stiffness of the structure was obtained using cracked section properties of the beam and full cross-section of the columns. The stiffness contribution of the masonry panels was not taken into account because the panels were separated from the structural frame by a 25 mm-thick seismic gap that was filled with soft mortar to accommodate 1.5% interstory drift. The bearings were modeled as a combination of a linear spring element and a viscous damping element. The dynamic properties of the bearing elements were selected to match the force-displacement relationship from the full-scale bearing tests. A series of ground motions with two orthogonal components from past earthquakes were selected based on site-specific design spectra to represent the maximum design earthquake (MCE) and the maximum probable earthquake (MPE) seismic risk levels.

The results show that the HDNR bearings used in the demonstration building were very effective in isolating the superstructure from the ground motions. The floor maximum accelerations were smaller than the ground maximum acceleration. The maximum displacements at the isolation level were within the design values. The interstory drifts were reduced drastically when compared to the fixed-base model. The demonstration building in Indonesia is a case study in the process of implementing seismic isolation technology using HDNR bearings, and will serve as a lesson for the implementation of isolation in other developing countries as an alternative approach to protecting structures beyond life-safety criteria.

KEYWORDS

natural rubber bearing, base-isolation, seismic isolation, low-cost isolator, low-cost housing, earthquake protection, demonstration building.

INTRODUCTION

The construction of a four-story reinforced concrete building, supported on high-damping natural rubber (HDNR) isolators, in the south of Java, Indonesia was completed in 1994. The construction of this demonstration building was sponsored by the United Nations Industrial Development Organization (UNIDO) to introduce base-isolation technology to developing countries. For any innovative system to be widely adopted in developing nations, it must be cost-effective and technically efficient, thus, the design and construction of the superstructure of the isolated building should not deviate substantially from common practice and should use building codes for fixed-base buildings and vernacular building materials.

In base-isolated buildings, the earthquake forces transmitted to the superstructure or the floor accelerations are usually smaller than the peak ground acceleration (PGA) because the majority of the earthquake energy is not transmitted to the superstructure, but is transformed into large displacements at the seismic isolation level. Well-designed seismic isolation devices, such as HDNR bearings, should be able to accommodate very large horizontal displacements resulting from an earthquake without losing the ability to carry vertical and horizontal loads. Typically, two levels of seismic risk are defined for isolated structures. The Maximum Design Earthquake (MDE) represents the level of shaking expected during the lifetime of the building and it is used to design the isolator and the superstructure. The Maximum Credible Earthquake (MCE) is the largest input possible given the geological framework of the building site. The isolation system as a whole should be designed and tested to remain stable for the MCE input level.

Description of the Demonstration Building

The demonstration building in Indonesia is located in the southern part of West Java, about one kilometer southwest of Pelabuhan Ratu. It is a four-story moment-resisting reinforced concrete structure with masonry infill walls that are supported by sixteen high-damping natural rubber elastomeric bearings. The isolation bearings are located on the ground level and employ a recessed-endplate connection detail. This configuration is very easy to install and is cost-effective, thus lending itself as a viable solution for isolation in low-cost housing applications. The building is 7.2 m by 18.0 m in plan, and the height to the roof above the isolators is 12.8 m. The building accommodates eight apartment units. The walls that enclosed each unit are made out of unreinforced masonry with special seismic gaps filled with soft mortar. This seismic gap structurally separates the walls from the main frame.

The site-specific seismicity for this project was assessed by Beca Carter Holling and Ferner (BCHF) of New Zealand. They had earlier produced the response spectra incorporated into the Indonesian Code for the earthquake-resistant design of buildings (BCHF, 1979). The site-specific response spectra were developed for various levels of earthquake risk. Figure 1 shows five curves of acceleration spectra representing respectively a 20-year return period (serviceability check), a 200-year return period (recommended design - MDE), a 500-year return period, a 1000-year return period (Maximum Probable Earthquake - MPE), and a Maximum Credible Earthquake (MCE).

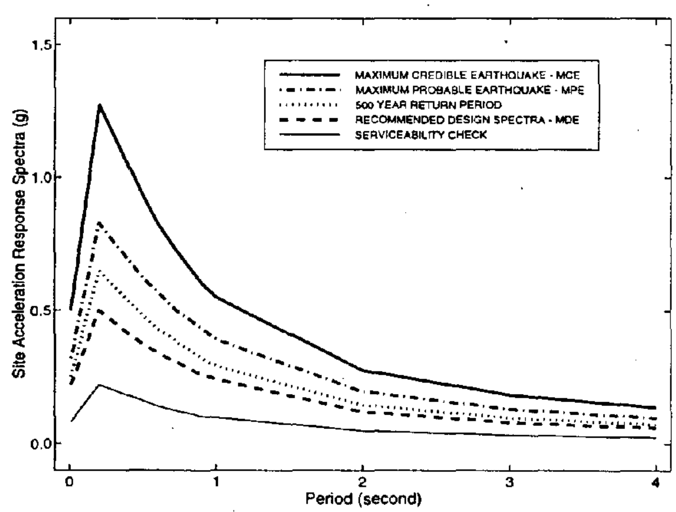

Fig. 1. BCHF site response spectra

The isolation system was designed so that the period of the isolated building is 2 seconds with 10% of critical damping during a MDE, and no catastrophic failure will take place in the event of a MPE. The design displacement of the isolator is 101 mm corresponding to 104% shear strain, and the displacement at the MPE input level is 184 mm equivalent to 189% shear strain. The bearings were designed and fabricated by the Malaysian Rubber Producers' Research Association (MRPRA) in Hertford, UK. Two different HDNR compounds and a single bearing size were used to achieve overall economy on fabrication, installation, and maintenance of the isolation system. The bearings were connected to the superstructure and foundation using recessed endplates which is simpler and more cost-effective than a standard bolted connection. The dynamic properties of the bearings were obtained from full-size bearing tests conducted at the Earthquake Engineering Research Center (EERC), University of California at Berkeley (Taniwangsa *et al.*, 1995).

There are currently no guidelines for seismically-isolated buildings in the Indonesian Codes. The superstructure of the building was designed according to the Indonesian Building Code by the Institute of Human Settlements (IHS) of Indonesia. It was designed as a fixed-base building, expected to behave elastically for a base shear of 0.07 g, which is about one third of the spectral value of 0.2 g corresponding to a 20-year return period. The Indonesian code allows the development of plastic hinges in a significant number of primary structural members at the full spectral value corresponding to a 20-year return period, and the structure has to satisfy life safety requirements for a spectral acceleration of 0.55 g (corresponding to the MDE). Minteck Exploration and Drilling Services, under the supervision of BCHF, determined the geological conditions underneath the building by drilling a borehole 65 m deep. There is a thin layer (about 0.5 m) of sandy silt with gravel covering unweathered rock layers that support the foundation of the building.

ANALYTICAL MODEL

A three-dimensional time history analysis of the building was carried out using the computer program 3D-Basis-Tabs (Nagarajaiah *et al.*, 1993). This program is a combination of the 3D general purpose program, ETABS, and a specific program to model isolation systems, 3D-BASIS. A mathematical model encompassing both the superstructure and the seismic isolation system was first developed. This model was then subjected to a series of recorded ground motions representative of the site response spectra for the MDE and the MPE seismic risk levels, as well as the serviceability checks.

Superstructure Model

The superstructure of the demonstration building was modeled as a three-dimensional frame with linear elastic behavior. The beams and columns were modeled using beam-column elements in ETABS. The stiffness of the structure was computed using cracked section properties of the beams and full cross-sections of the columns. The stiffness contribution of the unreinforced masonry walls was not taken into account because the interstory drifts of the base-isolated model were much less than the drifts of the fixed-based model. The seismic gaps, which were filled with the soft mortar that separated the walls and the structural frame, were large enough to accommodate the anticipated maximum interstory drifts due to the earthquake ground motions and isolating the masonry panels from the reinforced concrete frames.

The distribution of the structural elements at each floor was symmetrical in both directions, and the distribution of the mass was slightly asymmetrical in the longitudinal direction; however, the degree of eccentricity was very small, less than 3% of the length of the building. The story masses were lumped at the center of mass of each floor. The mass values included gravity loads and one-half of the live-load. The first nine modes of the fixed-base superstructure were calculated. Figure 2 shows the first three periods and their corresponding mode shapes. The first period is 0.62 seconds, corresponding to the longitudinal direction; the second

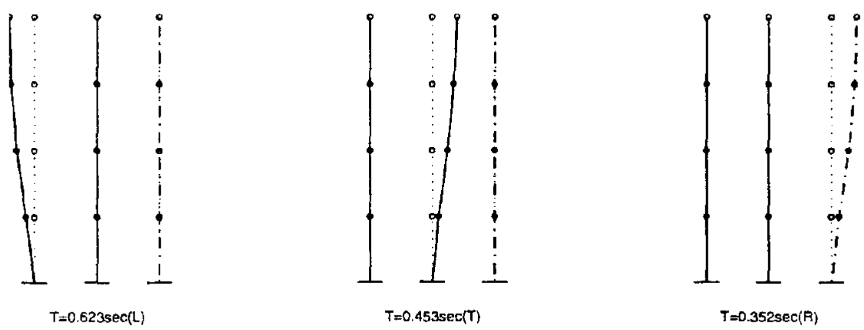

Fig. 2. First three mode shapes and periods of the demonstration building

mode is 0.45 seconds, corresponding to the transversal direction; and the third mode is 0.35 seconds, corresponding to the first rotational mode of vibration. These periods of the superstructure were sufficiently separated from the 2 second horizontal period of the isolation system. Five percent modal damping was assumed for all modes.

The model of the superstructure was verified by comparing the analytical studies and experimental results on a one-third scaled model of the lower portion of the frames that was built and tested at EERC (Taniwangsa *et al.*, 1996). The analytical model accurately predicted the response of the building under the set of ground motions representing various levels of seismic risk in the BCHF site spectra.

Isolation System Model

Two rubber compounds, to be designated as "soft" and "hard", were used to isolate the building. This allows for the use of one size of bearing to accommodate uneven column loads. Six soft bearings were located under the columns of the exterior frames in the transverse direction, while ten hard bearings were located under the remaining columns.

Each bearing was modeled as a combination of a linear spring element and a viscous damping element. The spring constant and the damping value were appropriately adjusted to account for input intensity. The damping value was also tuned to include the influence of the axial load on the bearing so that an accurate representation of bearing response was obtained over the range of inputs. The dynamic properties of the bearing elements were selected to match the force-displacement relationship obtained from the full-scale bearing tests. A typical shear force-displacement hysteresis curve of a bearing test (Fig. 3(a)) shows that the secant stiffness is linear and similar behavior is observed for all shear strain levels under different axial pressures. Figure 3(b) shows the relation between the shear stiffness and shear strain for the soft bearings under the design pressure. The assumptions in the modeling of these bearings were validated by real-time tests (Taniwangsa *et al.*, 1995).

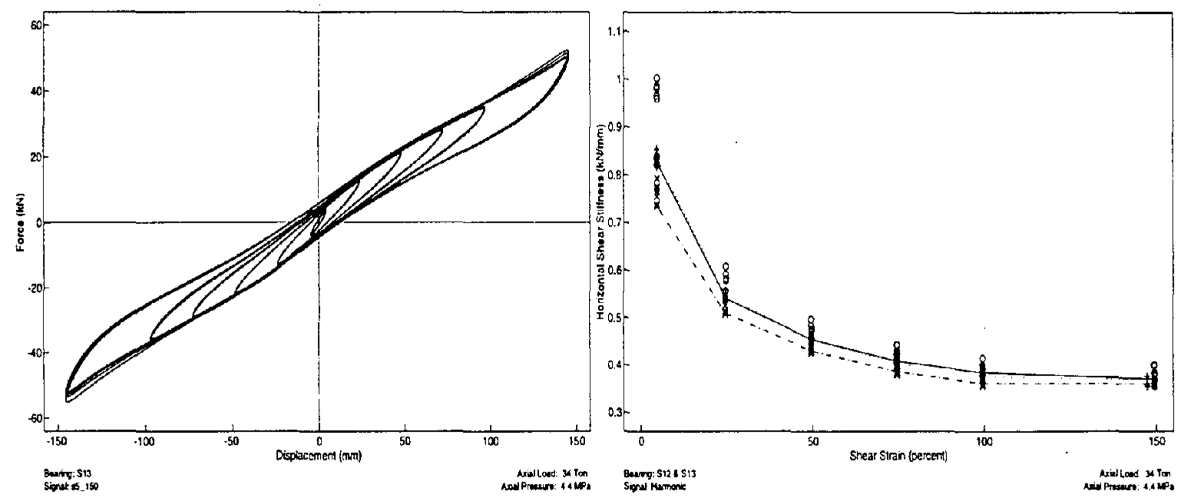

Fig. 3. (a) Bearing force vs. displacement and (b) Shear stiffness vs. shear strain

Selection of Input Ground Motions

The site response spectra for various seismic risk levels were developed by BCHF using a probabilistic approach because no previous strong motion records were available in the vicinity. These site-specific spectra were used as target spectra in selecting the input motions from the past earthquake record data base. In order to perform a three-dimensional time history analysis, the records should have two horizontal components and the elastic response spectra of those records should match the target spectra reasonably well, so that it is not necessary to conduct acceleration and/or duration scaling (Clark P., *et al.*, 1993). Table 1 shows the seven sets of ground motion used in the analysis. The 1985 Chilean and Michoacan earthquakes were selected because they were large earthquakes with a similar subduction zone mechanism to that of the Java trench earthquake source. The 1994 Northridge, the 1989 Loma Prieta, the 1986 Palm Springs, and the 1990 Uplands earthquakes, earthquakes with a wide range of sources and magnitudes, represent the possibility for moderate intensity strike-slip earthquake mechanism within the highly-faulted region of the building site.

In the analysis, the building was subjected simultaneously to the pair of ground motions, with the strongest component applied in the weakest direction of the structure, in order to get the results from the most rigorous case. A serviceability check is critical in assessing the response of a base-isolated structure because during small earthquakes, the horizontal force is often not large enough to bring the isolation system to the low stiffness levels anticipated at the design shear strain levels (see Fig. 3(b)), the isolation system is therefore not effective and at that point the building will behave more like a fixed-base structure.

Table 1: Ground motions used in the analysis

Earthquake	Date	Magnitude	Station	Epicentral Distance	Comp.	PGA(g)
Chile	3-Mar-85	Ms=7.8	Llolleo	4.5 km	N10E	0.66
					S80E	0.41
Michoacan	19-Sep-85	Ms=8.1	Caleta de	22 km	N00E	0.14
			Campos		N90E	0.14
Palm Springs	8-Jul-86	Ml=5.9	Desert Hot	12 km	N00E	0.30
			Spring		N90E	0.27
Loma Prieta	17-Oct-89	Ms=7.1	Corralitos	7 km	N00E	0.63
					N90E	0.48
Loma Prieta	17-Oct-89	Ms=7.1	Capitola	9 km	N00E	0.48
					N90E	0.42
Uplands	28-Feb-90	Ml=5.5	Rancho	12 km	N00E	0.14
			Cucamonga		N90E	0.10
Northridge	17-Jan-94	Ms=6.8	Pacoima dam	19 km	N175E	0.42
			Down-stream		N265E	0.44

ANALYTICAL RESULTS

Because the model used for the isolation bearings is strain dependent, the time-history analysis of the isolated building is an iterative procedure. First the expected strain in the isolators is assumed based on the intensity of the input ground motion. The values of elastic springs and viscous dampers representing the rubber bearings are chosen according to that estimated strain level. After the initial analysis is performed, the horizontal deformation at the isolation level obtained from time-history analysis is compared to the estimated strain values. If the assigned and calculated deformation levels at the isolation level are substantially different, the calculated deformation level is used to determine new parameters of the bearing model; the process is repeated until the assumed and calculated deformation levels are of the same order. The results of the analyses were presented in terms of the combined peak floor accelerations and the normalized peak accelerations. The combined peak floor displacement and the inter-story drifts are also discussed. The variation of the column loads during the earthquake should be verified to assure that the column loads remained in compression, because the recessed connection of the isolators would not be able to transfer the shear force to the superstructure under tensile loads.

Prediction of Maximum Accelerations

The time-history analysis was carried out for all selected ground motions shown in Table 1. The combined peak floor accelerations were obtained by combining the maximum floor acceleration of each direction using the square root of the sum square method. The peak ground accelerations of both direction were also combined by the same method to obtain combined peak ground acceleration. Figure 4(a) shows the distribution of the combined peak acceleration along the height of the building. The maximum acceleration responses on the superstructure corresponding to the input ground motion at the MPE risk level (an earthquake with return period of 1000 years) are around 0.2 g. According to the Indonesian Earthquake Code, spectral accelerations of 0.2 g correspond to the full spectral value of an earthquake with a 20-year return period, and the structure may develop plastic hinges in a number of primary members.

The Uplands earthquake recorded at the Rancho Cucamonga was selected to represent the serviceability level earthquake, which is a more frequent earthquake with a smaller spectral acceleration values. Usually under this level of earthquake, the isolation system is not effective because the earthquake forces are not large enough to pass the threshold of the other serviceability horizontal loads, i.e., wind. The maximum floor acceleration of the building due to these ground motions was around 0.05 g. For this level of response, the demonstration building should behave elastically because the superstructure was designed as a fixed-base building with elastic behavior under 0.07 g spectral acceleration.

Figure 4(b) show the normalized peak acceleration to the corresponding peak ground acceleration. The floor acceleration responses were always smaller than the PGA, including that for the smallest earthquake in this study (with a PGA of 0.10 g). The distribution of the normalized maximum accelerations due to the Uplands earthquake (serviceability check), and the Palm Springs and Caleta earthquakes (MDE) has an inverted triangle shape, while the distribution due to earthquakes selected to represent the MPE was more uniform.

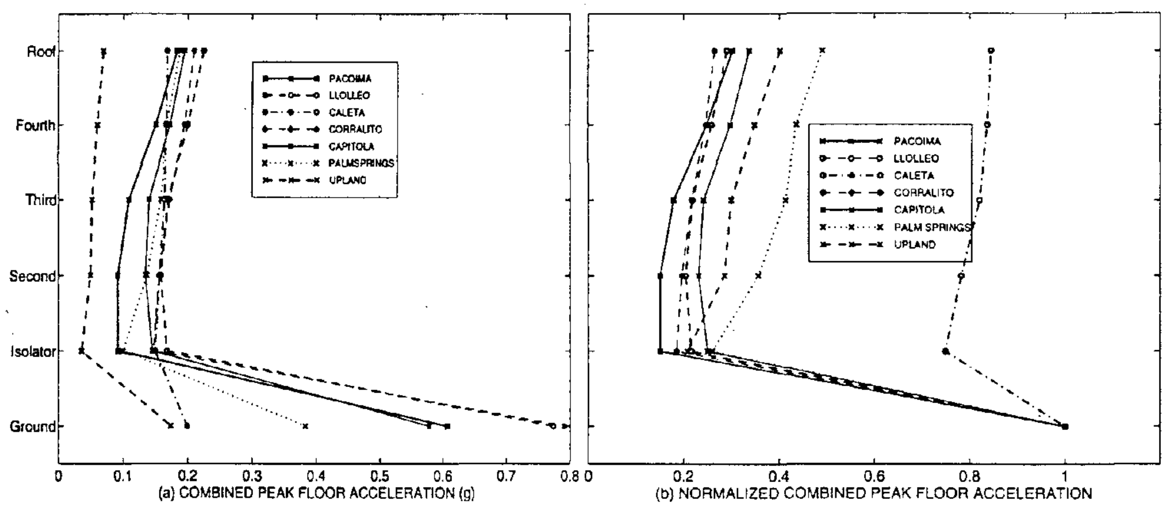

Fig. 4. (a) Combined peak floor acceleration and (b) Normalized peak acceleration

Prediction of Maximum Displacements

The combined peak floor displacements along the height of the building are shown in Fig. 5(a). The shapes of the maximum displacement distribution are similar to the theoretical first mode shape of the isolated building (Kelly, 1992) where a large portion of the building displacement is concentrated at the isolation level.

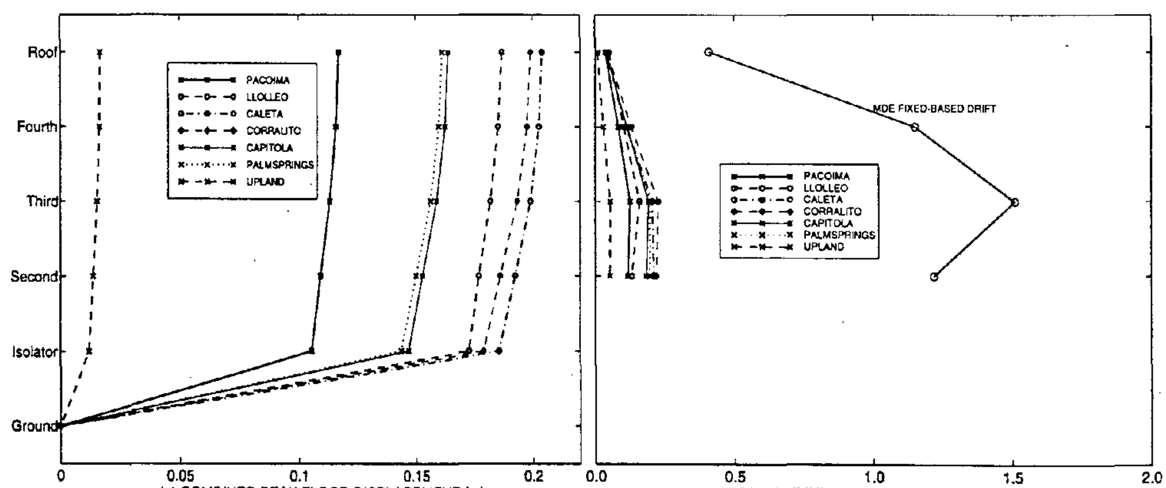

Fig. 5. Distribution of the maximum displacement

The maximum displacement of the isolation system due to all records in this study was less than the deflection at MPE level of 0.184 m. The isolator displacements due to the Caleta, Corralitos and Llolleo ground motions were very closed to this value. The displacement due to the Pacoima down-stream ground motion corresponded to the isolator design deflection, which was 0.104 m.

Figure 5(b) shows the distribution of the maximum interstory drifts. The drift of the base-isolated model is almost negligible, with a maximum value of less than 0.3% for all of the records. If the building were fixed-base instead of base isolated, the interstory drift due to a MDE ground motion could reach a value of 1.5%, which is five times larger than the drift of the base-isolated building. The interstory drift is a very important response parameter in the prediction of the performance of the non-structural elements and building contents, and, therefore, in the overall performance of the building.

Variation of Axial Loads on the Isolation Bearings

Because the connections between the isolation bearings and the building foundation were not traditional bolted but recessed, the contact area of the isolation bearings with the pedestal plates and the column end-plates became a very important issue. It was necessary to determine whether the axial load of a column changed sign during the earthquake, implying local column uplift. If the columns are in tension, the isolation bearings under these columns will not participate in carrying the horizontal shear force; and hence the earthquake force will be redistributed to the other isolation bearings, remaining under compression.

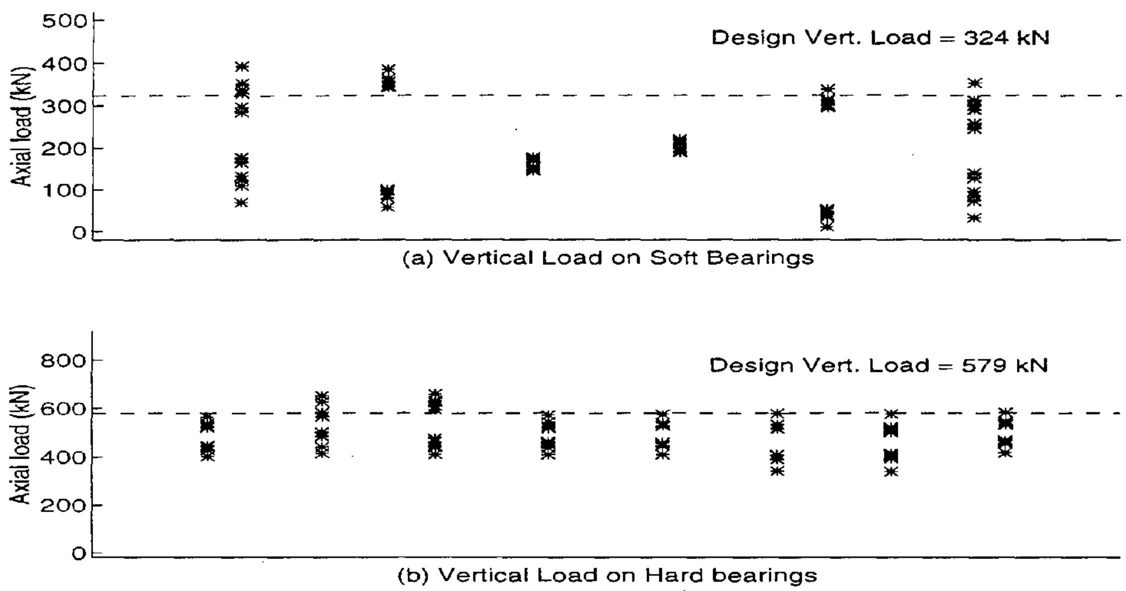

Fig. 6. Maximum and minimum vertical loads on the isolation bearings

In this study, the maximum and minimum axial loads in each column computed from the dynamic analysis were compared to the design axial load for each bearing type. Figure 6(a) shows the scatter plot of the maximum and minimum axial loads for the soft compound bearings. The axial loads in each column were always in compression. These bearings were located under the external transverse frames. The fluctuation of the axial load of these soft compound bearings was in the range of 20 to 392 kN. Figure 6(b) is a scatter plot of the maximum and minimum axial loads for the hard compound bearings. The axial loads remained under compression during the earthquakes, fluctuating +35% and -40% around the design axial load of 579 kN. At no time does any bearing go into tension, thereby eliminating the concern of column uplift and loss of bearing force-carrying capacity.

CONCLUSIONS

The results of the time-history analyses of an analytical model of the base-isolated demonstration building in Indonesia show that the HDNR bearings used in this building are very effective in isolating the superstructure from the ground motions with high PGA (above 0.6 g), usually for the ground motions representing the MPE. For this level of ground shaking, the combined peak roof accelerations were about 25 percent of the PGA. The effectiveness of the isolation system in reducing the shear force transmitted to the superstructure tended to decrease as the PGA decreased. When the PGA of the selected ground motions were in the range of 0.14 g to 0.30 g (a MDE risk level), the maximum roof accelerations were in the range of 60% to 90% of the PGA. The ground motion representing the serviceability check earthquake had a PGA of 0.14 g, and the maximum roof acceleration was only 40% of PGA. The distribution of the maximum floor acceleration over the height of the building due to the ground motions with high PGA tended to be more uniform, while for lower PGA the distribution was an inverted triangle shape.

In all cases there was no amplification of the PGA to the superstructure. The maximum floor acceleration on the superstructure corresponding to the input ground motion at the MPE risk level (an earthquake with return period of 1000 years) were around 0.2 g, which is comparable to the full spectral value of an earthquake with a 20-year return period for fixed-base design criteria.

The distribution of the maximum displacement is similar to the first mode shape of the isolated building, and in all cases, the displacements in the isolation bearings were smaller than the MPE deflection of 184 mm. The maximum interstory drifts were less than 0.3%, one fifth the interstory drift of the fixed-base building under a MDE earthquake. This study also verified that all the isolation bearings remained in compression under the all selected ground motions.

A well designed, fabricated, installed, and maintained HDNR isolation system can be an excellent choice in providing protection from strong earthquakes for public buildings, such as housing, schools, and hospitals. Isolation reduces the floor accelerations and interstory drifts to ensure earthquake protection beyond life safety, and provides better performance in terms of building contents, non-structural elements, and serviceability after major earthquakes.

ACKNOWLEDGEMENTS

The authors very much appreciate the support of Dr. Keith Fuller of MRPRA and Dr. Madgy Youseff of UNIDO. The assistance of the EERC laboratory staff in the experimental phases of this project is also greatly appreciated. We would also like to thank Claire Johnson for assisting in preparing the manuscript.

REFERENCES

Beca Carter Hollings & Ferner, *et al.* (1979), *'Indonesian Earthquake Study', Vol. 3-5.*

Clark, P.W., *et al.*, (1993), 'Performance Considerations for Isolation Systems in Regions of High Seismicity', *Proceeding, Seminar on Seismic Isolation, Passive Energy Dissipation, and Active Control*, Vol.**1**, ATC 17-1, San Francisco, pp. 29-40.

Kelly, J.M. (1992), *'Earthquake-Resistant Design with Rubber'*, Springer-Verlag.

Nagarajaiah, S., *et al.*, (1993), '3D-Basis-Tabs: Computer Program for Nonlinear Dynamic Analysis of Three Dimensional Base Isolated Structures', Report No. *NCEER-93-0011*, State University of New York at Buffalo.

Taniwangsa.W., *et al.*, (1994), 'Analytical Response Predictions of the UNIDO Demonstration Building at Pasir Badak, Indonesia', *Proceeding, Workshop on The Use of Natural Rubber-Based Bearings for Earthquake Protection of Small Buildings*, Jakarta.

Taniwangsa.W., *et al.*, (1995), 'Natural Rubber Isolation Systems for Earthquake Protection of Low-Cost Buildings', Report No. *UCB/EERC 95-12*, Earthquake Engineering Research Center, University of California at Berkeley.

Taniwangsa.W., *et al.*, (1996), 'Analytical and Experimental Studies on the Reinforced Concrete Frame Filled with Masonry Panels', *to be published.*

EXPERIMENTAL VERIFICATION OF DISPLACEMENT-BASED DESIGN PROCEDURES FOR SLENDER RC STRUCTURAL WALLS

CHRISTOPHER P. TAYLOR[1], JOHN H. THOMSEN IV[2], and JOHN W. WALLACE[1]

[1]Department of Civil Engineering, Clarkson University, Potsdam, NY, USA 13699-5710

[2]Degenkolb Engineers, 350 Sansome St., Suite 900, San Francisco, CA, USA 94104

ABSTRACT

This paper presents the results of experimental studies of large scale wall specimens with rectangular, tee-shaped, and barbell-shaped cross sections to verify of a recently developed displacement-based design procedure. This procedure evaluates the need for special transverse reinforcement at the wall boundaries to provide concrete confinement and suppress buckling of the longitudinal reinforcement. Six wall specimens were tested; three with rectangular cross sections, two with tee-shaped cross sections, and one with a barbell shaped cross section. One of the rectangular walls and the barbell shaped walls included large openings at the base of the wall near the boundary. The specimens were tested under reverse cyclic loading and a constant axial load of approximately $0.10A_gf'_c$. The conclusions of the study are: (1) displacement-based design is a flexible design tool, (2) experimental studies validate the use of displacement-based design, (3) special attention is required for the design of walls with tee-shaped cross sections, and (4) a strut and tie model used in conjunction with a displacement-based design procedure is an effective way to design slender walls with openings in the plastic hinge region.

KEYWORDS

Displacement-based design, performance-based design, ductility, structural wall, shear wall, openings, unsymmetric, experimental, testing, strut and tie model, effective flange width

INTRODUCTION

The use of reinforced concrete structural walls is common for resisting lateral forces imposed by wind or earthquakes. In areas of high seismic risk, it is usually not feasible to design a structural wall to remain elastic during a severe earthquake (Wallace and Moehle, 1992); therefore, inelastic deformations are expected, usually at the base of the wall. Allowing inelastic deformations reduces the force that the wall must resist, provides a "fuse" to limit damage to other elements in the structure, and can provide significant damping. In order to exhibit stable, inelastic behavior, the wall must be specially detailed, that is, transverse reinforcement must be provided in regions of high strain.

Prior to 1994, US code provisions regarding the design of reinforced concrete structural walls focused on strength requirements (i.e. ACI 318-89; UBC-1991). Adequate deformability was achieved through the use of heavily confined boundary elements (typically wider than the wall web, resulting in a barbell shaped cross section) whenever the extreme fiber stress due to combined axial and lateral loads exceeds $0.2f'_c$. The confinement within the boundary elements must continue over the wall height until the extreme fiber stress falls below $0.15f'_c$. These boundary elements must be capable of resisting gravity loads and overturning moments without the aid of the wall web. These requirements often made it costly to use a predominantly structural wall system, especially in areas of high seismic risk. Studies have shown that these code requirements are overly conservative for a majority of building systems that utilize reinforced concrete structural walls for lateral load resistance (Ali and Wight, 1991; Wood, 1991; Wallace and Moehle, 1992).

During the 1985 earthquake near Viña del Mar, Chile, the approximately 400 modern reinforced concrete buildings were subjected to strong ground motions. In general, these buildings performed very well. The good performance of these buildings was attributed to the relatively large number of structural walls which reduced the deformations imposed on the walls; therefore, specially detailed boundary regions were not required. Analytical studies were performed to evaluate several Chilean buildings and to extrapolate the findings to U.S. practice (Wallace and Moehle, 1992; 1993; Wallace, 1994). These studies focused on establishing likely response characteristics (wall deformation capacity) of shear wall buildings to estimate design requirements. The analytical studies were compared with experimental studies performed on structural walls of rectangular or nearly rectangular cross section (Carvajal and Pollner, 1983; Oesterle et al., 1976; Shiu et al., 1981; Oesterle, 1986; and Ali and Wight, 1991). The results indicated that the analytical procedure used to estimate the drift capacities tends to yield conservative estimates of wall deformation capacity, and that this procedure provides a simple, effective method for determining the need for confining steel at structural wall boundaries. Subsequent analytical studies of reinforced concrete structural walls has lead to the development of a displacement-based design procedure (Wallace and Moehle, 1992; 1994). The procedure uses lateral drift, as opposed to strength, and directly relates computed building response and wall attributes to the need to provide transverse reinforcement at the wall boundaries based on preventing concrete crushing and suppressing buckling of the longitudinal reinforcement.

Although the displacement-based (performance-based) analytical procedure has been well documented, experimental studies have not been conducted to verify the analytical procedure. In particular, the analytical procedure uses monotonic force-deformation relations (moment-curvature relations) to assess the need for transverse reinforcement at the wall boundaries. In addition, very little experimental information is available to assess the performance of rectangular walls with moderate amounts of transverse reinforcement at the wall boundaries. Essentially no data are available for walls with unsymmetrical cross sections, or for walls with openings at the base. Given these needs, a comprehensive experimental program was undertaken as outlined in the following sections.

EXPERIMENTAL STUDIES

Experimental verification of the proposed displacement-based design approach involved the testing of six approximately quarter-scale wall specimens. The walls tested were: two solid rectangular walls, two solid tee-shaped walls, one rectangular wall with an opening, and one barbell shaped wall with an opening (Figs. 1 to 3). The walls were 12 ft (3.66 m) high and 4 ft (1.22 m) long, resulting in an aspect ratio of 3. A wall thickness of 4 inches (102 mm) was used. Typical material properties were selected, f'_c=4 ksi (27.6 MPa) and f_y=60 ksi (414 MPa). Further details can be found in Thomsen and Wallace (1995) for the solid walls and in Taylor and Wallace (1995) for the walls with openings.

A displacement-based design procedure was used to select transverse reinforcement at the wall boundaries. Based on analytical studies of prototype buildings (Thomsen and Wallace, 1995), each wall was designed for 1.5% lateral drift. Transverse reinforcement was provided to ensure that the walls could reach the design curvature. For strains exceeding 0.004, special detailing was used to provide concrete confinement and to suppress buckling of the longitudinal reinforcement. The flanges were considered for the tee-shaped walls and

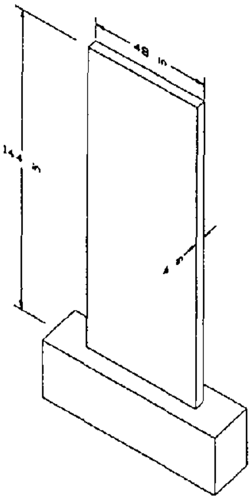

Fig. 1 Rectangular Specimen

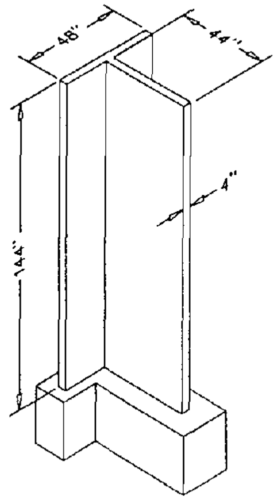

Fig. 2 Tee-Shaped Specimen

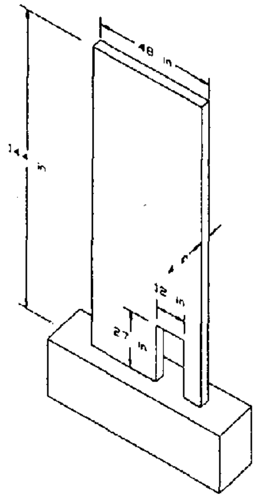

Fig. 3 Rectangular with Opening

the openings were considered for the walls with openings; therefore, the normal strain distributions computed for positive and negative lateral loading differ. Higher concrete compressive strains are predicted for the tee-shaped wall when the flange is in tension, and for the wall with an opening when the "column" is in compression (defined as negative loading in the experimental program for both wall types). Figure 4 shows the reinforcement provided for the rectangular wall with an opening. The reinforcement for the other rectangular wall sections were similar. Figure 4 shows that a greater amount of transverse reinforcement was provided in the column, next to the opening, where greater compressive strains were expected. Analysis of the tee-shaped wall also indicated that considerably greater amounts of transverse reinforcement spaced over a greater depth was needed at the web boundary. In contrast, based on the computed normal strain distribution for the tee-shaped walls, very little transverse reinforcement was needed at the web-flange intersection.

For the solid rectangular wall (RW2), minimum web reinforcement was used (deformed US #2 bars @ 7.5 inches; $\rho = 0.00327$) since the shear stress at wall flexural yielding was only $2.5\sqrt{f_c'}\ psi$ $(0.21\sqrt{f_c'}\ \text{MPa})$. For the tee-shaped wall, the design shear force was computed from the flexural capacity of the wall assuming all of the flange longitudinal reinforcement was effective as tension steel; therefore, the flexural capacity of the Tee-shaped wall was approximately twice that for the rectangular wall and greater amounts of web steel was provided deformed US #2 bars @ 5.5 inches (6.4 mm @ 140 mm), $\rho = 0.00445$.

Since conventional techniques are not effective for the shear design of discontinuous regions, shear reinforcement for the walls with openings was selected using strut and tie models. A refined model was developed for each wall in each direction. The models indicated that, when the column was in compression, a concentration of horizontal steel was required over the opening to drag the shear force back into the solid panel. Use of a strut and tie model ensured that an adequate load path was provided to carry the applied horizontal load from the top of the wall down to the base. Although the strut and tie model does not assess the need for vertical web reinforcement, equal amounts of horizontal and vertical web steel were provided in the panel region at the base of the wall. Analytical studies (Sittipunt and Wood, 1994) suggest that diagonal reinforcement is the most efficient distribution of web reinforcement. Although less efficient, a uniform mesh of horizontal and vertical reinforcement was used for ease of construction.

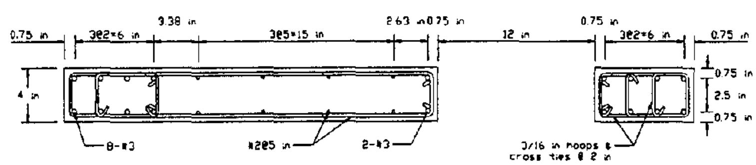

Fig. 4 Cross Section at Base of Wall with Opening

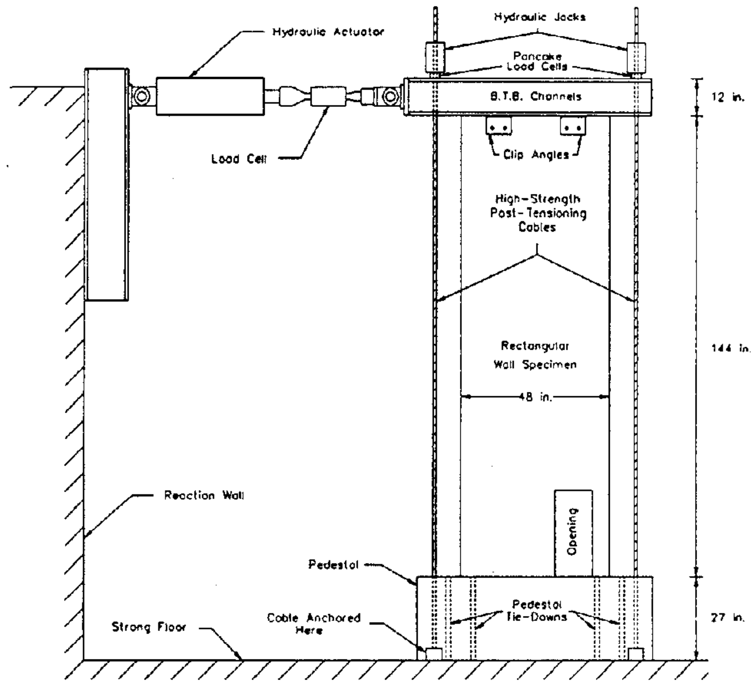

Fig. 5 Test Setup

Instrumentation was provided to measure loads, displacements and strains at critical locations. All measurements were read by a computer data acquisition system at 32 points throughout each cycle. Lateral load was measured with a load cell placed between the actuator and the load transfer assembly. Axial loads were measured with hollow core load cells placed between the top chucks and the jacks. The horizontal displacement profile of each specimen was measured using wire potentiometers at four locations over the wall height. The wire potentiometers were mounted on a steel reference frame connected independently to the floor. Linear potentiometers were provided at each end of the pedestal to determine the vertical displacement of the pedestal, from which the pedestal rotation was calculated. To obtain the rotation at the base of the wall (over approximately the plastic hinge length), wire pots were mounted at the first story height and connected to the pedestal to measure the vertical displacement of each side of the wall. Shear deformations were measured using wire potentiometers mounted in an "X" configuration over the bottom two stories. Vertical strain along the base of each wall was measured three ways. First, steel strain gages were attached to many of the reinforcing bars just above the base of the wall and at the first story level. Second, concrete strain gages were embedded at various locations along the base of the wall. Finally, linear voltage differential transducers (LVDT's) were used to measure vertical displacement along the base of the wall over a gage length of approximately 9 inches (229 mm).

The base of each specimen was fixed to a strong floor and the top was free to rotate (Fig. 5). Out of plane movement was restrained at the top of the walls. A constant axial load of approximately $0.10A_g f'_c$ was maintained for the duration of each test. Reverse cyclic horizontal loading was applied slowly at the top of each specimen in the plane of the wall or web in the case of the tee-walls. Typically, two complete cycles were performed at each drift level; however, four cycles were typically performed at lateral drift levels of 1.0 and 1.5%. The drift levels investigated were approximately 0.10%, 0.25%, 0.50%, 0.75%, 1.0%, 1.5%, 2.0%, 2.5%, and 3.0%.

EXPERIMENTAL RESULTS

Lateral Load Versus Top Displacement

Figures 6 through 8 show the applied lateral load versus top displacement relations (note that the vertical axis are different for Fig. 7). The applied lateral load was measured using a load cell mounted between the hydraulic actuator and the top loading assembly. Top displacement was measured using a wire potentiometer. In general, excellent performance was observed for the wall specimens. Lateral drift levels of 2 to 2.5% were applied before significant deterioration was observed. For each specimen, the point of yielding can be identified to occur at approximately 0.75% drift. For the tee-shaped wall, the post-yield stiffness is

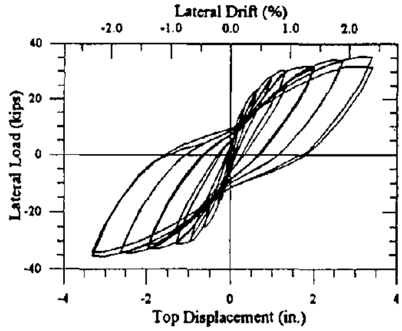

Fig. 6 RW2: Load vs. Disp.

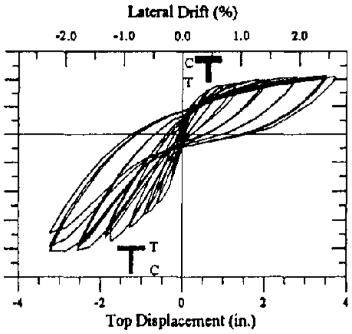

Fig. 7 TW2: Load vs. Disp.

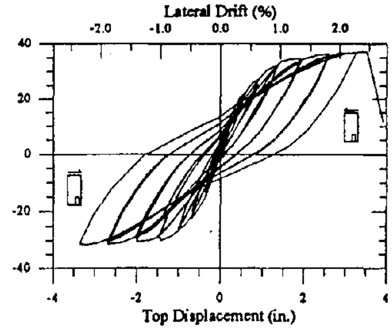

Fig. 8 RW3-O: Load vs. Disp.

significantly greater and the strength is nearly double when the web is in compression due to the large neutral axis depth caused by the large amount of tension steel within the flange. Figure 7 shows that tee-shaped walls do not perform simply as two rectangular walls as may be assumed in design. For the walls with openings, the strength and stiffness in the positive direction are only slightly greater than in the negative direction for each specimen. The similar strengths and stiffnesses were the result a shallow neutral axis depth; thus, the opening had little effect on the flexural behavior of the wall. The full loops in Figs. 6 through 8 indicate that, with proper reinforcement, rectangular walls, tee-shaped walls, and rectangular walls with an opening at the base can exhibit stable hysteretic behavior and significant ductility.

Strain Profiles at Wall Base

The strain profiles at the base of the wall were calculated from the LVDT's (Figs. 9 through 13). Strains were calculated by dividing the displacement recorded from the LVDT's by the gage length of approximately 9 inches (23 cm). The design strains were taken from moment-curvature analyses based on the curvature demand at the wall base for the design drift level 1.5 % (Wallace and Moehle, 1992). The strain profiles for the four solid walls are nearly linear, thus the assumption of a linear strain distribution is reasonable even though cyclic loads were applied to the wall specimens and the analytical procedure is based on a monotonic moment-curvature analysis.

For the walls with openings, when the lateral drift exceeds approximately 0.75% drift, the strain profiles become nonlinear. The column and the panel act somewhat independently in flexure, resulting in greater curvature in the panel and in the column. This is most prominent in the column (Figs. 10 and 11). This increase in curvature at the base of the column was accompanied by a decrease in curvature at the top of the column, indicating that the column was subjected to reverse curvature.

For the tee-shaped walls with the flange in compression (Fig. 12), very low strains are predicted and measured; therefore, evaluation of this case is not critical. For the T-shaped wall with the flange in tension (Fig. 13), large compression strains developed in the web. It is noted that the design strain distribution plotted

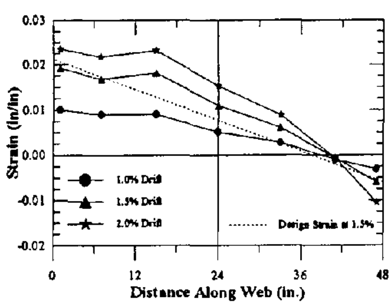

Fig. 9 RW2: Strain Profile

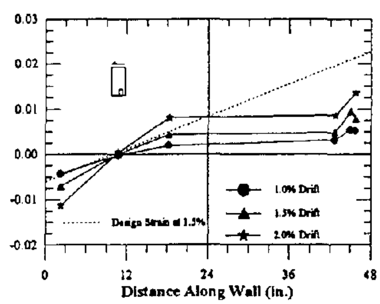

Fig. 10 RW3-O: Strain Profile
Column in Tension

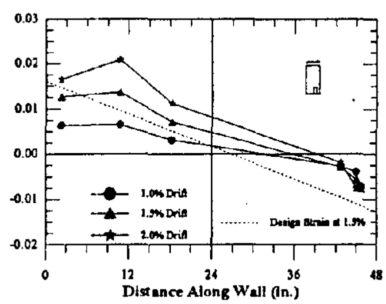

Fig. 11 RW3-O: Strain Profile
Column in Compression

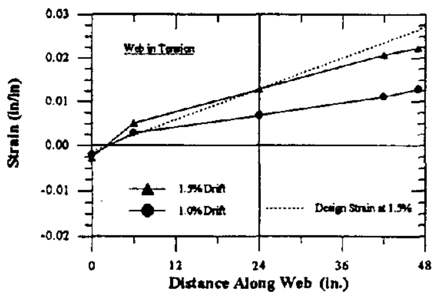

Fig. 12 TW2: Strain Profile - Web in Tension

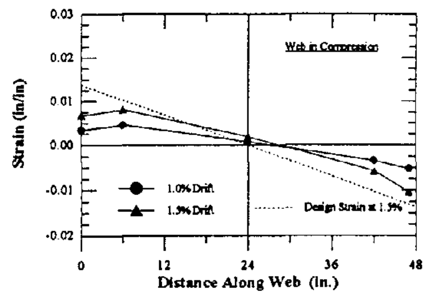

Fig. 13 TW2: Strain Profile - Web in Compression

in Fig. 13 is based on assuming the entire tension flange is effective; experimental results indicate that this was a reasonable assumption. In addition, the experimental results plotted in Fig. 13 have not been corrected for pedestal rotation which accounted for approximately 0.3% drift at an imposed drift level of 1.5%; therefore, the comparison between experimental and analytical strain distributions would be slightly better if this effect were included. The large compressive strains that develop at the web boundary are much greater than those for the rectangular walls due to the contribution of the flange reinforcement as tension steel. This high strain must be identified when evaluating the need for transverse reinforcement; therefore, tee-shaped walls should not be designed simply as two rectangular walls joined together and the influence of the flange must be evaluated. For evaluating detailing requirements at the web boundary (as well as shear reinforcement), a high estimate for the effective flange width should be used to ensure adequate performance.

Moment - Curvature Relations

The experimental moment-curvature relations for the rectangular wall with an opening are compared with analytical results at the first peak of each drift level in Figs. 14 and 15. In addition, the design ultimate curvature is noted on the figure for reference. The analytical results were calculated using the BIAX (Wallace, 1992) computer program with a Saatcioglu & Razvi (1992) model for confined concrete. For the experimental curves, the moment was taken as applied horizontal load times the height to the point of application above the wall base (150 in; 3.81 m). The experimental curvature was calculated two ways: 1) as the slope of a best fit line through the strains determined from the LVDT's at the base of the wall, and 2) by dividing the rotation at the first story level by an assumed plastic hinge length of 30 inches (762 mm). For the solid walls, in general, very good agreement was observed between analytical and experimental moment-curvature relations (similar to results plotted in Fig. 14); therefore, these results are not shown. For the wall with an opening, the comparisons show that, although the actual strain distributions were not linear, both the peak moments and the curvatures were predicted very well, especially for the case with the column in tension (Fig. 14). For the case with the column in compression (Fig. 15), a reduction in stiffness is noted and the flexural capacity is overestimated using a monotonic moment-curvature analysis. The reduction in stiffness is likely due to the Bauschinger effect caused by cyclic loading. The slightly under predicted ultimate moment

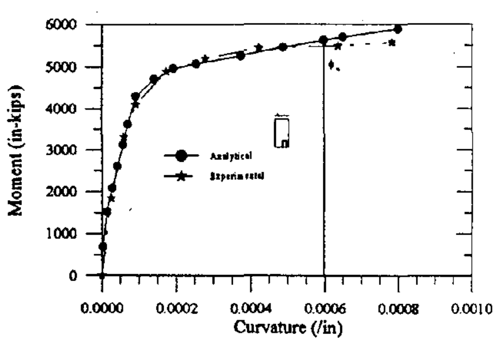

Fig. 14 RW3-O: Moment-Curvature
Column in Tension

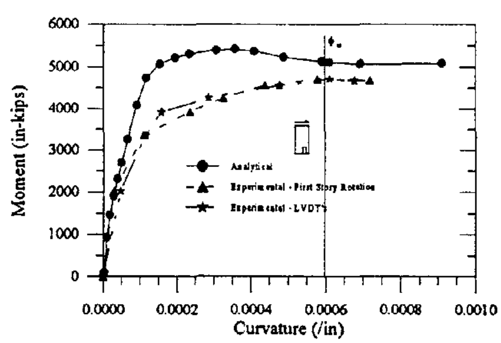

Fig. 15 RW3-O: Moment-Curvature
Column in Compression

capacity is attributed to the contribution of the diagonal compression struts to the stress in the longitudinal steel.

Strut and Tie Models

Although, for solid walls with the same overall dimensions, shear was found to play a small role in the specimen behavior, for the specimens with openings, shear contributed approximately 25% of the overall top lateral displacement. As well, conventional code approaches are ineffective for walls with relatively large openings. Strut and tie models were found to be a flexible and effective tool for the shear design of discontinuous regions. Provided a reasonable model is selected, this method will result in a conservative design. A reasonable model is one in which the orientation of model elements does not vary too far from the elastic principle stresses. Strain gage data indicated that the additional horizontal web reinforcement provided above the opening to drag the shear back into the wall panel at the base of the wall was effective. The strain gage data also revealed that the load path assumed in the design process was not always followed when alternative, stiffer, load paths were available. Although the strut and tie model did not indicate a need for vertical web reinforcement, and analytical studies suggested that diagonal reinforcement should be provided, a mesh of horizontal and vertical web reinforcement was provided. Test results indicate good inelastic performance with this reinforcing arrangement.

CONCLUSIONS

In areas of high seismic risk, structural walls are not designed to remain elastic during a severe earthquake; therefore, inelastic deformations are expected, usually at the base of the wall. In order to exhibit stable, inelastic behavior, the wall must be specially detailed, that is, transverse reinforcement must be provided in regions of high strain. Experimental results show that, when properly reinforced, slender structural walls can exhibit stable hysteretic behavior and significant ductility.

The experimental studies presented in this paper have shown that displacement-based design methodologies are an effective tool for evaluating structural wall behavior. Using a displacement-based approach results in wall designs that are directly related to the building configuration, as well as the wall aspect ratio, the wall axial load, the wall cross sectional configuration, and the wall reinforcing ratios. This procedure worked well to ensure that the concrete in the boundary elements had adequate confinement to prevent crushing at high strains. The agreement between the predicted and experimental strain distributions and moment curvature relations verify that displacement-based design procedures are appropriate for design and evaluation of slender structural walls. For slender walls with openings, combining a displacement-based design approach for evaluating required transverse reinforcement at the wall boundaries with a strut and tie model to evaluate required shear reinforcement proved effective. Although measured strain distributions were not linear for the walls with openings, comparisons between predicted and measured moment-curvature relations indicate that reliable results can be obtained.

REFERENCES

Ali, A. and Wight, J.K. (1991), "Reinforced Concrete Structural Walls with Staggered Door Openings," *Journal of Structural Engineering*, ASCE, Vol. 117, No. 5, pp. 1514-1531, May 1991.

Carvajal, O. and Pollner, E. (1983), "Muros de Concreto Reforzados con Armaduro Minima," *Boletin Techico*, Universidad Central de Venezuela, Facultad de Ingenieria, Ano 21 (72-73), Enero-Diciembre, 5-36 (in Spanish).

Oesterle, R.G., Fiorato, A.E., Johal, L.S., Carpenter, J.E., Russel, H.E., and Corley, W.G. (1976), "Earthquake Resistant Structural Walls - Tests of Isolated Walls," *Report to the National Science*

Foundation, Construction Technology Laboratories, Portland Cement Association, Skokie, IL, November, 1976.

Oesterle, R.G. (1986), "Inelastic Analysis of In-Plane Strength of Reinforced Concrete Shear Walls," *PhD Dissertation*, Northwest University, Evanston, IL, June 1986.

Saatcioglu, M. & Razvi, S.R. (1992), "Strength and Ductility of Confined Concrete," *Journal of Structural Engineering*, ASCE, Vol. 118, No. 6, pp. 1590-1607, 1992.

Shiu, K.N., Daniel, J.I., Aristizabel-Ochoa, J.D., Fiorato, A.E., and Corley, W.G. (1981), "Earthquake Resistant Structural Walls - Tests of Walls with and without Openings," *Report to the National Science Foundation*, Department of Civil Engineering, University of Illinois at Urbana-Champaign, December 1993.

Sittipunt, C. and Wood, S.L. (1993), "Finite Element Analysis of Reinforced Concrete Shear Walls," Civil Engineering Studies, Structural Research Series No. 584, University of Illinois, Urbana, December 1993.

Taylor, C.P. and Wallace, J.W. (1995), "Design of Slender Reinforced Concrete Structural Walls With Openings," *Report No. CU/CEE-95/13*, Department of Civil and Environmental Engineering, Clarkson University, Potsdam, NY, December 1995.

Thomsen IV, J.H. and Wallace, J.W. (1995), "Displacement-Based Design of RC Structural Walls: An Experimental Investigation of Walls with Rectangular And T-Shaped Cross-Sections," *Report No. CU/CEE-95/06*, Department of Civil and Environmental Engineering, Clarkson University, Potsdam, NY, June 1995.

Wallace, J.W. (1992), "BIAX: Revision 1 - A Computer Program for the Analysis of Reinforced Concrete and Reinforced Masonry Sections," *Report No. CU/CEE-92/4*, Structural Engineering, Mechanics and Materials, Clarkson University, 1992.

Wallace, J.W., (1994), "Displacement-Based Design of Reinforced Concrete Structural Walls," *Proceedings*, Fifth U.S. National Conference on Earthquake Engineering, Chicago, IL, Vol. II, pp. 191-200, July 1994.

Wallace, J.W. and Moehle, J.P. (1992), "Ductility and Detailing Requirements of Bearing Wall Buildings," *Journal of Structural Engineering*, ASCE, Vol. 118, No. 6, pp. 1625-1644, June 1992.

Wallace, J. W. and Moehle, J. P. (1993) "An Evaluation of Ductility and Detailing Requirements of Bearing Wall Buildings Using Data from the 3 March 1985 Chile," Earthquake Spectra, Vol. 9, No. 1, February, 1993, pp. 137-156.

Wood, S.L. (1991) "Performance of Reinforced concrete Buildings During the 1985 Chile Earthquake: Implications For the Design of Structural Walls," Earthquake Spectra, Vol. 7, No. 4, November 1991, pp. 607-638.

REHABILITATION OF INFILLED NON-DUCTILE FRAMES WITH POST-TENSIONED STEEL BRACES

Amador Terán-Gilmore

Departamento de Materiales, Universidad Autónoma Metropolitana,
Av. San Pablo 180, Colonia Reynosa, Mexico 02200, D.F.

ABSTRACT

In recent years, it has been shown that the seismic performance of existing buildings can be enhanced considerably by bracing them with post-tensioned rods or cables. The use of this upgrading technique yields several advantages, such as architectural versatility, low cost, fast and clean construction, and does not add any significant reactive mass to the existing facility. This paper has the following objectives: to investigate the use of post-tensioned steel braces for the seismic rehabilitation of non-ductile frame buildings with unreinforced masonry infills; to discuss some of the issues that need to be considered for the design of the rehabilitated building; to assess the advantages of the use of this technique by studying the seismic performance of an infilled non-ductile frame building before and after it has been upgraded with post-tensioned braces; and finally, to offer conclusions and research recommendations.

KEYWORDS

Unreinforced masonry, seismic performance, displacement control, interstory drift, seismic rehabilitation

INTRODUCTION

During the rehabilitation of an existing building, the design options available to the designer are limited by the existence of a building that usually has some structural deficiencies. To make possible the successful rehabilitation of an existing building, the designer needs to identify its structural weaknesses through the understanding of its local and global mechanic characteristics. In the case of non-ductile frame buildings infilled with unreinforced masonry (URM) walls, this understanding should not only include the characteristics of the frame members, but also those of the infills. Given the poor performance of URM buildings and elements during past and recent earthquakes, the notion that this material should not be used to resist lateral loads is widely extended. Nevertheless, recent research has challenged this notion while demonstrating that as with any other structural material, the use of URM to resist seismic loads has advantages and disadvantages, depending on how the URM is used.

The efficient rehabilitation of an existing building is possible when all its existing structural materials and elements can be used to help resist the seismic loads once the building is rehabilitated. This may be achieved in infilled frames if the large natural sources of strength, stiffness and viscous and hysteretic energy dissipation provided by the infills are taken advantage of. That is, rather than eliminating the infills' contribution to resist the seismic loads, it is necessary to consider that the presence of URM infills may improve the overall seismic performance of a frame building. Under these circumstances, the main challenge confronted by the designer can be summarized with the following question: What changes can and should be introduced to the mechanic characteristics of the building, through the use of post-tensioned (PT) steel braces, in such a way that the infills are put to work according to their strengths rather than their weaknesses?

SEISMIC PERFORMANCE OF URM ELEMENTS

The overall earthquake-resistant capacity of URM elements is considerably higher than was previously thought. URM walls and infills have a considerably larger strength than that at first cracking, a significant inelastic deformation capacity and if their in-plane deformation is limited within certain values, a fairly stable hysteretic behavior. Even after several loading cycles, URM elements are able to carry a large percentage of their peak strength for relatively large drift. Thus, it is not surprising that URM infills that are properly introduced into frame buildings enhance considerably the ultimate strength and stiffness of these buildings, and even their energy dissipation capacity (Klingner and Bertero, 1976; Schuller *et al.*, 1994).

Depending on the loading condition, the relative strength and stiffness of the frame and infills, the bond between them, and the mechanic characteristics of the masonry, a number of failure mechanisms are possible in an infilled frame. The designer should be aware of these mechanisms, and accordingly, avoid undesirable modes of failure. Other issue that deserves consideration is the multi-directional nature of ground motion. Drift and acceleration are the most relevant in-plane and out-of-plane seismic demands, respectively, in URM infills. It has been observed that in-plane damage reduces the out-of-plane strength of an infill, especially for those having large slenderness ratios (Sakamoto, 1978; Angel and Abrams, 1994). Usually, out-of-plane failure should not be a design concern because URM infills possess high out-of-plane strength (Angel and Abrams, 1994). Nevertheless, some experimental results and the out-of-plane failure of URM infills during past earthquakes suggest that large in-plane demands in combination with significant out-of-plane demands may result in out-of-plane failure (Teran *et al.*, 1995).

BASIC BEHAVIOR OF A PT STEEL BRACE

Figure 1a shows the deformation vs. force curve of an axially loaded cable (or rod). As shown, the cable buckles elastically when subjected to compressive strains; while it can develop its yielding strength under tension. Figure 1b illustrates the behavior of the same cable subjected to cyclic loading. As shown, all inelastic tensile elongation accumulates every time the cable yields in tension. Figure 2a shows a counterpart of Fig.1a for a prestressed cable. As shown, both figures are similar, except that there is an initial state of stress and strain in the prestressed cable, which is accounted for in Fig.2a by shifting the origin of the force vs. displacement axes. Because of this shift, the cable can now "resist" compressive forces (a reduction of its initial tension can be interpreted as the cable developing a compressive force). Note that a reduction in the initial prestress of the cable implies a reduction in its capacity to "resist" compression, as can be concluded by following the path OABC in Fig.2b (Teran *et al.*, 1995). Figures 1 and 2 provide help in understanding the consequences that excessive yielding or buckling of a PT brace can have in its seismic performance: first, yielding (loss of prestress) reduces its ability to "resist" compressive forces; second, yielding (axial elongation) results in the reduction of its lateral stiffness; and third, net compressive strains in the brace (buckling) can lead to sudden and undesirable changes in the strength and deformation demands in the existing frame members. The axial strength and the amount of prestress provided to the braces should be designed to prevent their buckling and/or excessive yielding.This is only possible if a reasonable estimate of the maximum drift demand in the braces is available.

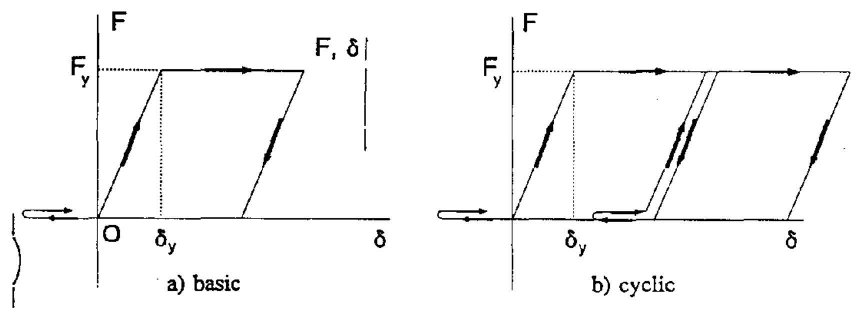

Fig. 1 Axial displacement vs. axial load behavior of rod or cable

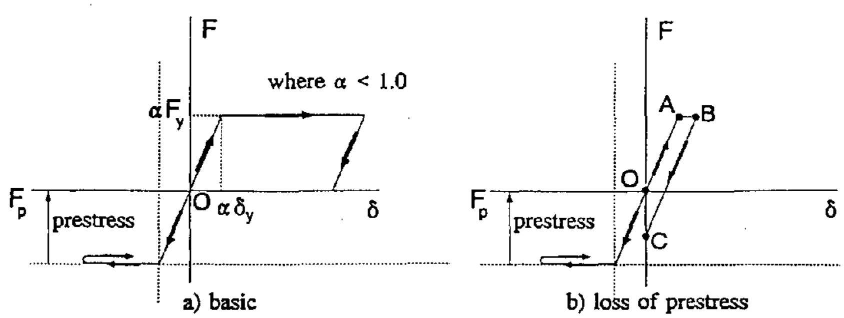

Fig.2 Axial displacement vs. axial load behavior of prestressed rod or cable

The use of high levels of prestress, so that the PT braces may moderately yield in tension at relatively small drifts, has been recently discussed (Pincheira and Jirsa, 1992). Although this is an attractive option, it should be considered carefully, because braces with high levels of prestress are likely to yield, and thus of partially loosing their high level of prestress during the small and moderate seismic events that usually occur prior to the safety level ground motion.

USE OF PT BRACES FOR REHABILITATION OF INFILLED NON-DUCTILE FRAMES

The use of PT steel braces in seismic rehabilitation is a relatively new technique that can be applied efficiently to rehabilitate existing low and middle-rise frame buildings by providing significant increases in the lateral stiffness and strength of these buildings (Rioboo, 1989; Pincheira and Jirsa, 1992).

Previous to the rehabilitation of an existing building, it is desirable to carefully define the design goals of this rehabilitation. One way of defining the design goals consists of first defining qualitatively what constitutes an acceptable behavior (performance criteria) of the upgraded building, an then to quantify this qualitative definition by setting limits on the global and local seismic demands of the upgraded building. For instance, damage in frame members and in-plane damage in URM infills can be controlled by limiting their deformation and energy dissipation demands, while out-of-plane damage control in the infills can be achieved by limiting their in-plane damage and out-of-plane acceleration. The design of an adequate PT bracing system can be based on different performance criteria. Once these criteria have been established and quantified, different philosophies of design can be used to satisfy them. Essential to the good performance of the upgraded infilled non-ductile frame is to keep the frame members from developing non-ductile failures, preventing the collapse of the URM infills and preventing the PT braces from yielding in excess or buckling. To achieve this performance criteria, the following philosophy of design is suggested: design the PT braces to remain elastic and to control the story drift in the building to avoid the failure or collapse of the non-ductile frame members and the URM infills. Controlling the drift demand on a building through its rigidization while keeping the non-ductile frame members and PT braces essentially elastic is very likely to result in large increases in the base shear and story acceleration demands in the upgraded building. Nevertheless, provided the deformation demands on the URM infills are controlled within certain limits, they can supply a large and fairly stable source of viscous and hysteretic energy dissipation that will reduce these increases.

It should be emphasized that the good performance of the frame members, infills and PT braces in the upgraded building can only be achieved through drift control. This implies that the quantification of the performance criteria can be attempted by setting limits to the maximum drift or interstory drift index, IDI, demand in the building. An attractive aspect of the use of PT braces in rehabilitation is the wide range of lateral stiffness that can be considered during their design. Once the stiffness of the existing structure is evaluated, a bracing system with adequate stiffness can be easily developed. In the particular case described here, the braces should allow the structure to deform enough so as to allow the infills to contribute to resist the seismic loads, while controlling this deformation so as to let the infills provide this contribution in a stable manner and to keep the non-ductile frame members from failing. Although PT braces are usually designed to remain elastic, they can be fabricated from different types of steel, in such a way that they can be designed for a wide range of elastic deformation.

Due to the prestress in the PT braces, an initial state of stress is induced into the existing elements. Because of the large plan area of the infills, the presence of the braces induces a moderate state of compression that is likely to enhance the behavior of the infills. If so, it is desirable to brace the infilled frames of the building. Some advantages of using PT braces are: usually it is possible to distribute and design them in such a way as to avoid modifying the existing foundation; they add small reactive mass; there is no concern for inelastic buckling of the braces; clean and fast construction process; multiple architectonic possibilities; and they provide an efficient and economic solution. To achieve an adequate rehabilitation of an infilled frame using PT braces, it is necessary to check several aspects of the global and local behavior of the upgraded building: the change in behavior and failure mode of the existing frame members; the effects of the change in the dynamic characteristics of the building; the connection of the braces to the existing structure; and the use of the bracing system to correct significant strength and stiffness irregularities in plan and height (Teran *et al.*, 1995).

EXAMPLE OF REHABILITATION OF AN INFILLED NON-DUCTILE FRAME BUILDING

A six-story reinforced concrete (RC) infilled non-ductile frame building (CSMIP Station No. 23544) was selected to illustrate the use of PT braces. This building has insufficient lateral strength and stiffness, as well as large mass, stiffness and strength irregularities in plan and height. CSMIP Station No. 23544 was constructed in 1923, and has a penthouse, a mezzanine and a basement level. The floor system consists of a 3" thick one-way slab system. Some of the frames of the building, including the four perimetral frames, are infilled with URM. Figure 3 shows plan views of the building while Fig.4 shows the elevation view of 5 frames parallel to the E-W direction. Due to the inappropriate distribution of the infills in plan and the presence of a mezzanine and a penthouse, large mass and stiffness eccentricities in plan exist in the E-W and N-S directions; while the irregular distribution of infills through height produce the existence of a flexible and weak first story (soft story). The sizes of the beams are fairly constant over height. Columns are square and their size decrease considerably in higher stories. Transverse reinforcement in the columns is provided by closely spaced spirals. The exact detailing of the longitudinal steel in beams and columns is not known, but the fact that this building was designed for gravitational loads in 1923 strongly suggests that the frame members may not reach their ultimate or even their yield flexural strength.

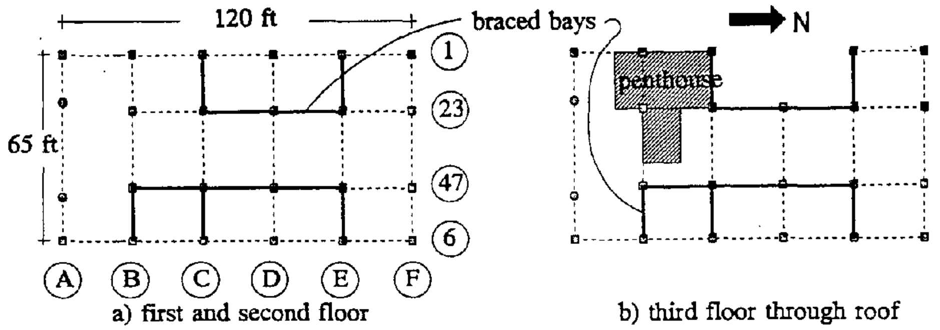

Fig.3 Plan view of CSMIP Station No. 23544

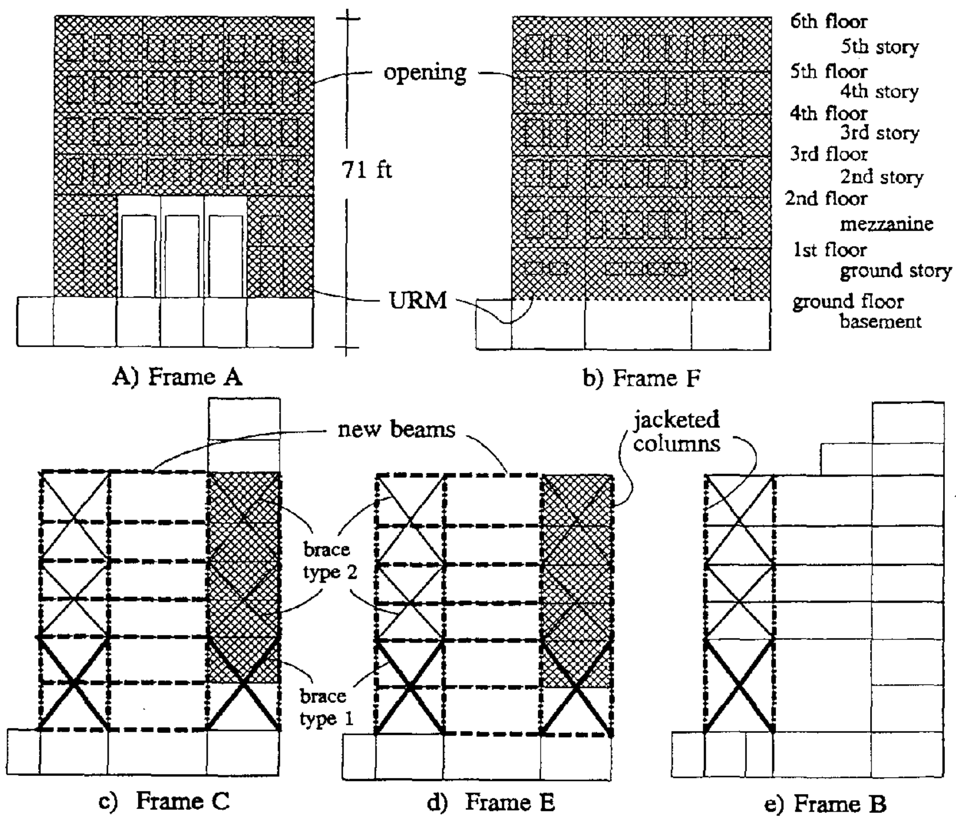

Fig.4 Elevation view of frames in E-W direction

Modelling Considerations

Under cyclic loading beyond cracking, URM infills suffer large degradation of stiffness and strength, and their viscous damping coefficient usually increases considerably with respect to that of the virgin infill (Klingner and Bertero, 1981). Because of the above, the large variability of the mechanic characteristics and geometry of the infills, and the fact that their lateral stiffness and strength are very sensitive to the quality control of the material and to workmanship, the analysis of an infilled frame building usually involves a large uncertainty.

At some stage of their lateral behavior, infills usually suffer extensive diagonal cracking which foments the formation of a lateral load-resisting mechanism based on one or more compression struts. Thus, infills can be modelled as equivalent struts whose properties may be determined from their lateral force vs. lateral deformation curves determined experimentally or analytically. Considerations done to model the URM infills with equivalent struts for the linear and nonlinear analyses reported herein are discussed in Teran *et al.* (1995). Cracking of the concrete was accounted for in the estimation of the stiffness of the RC members for the above mentioned analyses. For planar (2D) nonlinear analyses, a lumped plasticity model was used for the RC members, while for three-dimensional (3D) nonlinear analyses, a fiber model was used (Teran *et al.* 1995).

Seismic Performance of the Building Before and After its Rehabilitation

As mentioned before, the quantification of the performance criteria can be made through setting limits to the maximum IDI demand in the upgraded building. Table 1 shows this quantification, which is discussed in detail in Teran *et al.* (1995). Usually, energy dissipation should also be considered in the quantification of the performance criteria, but in the current case, this was done indirectly through setting drift limits in such a way that the URM infills are likely to exhibit stable hysteretic behavior. The critical IDI is 0.005 and is associated to the performance criteria for the URM infills. Because an adequate performance of the upgraded building depends on controlling its maximum IDI demand through controlling its lateral displacement, a displacement (δ) design spectra was established simultaneously with a strength (S_a) design spectra for the safety limit state. The site spectra, illustrated in Fig.5, were obtained for a viscous damping coefficient (ξ) of 0.05 and according to the guidelines of SEAOC (1993).

Table 1. Quantification of performance criteria for safety

Response Condition: SAFETY	Condition to satisfy performance criteria	Quantification of IDI to satisfy performance criteria
State of RC members	Elastic	Can at least undergo IDI demands of 0.005
State of URM infills	Stable hysteretic behavior	Less or equal to 0.005
State of PT braces	Elastic	To be designed
State of nonstructural elements	Pre-collapse	Less or equal to 0.0125

Although in the original research work the rehabilitation was carried out in both the N-S and E-W directions (Teran *et al.*, 1995), in this paper only the behavior in the E-W direction of the building is discussed. The fundamental mode of translation (T) and the seismic coefficient (S_a/g) of the original building in this direction were estimated as 1.0 sec and 0.14, respectively. Fig.5a shows that a single-degree-of-freedom system (SDOFS) having a S_a/g of 0.14 and a T of 1.0 sec would suffer a displacement ductility demand, μ, of about 4 when subjected to the design ground motion; while Fig.5b shows that the same SDOFS would have a displacement demand around 8".

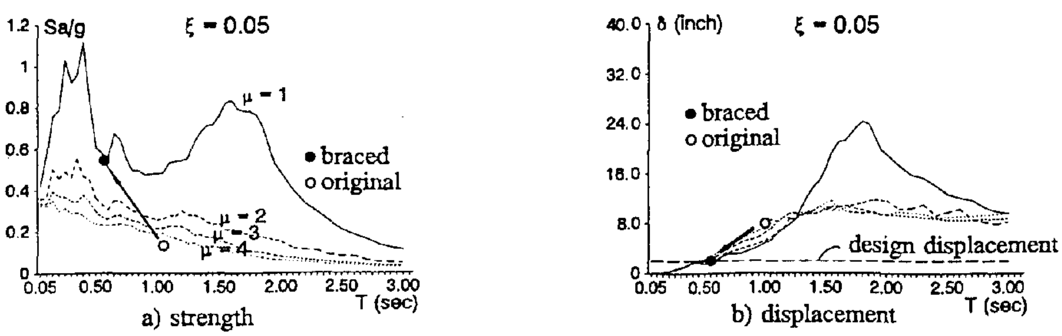

Fig.5 Design Spectra

Figure 6 shows the roof displacement (δ_{roof}) vs. base shear (V_b) curve obtained from a 2D nonlinear pushover analysis of the original building, while Figs.7 and 8 show floor displacement and IDI envelopes obtained from a 2D nonlinear time-history analysis of the original building subjected to a ground motion having a seismic input consistent with that of the design spectra. Note that in Figs.7 and 8, both the negative and positive envelopes are plotted in the same side of the displacement or IDI axis. As shown in Fig.7, the maximum δ_{roof} demand obtained from the nonlinear analysis (around 10") is consistent with the δ of 8" obtained in the SDOFS on Fig.5b; while the IDI demands in the lower stories reach values of around 0.02, which as suggested in Fig.8, are too large for the non-ductile frame members and URM infills to accommodate. Fig.9, which shows how the six floor diaphragms move relative to each other and to the ground (discontinuous rectangle) according to a 3D nonlinear pushover analysis, suggests that the building does not exhibit a significant torsional response when loaded in the E-W direction, and thus that the 2D results may be used to assess the response of the building.

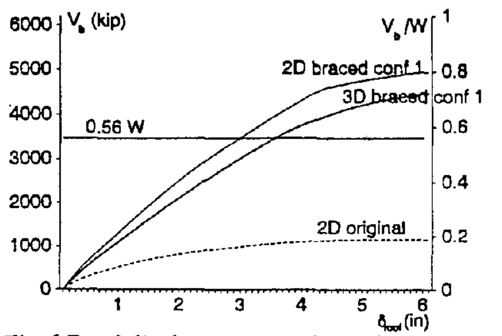

Fig.6 Roof displacement vs. base shear curves obtained from nonlinear pushover analyses

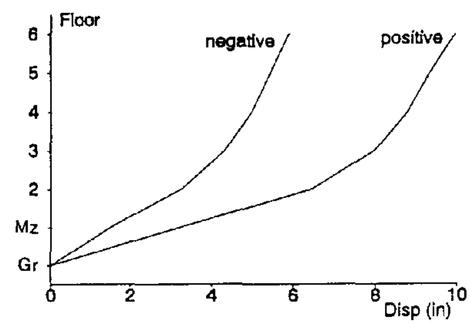

Fig.7 Floor displacement envelopes from 2D non-linear time-history analysis of original building

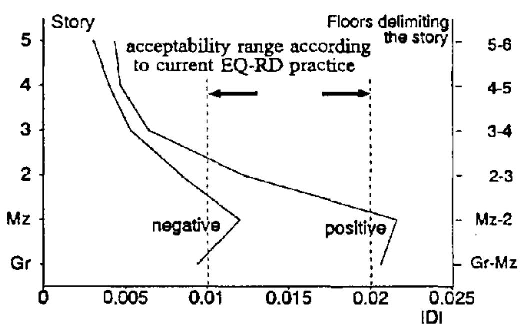

Fig.8 IDI envelopes from 2D nonlinear time-history analysis of original building

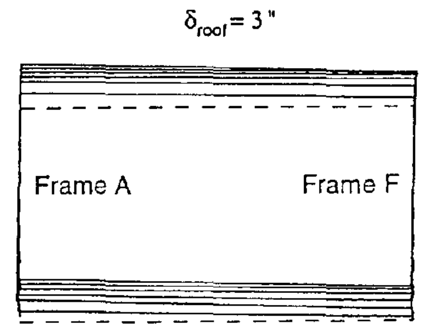

Fig.9 Floor displacement envelope from 2D non-linear time-history analysis of original building

It was estimated that the maximum IDI demand in the rehabilitated building reaches a value of 0.005 approximately when its δ_{roof} reaches a value of 2.5", which corresponds to a δ of about 2" in its equivalent SDOFS model (Teran *et al.*, 1995). Thus, to limit the maximum IDI demand in the building to a value of 0.005, it is necessary to first reduce the T of the building from 1.0 to about 0.55 sec, as schematically shown in Fig.5b. Once the maximum T has been set as 0.55 sec, it is possible to determine the design strength by considering that the braces are designed to remain elastic, and thus that μ is equal to 1, as shown in Fig.5a. This yields a S_a/g of about 0.56 (design V_b of 0.56W, where W is the reactive weight of the building). Note that using design spectra corresponding to a ξ of 0.05 is usually conservative, because it neglects the energy dissipation provided by the infills. The PT bracing system was designed to meet the requirements illustrated in Fig.5. As shown in Figs.3 and 4, braces were located in internal frames to avoid disturbing the architecture of the facades. Each diagonal in Fig.4 represents two braces, which are provided one at each side of the frame members to avoid creating undesirable loading conditions. Every brace spans two floors and, as shown in Figs.4c to 4e and Table 2, two different type of braces were used. Braces with bigger cross section were provided in the lower two stories to diminish the existing strength and stiffness irregularities in height. Initially two brace configurations were considered: configuration 2, which includes the 5 braced bays in the E-W direction shown in Figs.3 and 4; and configuration 1, which includes only 4 braced bays because the one shown in Fig.4e is eliminated. The braces are made of cable wire with a minimum yield stress ranging from 140 to 160 ksi, half of which is used for post-tensioning. As shown in Fig.4, the majority of columns located in Frames B, C and E need to be jacketed to resist the large axial forces induced to them by the braces, while some beams need to be added to avoid the buckling of the one-way slab floor system. Also, given the large axial force induced at the base of the columns that support the braces, the existing basement and foundation need to be modified and upgraded (Teran *et al.* 1995).

The T corresponding to the upgrade configurations 1 and 2 are 0.70 and 0.62 sec, respectively. Fig.6 shows the

Table 2. Sizes of the PT braces

Brace type	Required area (in^2)	Nominal diameter (in)	Provided area (in^2)
1	5.2	3 1/8	5.86
2	2.6	2 1/8	2.71

δ_{roof} vs. V_b curves obtained from 2D and 3D nonlinear pushover analysis of upgrade configuration 1. As shown, the target V_b of 0.56W is reached for a δ_{roof} larger than the target value of 2.5" set for δ_{roof}, because the actual T of 0.70 sec is larger than its design counterpart of 0.55 sec. Figures 10 and 11, which were obtained from 3D time-history elastic analyses, show IDI envelopes corresponding to the end frames (A and F) of the building when upgrade configurations 1 and 2, respectively, are subjected to a ground motion with seismic input consistent with that of the design spectra. As shown, both configurations are able to control successfully the maximum IDI demand to values less than 0.005 while eliminating the formation of the original soft story. Nevertheless, the difference between the IDI demands of Frame A and F in Figs.10 and 11 suggest that while configuration 2 is able to control the torsional response of the upgraded building, configuration 1 can not, specially in the ground story. Figures 12 and 13, which show floor displacement and IDI envelopes, respectively, obtained from the 2D nonlinear time-history analysis of configuration 1 subjected to the same seismic input mentioned above, shows that the δ_{roof} and IDI demands have been controlled within their target design values of 2.5" and 0.005, respectively, while the deformation demands through height are fairly constant. Figures 12 and 13 strongly suggest that if the torsional response of the building is not significant, 4 braced bays (configuration 1) should be enough to achieve the design goals of the rehabilitation. Nevertheless, as suggested in Fig.10 and shown in Fig.14, which was obtained from the 3D nonlinear pushover analysis of configuration 1, there is a large torsional response associated to configuration 1. One last configuration was considered for the bracing system: configuration 3, which has only 4 braced bays which include all the braced bays shown in Figs.4c to 4e except for the first braced bay of Frame C. Figure 15, obtained from the 3D nonlinear pushover analysis of configuration 3, shows that for this case, the torsional effects are practically eliminated. A nonlinear 2D time-history analysis was not carried out on confi- guration 3, because its response should be very similar to that shown in Figs.12 and 13. Nonlinear 3D time-history analyses of the upgraded version of the building were not carried out because of the extremely large computational demands associated to such analysis, and thus, it was not possible to assess in a reasonable way the simultaneous in-plane and out-of-plane demands (IDI and out-of-plane acceleration, respectively) in the URM infills.

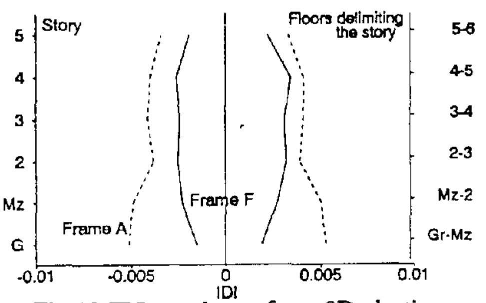

Fig.10 IDI envelopes from 3D elastic analysis of configuration 1

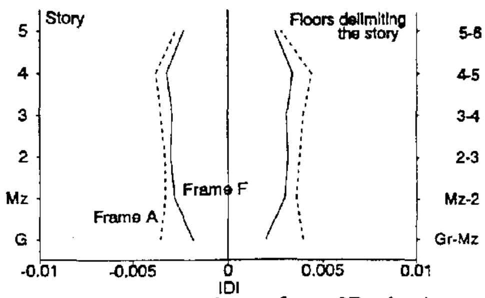

Fig.11 IDI envelopes from 3D elastic analysis of configuration 2

CONCLUSIONS AND RESEARCH NEEDS

The rehabilitation of an existing infilled non-ductile building using PT braces is an attractive option. Usually, it is possible to achieve large and economic increases in the lateral strength and stiffness of the existing building.

The use of PT braces to upgrade infilled non-ductile frames may be limited to low-rise and squat medium-rise buildings due to the high axial forces that may be induced in the existing columns that in turn create structural problems that are difficult and costly to fix. The correct rehabilitation of an infilled non-ductile building is only possible if the performance criteria for the upgraded building is defined qualitatively and quantitatively according to the mechanic characteristics of the existing structural and nonstructural elements. Because a rational way to quantify these performance criteria is through setting limits to the maximum drift demands in the building, a displacement- based design procedure should be used simultaneously with the use of design spectra specifically obtained for the site.

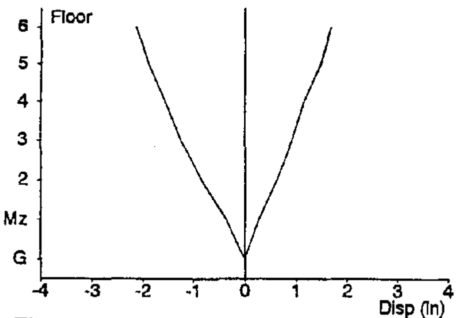

Fig.12 Floor displacement envelopes from 2D nonlinear analysis of configuration 1

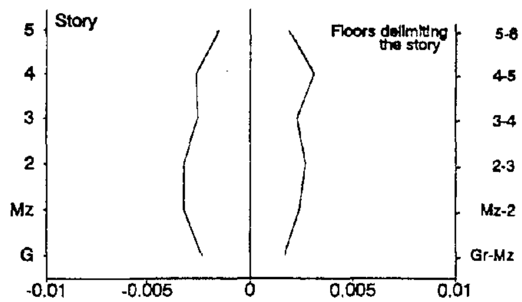

Fig.13 IDI envelopes from 2D nonlinear analysis of configuration 1

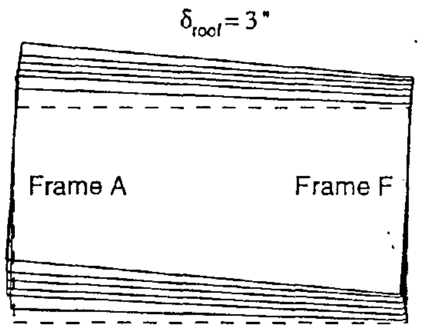

Fig.14 Displaced floor diaphragms according to 3D pushover analysis of configuration 1

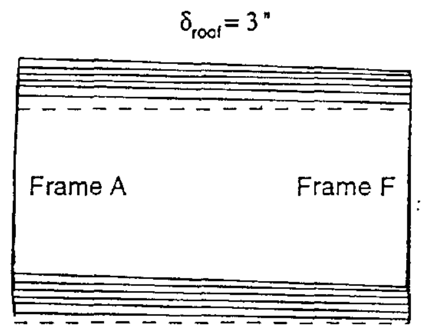

Fig.15 Displaced floor diaphragms according to 3D pushover analysis of configuration 3

Considerable research needs to be carried out to clarify several issues of the in-plane and out-of-plane behavior of URM infills, including the effects of multi-directional loading in their seismic performance and the development of reliable analytical methods and tools to model their behavior. The comparison of the results obtained from the elastic and nonlinear analyses of the upgraded building suggests that elastic analyses may be used reasonably well to estimate the response of infilled frame buildings rehabilitated with PT braces; nevertheless, it is necessary to develop methods to account for the energy dissipation provided by the URM infills (such as the use of an equivalent viscous damping coefficient).

ACKNOWLEDGEMENTS

The investigation reported in this paper was supported by the National Science Foundation under grant No. BCS-9221527. The author wishes to express his gratitude to Prof. Vitelmo Bertero, Prof. Jesus Iglesias, Prof. James Jirsa and Nabih Youseff. Special thanks are due to Maureen Doyle for editing this paper.

REFERENCES

Angel, R. and D.P. Abrams (1994). Out-of-plane strength evaluation of URM infill panels. Report NCEER-94-0004.

Klingner, R.E. and V.V. Bertero (1976). Infilled frames in earthquake-resistant construction. Report EERC 76-32.

Pincheira, J.A. and J.O. Jirsa (1992). Post-tensioned bracing for seismic retrofit of RC frames. Proceedings of the 10th World Conference on Earthquake Engineering, Vol. 9, pp. 5199-5204.

Rioobo, J.M. (1989). Sistema de rigidizacion y refuerzo de estructuras mediante cables de presfuerzo. Proceedings of the VIII Congreso Nacional de Ingenieria Sismica (Mexico), Vol. III, G74-G82.

Sakamoto, I. (1978). Seismic performance of nonstructural and secondary structural elements. Report UCB/EERC 78/10.

Schuller, M. et al. (1994). Performance of masonry-infilled R/C frames under in-plane lateral loads: experiments. Report NCEER-94-0004.

SEAOC Hazardous Building Subcommittee for Infilled Frames (1993). Guidelines for analysis of existing frame structures with concrete or masonry infill.

Teran-Gilmore, A. et al. (1995). Seismic rehabilitation of framed buildings infilled with unreinforced masonry using post-tensioned steel braces. Report UCB/EERC 95/06.

DESIGN OF A SEISMIC UPGRADE FOR OUTRIGGER KNEE JOINTS

C. R. THEWALT
Dept. of Civil and Env. Eng., 721 Davis Hall,
University of California, Berkeley, CA 94720-1710, USA

B. STOJADINOVIĆ
Dept. of Civil and Env. Eng., 2380 G. G. Brown Bldg.,
University of Michigan, Ann Arbor, MI 48100-2125, USA

ABSTRACT

Observations after the 1989 Loma Prieta earthquake suggest that older outrigger bridge bents may be susceptible to damage under three dimensional earthquake motions. In particular, older joints are weak and brittle and long outrigger beams may have insufficient torsional capacity.

The performance of the existing outrigger knee joint systems was evaluated by testing two half-scale as-built models. Two upgrade schemes, a ductile and a strong strategy, are proposed and tested on prototype specimens. Upgrade design guidelines are made using the steel jacket implementation of the strong upgrade strategy. A combination of displacement and force based design procedures is recommended to insure that the upgraded outrigger knee joint system satisfies the imposed demands. The recommendations for detailing the steel jacket upgrade and a set of tools for predicting the performance of the upgraded outrigger knee joints complete the guidelines.

KEYWORDS

Reinforced concrete, Seismic upgrade, Beam-column plastic hinge, Design of confinement, Structural joint

INTRODUCTION

The urgent need for seismic upgrading of elevated freeways was underscored by the collapses and extensive damage incurred during the 1989 Loma Prieta earthquake. The California Department of Transportation (Caltrans) initiated a large research effort aimed at devising an effective and economical seismic upgrade strategy for the elevated freeway structures built in the 1950's and 60's. One component of the research effort was the investigation of outrigger beam and knee joint systems found in elevated freeway bents (Figure 1). The investigation had two principal goals: to evaluate the behavior of the existing outrigger knee joint systems under combined transverse and longitudinal loading and to devise and experimentally verify upgrading strategies suitable for improving the seismic performance of existing outrigger knee joints [Stojadinović 95].

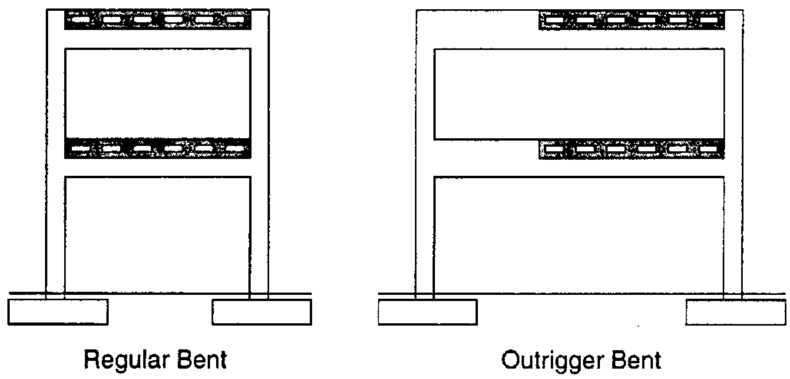

Figure 1: Elevated freeway bents.

Half scale models of typical existing outrigger knee joints were used for experimental evaluation of the behavior of the outrigger knee joint systems. The model/prototype stress identity similitude requirements and the length scale factor of 2 governed the specimen design process. The specimen details and the material properties were chosen to reflect the features of the elevated freeway structures designed in the San Francisco Bay Area during 1950's and 1960's.

For testing convenience the specimens were placed in the loading frame in up-side-down position (Figure 2). The loading pattern was designed to reproduce the overall effects of the earthquake-induced simultaneous bi-directional horizontal motion as well as the effect of gravity and frame action in the bent. The loading was applied in a quasi-static manner by controlling the actuator displacements using a computer. Two types of horizontal displacement patterns were used in the experiments (Figure 2): the clover-leaf pattern and the cross-and-circle pattern. During an experiment, the specimen was subjected to a repeated application of the chosen displacement pattern with a gradually increasing magnitude until failure. The cross-and-circle pattern has the advantage of supplying good planar data as well as three dimensional response data, but it is very demanding in terms of cumulative ductility.

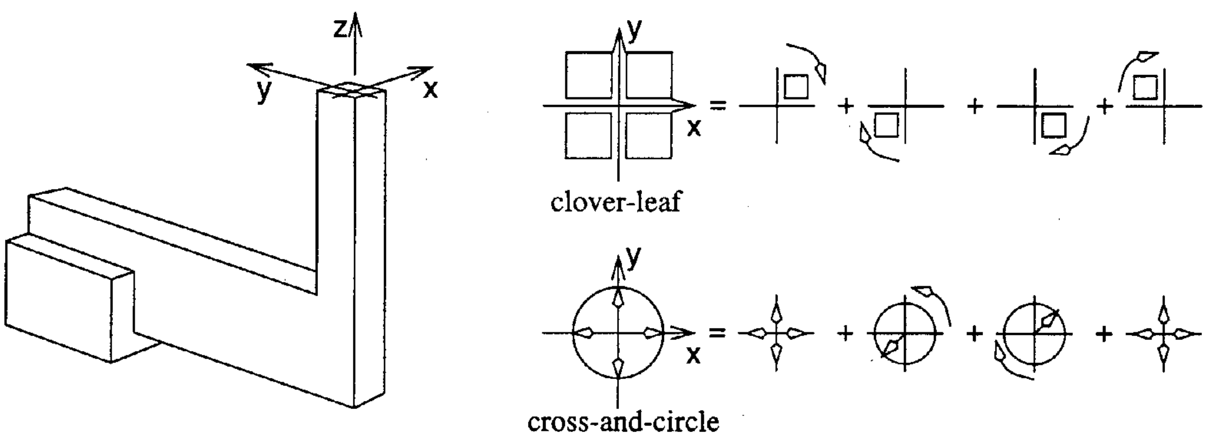

Figure 2: Specimen setup and loading patterns.

AS-BUILT SPECIMENS

The performance of existing specimens was established by testing two specimens, one with a long outrigger beam and the other with a short outrigger beam. The confinement and detailing of the existing outriggers and knee joints is unsatisfactory. The outrigger beam shear reinforcement consists of open stirrups closed with U-caps, placed approximately one quarter of the depth of the beam apart. The longitudinal bars at the bottom of the beam are developed in the knee joint over a length of 20 bar diameters. The joint contains no confining steel, since neither the beam nor the column transverse steel is extended into the joint.

Diagonal cracking appeared on both as-built specimens during the pre-yield cycles. The combination of shear and torsion produced a set of inclined diagonal cracks on the sides of the beam of the long outrigger specimen. The failure of both specimens occurred soon after yielding of column reinforcement. The sides of the joint dilated first, followed by splitting of the layer of column bars from joint core on the exterior face of the joint.

The failure was sudden and brittle (Figure 3). As expected, the unconfined joints were unable to transfer the cyclic joint shears. The long outrigger beam torsional capacity was also found to be inadequate due to the lack of closed stirrups. The deficient details of the existing outriggers contribute to the poor behavior of both as-built specimens.

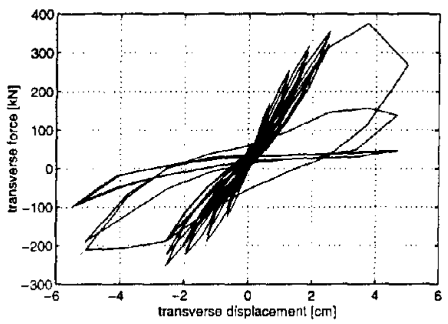

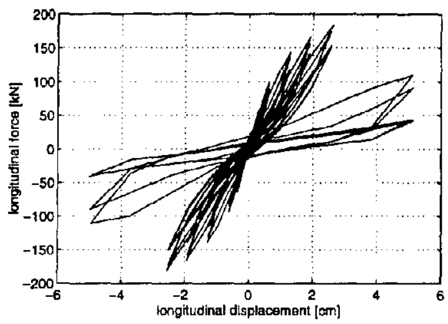

Figure 3: Force/displacement behavior of the short as-built specimen.

PROTOTYPE UPGRADES

The seismic upgrade of existing outrigger knee joints has to prevent their catastrophic failure and to increase their deformation and energy dissipation capacity. The strengthened outrigger knee joints should behave as well as the rest of the upgraded bridge structure and should be easy to inspect and repair after an earthquake. Experiments on the as-built specimens show that the elements of the outrigger knee joint system should be modified to form a stable, ductile, energy dissipating system with a well-controlled failure mechanism. The damage in the knee joint region should be minimized. Two upgrade strategies, designed to accomplish these goals, were proposed: the ductile upgrade strategy and the strong upgrade strategy.

Ductile Upgrade Strategy

The ductile upgrade strategy is designed to increase the stable deformation capacity of the outrigger system. The ductile scheme hinges at multiple locations causing distributed damage throughout the specimen. A plastic hinge forms in the column in response to transverse loading. In the longitudinal direction, hinging occurs in flexure/torsion of the beam.

A reinforced concrete jacket was used on the prototype ductile upgrade. Two 15 centimeter thick side bolsters connected with closed stirrups and T-headed through-bars strengthened the beam. The bolster horizontal reinforcement was wrapped around the outside face of the joint to increase confinement, arrest joint dilation and prevent the column bar bond-splitting failure observed in the as-built tests.

The ductile upgrade prototype behaved as expected, with two distinct plastic hinge zones providing a high level of ductility and energy dissipation. In addition, the forces transferred to the bridge deck were minimized. However, the distributed hinging produced a comparatively large amount of distributed damage, making the upgraded outrigger knee joint system hard to repair after a strong earthquake.

Strong Upgrade Strategy

The strong upgrade strategy was designed to form a stable system with large deformation capacity that concentrated all damage in the column plastic hinge zone. The column was designed to hinge under both transverse and longitudinal loads. The knee joint, the beam and the beam/bridge deck interface were strengthened to the level required to carry the ultimate forces transferred through the column plastic hinge. It should be noted that the forces transfered to the superstructure are larger using this scheme than with the ductile upgrade.

The original strong upgrade prototype used steel jacketing made of 12.5mm A36(USA) plate. The jacket was welded together around the beam and the knee joint, strengthened with threaded through-bars and injected with epoxy. The column of the prototype system was not altered.

As expected, the prototype strong upgrade developed a plastic hinge in the column. The hinge provided the plastic rotation capacity necessary for a ductile behavior of the upgraded system. As a consequence of plastic deformation, virtually all of the damage was concentrated in the column hinge. However, the jacket anchors at the beam/bridge deck interface failed under longitudinal loading, suggesting the final upgrade design must take into account the possibility of significant beam weak axis bending.

FINAL UPGRADE DESIGN

The extent of damage caused by multiple plastic hinge zones makes the ductile upgrade strategy less attractive than the strong upgrade despite its excellent energy dissipation characteristics. The strong upgrade strategy offers a simple ductile solution applicable to outrigger systems with both short and long beams. Therefore, the strong upgrade strategy was chosen for the final design of the outrigger knee joint system upgrades.

Two versions of the final upgrade strategy were tested. A final upgrade employing a post-tensioned reinforced concrete jacket was tested on one long outrigger specimen. The concrete jacket was made up of two 22.5 centimeter thick bolsters resembling the ductile upgrade prototype. Post-tensioning was designed to secure the beam/bridge deck connection and increase the torsional resistance of the beam.

Another final upgrade design (Figure 4), using a 6 mm A572-50(USA) steel plate jacket, was tested on two specimens, one with a long and the other with a short outrigger beam. The jackets were welded together, tied through the middle of the cap beam with one row of threaded through-bars and injected with epoxy. The anchorage of the beam jacket to the bridge deck was carefully detailed to make cap beam post-tensioning unnecessary.

The columns of all three final design specimens were upgraded to achieve large curvature ductility while minimizing the increase in the strength of the column plastic hinge. A grouted cylindrical casing using 3 mm thick A572-50(USA) curved steel plate was placed around the column. The casing was closed from above and below by four pairs of end-plates. The anticipated rotation of the plastic hinge dictated a 2.5 centimeter clearance between the beam jacket and the column casing. The shear capacity of the

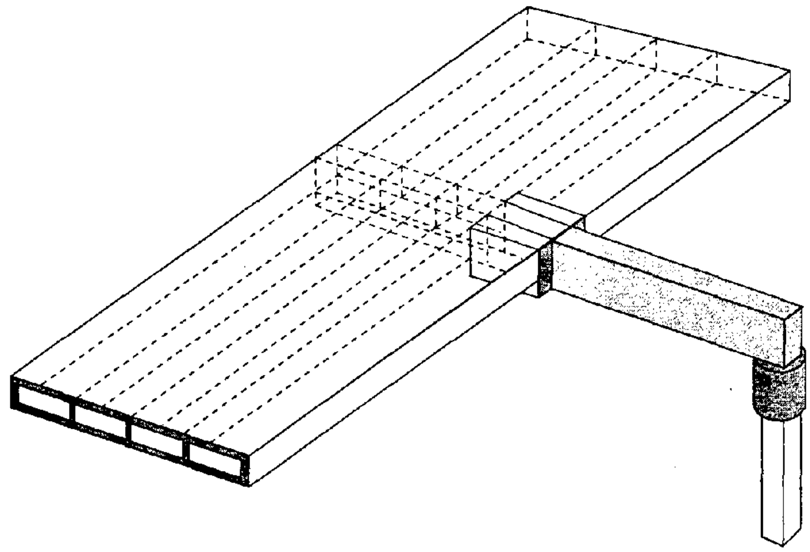

Figure 4: Final upgrade strategy implemented using a steel jacket.

as-built column was determined to be sufficient to hinge the column in bending. Therefore, the steel casing was extended only part-way down the column, along a length determined from the ratio of the ultimate moment capacity of the column hinge and the yield moment strength of the as-built column. Aesthetic or constructibility issues may make a full length column jacket more attractive but it is not needed to achieve the desired system behavior.

The behavior of all three final upgrade specimens was excellent. The strengthened beam and knee joint were sufficiently strong to concentrate virtually all of the damage in the column hinge region. The improvement in the behavior achieved by the strong upgrade is evident from the force/displacement response of the upgraded short outrigger specimen (Figure 5). The specimens maintained significant strength at large deformation and the loops were broad and not pinched.

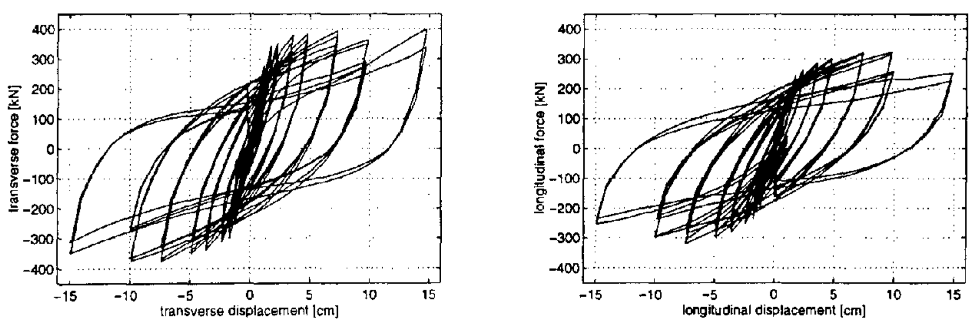

Figure 5: Force/displacement response of the upgraded short outrigger.

The reason for the significantly improved global behavior lies in the ductile moment/curvature response of the upgraded column plastic hinge (Figure 6). Measured response of the upgraded hinge shows stable behavior up to curvature ductility level of 21 and considerable energy dissipation. This behavior was achieved by confining the concrete of the hinge cross section using a steel casing. Even though the casing was quite thin the strains in the casing remained well below yield throughout the experiment.

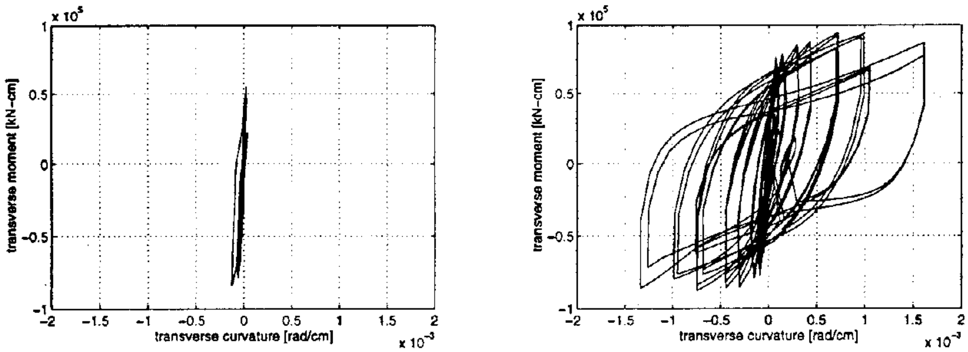

Figure 6: Moment/curvature response of the as-built and the upgraded short outrigger specimen.

DESIGN GUIDELINES AND ANALYSIS TOOLS

Design guidelines [Stojadinović 95] were developed using the information from the experimental and analytical investigation. The guidelines define the necessary steps to design and implement the strong upgrade strategy using a steel plate jacket on existing outrigger knee joint systems. The principal part of the design guidelines is the upgrade design procedure. The procedure has a displacement-based and a force-based part.

The displacement-based part of the design procedure ensures that the upgraded column hinge has sufficient sustained plastic rotation capacity to satisfy the desired outrigger knee joint system drift demand. The design procedure starts by specifying the drift demand on the outrigger knee joint system. The curvature ductility demand on the column plastic hinge is computed using a plastic hinge model under the assumption that all of the system deformation is generated in the hinge zone.

The column hinge confinement is then designed to provide the required curvature ductility. The value of effective confinement pressure is determined iteratively using moment-curvature information from a fiber cross section analysis program. The program employs realistic material models [Mander 84] for unconfined and confined concrete and for the reinforcing steel.

The original section analysis program [Thewalt 94] has been completely rewritten and is now called called APS (Analysis of Plane Sections). The new program has many enhancements over the original version, including: (1) decreased memory demands so that the program can easily run on PC computers; (2) a new solution algorithm that allows for stable force control solution even when multiple stiffness terms go zero or negative; (3) three user definable normalized tolerances to control stress error, path deviation error, and convergence error; and (4) an incremental stiffness update on fiber strain reversals that dramatically improves performance.

Figure 7 shows how the iterative design process is applied to the column hinge cross section of the short upgraded specimen by examining the behavior of an extreme core fiber. Confinement is adjusted until the core concrete does not crush at the desired curvature. The confinement pressure exerted at yield of the column casing was varied from 0 to 5.5 MPa. The improvement in the stress/strain response of the extreme concrete core fiber is reflected in the enhancement of curvature ductility and increase in moment capacity of the column hinge. The dashed line represents the state of the cross section at the design curvature demand level. The circles on the right graph represent the state of the cross section when the first fiber of the concrete core is crushed.

Knowing the ultimate capacity of the upgraded column hinge, including effects like strain hardening, the remaining elements of the upgrade outrigger knee joint system are designed following force-based procedures. The nominal strength capacities of the remaining elements are designed to satisfy the

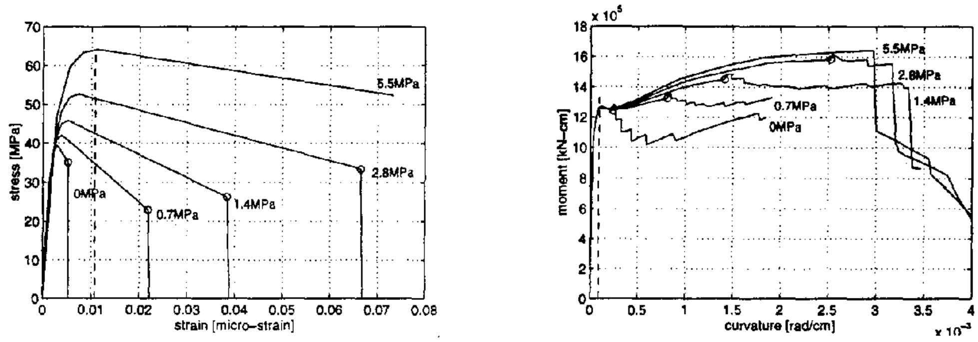

Figure 7: Iterative design of column hinge confinement.

strength demands imposed by the ultimate capacity of the column hinge.

CONCLUSION

The experimental investigation of the as-built outrigger knee joint systems confirmed their vulnerability. The joint region and the torsional strength of the outrigger beam were found to be the primary weak links of the system. Seismic upgrading was found to be necessary to avoid the brittle behavior observed in the as-built tests.

Two upgrade strategies for existing outrigger knee joint systems were proposed and evaluated. The final upgrade strategy is based on the capacity design principle of concentrating the damage in the column plastic hinge and strengthening the remaining elements of the outrigger knee joint system. Variations of the final upgrade design were tested on three specimens and all performed very well.

A demand/capacity procedure for designing the seismic upgrade of existing outrigger knee joints was developed. The design procedure is based on careful detailing of the column plastic hinge to provide adequate and sustained plastic rotation capacity. The design procedure, together with several detailing solutions and section analysis program form a set of design guidelines presented in [Stojadinović 95]. The final report also investigates issues of how the observed local behavior can be included in simplified global nonlinear analyses.

REFERENCES

[Mander 84] J. B. Mander, M. J. N. Priestley, and R. Park. "Seismic design of bridge piers." Technical Report 84-2, Department of Civil Engineering, University of Canterbury, Christchurch, New Zealand, February 1984.

[Stojadinović 95] B. Stojadinović and C. R. Thewalt. "Upgrading bridge outrigger knee joint systems." Technical Report UCB/EERC-95/03, Earthquake Engineering Research Center, University of California, Berkeley CA 94720, 1995.

[Thewalt 94] C. R. Thewalt and B. Stojadinović. "A stable reinforced concrete section analysis procedure." *ASCE Structural Engineering Journal*, 120(ST10):3012–3024, October 1994.

CYCLIC BEHAVIOR OF RC BEAM-COLUMN KNEE JOINTS CONSTRUCTED USING CONVENTIONAL AND HEADED REINFORCEMENT

JOHN W. WALLACE[1], SCOTT W. . McCONNELL[2], PIUSH GUPTA[1]

[1]Department of Civil Engineering, Clarkson University, Potsdam, NY, USA 13699-5710
[2]Schoor-Depalma, 200 State Highway 9, P.O. Box 900, Manalapan, NJ 07726-0900

ABSTRACT

A comparison is made of the reversed cyclic behavior of reinforced concrete exterior and knee joints constructed utilizing conventional reinforcement anchorages and headed reinforcement anchorages. The comparison is based on the experimental results of two exterior and five knee joint specimens tested as part of an extensive experimental program. An overview of the experimental study is presented prior to evaluating the effectiveness of the specimens constructed using headed reinforcement. Behavior of the specimens constructed using headed reinforcement eased specimen fabrication and concrete placement, as well, the behavior was as good as, or better than similarly constructed specimens constructed with standard 90 degree hooks. For knee joints, the test results indicate the need to provide transverse reinforcement at the heads to restrain.

KEYWORDS

Beam-column joints, joints, knee joints, headed reinforcement, T-headed bars, mechanical anchorage, experimental, cyclic loads, exterior joints, headed rebar.

INTRODUCTION

ACI-ASCE Committee 352 publication ACI 352-91 sets various design guidelines for achieving proper anchorage of longitudinal bars terminating within a joint. For high seismic zones, load reversals in the joint can lead to significant bond deterioration along straight bar anchorages; therefore, ACI 352-91 requires that 90 degree hooked anchorages be used when longitudinal reinforcement is terminated within the joint. The use of hooked anchorages tends to increase steel congestion, making the construction process more difficult. In addition, geometric limitations often prevent the use of larger diameter reinforcing bars due to construction limitations arising from lengthy hook extensions and large bend diameters. In these cases, the use of reinforcement with mechanical anchorages has obvious advantages; however, the use of mechanical anchorages may produce high local stresses. Therefore, experimental studies of specimens constructed with mechanical anchorages are needed to assist in the development of design guidelines.

OBJECTIVES AND SCOPE

The overall research project involved experimental and analytical studies of beam-column joints subjected to slowly varying, reversed cyclic loads. A total of eighteen beam-column knee joint specimens and two beam-column exterior joint specimens were tested. The scope of this report is limited to evaluating: (1) joint shear strength requirements for knee joints and (2) the effectiveness of the specimens constructed with headed bars. Where possible, the performance of specimens constructed with headed reinforcement is compared with the test results of similarly constructed specimens in which anchorage within the joint was provided with standard hooks. Additional information on the studies is available in the following reports (Cote and Wallace, 1994; McConnell and Wallace, 1994; 1995; Gupta and Wallace, 1996).

OVERVIEW OF ACI-ASCE COMMITTEE 352 REQUIREMENTS

Design requirements for reinforced beam-column joints for typical structures are specified by ACI-ASCE Committee 352 Report 352-91. Report 352-91 provides guidelines for both ``non-seismic" (Type 1) and ``seismic" (Type 2) design applications; emphasis is placed on Type 2 connections within this paper. ACI 352-91 defines a Type 2 joint as a joint that ``connects members designated to have sustained strength under deformation reversals into the inelastic range." Specific requirements for Type 2 joints are reviewed in the following paragraphs.

ACI 352-91 recommends that the nominal moment strength of the columns be at least 1.4 times the nominal moment capacity of the adjoining beams to ensure that a majority of the inelastic deformations occur in the beam rather than the column (to avoid the formation of a ``soft-story"). It is noted that achieving this ratio is difficult for knee joints; however, this requirement need not be satisfied for knee-joints, because column hinging is typically no more critical than beam hinging.

The ACI 352-91 requirements for joint shear strength are based on (1):

$$\phi V_n = \phi\gamma\sqrt{f'_c}\,b_j h \geq V_u \tag{1}$$

where ϕ=0.85, V_n is the nominal shear strength of the joint, b_j is the effective width of the joint, h is the depth of the column, and γ is a factor that depends on the joint type and classification. For a Type 2 exterior and corner (other) joints, γ is taken as 15 and 12 for f'_c in psi, and 1.2 and 1.0 for f'_c in MPa. No specific recommendations are given for knee joints; therefore, a value of 12 (for f'_c in psi) may be used, although no comprehensive studies have been conducted to establish if this is reasonable.

The ACI 352-91 report specifies that the critical section for development of reinforcement should be at the outside edge of the column core for Type 2 joints. Furthermore, all terminating bars should be hooked within the transverse reinforcement of the joint using a 90 degree standard hook. The development length should be computed as:

$$l_{dh} = \frac{\alpha f_y d_b}{75\sqrt{f'_c}}\ in. \quad = \quad \frac{\alpha f_y d_b}{6.225\sqrt{f'_c}}\ \text{mm} \tag{2}$$

where f_y and f'_c are in terms of psi and MPa for l_{dh} in inches and mm, respectively. The term α represents a stress multiplier used to account for strain hardening and over strength of the reinforcing bars. A minimum value of α = 1.25 is recommended for Type 2 joints. For f'_c = 4000 psi (27.4 MPa), f_y = 60 ksi (420 MPa), and α= 1.25, the development length is approximately 15.8 bar diameters.

The committee also makes recommendations for providing adequate transverse reinforcement in the form of spirals or rectangular hoops with crossties for both Type 1 and Type 2 joints. For Type 2 joints, the total cross-sectional area of transverse reinforcement within the joint in each direction should be:

$$A_{sh} = 0.3\,\frac{s_h h'' f'_c}{f_{yh}}\left(\frac{A_g}{A_c} - 1\right) \geq 0.09\, s_h h''\,\frac{f'_c}{f_{yh}} \tag{3}$$

The center-to-center spacing between layers of transverse reinforcement, s_h should not exceed the least of one-quarter of the minimum column dimension or 4 inches (101.6 mm). ACI 352 requirements were used to assist in the planning of the experimental research program as well as to evaluate the test results.

EXPERIMENTAL RESEARCH PROGRAM

The overall research program involved testing twenty beam-column joint specimens. A brief description of the specimens is provided in the following subsections. Design of specimen BCEJ2 was based on requirements for low seismic regions; therefore, results are not presented.

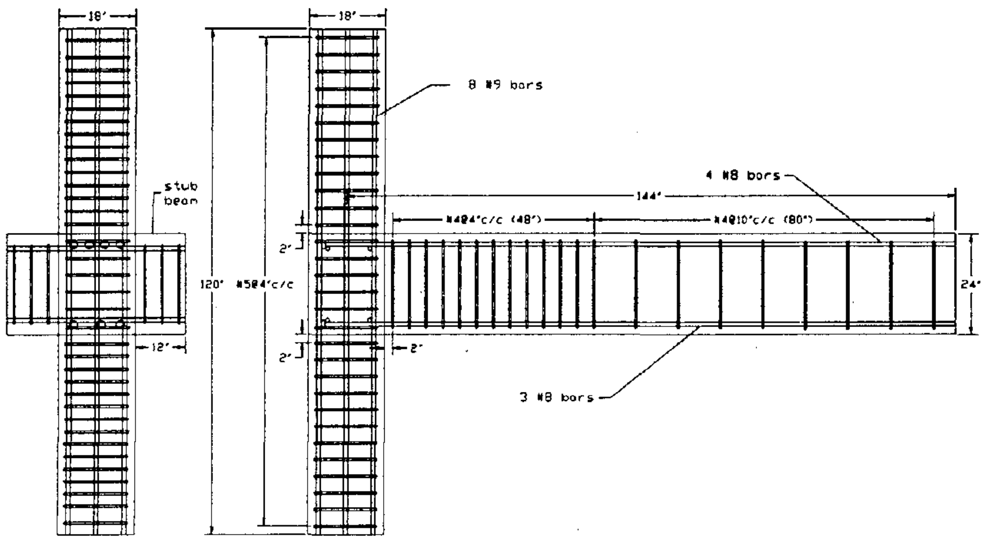

Fig. 1. Specimen BCEJ1 Reinforcing Details

Specimen Description

Overall dimensions for the exterior and knee joint specimens tested are shown in Figure 1 - 3. For all specimens, a concrete compressive strength of 4,000 psi (27.6 MPa) and a reinforcement yield stress of 60,000 psi (413.7 MPa) were used for design purposes.

In specimens KJ1-KJ13, hooked beam and column anchorages were provided within the joint as required by ACI 352-91. In specimens KJ16-KJ18 headed bars were used to anchor both column and beam reinforcement

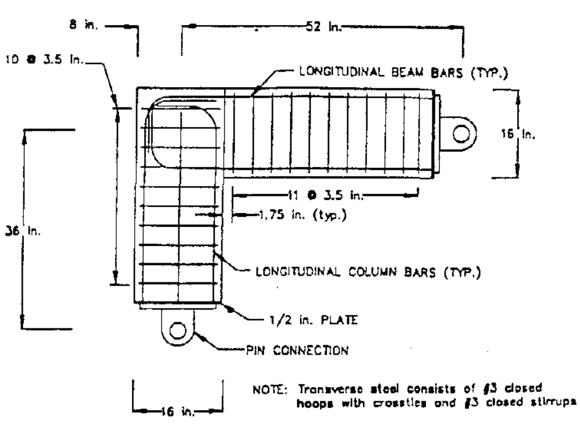

Fig. 2a. Knee Joint Specimen Geometry

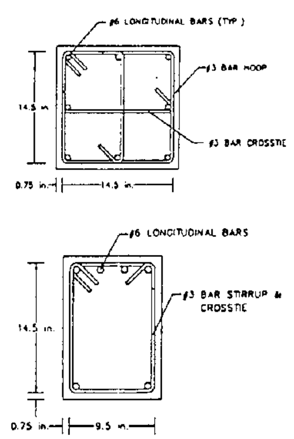

Fig. 2b. Knee Joint Specimen Cross Sections

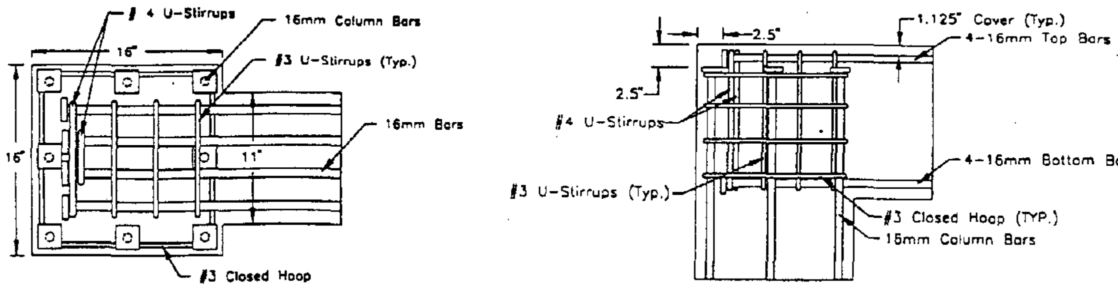

Fig. 3. Reinforcing Details for Specimen KJ17

within the joint, whereas in specimens BCEJ1 and BCEJ2 headed reinforcement was used to anchor beam longitudinal reinforcement. For specimens KJ16-KJ18, the headed anchorages were fabricated by Headed Reinforcement Canada using a friction welding technique to attach steel plates to the reinforcement (Norwegian Tempcore steel). For the reinforcement used in these specimens (16 and 20 mm diameter bars), the steel plates were approximately 2" x 2" x 1/2" (50 mm x 50 mm x 12 mm). For specimens BCEJ1-BCEJ2, a tapered, threaded connection provided by ERICO, INC was used to anchor circular plates (diameter = 2.25 in.; thickness = 1.375 in.) to the longitudinal reinforcement. Figures 3 shows the plan and elevation joint details for KJ17; details for BCEJ1 are provided in Figure 1. A 12 in. (25.4 mm) long beam stub was cast on either side of the joint to represent the confinement provided by the transverse beams that typically frame into the joint.

The ratio of the beam flexural strength to the column flexural strength was approximately unity for the knee joint specimens and 1.65 for BCEJ1. The joint shear demand was approximately 6, 9, and 12 $\sqrt{f_c'}$ psi (0.5, 0.75, and 1.0 $\sqrt{f_c'}$ MPa) for the knee joint specimens KJ1-KJ15, depending on the amount of beam longitudinal reinforcement. The design joint shear stresses were approximately $6\sqrt{f_c'}$ psi for specimens KJ16-KJ17, $9\sqrt{f_c'}$ psi for specimen KJ18, and $12\sqrt{f_c'}$ psi BCEJ1.

The tension development length provided within the joint core slightly exceeded that required for a standard hook for specimens KJ16 and KJ17, was approximately equal to that required for a standard hook for specimen KJ18, and was slightly less than that required for a standard hook for specimen BCEJ1 ($12.5d_b$ versus a required length of $15.8\ d_b$) the compression development length provided was 84%, 67%, and 88% of that required by ACI 318 Section 12.3 (including a multiplier of 0.8 to account for confinement) for specimens KJ16-KJ17, KJ18, and BCEJ1, respectively.

Horizontal transverse reinforcement within the joint region for specimens KJ4 and KJ7, and KJ16-KJ18 consisted of #3 (9.5 mm) US Grade 60 hoops with two crossties spaced at 3.5 inches (88.9 mm). Double leg, inverted, ''U-shaped" stirrups were also provided at a spacing of 3.5 in. (88.9 mm) in KJ4, KJ7, and KJ16 to confine the top face of the joint. For specimens KJ17 and KJ18, an additional U-shaped stirrup was used at the heads to restrain pullout (Fig. 3). For specimen BCEJ1, the spacing of transverse reinforcement in the joint region (hoop and two crossties) was approximately 4 inches (101.6 mm).

The average concrete compressive strengths at the testing date were: 7480, 4765, 5390, 5450, 5540, and 5190 psi (51.6, 32.9, 37.2, 38.2, 35.8 MPa) for specimens KJ4, KJ7, KJ16-KJ18, and BCEJ1, respectively. It should be noted that the stress-strain characteristics of the US Grade 60 reinforcement differ slightly from that of the Norwegian Tempcore reinforcement used for specimens KJ16-KJ18 (relatively little strain hardening occurred in the Tempcore steel), and that stress strain relations are not yet available for the reinforcement used in BCEJ1. Yield strength of the US Grade 60 longitudinal and transverse reinforcement used in the knee joints was approximately 65 ksi (44.8 MPa) for all specimens and bar sizes, whereas the yield stress was 71 (49.0 MPa) and 77 ksi (53.1 MPa) for the 16 mm and 20 mm bars, respectively, used in specimens KJ16-KJ18.

Specimen Testing and Instrumentation

The knee joints were tested in a statically determinate test setup with the column in an upright position. A schematic of the testing apparatus is shown in Figure 4. With this setup, the axial load in the beam and column varies in proportion with the applied load. The affects of axial load on member capacity were included in the specimen design and analysis. The exterior joints were also tested in an upright position (Figure 5). No axial load was applied to the column.

Instrumentation was used to measure lateral load, lateral displacement, rotations, concrete cover and joint core strains, and strain in the longitudinal and transverse reinforcement. Reversed cyclic loading was applied under displacement control. A minimum of two complete cycles were performed at each drift level in all specimens. The strain in the longitudinal and transverse reinforcement was measured through the use of strain gages. Several gages were provided along the top beam bars for specimens KJ16-KJ18 to evaluate the effectiveness of the headed reinforcement.

EVALUATION OF EXPERIMENTAL RESULTS

The primary objectives of this paper are to evaluate the potential of using headed anchorages with beam-column joint regions; therefore, only selected results from the overall research program are presented. For the knee joint specimens, a direct comparison between specimens constructed with headed reinforcement and similarly reinforced specimens where the anchorage within the joint was provided with 90 hooks (referred to as conventionally reinforced) is available. The conventionally reinforced specimen most comparable to specimens KJ16 and KJ17 is KJ4; whereas, specimen KJ7 most closely resembles the reinforcement placed in specimen KJ18. Specimen behavior and performance are discussed in the following subsections. Conclusions are based on the observed behavior as well as comparative evaluations. Some general results of the overall research program are presented first, followed by specific observations for the specimens with headed reinforcement.

Joint Shear Capacity

One objective of the knee joint research program was to evaluate joint shear capacity by varying the amount of longitudinal reinforcement provided in the beams and columns. Results indicate that if the joint shear demand is kept below $6\sqrt{f_c'}$ psi ($0.5\sqrt{f_c'}$ MPa), then good joint performance was achieved with little damage observed within the joint (KJ1-KJ4, KJ14-KJ17). Beam flexural hinging was typically observed for these specimens and good load deformation behavior was measured (Fig. 6). For specimens with sufficient

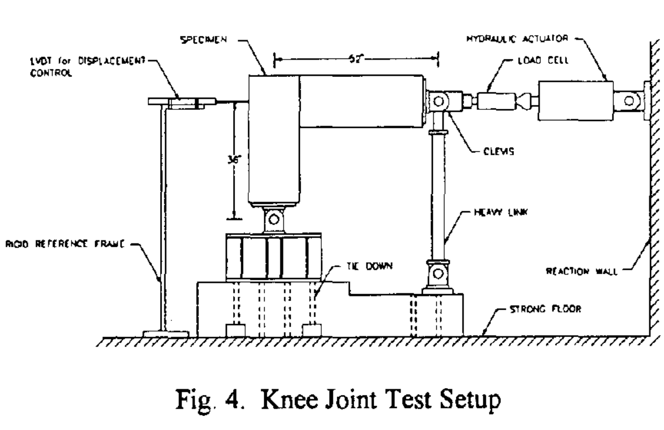

Fig. 4. Knee Joint Test Setup

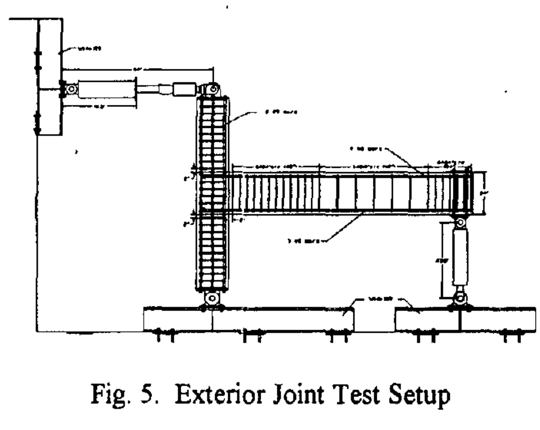

Fig. 5. Exterior Joint Test Setup

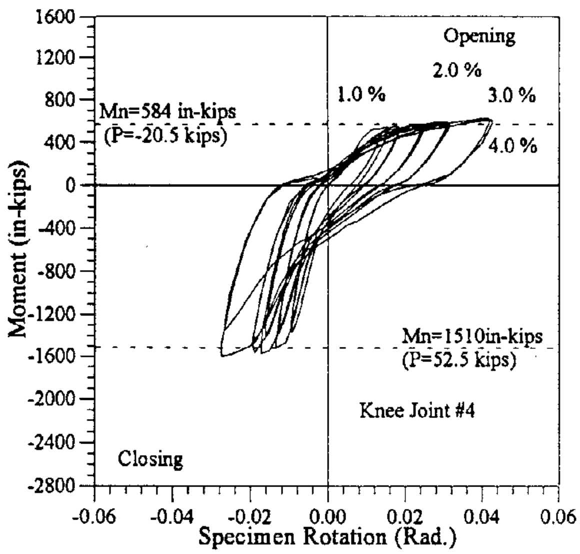

Fig. 6. Beam Moment vs. Specimen Rotation: KJ4

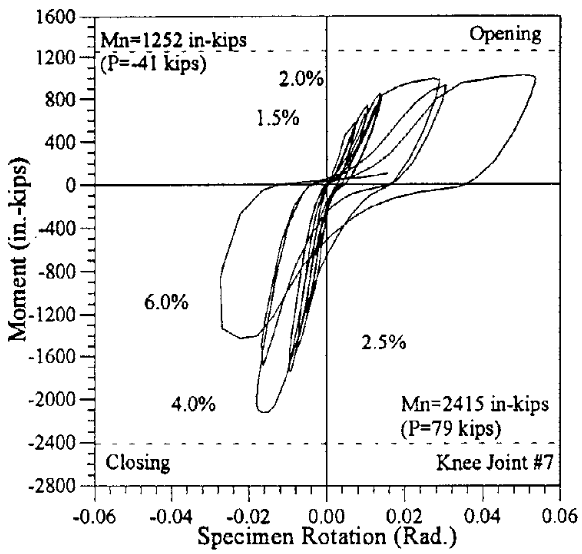

Fig. 7. Beam Moment vs. Specimen Rotation: KJ7

beam flexural reinforcement to achieve joint shear stresses of 9 to $12\sqrt{f_c'}$ psi (0.75 to $1.0\sqrt{f_c'}$ MPa), the maximum joint shear stress under closing moments obtained ranged from 7.4 to $9.2\sqrt{f_c'}$ psi (0.62 to $0.77\sqrt{f_c'}$ MPa), with an average value of $8.0\sqrt{f_c'}$ psi ($0.67\sqrt{f_c'}$ MPa). For all of these specimens, the full moment capacity of the beam could not be reached and substantial joint damage was observed. As a result, somewhat poor overall performance was observed (KJ7, Fig. 7). The horizontal dashed lines in Fig. 6 and 7 indicate the nominal moment capacities of the beam under both positive and negative bending. Due to joint deterioration, the specimens were unable to achieve the full flexural capacity of the beams. Based on the test results, beam-column knee joints without transverse beams are not capable of achieving a joint shear level of $12\sqrt{f_c'}$ as would be suggested in the Committee 352 report. For a knee joint with 4 adjacent unrestrained sides (the knee-joints were tested without transverse beams), a γ factor of 8 is probably a realistic limiting value.

Headed Reinforcement Anchorages

Specimen BCEJ1 was designed to meet ACI Committee 352 requirements except that headed reinforcement was used to anchor the beam top and bottom bars. No other alterations were made, although an attempt was made to place column hoops in line with the heads of the beam bars to provide additional restraint against pushout. Experimentally measured moment-rotation behavior (moment at column face versus the rotation measured over the 24 in. (609.6 mm) of the beam) is plotted in Fig. 8. Excellent behavior was observed, with little deterioration in flexural strength noted even at 6% lateral drift (note that no axial load was applied to the columns). Based on the test results, it is apparent that the use of headed reinforcement is a viable alternative to the use of standard hooks in exterior beam column joints. It is noted that the headed reinforcement was anchored approximately 13 beam bar diameters into the joint (roughly equivalent to the embeddment required for a standard hook). It is likely that shorter embeddments could be used as test results on isolated anchors (Bode and Roik, 1987) indicate that an embeddment of 8 to 10 bar diameters is adequate; however, additional testing is needed to verify this for bars anchored within a joint region. Pushout of the column cover concrete did not affect the lateral load capacity of the specimen even though only 88% of the compression development length was provided.

Testing of the knee joint specimens with headed bars was conducting in two phases due to the special problems associated with this joint configuration (four unrestrained joint faces). Specimen KJ16 was constructed to be essentially the same as the conventionally reinforced specimens (except with headed bars replacing the standard 90 degree hooks). Test indicated the need to provide additional reinforcement to restrain pullout of the beam top bars. Based on the test results for KJ16, additional reinforcing was provided in specimens KJ17 and KJ18 to restrain the heads of the beam top bars (Fig. 3). The area of the U--stirrups at the heads of the beam top bars was selected such that the stirrups would be capable of resisting one half of the total tension force developed in the beam top bars. The resistance provided by the three remaining single U-stirrups and by the cover concrete were neglected. No additional transverse reinforcement was used in the column.

The moment-rotation hysteresis loops for specimen KJ17 are plotted in Fig. 9 and indicate that large ductilities were achieved under both opening and closing moments. For specimen KJ17, the horizontal shear demand placed on the joint was kept below $6\sqrt{f_c'}$ psi ($0.5\sqrt{f_c'}$ MPa); therefore, good joint behavior was expected based on the results of the specimens constructed with conventional reinforcement anchorages. For this joint shear stress level, flexural hinging occurred in the beam adjacent to the column face.

Compared with KJ4 (Fig. 6), the relations for KJ17 reveal that the performance of the specimen constructed with headed reinforcement is as good as the specimen constructed with conventional reinforcement. Slight differences are evident in Fig. 6, compared with Fig. 9. These differences include: (1) KJ17 exhibits slightly greater stiffness than KJ4, probably due to less slip of the reinforcement, and (2) KJ17 achieves slightly lower flexural capacity than KJ4, likely due to the differences in the strain-hardening characteristics of the bars.
In specimen KJ17, some pushout of the concrete at the back of the joint occurred due to compressive forces in the beam bottom bars and localized bending of the column bar at the middle of the back face was noted. However, the concrete spalling and column bending mentioned above did not occur until very high drift demands (6%) were imposed on the specimen. This behavior was not evident in specimens KJ16 and KJ18 which were not subjected to such extreme deformation demands, indicating that the provided compression development length (85% and 67% of the ACI required compression development length for KJ17 and KJ18, respectively), detailing, and concrete cover are sufficient under the maximum displacement demands reasonably expected to occur in structural systems.

Specimen KJ18 performed noticeably better than specimen KJ7, which was reinforced using conventional 90 degree hooks. This is primarily due to less reinforcement slip occurring when the headed anchorages are used. Excessive anchorage slip occurred in the top beam bars under large displacement demands in KJ7. Initial crack formation occurred along the straight portion of these bars and eventually extended around the bends as the hook extensions pushed outward on the concrete cover at the back of the joint.

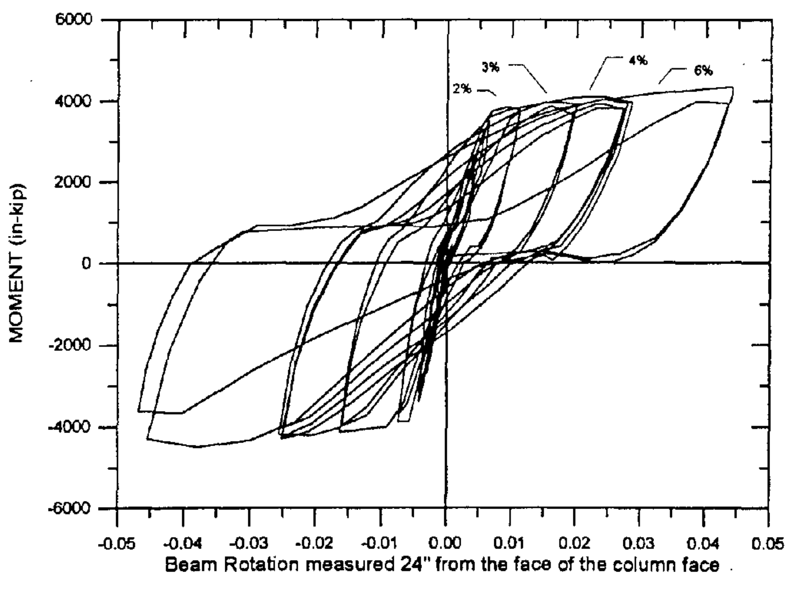

Fig. 8. Beam Moment vs. Rotation: BCEJ1

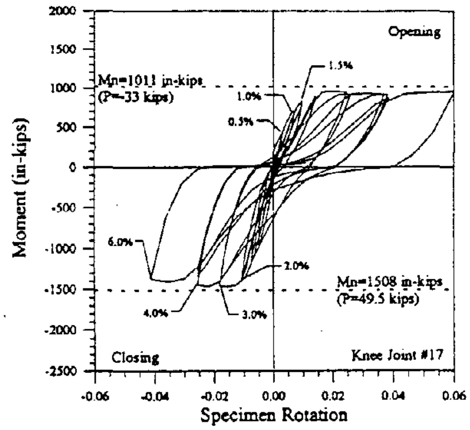

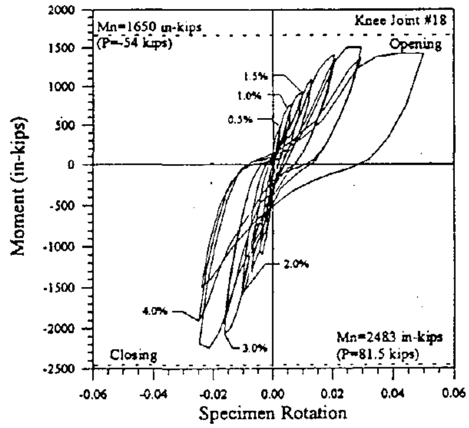

Fig. 9. Beam Moment vs. Specimen Rotation: KJ17 Fig. 10. Beam Moment vs. Specimen Rotation: KJ18

CONCLUSIONS

Results of a experimental and analytical study of knee and exterior joints was summarized and ACI Committee 352 recommendations were assessed. Based on this study, the following conclusions were reached: (1) The joint shear strength value implied for knee joints in ACI 352-91 ($12\sqrt{f_c'}$ psi; $1.0\sqrt{f_c'}$ MPa) is unconservative for the case where no transverse beams are provided. Based on test results, a limiting value of $8\sqrt{f_c'}$ psi ($0.67\sqrt{f_c'}$ MPa) should be used. (2) The use of headed reinforcement in exterior beam-column joints is a viable option and presents no significant design problems. (3) Performance of beam-column knee joints constructed with headed reinforcement performed as well as similar specimens with 90 degree hooks; however, additional transverse reinforcement may be needed to ensure that the heads are adequately restrained against pullout. (4) The use of headed reinforcement allows for easier construction by alleviating congestion of joint reinforcement, and thus easing concrete placement.

ACKNOWLEDGEMENTS

The work presented in this report was supported by funds from the U.S. National Science Foundation for the conventionally reinforced specimens and Headed Reinforcement Canada and ERICO USA for the specimens with headed reinforcement. Opinions, findings, conclusions, and recommendations in this paper are those of the authors and do not necessarily represent those of the sponsors.

REFERENCES

"Recommendations for Design of Beam-Column Joints in Monolithic Reinforced Concrete Structures," ACI 352-91, ASCE-ACI Committee 352, American Concrete Institute, Detroit, MI, 1991.

Bode, H.; Roik, K., "Headed Studs - Embedded in Concrete and Loaded in Tension," *ACI Special Publication SP103-4*, 1987, pp. 61-88.

Cote, P. A.; Wallace, J. W., "A Study of Reinforced Concrete Knee Joints Subjected To Cyclic Lateral," *Report No. CU/CEE-94/04*, Department of Civil and Environmental Engineering, Clarkson University, Potsdam, NY 13699-5710, February 1994.

Gupta, P.; Wallace, J. W., "Cyclic Lateral Load Behavior of Exterior Beam-Column Joints Utilizing ERICO TERMINATOR Anchors," *Report No. CU/CEE-96/??*, Department of Civil and Environmental Engineering, Clarkson University, Potsdam, NY 13699-5710, 1996 (In Process).

McConnell, S. W.; Wallace, J.W., "Behavior of Reinforced Concrete Beam-Column Knee Joints Subjected To Reversed Cyclic Loading," *Report No. CU/CEE-95/07*, Department of Civil and Environmental Engineering, Clarkson University, Potsdam, NY 13699-5710.

SEISMIC REHABILITATION USING SUPPLEMENTAL DAMPING SYSTEMS

A. S. WHITTAKER, M. C. CONSTANTINOU, and C. A. KIRCHER

(AW) Earthquake Engineering Research Center, University of California, Berkeley, CA, 94804
(MC) State University of New York, Buffalo, NY, 14260
(CAK) Kircher and Associates, Mountain View, CA, 94041

ABSTRACT

Recent earthquakes in the United States (1989 Loma Prieta and 1994 Northridge) and Japan (1995 Hyogo-ken-Nanbu) have clearly demonstrated the need to rehabilitate (retrofit) vulnerable buildings. On the West Coast of the United States, vulnerable construction generally predates the mid 1970's, although there exist many more modern buildings requiring retrofit. Such rehabilitation in the United States has been hampered by the lack of guidelines and commentary for design professionals and building officials.

Guidelines and commentary for the seismic rehabilitation of buildings are now being developed in the United States with funding from the Federal Emergency Management Agency (FEMA). The project will be completed in 1997. One key component of the project is incorporating provisions for supplemental damping systems. This effort is timely because damping hardware is now being proposed for seismic rehabilitation.

This paper describes the means by which energy dissipation hardware is classified for analysis purposes, and outlines modeling and analysis procedures being developed for use with energy dissipation systems. Recommendations for further study are also described.

KEYWORDS

analysis; damping; energy; nonlinear; pushover; rehabilitation; seismic.

INTRODUCTION

Seismic framing systems must be capable of absorbing and dissipating energy in a non-degrading manner for many cycles of substantial deformation. In modern conventional construction, energy dissipation occurs in plastic hinge zones in members of the structural frame that routinely form part of the gravity load resisting system. Such energy dissipation is accompanied by substantial nonlinear response (characterized by ductility) and constitutes damage to the seismic framing system. As evinced by experiences following the 1994 Northridge earthquake, structural damage is often difficult and expensive to repair following an earthquake. Older construction is generally characterized by little to no ductility, rapid stiffness and strength degradation following yielding, and poor energy dissipation characteristics.

Recent earthquakes in the United States (1989 Loma Prieta and 1994 Northridge) and Japan (1995 Hyogo-ken-Nanbu) have clearly demonstrated the need to retrofit vulnerable buildings. On the West Coast of the United States, vulnerable construction generally predates the mid 1970's, although there exist many more modern buildings requiring retrofit.

One major goal of seismic rehabilitation is to limit deformations to protect the older construction from damage, that is, to prevent substantial nonlinear response in the older, nonductile framing elements. The designer, using conventional construction such as reinforced concrete shear walls and steel braced frames, has the objective of forcing the seismic energy dissipation (damage) into the new, ductile elements. The drawback to this strategy is that many of the new elements may be substantially damaged following an earthquake. This damage may be difficult and expensive to repair.

The objective of adding damping hardware to existing construction is to dissipate much of the earthquake-induced energy in *disposable* elements not forming part of the gravity framing system — thus permitting easy, and relatively inexpensive, replacement (if necessary) following an earthquake. As such, the implementation of damping hardware is conceptually attractive for seismic rehabilitation. However, the absence of guidance and resource material has hindered the use of such hardware.

Widespread seismic rehabilitation of older construction in the United States has been hampered by the lack of guidelines for design professionals and building officials. This lack of resource material is being rectified by the preparation of guidelines and commentary for seismic rehabilitation — a project widely known as ATC-33. This national project is being funded by the Federal Emergency management Agency. One key component of Project ATC-33 is to develop procedures for the implementation of supplemental damping systems.

This paper is loosely based on the commentary to the guidelines that the authors developed for the 75 percent submittal for Project ATC-33. The paper describes the means by which damping (energy dissipation) hardware is classified for analysis purposes, and outlines modeling and analysis procedures being developed for use with damping systems. Gaps in current knowledge are identified at the end of the paper.

Much experimental research has been conducted on the use of supplemental damping hardware for new and retrofit seismic construction. This research is not described in the paper. The reader is referred to Aiken (1990, 1993), Bergman (1993), Chang (1991), Constantinou (1993), Reinhorn (1995), and Whittaker (1989) for detailed information.

CLASSIFICATION OF SUPPLEMENTAL DAMPING SYSTEMS

On the basis of their behavior, passive supplemental dampers are classified in the ATC-33 *Guidelines* and *Commentary* (ATC, 1995) as hysteretic, velocity-dependent, or other. Examples of hysteretic systems include devices based on yielding of metal and friction. Figure 1 shows sample force-displacement loops of hysteretic dampers. Examples of velocity-dependent systems include dampers consisting of viscoelastic solid materials, dampers operating by deformation of viscoelastic fluids (e.g., viscous shear walls), and dampers operating by forcing fluid through an orifice (e.g., viscous fluid dampers). Figure 2 illustrates the behavior of these velocity-dependent systems.

Other systems have characteristics which cannot be classified by one of the basic types depicted in either Figs. 1 or 2. Examples are dampers made of shape memory alloys, frictional-spring assemblies with recentering capabilities and fluid restoring force/damping dampers. For information on these dampers, the reader is referred to ATC (1993), EERI (1993) and Soong and Constantinou (1994). Only hysteretic and velocity-dependent dampers are discussed in this paper.

Some types of supplemental damping systems can substantially change the force-displacement response of a building by adding strength and stiffness. Such influence is demonstrated in Fig. 3 for metallic-yielding, friction, and viscoelastic dampers. Note that these figures are schematic only and that the force-displacement relation for the central figure assumes that the framing supporting the friction dampers is rigid. Viscous damping systems will generally not substantially change the force-displacement response of a building.

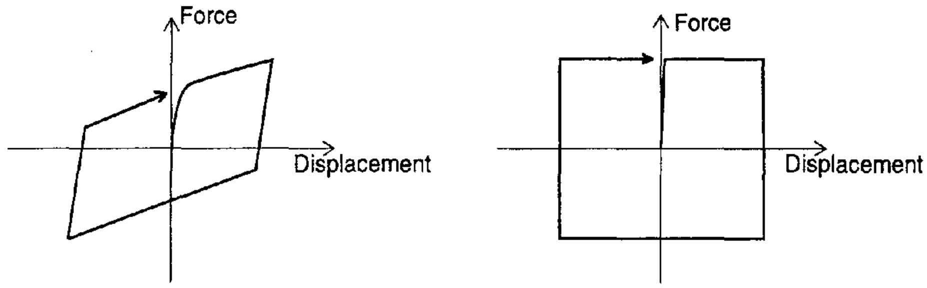

a. Metallic-yielding damper b. Friction damper

Fig. 1. Force-displacement relations for hysteretic dampers

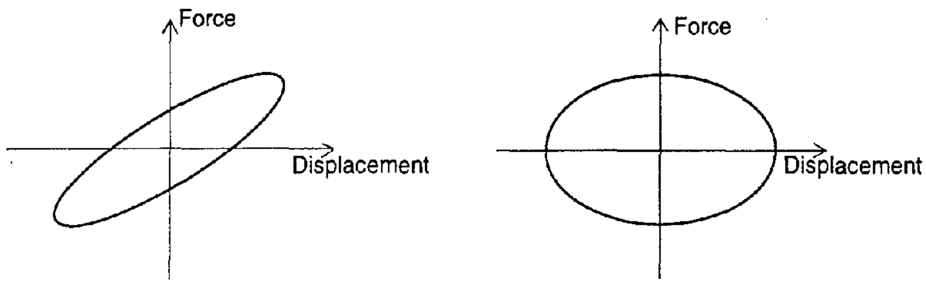

a. Viscoelastic damper b. Viscous damper

Fig. 2. Force-displacement relations for velocity-dependent dampers

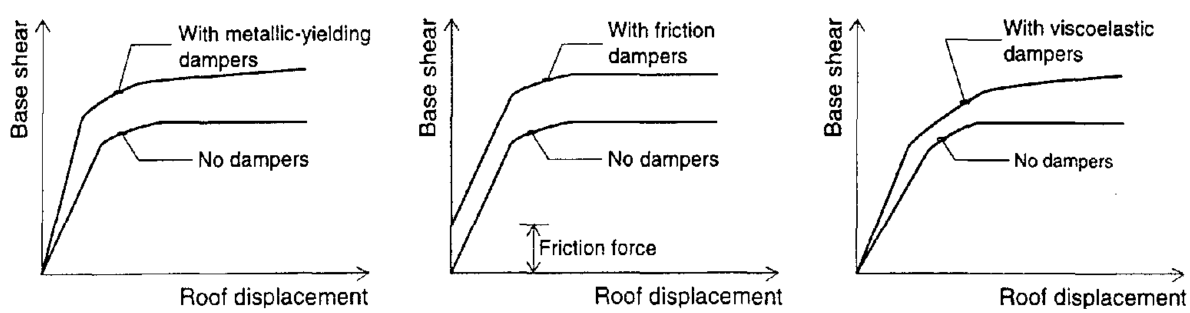

Fig. 3. Influence of selected supplemental dampers on the force-displacement relation of a building

CHARACTERIZATION OF SUPPLEMENTAL DAMPING SYSTEMS

For the purpose of this discussion, damping systems are classified as either hysteretic or velocity-dependent. The following discussion provides information on the characterization of individual dampers for use in modeling and nonlinear analysis.

Hysteretic Dampers

Hysteretic dampers exhibit bilinear or trilinear hysteretic, elasto-plastic or rigid-plastic (frictional) behavior, which can be easily captured with structural analysis software currently in the marketplace. Details on the modeling of metallic-yielding dampers may be found in Whittaker (1989); the steel dampers described by Whittaker exhibit stable force-displacement response and no temperature dependence. Friction devices are described by Aiken (1990) and Nims (1993); the devices tested by Aiken and Nims responded with box-like hysteresis and no temperature dependence.

Velocity-Dependent Dampers

Solid viscoelastic dampers typically consist of constrained layers of viscoelastic polymers. They exhibit viscoelastic solid behavior with mechanical properties dependent on frequency, temperature and amplitude of motion. A force-displacement loop of a viscoelastic solid device under sinusoidal motion of amplitude Δ_0 and frequency ω is shown in Fig. 4a. The force in the damper may be expressed as:

$$F = K_{eff}\Delta + C\dot{\Delta} \tag{1}$$

where K_{eff} is the effective stiffness, C is the damping coefficient, and Δ and $\dot{\Delta}$ are the relative displacement and relative velocity between the ends of the damper, respectively. The effective stiffness of the damper is calculated as:

$$K_{eff} = \frac{|F^+| + |F^-|}{|\Delta_0^+| + |\Delta_0^-|} \tag{2}$$

where F^+ and F^- are the forces in the damper at damper displacements Δ_0^+ and Δ_0^-, respectively. The damping coefficient (C) is calculated as:

$$C = \frac{W_D}{\pi\omega\Delta_0^2} \tag{3}$$

where W_D is the area enclosed within the hysteresis loop. The effective stiffness is also termed the storage stiffness (K'). The damping coefficient C is often defined in terms of the loss stiffness (K'') as follows:

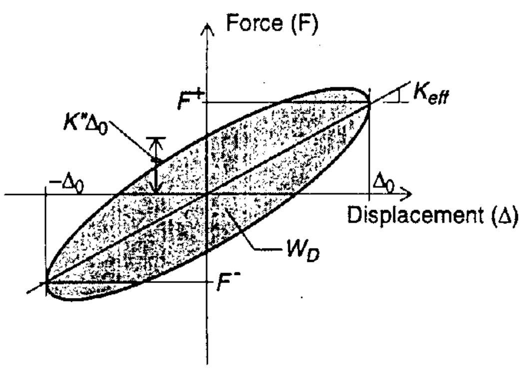

a. Viscoelastic damper

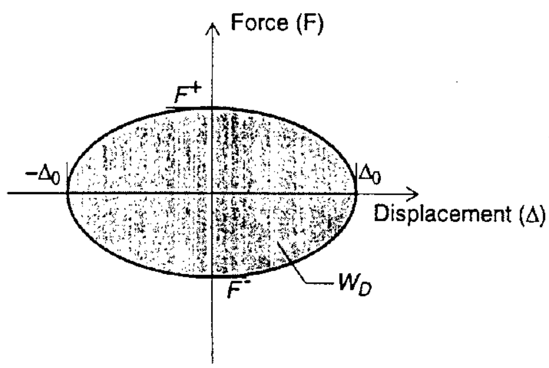

b. Viscous damper

Fig. 4. Parameter definition for velocity-dependent dampers

$$C = \frac{K''}{\omega} \tag{4}$$

Parameters K_{eff} and C are dependent on the frequency, temperature and amplitude of motion; the frequency and temperature dependence of viscoelastic polymers generally vary as a function of the composition of the polymer (Bergman, 1993). Modeling of viscoelastic solid behavior over a wide range of frequencies is possible by use of advanced models of viscoelasticity (Kasai, 1993). Simpler models such as the standard linear solid model (a spring in series with a Kelvin model), which can be implemented in commercially-available structural analysis software, are capable of modeling behavior over a small range of frequencies, which will generally be satisfactory for most rehabilitation projects.

Fluid viscoelastic devices which operate on the principle of deformation (shearing) of viscoelastic fluids (ATC, 1993) have behavior which resembles that of solid viscoelastic devices. However, fluid viscoelastic devices have zero effective stiffness under static loading conditions. Fluid and solid viscoelastic devices are distinguished by the ratio of the loss stiffness (K'') to the effective or storage stiffness (K'). This ratio approaches infinity for fluid devices and zero for solid viscoelastic devices as the loading frequency approaches zero. Fluid viscoelastic behavior may be modeled with advanced models of viscoelasticity (Makris, 1993). However, for most practical purposes, the Maxwell model (a spring in series with a dashpot) can be used to model fluid viscoelastic devices.

Pure viscous behavior may be produced by forcing fluid through an orifice (Soong and Constantinou, 1994; Constantinou, 1993). The force output of these devices (Fig. 4b) has the general form:

$$F = C_0|\dot{\Delta}|^{\alpha}\,\mathrm{sgn}\,(\dot{\Delta}) \tag{5}$$

where $\dot{\Delta}$ is the velocity, α is an exponent in the range of 0.1 to 2.0, and sgn is the signum function. The simplest form is the linear fluid damper for which the exponent is equal to 1. In this paper, discussion on fluid viscous devices is limited to linear fluid dampers; for a detailed treatment of nonlinear fluid dampers, the reader is referred to Soong and Constantinou (1994)

ANALYSIS AND MODELING PROCEDURES

Two analysis procedures have been developed for the implementation of supplemental damping systems. To date, only procedures for simplified nonlinear analysis (also known as *pushover* analysis) and nonlinear dynamic analysis have been drafted for Project ATC-33. Simplified elastic analysis procedures are not yet available. The application of the nonlinear static analysis procedure, to the design of different damping systems for the seismic rehabilitation of buildings, is described below. The reader is referred to the list of references at the end of this paper, and the literature in general for information on nonlinear dynamic analysis.

A discussion on modeling supplemental dampers for the purpose of nonlinear static analysis follows the description of the nonlinear static analysis procedure.

Nonlinear Static Analysis Procedure

The purpose of this procedure is to evaluate the response of a rehabilitated building by a procedure which is simpler than nonlinear response history analysis but more realistic and comprehensive than linear elastic analysis. The simplified nonlinear analysis procedure may be used for the analysis of rehabilitated buildings incorporating supplemental dampers provided (a) the building with the energy dissipation devices is classified as regular in plan, (b) biaxial effects in framing members that resist seismic forces in orthogonal directions are appropriately accounted for, and (c) the fundamental modal mass in each principle translational direction exceeds 80 percent of the total mass in that direction.

In the nonlinear static analysis procedure the structure is represented by a two-or-three-dimensional mathematical model which accounts for all important response characteristics, including those of the supplemental damping system. (The supplemental damping system is composed of the dampers and the structural members that transfer forces between the dampers and the remainder of the seismic framing system.) Lateral loads are applied in a predetermined pattern and the structure is incrementally pushed to a target displacement (D). A force-displacement relation for the building is thereby developed. Typically, the force variable is base shear and the displacement variable is roof displacement. The target displacement is established by analysis of the seismic hazard. In Project ATC-33, the seismic hazard is characterized by a 5-percent damped response spectrum. Further, the calculation of the target displacement is based on the assumption that for periods greater than approximately 0.5 second (for a rock site), displacements are preserved in a mean sense, that is, mean elastic displacements are approximately equal to mean inelastic displacements. (Note that the degree of scatter in the ratio of elastic and inelastic displacements may be substantial.)

The reader is referred to ATC (1995) and the literature for additional information on nonlinear static analysis.

Modeling Supplemental Dampers

Hysteretic Dampers. Hysteretic energy dissipation devices should be explicitly modeled by bilinear, elasto-plastic or rigid-plastic elements for nonlinear static analysis. There are no rigorous procedures for the linearization of hysteretic dampers. The mathematical model of the rehabilitated building should include all important characteristics of the hysteretic dampers and their supporting framing. The fundamental period of this model should be used to estimate the target displacement.

Velocity-dependent Dampers. The only velocity-dependent dampers currently considered for seismic rehabilitation applications are viscoelastic and viscous dampers. Accordingly, only these types of velocity-dependent dampers are discussed in this section.

Viscoelastic dampers exhibit effective stiffness which is generally dependent on frequency of motion, amplitude of motion, and temperature. Viscoelastic devices should be modeled for the purpose of nonlinear analysis as either linear or nonlinear springs representing the effective stiffness of the device at a fixed temperature and frequency. Multiple analyses using different temperature-based effective stiffnesses should be undertaken to address the temperature dependence of the viscoelastic material. The effective stiffness calculation should be based on an excitation frequency equal to the inverse of the effective period of the rehabilitated building (including the viscoelastic dampers) at the target displacement.

The mathematical model of the rehabilitated building must include the stiffness characteristics of the viscoelastic dampers and their supporting framing. The fundamental period of this model should be used to estimate the target displacement from a response spectrum that is modified from the 5-percent spectrum to account for the viscous damping provided by the dampers.

Modification of the spectral displacement demand is a key step in the analysis process. The first mode damping (ξ) provided by the viscoelastic dampers can be estimated as follows. The energy dissipated (W_D) in one cycle of loading to the target displacement can be estimated as:

$$W_D = \frac{2\pi^2}{T_{eff}} \sum C_j \Delta_{rj}^2 (\cos\theta_j)^2 \tag{6}$$

where C_j is the damping coefficient of damper j, θ_j is the angle of inclination of damper j to the horizontal, Δ_{rj} is the relative axial displacement of the ends of damper j at the target displacement (D), T_{eff} is the effective fundamental period of building at the target displacement, and the summation extends over all dampers. This calculation is iterative because the target displacement is a function of the damping provided by the viscoelastic energy dissipators.

The first mode damping provided by the viscoelastic dampers can be estimated as:

$$\xi = \frac{1}{2\pi}\left(\frac{W_D}{KD^2}\right) \tag{7}$$

where W_D is calculated per eq. (6), and K is the effective stiffness of the rehabilitated building at the target displacement (D). The modal damping ratio used to calculate the target displacement is then calculated by adding (a) the first mode damping provided by the viscoelastic dampers, and (b) the structural damping in the building frame — typically assumed to be 5 percent of critical. This iterative procedure is complete when the modal damping ratio used to calculate W_D is approximately equal to the modal damping ratio calculated following the subsequent evaluation of eq. (7).

The member forces calculated from the nonlinear static analysis do not include the viscous forces developed in the viscoelastic dampers. Separate analysis should be performed to capture the viscous forces. The reader is referred to ATC (1995) for further information.

Fluid viscous dampers do not exhibit stiffness unless the excitation frequency is high. As such, the model of the rehabilitated building need not include such dampers for the purpose of nonlinear static analysis — the viscous dampers serve only to improve the energy dissipation characteristics of the rehabilitated building. The fundamental period of the mathematical model should be used to estimate the target displacement from a response spectrum that is modified from the 5-percent spectrum to account for the damping provided by the viscous dampers. If the response of the viscous dampers is temperature dependent, multiple analyses will be required to capture the maximum force output and minimum energy dissipation of the dampers.

Modification of the spectral displacement demand is a key step in the analysis process. The first mode damping ratio (ξ) provided by the viscous dampers can be estimated by calculation of the energy dissipated (W_D) by all of the dampers in the building, in one cycle of loading to the target displacement, as follows:

$$W_D = \frac{2\pi^2}{T_{eff}} \sum C_{0j} \Delta_{rj}^2 (\cos\theta_j)^2 \tag{8}$$

where C_{0j} is the damping coefficient of damper j, the summation extends over all dampers, and all other terms are as defined above. This calculation is iterative because the target displacement is a function of the damping provided by the viscous dampers.

The remainder of the procedure for viscous dampers is virtually identical to that described above for viscoelastic dampers and is not repeated here. Following convergence of the procedure, the effects of forces in the viscous dampers must be included in the calculation of the maximum frame forces. The reader is referred to ATC (1995) for more information.

SUMMARY AND CONCLUSIONS

Recent damaging earthquakes have demonstrated that substantial earthquake risk mitigation can only be realized in the United States through rehabilitation of the vulnerable building stock. This effort will be made easier by the publication and promulgation of the ATC-33 Guidelines and Commentary (ATC, 1995). A key component of the ATC-33 project is the development of guidelines for the implementation of hysteretic and velocity-dependent damping hardware. This paper has been based in part on the authors' work on the ATC-33 project. Background information on selected types of damping hardware, and guidance on modeling dampers and the use of nonlinear static analysis for seismic rehabilitation has been presented. Similar procedures can be used for new construction.

The authors' research work in the field of supplemental damping, and activities associated with Project ATC-33, have identified substantial gaps in the knowledge base. Such gaps include (a) a poor understanding of the interaction between hysteretic and velocity-dependent damping, (b) the lack of simplified elastic procedures for the implementation of supplemental dampers in new and retrofit construction, (c) inadequate verification of the nonlinear static analysis procedure, and (d) a paucity of information on optimal distributions of supplemental dampers. It is recommended that these gaps in our knowledge be the subject of focused research in the near future.

ANALYTICAL STUDIES OF PRE-NORTHRIDGE STEEL MOMENT-RESISTING CONNECTIONS

TZONG-SHUOH YANG† and EGOR PAUL POPOV‡

†ISEC, Inc., 505 Montgomery, Suite 1640, San Francisco, CA 94111, USA.
‡Department of Civil Engineering, University of California, Berkeley, CA 94720, USA.

ABSTRACT

This paper presents the analytical studies of pre-Northridge earthquake welded beam-to-column connections used in typical moment-resisting steel frames. This paper assumes no defects in welding material, welding procedure, and workmanship. The purpose of these studies is to give explanations on both fracture locations and failure modes of aforementioned connections in rational ways. The stress concentration at the juncture of welded beam flange and column flange is analyzed by three-dimensional elastic-plastic finite elements. The result clearly explains why the weak beam flange breaks off right at the weld due to triaxial actions in that region with no apparent yielding. The effect of backing bar in connection failure is analyzed next by fracture mechanics methods. The unfused backing bar surface next to the column flange is interpreted as an artificial crack. Flange tension by bending of beam opens the artificial crack and initiates the rupture. The stress intensity factors at the artificial crack tips of both top and bottom backing bars are calculated by the J-integral method. The result explains why the rupture mostly started at the bottom flange but not at the top flange. Finally, the analytical cyclic load-deflection curves are compared with the SAC[1] full-size specimens tested at UC Berkeley. Good agreements between the analytical results and the experimental tests conclude the paper.

KEYWORDS

Steel moment-resisting connection; brittle failure; backing bar; fracture mechanics; nonlinear finite element analysis; stress intensity factor; J-integral; cyclic test; hysteresis.

INTRODUCTION

Before the 1994 Northridge earthquake, steel moment-resisting frames (MRFs) were considered ductile by engineers. The dream was broken suddenly after the earthquake. Many brittle failures were reported throughout the greater Los Angeles area (Youssef *et al.*, 1995). A typical welded beam-to-column moment resisting connection is shown in Fig. 1. The top and bottom flanges of the beam are welded directly to the column by full penetration groove welds. The beam web is bolted or welded to a shear plate, which is attached to the column by welding. The most serious rupture modes of such connections are shown in Fig. 2. The failure modes are catastrophic because they fracture at extremely high speeds without exhibiting prior ductile behavior. This violates the precept of the ductile MRF. This paper is based on a report by the authors (Yang and Popov, 1995).

[1] SAC is an acronym for Structural Engineers Association of California, Applied Technology Council, and California Universities for Research in Earthquake Engineering.

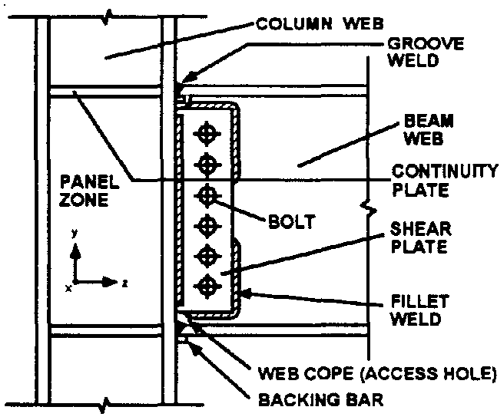

Figure 1: A typical welded beam-to-column connection.

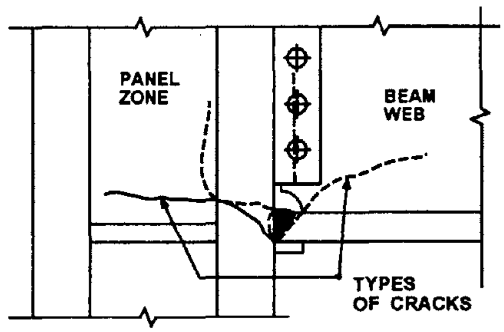

Figure 2: Some failure modes of the welded beam-to-column connection.

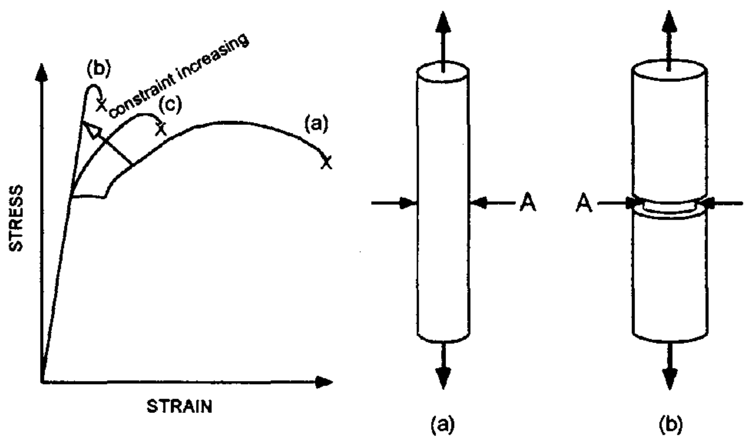

Figure 3: Simple tensile test of steel specimens with the same critical cross section area: (a) cylindrical bar, and (b) grooved cylindrical bar.

PROPERTIES OF STRUCTURAL STEEL

The stress-strain curve of a small diameter uniform cylindrical steel bar ((a) in Fig. 3) loaded longitudinally to failure, will be ductile (curve (a) in Fig. 3). A small diameter bar of uniform cross-section is not restrained in the lateral direction, and allows Poisson contraction, which leads to specimen necking down and the development of shear slip layers (Lueders lines) during failure. However, for a cylindrical bar with a groove or notch, such as bar (b) in Fig. 3, even though the cross sectional area at the groove is the same as bar (a), the tensile stress-strain curve is completely different. When loaded in tension, the grooved part will have the largest stress, due to the constraint of the larger sections outside the groove, no lateral contraction or shear flow can develop at the groove. The failure of bar (b) is caused by triaxial action resulting in a brittle failure with no apparent yielding. Its stress-strain curve is similar to curve (b) in Fig. 3 (MacGregor, 1931). It can be seen in Fig. 1 that the welded beam flange cannot be deformed in both x and y directions because it is welded to a large column flange with continuity plates. The welded beam-to-column connection is essentially like a grooved bar except with a different shape.

Another important fact regarding the mechanical properties of today's steel is that the yield strength of A36 steel is no longer 36 ksi. The average yield strength of A36 steel is about 48 ksi, the ultimate strength of A36 steel is about 70 ksi. The misleading ASTM requirement for minimum strength with no specified maximum results in a melee of actual strengths in use of which the designer is unaware. This prevailing condition makes it impossible to design rationally.

Table 1: Four possible failure types of a steel MRF connection.

Failure Type	Minimum Capacity	Failure Mode
1	C_m^b or C_v^b	beam flange or shear plate rupture
2	C_m^c or C_v^c	fracture through column web or divot pullout from column flange
3	C_{cr}^b	buckling of beam near connection and formation of plastic hinge
4	C_{cr}^c	buckling of column near connection and formation of plastic hinge

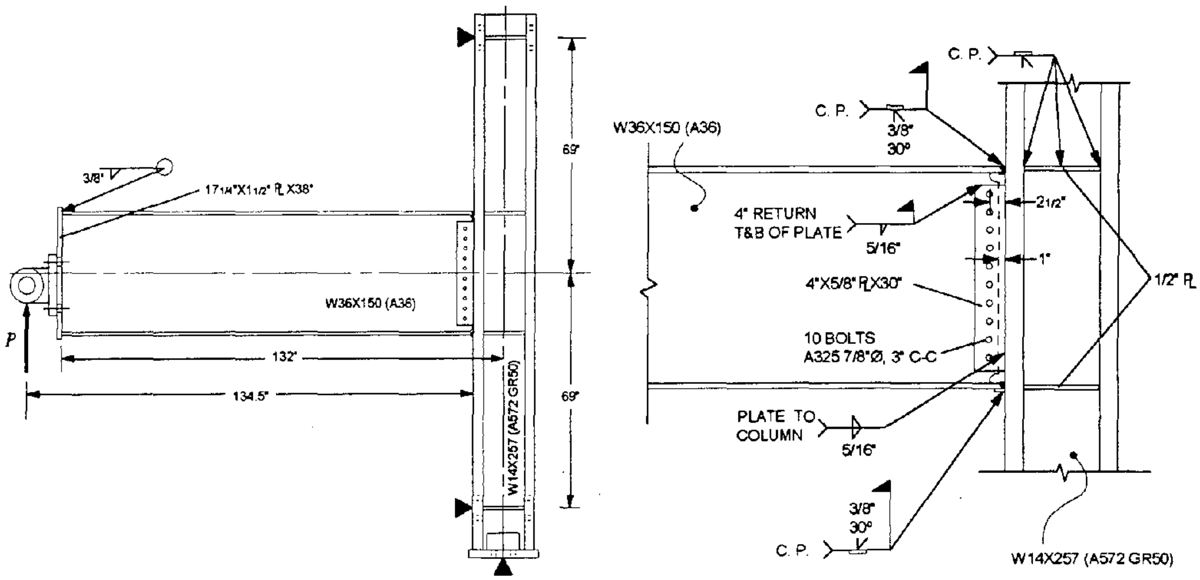

Figure 4: Detail of the SAC PN specimens.

DESIGN STRATEGY

The most essential characteristic of the MRF is the requirement that plastic hinges be formed near connections during severe loading conditions. These plastic hinges provide strength and ductility to dissipate energy hysteretically. As it is impossible to develop large plastic deformation right at the beam-column weld location, the plastic hinges can only be formed at the beam or column section near the connection. The possible failure modes at the connection are given in Table 1. The subscripts m, v and cr are the *moment*, *shear* and *local buckling* capacity of the member, respectively. The superscripts b and c are used to designate *beam* and *column*, respectively. The actual resisting capacity of a connection is controlled by the minimum of these six values. The minimum resisting capacity is based on the failure type. In Table 1, Types 1 and 2 correspond to sudden brittle fractures and should be avoided. By developing plastic hinges near the connections, Type 3 and 4 mechanisms assure good strength and ductility. For beam flange connections welded directly to the column flange, the resisting capacity C_m^b is always smaller than the ultimate moment capacity of the beam. Therefore, in order to develop a Type 3 mechanism, either cover plates or a non-compact beam section must be used.

THREE SAC PRE-NORTHRIDGE SPECIMEN TESTS

In order to help understand the strength and ductility of the welded moment resisting connections, three specimens have been fabricated according to the standards used before the 1994 Northridge earthquake. These were tested at UC Berkeley under the guidance of the SAC Joint Venture. The dimensions and and connection detail of these specimens are shown in Fig. 4. Cyclic loads are applied to the beam tip by an actuator. During fabrication of the specimens, two A572-Gr50 beams were erroneously used for the first two specimens PN1 and PN2. The third specimen PN3 was made correctly. The material properties of these three specimens based on mill certificates are given in Table 2. Notice that the yield strength of these specimens is much higher than the ASTM minimum. The test results of these specimens are shown in Table 3.

Table 2: Material properties of the SAC Joint Venture PN specimens.

Specimen Number	Material Size & Spec	Yield Strength F_y	Ultimate Strength F_u
PN1, PN2 & PN3 Column	W14×257 A572-Gr50	53.5 ksi	72.5 ksi
PN1 & PN2 Beam	W36×150 A572-Gr50	62.6 ksi	74.7 ksi
PN3 Beam	W36×150 A36	56.8 ksi	68.7 ksi

Table 3: Test results of the SAC Joint Venture PN specimens.

Specimen Number	Load (kips)	Displacement Total (inches)	Displacement Beam (inches)	Post-yield cycles	Date & Temperature
PN1 - P_{yield}	154	1.31	1.15	$4\frac{1}{4}$	02/09/95
P_{peak}	225	2.91	2.63		60° F
PN2 - P_{yield}	153	1.34	1.11	$1\frac{1}{4}$	02/16/95
P_{peak}	201	1.94	1.71		50° F
PN3 - P_{yield}	138	1.12	1.02	$4\frac{1}{4}$	02/28/95
P_{peak}	199	3.02	2.88		60° F

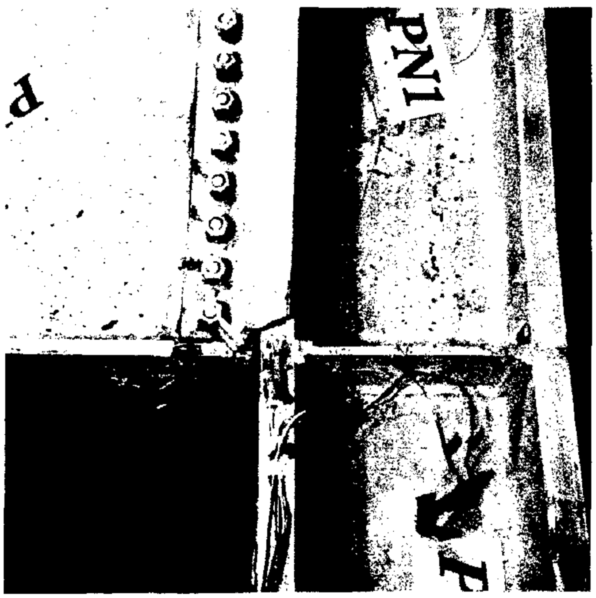

Figure 5: Photograph of SAC specimen PN1 after test.

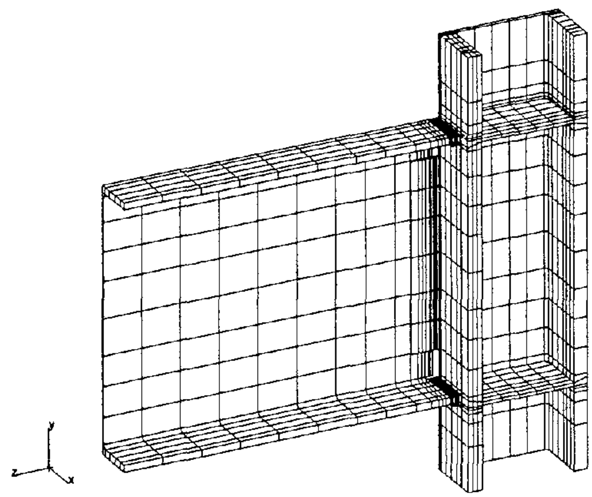

Figure 6: Finite element mesh for SAC Pre-Northridge PN connection. Only one half of the specimen is modeled.

Since the beams of three SAC specimens have compact sections and are made of strong material, the failure modes are of the rapid fracture type. The cracks in the PN1 and PN2 specimens initiated at the center of the bottom beam flange-column juncture. The crack rapidly propagated through the column flange and forked out into two cracks in the column web (Fig. 5). The fracture patterns in PN1 and PN2 were similar except that the post-yield cycles developed by PN2 were smaller. Specimen PN3 had a different fracture pattern. The crack initiated at the center of the bottom beam flange-column juncture, then fractured the entire bottom beam flange. All three specimens performed unsatisfactorily and failed in abrupt fractures.

NONLINEAR FINITE ELEMENT ANALYSIS

The stress distribution in the SAC specimens were modeled on eight-node brick elements using the ABAQUS finite element package (Hibbitt *et al.*, 1994). Part of the element mesh is shown in Fig. 6. The material properties used in the finite element model are based on the Mill Certificates as given in Table 2. The material properties were modeled by von Mises yield criterion with associated plastic flow.

To simulate the experimental loading condition, the same imposed beam tip displacements were used in the finite element computations. The experimental and analytical hysteresis loops for the SAC PN1 specimen are

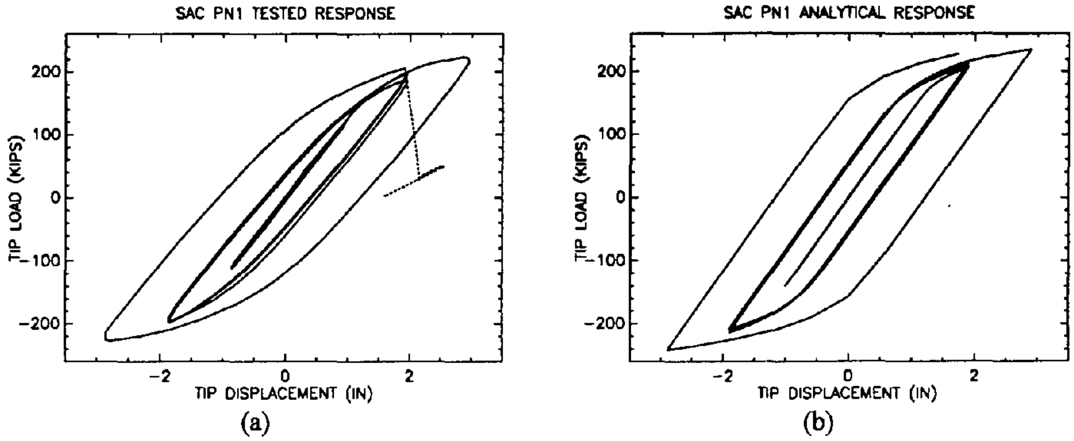

Figure 7: (a) Experimental and (b) analytical hysteresis loops of SAC PN1 specimen.

presented in Figs. 7. Analytical results for SAC PN2 were similar as the design of this specimen was identical to SAC PN1 specimen. The hysteresis loops for SAC PN3 were similar, but were somewhat wider, since this specimen had a beam of A36 steel.

A perspective view of the connection stress distribution is shown in Fig. 8. The highest stressed spots are at the beam flange weld and in the panel zone. The material yielding in the panel zone starts at the center and then gradually expands outward. During the test, the whitewash was continuously breaking off in the panel zone. The SAC PN1/PN2 stress distributions for the bottom beam flange along the line of groove weld are shown in Fig. 9. Curves shown are for beam tip loads of 21, 41, 62, 82, 103, 117, 142, 200, and 225 kips. Shearing stresses are not shown because their values are small.

THE EFFECT OF THE BACKING BAR

If the backing bar has not been removed after welding, the unfused interface between the backing bar and the column flange acts as a fine crack (Fig. 10). Theories for analyzing the stress field near cracks are now well-established (Irwin, 1956). For a crack aligned in the y direction, K is the stress intensity factor (SIF), and is a function of r, θ in the cylindrical polar coordinates of a point with respect to the crack tip. Each case is characterized by the SIF having a spatial distribution of stresses. The unstable fracture occurs when the SIF K at the crack tip reaches a critical value K_c. To prevent a fracture failure, the computed SIF K must be less than the critical SIF, or fracture toughness, K_c. The "artificial crack" between the unfused backing bar and the column flange can be characterized as an edge crack. Tension in a beam flange due to bending opens the crack.

In order to evaluate the SIF at the connection, the backing bars together with the artificial cracks mentioned previously are introduced in the finite element model (see Fig. 6). The J contour integrals along the top and the bottom backing bar crack tip were evaluated following the formulation by Rice (1968). The available critical SIFs for the 1.5-in.-thick A572 Grade 50 specimens were used to approximate the critical SIFs for A572 Grade 50 steel used in the model (Novak, 1976). The approximate equivalent K_I values from the computed J values for the top and the bottom backing bars for PN1 and PN2 are shown in Fig. 11. In the figures, K_I values are plotted against beam width and analysis steps. It can be seen that the largest K_I occurs at the center of the beam flange-backing bar juncture. If the connection fractures, it will start at the point with the largest SIF.

It is instructive to re-plot the largest SIF vs. the applied tip load (see Fig. 12). The growth of K_I due to cyclic load can be seen. The most interesting finding in the figure is that the bottom backing bar K_I at any given time is larger than that of the top backing bar. This clearly explains why most of the connection fractures during the Northridge earthquake initiated at the bottom backing bar. The SAC PN1 and PN2 specimens are theoretically identical, but the PN1 specimen sustains more cycles of loading than PN2. One of the explanations for this is the different temperature. PN2 was tested on a cooler day. The low K_{Ic} value at the lower temperature meant PN2 fractured earlier.

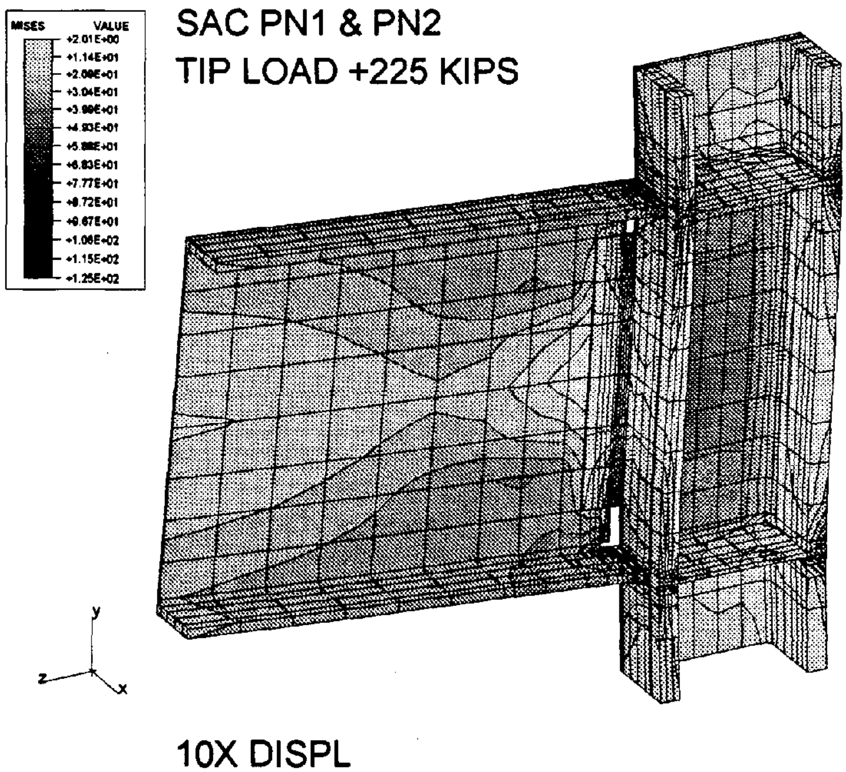

Figure 8: Von Mises Stress contours for SAC PN1/PN2 under 225 kips tip load.

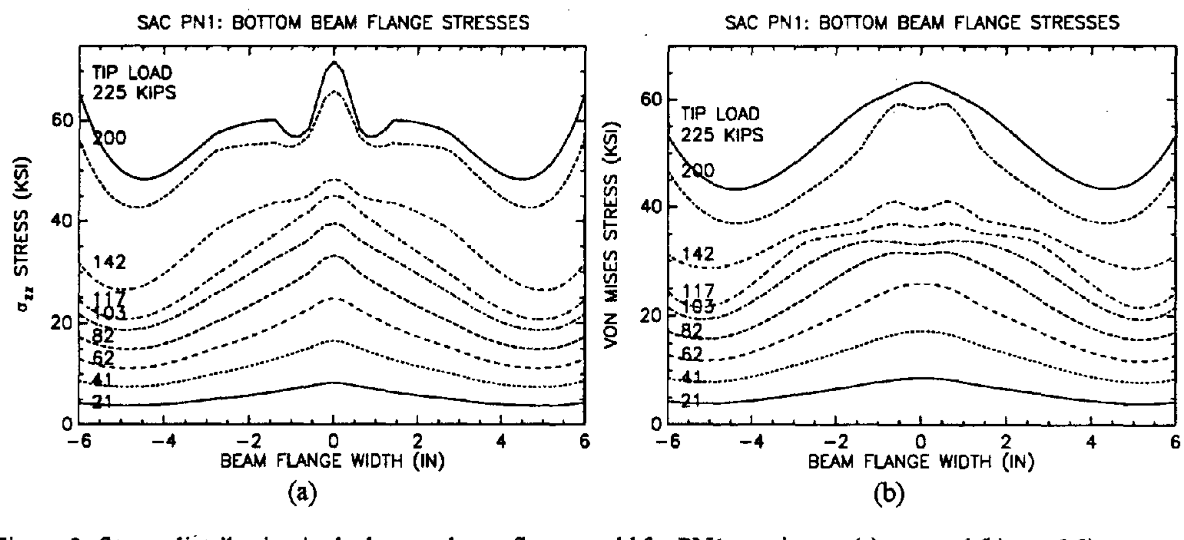

Figure 9: Stress distribution in the bottom beam flange weld for PN1 specimen: (a) σ_{zz}, and (b) von Mises stress.

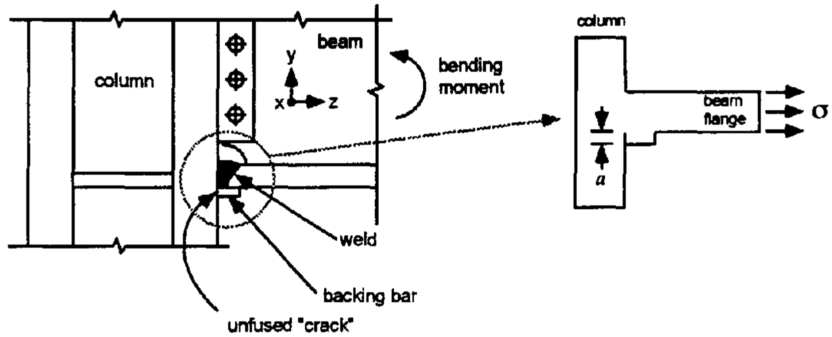

Figure 10: The unfused backing bar surface forms an artificial edge crack.

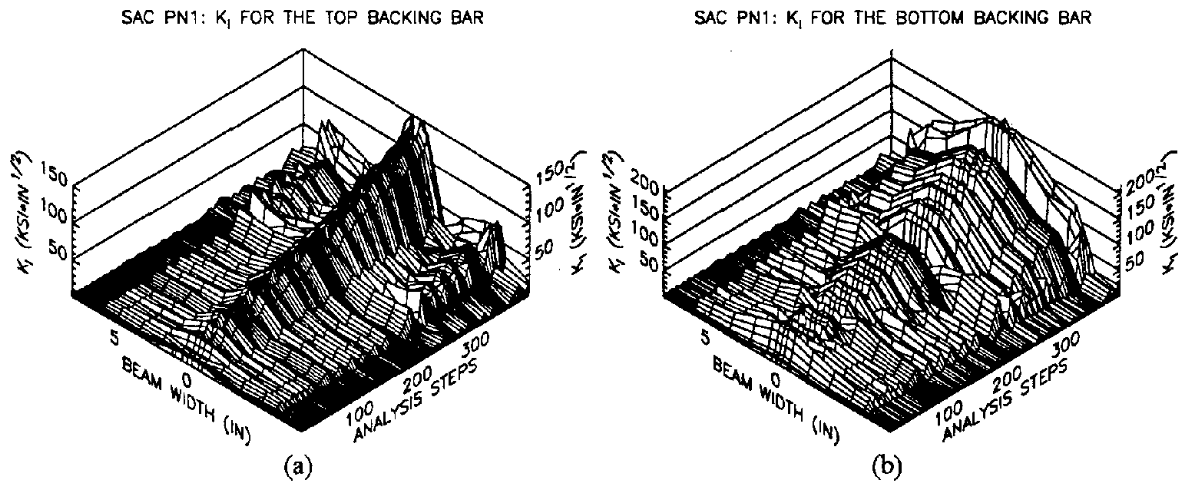

Figure 11: SIFs plotted across beam width and number of analysis steps at (a) top and (b) bottom backing bars.

There are two ways to reduce the deleterious effect of the backing bar. A direct method is to remove it using a carbon arc. Once the backing bar has been removed, the artificial crack no longer exists. The advantage of this method is that the root pass of the weld can be examined. But this method has some probability of damaging a good weld above the backing bar. Another method to reduce the SIF caused by the backing bar is to apply a fillet weld under it to close the crack. But one must use other non-destructive tests to ensure that the root pass of the weld is good. A center crack occurring away from the edges has a smaller SIF.

CONCLUSION

The connection made by directly welding a compact beam flange to a column cannot attain the plastic moment of the beam. Triaxial loading makes steel at a connection fail without exhibiting yielding ductile behavior. This is due to the state of stress and not because of the material property. The demand for ductility should be dependent on the material yielding near the connection area.

Material properties of steel, such as yield strength and ultimate strength, should be regulated to have a narrow range instead of prescribing only the minimum strength. Otherwise, an engineer cannot design a structure with tolerable bounds on response.

The unfused surface between the backing bar and the column can be characterized as an edge crack. During load reversals, the SIF at the bottom backing bar crack is higher than that at the top backing bar, resulting in greater probability of initial fracture at the bottom weld during an earthquake. Welded connections exposed to outside temperatures should be designed very carefully because steel has a lower critical SIF at low temperatures.

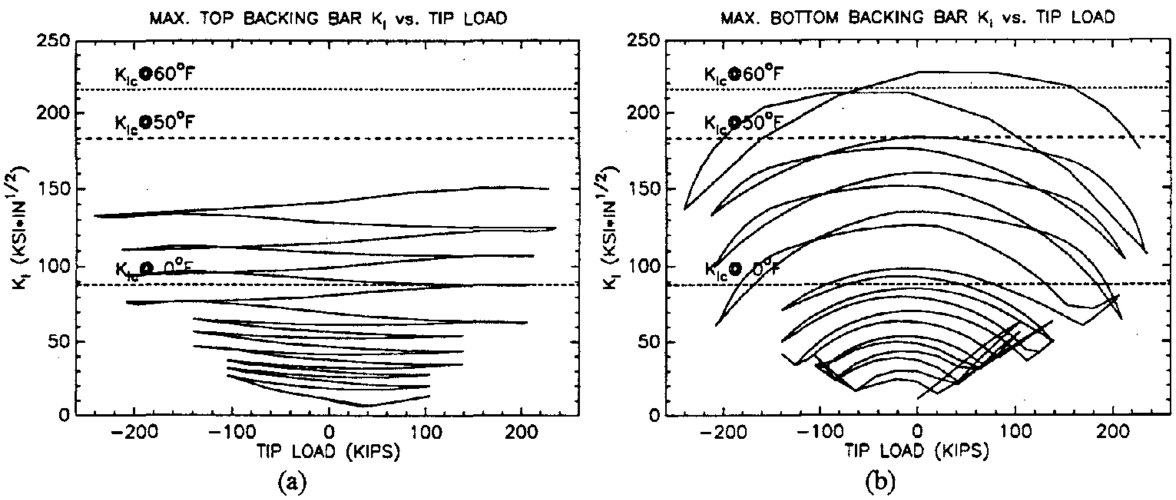

Figure 12: Maximum SIFs vs. tip load at (a) top and (b) bottom backing bars for SAC PN1 and PN2 specimens.

ACKNOWLEDGEMENTS

This paper was completed with the support of the National Science Foundation under the grant (CMS-9416457) entitled "Re-evaluation of Conventional Seismic Beam-to-Column Flange Steel Connections". Professors Egor P. Popov and Stephen A. Mahin were the co-PIs. Special thanks are due to Drs. S.-C. Liu and M. P. Singh of NSF for encouraging this study. The cooperation of J. O. Malley, SAC Project Director for Topical Investigations, was much appreciated.

REFERENCES

Hibbitt, Karlsson, and Sorensen, Inc. (1994). *ABAQUS Version 5.4.*

Irwin, G. R. (1956). Onset of fast crack propagation in high strength steel and aluminum alloys. *Sagamore Research Conference Proceedings*, **2**, 289–305.

MacGregor, C. W. (1931). The yield point of mild steel. *Transactions of the American Society of Mechanical Engineers*, APM-53-15, 187–200.

Novak, S. R. (1976). Resistance to Plane-Stress Fracture (R-Curve Behavior) of A572 Structural Steel, *ASTM STP 591*. American Society for Testing and Materials, Philadelphia.

Rice, J. R. (1968). A path independent integral and the approximate analysis of strain concentration by notches and cracks. *Journal of Applied Mechanics*, **35**, 379–386.

Yang, T.-S. and Popov, E. P. (1995). Behavior of Pre-Northridge Moment Resisting Steel Connections. *Report No. UCB/EERC-95/08*, Earthquake Engineering Research Center, University of California, Berkeley.

Youssef, N. F. G., Bonowitz, D., and Gross, J. L. (1995). A Survey of Steel Moment-Resisting Frame Buildings Affected by the 1994 Northridge Earthquake. *Report No. NISTIR 5625*, National Institute of Standards and Technology, US Department of Commerce.

EARTHQUAKE ENGINEERING RESEARCH CENTER REPORT SERIES

EERC reports are available from the National Information Service for Earthquake Engineering (NISEE) and from the National Technical Information Service (NTIS). Numbers in parentheses are Accession Numbers assigned by the National Technical Information Service; these are followed by a price code. Contact NTIS, 5285 Port Royal Road, Springfield Virginia, 22161 for more information. Reports without Accession Numbers were not available from NTIS at the time of printing. For a current complete list of EERC reports (from EERC 67-1) and availablity information, please contact University of California, EERC, NISEE, 1301 South 46th Street, Richmond, California 94804-4698.

UCB/EERC-86/01 "A Study of Seismically Resistant Eccentrically Braced Steel Frame Systems," by Kasai, K. and Popov, E.P., January 1986, (PB87 124 178/AS)A14.

UCB/EERC-86/02 "Design Problems in Soil Liquefaction," by Seed, H.B., February 1986, (PB87 124 186/AS)A03.

UCB/EERC-86/03 "Implications of Recent Earthquakes and Research on Earthquake-Resistant Design and Construction of Buildings," by Bertero, V.V., March 1986, (PB87 124 194/AS)A05.

UCB/EERC-86/04 "The Use of Load Dependent Vectors for Dynamic and Earthquake Analyses," by Leger, P., Wilson, E.L. and Clough, R.W., March 1986, (PB87 124 202/AS)A12.

UCB/EERC-86/05 "Two Beam-To-Column Web Connections," by Tsai, K.-C. and Popov, E.P., April 1986, (PB87 124 301/AS)A04.

UCB/EERC-86/06 "Determination of Penetration Resistance for Coarse-Grained Soils using the Becker Hammer Drill," by Harder, L.F. and Seed, H.B., May 1986, (PB87 124 210/AS)A07.

UCB/EERC-86/07 "A Mathematical Model for Predicting the Nonlinear Response of Unreinforced Masonry Walls to In-Plane Earthquake Excitations," by Mengi, Y. and McNiven, H.D., May 1986, (PB87 124 780/AS)A06.

UCB/EERC-86/09 "EACD-3D: A Computer Program for Three-Dimensional Earthquake Analysis of Concrete Dams," by Fok, K.-L., Hall, J.F. and Chopra, A.K., July 1986, (PB87 124 228/AS)A08.

UCB/EERC-86/10 "Earthquake Simulation Tests and Associated Studies of a 0.3-Scale Model of a Six-Story Concentrically Braced Steel Structure," by Uang, C.-M. and Bertero, V.V., December 1986, (PB87 163 564/AS)A17.

UCB/EERC-86/11 "Mechanical Characteristics of Base Isolation Bearings for a Bridge Deck Model Test," by Kelly, J.M., Buckle, I.G. and Koh, C.-G., November 1987, (PB90 262 668)A04.

UCB/EERC-86/12 "Effects of Axial Load on Elastomeric Isolation Bearings," by Koh, C.-G. and Kelly, J.M., November 1987, PB88-179015(A06).

UCB/EERC-87/01 "The FPS Earthquake Resisting System: Experimental Report," by Zayas, V.A., Low, S.S. and Mahin, S.A., June 1987, (PB88 170 287)A06.

UCB/EERC-87/02 "Earthquake Simulator Tests and Associated Studies of a 0.3-Scale Model of a Six-Story Eccentrically Braced Steel Structure," by Whittaker, A., Uang, C.-M. and Bertero, V.V., July 1987, (PB88 166 707/AS)A18.

UCB/EERC-87/03 "A Displacement Control and Uplift Restraint Device for Base-Isolated Structures," by Kelly, J.M., Griffith, M.C. and Aiken, I.D., April 1987, (PB88 169 933)A04.

UCB/EERC-87/04 "Earthquake Simulator Testing of a Combined Sliding Bearing and Rubber Bearing Isolation System," by Kelly, J.M. and Chalhoub, M.S., December 1990, PB92-192962(A09).

UCB/EERC-87/05 "Three-Dimensional Inelastic Analysis of Reinforced Concrete Frame-Wall Structures," by Moazzami, S. and Bertero, V.V., May 1987, (PB88 169 586/AS)A08.

UCB/EERC-87/06 "Experiments on Eccentrically Braced Frames with Composite Floors," by Ricles, J. and Popov, E., June 1987, (PB88 173 067/AS)A14.

UCB/EERC-87/07 "Dynamic Analysis of Seismically Resistant Eccentrically Braced Frames," by Ricles, J. and Popov, E., June 1987, (PB88 173 075/AS)A16.

UCB/EERC-87/08 "Undrained Cyclic Triaxial Testing of Gravels-The Effect of Membrane Compliance," by Evans, M.D. and Seed, H.B., July 1987, (PB88 173 257)A19.

UCB/EERC-87/09 "Hybrid Solution Techniques for Generalized Pseudo-Dynamic Testing," by Thewalt, C. and Mahin, S.A., July 1987, (PB 88 179 007)A07.

UCB/EERC-87/10 "Ultimate Behavior of Butt Welded Splices in Heavy Rolled Steel Sections," by Bruneau, M., Mahin, S.A. and Popov, E.P., September 1987, (PB90 254 285)A07.

UCB/EERC-87/11 "Residual Strength of Sand from Dam Failures in the Chilean Earthquake of March 3, 1985," by De Alba, P., Seed, H.B., Retamal, E. and Seed, R.B., September 1987, (PB88 174 321/AS)A03.

UCB/EERC-87/12 "Inelastic Seismic Response of Structures with Mass or Stiffness Eccentricities in Plan," by Bruneau, M. and Mahin, S.A., September 1987, (PB90 262 650/AS)A14.

UCB/EERC-87/13 "CSTRUCT: An Interactive Computer Environment for the Design and Analysis of Earthquake Resistant Steel Structures," by Austin, M.A., Mahin, S.A. and Pister, K.S., September 1987, (PB88 173 339/AS)A06.

UCB/EERC-87/14 "Experimental Study of Reinforced Concrete Columns Subjected to Multi-Axial Loading," by Low, S.S. and Moehle, J.P., September 1987, (PB88 174 347/AS)A07.

UCB/EERC-87/15 "Relationships between Soil Conditions and Earthquake Ground Motions in Mexico City in the Earthquake of Sept. 19, 1985," by Seed, H.B., Romo, M.P., Sun, J., Jaime, A. and Lysmer, J., October 1987, (PB88 178 991)A06.

UCB/EERC-87/16 "Experimental Study of Seismic Response of R. C. Setback Buildings," by Shahrooz, B.M. and Moehle, J.P., October 1987, (PB88 176 359)A16.

UCB/EERC-87/17 "The Effect of Slabs on the Flexural Behavior of Beams," by Pantazopoulou, S.J. and Moehle, J.P., October 1987, (PB90 262 700)A07.

UCB/EERC-87/18 "Design Procedure for R-FBI Bearings," by Mostaghel, N. and Kelly, J.M., November 1987, (PB90 262 718)A04.

UCB/EERC-87/19 "Analytical Models for Predicting the Lateral Response of R C Shear Walls: Evaluation of their Reliability," by Vulcano, A. and Bertero, V.V., November 1987, (PB88 178 983)A05.

UCB/EERC-87/20 "Earthquake Response of Torsionally-Coupled Buildings," by Hejal, R. and Chopra, A.K., December 1987, PB90-208638(A15).

UCB/EERC-87/21 "Dynamic Reservoir Interaction with Monticello Dam," by Clough, R.W., Ghanaat, Y. and Qiu, X-F., December 1987, (PB88 179 023)A07.

UCB/EERC-87/22 "Strength Evaluation of Coarse-Grained Soils," by Siddiqi, F.H., Seed, R.B., Chan, C.K., Seed, H.B. and Pyke, R.M., December 1987, (PB88 179 031)A04.

UCB/EERC-88/01 "Seismic Behavior of Concentrically Braced Steel Frames," by Khatib, I., Mahin, S.A. and Pister, K.S., January 1988, (PB91 210 898/AS)A11.

UCB/EERC-88/02 "Experimental Evaluation of Seismic Isolation of Medium-Rise Structures Subject to Uplift," by Griffith, M.C., Kelly, J.M., Coveney, V.A. and Koh, C.G., January 1988, (PB91 217 950/AS)A09.

UCB/EERC-88/03 "Cyclic Behavior of Steel Double Angle Connections," by Astaneh-Asl, A. and Nader, M.N., January 1988, (PB91 210 872)A05.

UCB/EERC-88/04 "Re-evaluation of the Slide in the Lower San Fernando Dam in the Earthquake of Feb. 9, 1971," by Seed, H.B., Seed, R.B., Harder, L.F. and Jong, H.-L., April 1988, (PB91 212 456/AS)A07.

UCB/EERC-88/05 "Experimental Evaluation of Seismic Isolation of a Nine-Story Braced Steel Frame Subject to Uplift," by Griffith, M.C., Kelly, J.M. and Aiken, I.D., May 1988, (PB91 217 968/AS)A07.

UCB/EERC-88/06 "DRAIN-2DX User Guide.," by Allahabadi, R. and Powell, G.H., March 1988, (PB91 212 530)A12.

UCB/EERC-88/07 "Theoretical and Experimental Studies of Cylindrical Water Tanks in Base-Isolated Structures," by Chalhoub, M.S. and Kelly, J.M., April 1988, (PB91 217 976/AS)A05.

UCB/EERC-88/08 "Analysis of Near-Source Waves: Separation of Wave Types Using Strong Motion Array Recording," by Darragh, R.B., June 1988, (PB91 212 621)A08.

UCB/EERC-88/09 "Alternatives to Standard Mode Superposition for Analysis of Non-Classically Damped Systems," by Kusainov, A.A. and Clough, R.W., June 1988, (PB91 217 992/AS)A04.

UCB/EERC-88/10 "The Landslide at the Port of Nice on October 16, 1979," by Seed, H.B., Seed, R.B., Schlosser, F., Blondeau, F. and Juran, I., June 1988, (PB91 210 914)A05.

UCB/EERC-88/11 "Liquefaction Potential of Sand Deposits Under Low Levels of Excitation," by Carter, D.P. and Seed, H.B., August 1988, (PB91 210 880)A15.

UCB/EERC-88/12 "Nonlinear Analysis of Reinforced Concrete Frames Under Cyclic Load Reversals," by Filippou, F.C. and Issa, A., September 1988, (PB91 212 589)A07.

UCB/EERC-88/13 "Implications of Recorded Earthquake Ground Motions on Seismic Design of Building Structures," by Uang, C.-M. and Bertero, V.V., November 1988, (PB91 212 548)A06.

UCB/EERC-88/14 "An Experimental Study of the Behavior of Dual Steel Systems," by Whittaker, A.S. , Uang, C.-M. and Bertero, V.V., September 1988, (PB91 212 712)A16.

UCB/EERC-88/15 "Dynamic Moduli and Damping Ratios for Cohesive Soils," by Sun, J.I., Golesorkhi, R. and Seed, H.B., August 1988, (PB91 210 922)A04.

UCB/EERC-88/16 "Reinforced Concrete Flat Plates Under Lateral Load: An Experimental Study Including Biaxial Effects," by Pan, A. and Moehle, J.P., October 1988, (PB91 210 856)A13.

UCB/EERC-88/17 "Earthquake Engineering Research at Berkeley - 1988," by EERC, November 1988, (PB91 210 864)A10.

UCB/EERC-88/18 "Use of Energy as a Design Criterion in Earthquake-Resistant Design," by Uang, C.-M. and Bertero, V.V., November 1988, (PB91 210 906/AS)A04.

UCB/EERC-88/19 "Steel Beam-Column Joints in Seismic Moment Resisting Frames," by Tsai, K.-C. and Popov, E.P., November 1988, (PB91 217 984/AS)A20.

UCB/EERC-88/20 "Base Isolation in Japan, 1988," by Kelly, J.M., December 1988, (PB91 212 449)A05.

UCB/EERC-89/01 "Behavior of Long Links in Eccentrically Braced Frames," by Engelhardt, M.D. and Popov, E.P., January 1989, (PB92 143 056)A18.

UCB/EERC-89/02 "Earthquake Simulator Testing of Steel Plate Added Damping and Stiffness Elements," by Whittaker, A., Bertero, V.V., Alonso, J. and Thompson, C., January 1989, (PB91 229 252/AS)A10.

UCB/EERC-89/03 "Implications of Site Effects in the Mexico City Earthquake of Sept. 19, 1985 for Earthquake-Resistant Design Criteria in the San Francisco Bay Area of California," by Seed, H.B. and Sun, J.I., March 1989, (PB91 229 369/AS)A07.

UCB/EERC-89/04 "Earthquake Analysis and Response of Intake-Outlet Towers," by Goyal, A. and Chopra, A.K., July 1989, (PB91 229 286/AS)A19.

UCB/EERC-89/05 "The 1985 Chile Earthquake: An Evaluation of Structural Requirements for Bearing Wall Buildings," by Wallace, J.W. and Moehle, J.P., July 1989, (PB91 218 008/AS)A13.

UCB/EERC-89/06 "Effects of Spatial Variation of Ground Motions on Large Multiply-Supported Structures," by Hao, H., July 1989, (PB91 229 161/AS)A08.

UCB/EERC-89/07 "EADAP - Enhanced Arch Dam Analysis Program: Users's Manual," by Ghanaat, Y. and Clough, R.W., August 1989, (PB91 212 522)A06.

UCB/EERC-89/08 "Seismic Performance of Steel Moment Frames Plastically Designed by Least Squares Stress Fields," by Ohi, K. and Mahin, S.A., August 1989, (PB91 212 597)A05.

UCB/EERC-89/09 "Feasibility and Performance Studies on Improving the Earthquake Resistance of New and Existing Buildings Using the Friction Pendulum System," by Zayas, V., Low, S., Mahin, S.A. and Bozzo, L., July 1989, (PB92 143 064)A14.

UCB/EERC-89/10 "Measurement and Elimination of Membrane Compliance Effects in Undrained Triaxial Testing," by Nicholson, P.G., Seed, R.B. and Anwar, H., September 1989, (PB92 139 641/AS)A13.

UCB/EERC-89/11 "Static Tilt Behavior of Unanchored Cylindrical Tanks," by Lau, D.T. and Clough, R.W., September 1989, (PB92 143 049)A10.

UCB/EERC-89/12 "ADAP-88: A Computer Program for Nonlinear Earthquake Analysis of Concrete Arch Dams," by Fenves, G.L., Mojtahedi, S. and Reimer, R.B., September 1989, (PB92 139 674/AS)A07.

UCB/EERC-89/13 "Mechanics of Low Shape Factor Elastomeric Seismic Isolation Bearings," by Aiken, I.D., Kelly, J.M. and Tajirian, F.F., November 1989, (PB92 139 732/AS)A09.

UCB/EERC-89/14 "Preliminary Report on the Seismological and Engineering Aspects of the October 17, 1989 Santa Cruz (Loma Prieta) Earthquake," by EERC, October 1989, (PB92 139 682/AS)A04.

UCB/EERC-89/15 "Experimental Studies of a Single Story Steel Structure Tested with Fixed, Semi-Rigid and Flexible Connections," by Nader, M.N. and Astaneh-Asl, A., August 1989, (PB91 229 211/AS)A10.

UCB/EERC-89/16 "Collapse of the Cypress Street Viaduct as a Result of the Loma Prieta Earthquake," by Nims, D.K., Miranda, E., Aiken, I.D., Whittaker, A.S. and Bertero, V.V., November 1989, (PB91 217 935/AS)A05.

UCB/EERC-90/01 "Mechanics of High-Shape Factor Elastomeric Seismic Isolation Bearings," by Kelly, J.M., Aiken, I.D. and Tajirian, F.F., March 1990.

UCB/EERC-90/02 "Javid's Paradox: The Influence of Preform on the Modes of Vibrating Beams," by Kelly, J.M., Sackman, J.L. and Javid, A., May 1990, (PB91 217 943/AS)A03.

UCB/EERC-90/03 "Earthquake Simulator Testing and Analytical Studies of Two Energy-Absorbing Systems for Multistory Structures," by Aiken, I.D. and Kelly, J.M., October 1990, (PB92 192 988)A13.

UCB/EERC-90/04 "Unassigned," by Unassigned, 1990.

UCB/EERC-90/05 "Preliminary Report on the Principal Geotechnical Aspects of the October 17, 1989 Loma Prieta Earthquake," by Seed, R.B., Dickenson, S.E., Riemer, M.F., Bray, J.D., Sitar, N., Mitchell, J.K., Idriss, I.M., Kayen, R.E., Kropp, A., Harder, L.F., Jr. and Power, M.S., April 1990, (PB 192 970)A08.

UCB/EERC-90/06 "Models of Critical Regions in Reinforced Concrete Frames Under Seismic Excitations," by Zulfiqar, N. and Filippou, F.C., May 1990.

UCB/EERC-90/07 "A Unified Earthquake-Resistant Design Method for Steel Frames Using ARMA Models," by Takewaki, I., Conte, J.P., Mahin, S.A. and Pister, K.S., June 1990, PB92-192947(A06).

UCB/EERC-90/08 "Soil Conditions and Earthquake Hazard Mitigation in the Marina District of San Francisco," by Mitchell, J.K., Masood, T., Kayen, R.E. and Seed, R.B., May 1990, (PB 193 267/AS)A04.

UCB/EERC-90/09 "Influence of the Earthquake Ground Motion Process and Structural Properties on Response Characteristics of Simple Structures," by Conte, J.P., Pister, K.S. and Mahin, S.A., July 1990, (PB92 143 064)A15.

UCB/EERC-90/10 "Experimental Testing of the Resilient-Friction Base Isolation System," by Clark, P.W. and Kelly, J.M., July 1990, (PB92 143 072)A08.

UCB/EERC-90/11 "Seismic Hazard Analysis: Improved Models, Uncertainties and Sensitivities," by Araya, R. and Der Kiureghian, A., March 1988, PB92-193010(A08).

UCB/EERC-90/12 "Effects of Torsion on the Linear and Nonlinear Seismic Response of Structures," by Sedarat, H. and Bertero, V.V., September 1989, (PB92 193 002/AS)A15.

UCB/EERC-90/13 "The Effects of Tectonic Movements on Stresses and Deformations in Earth Embankments," by Bray, J. D., Seed, R. B. and Seed, H. B., September 1989, PB92-192996(A18).

UCB/EERC-90/14 "Inelastic Seismic Response of One-Story, Asymmetric-Plan Systems," by Goel, R.K. and Chopra, A.K., October 1990, (PB93 114 767)A11.

UCB/EERC-90/15 "Dynamic Crack Propagation: A Model for Near-Field Ground Motion.," by Seyyedian, H. and Kelly, J.M., 1990.

UCB/EERC-90/16 "Sensitivity of Long-Period Response Spectra to System Initial Conditions," by Blasquez, R., Ventura, C. and Kelly, J.M., 1990.

UCB/EERC-90/17	"Behavior of Peak Values and Spectral Ordinates of Near-Source Strong Ground-Motion over a Dense Array," by Niazi, M., June 1990, (PB93 114 833)A07.
UCB/EERC-90/18	"Material Characterization of Elastomers used in Earthquake Base Isolation," by Papoulia, K.D. and Kelly, J.M., 1990, PB94-190063(A08).
UCB/EERC-90/19	"Cyclic Behavior of Steel Top-and-Bottom Plate Moment Connections," by Harriott, J.D. and Astaneh-Asl, A., August 1990, (PB91 229 260/AS)A05.
UCB/EERC-90/20	"Seismic Response Evaluation of an Instrumented Six Story Steel Building," by Shen, J.-H. and Astaneh-Asl, A., December 1990, (PB91 229 294/AS)A04.
UCB/EERC-90/21	"Observations and Implications of Tests on the Cypress Street Viaduct Test Structure," by Bollo, M., Mahin, S.A., Moehle, J.P., Stephen, R.M. and Qi, X., December 1990, (PB93 114 775)A13.
UCB/EERC-91/01	"Experimental Evaluation of Nitinol for Energy Dissipation in Structures," by Nims, D.K., Sasaki, K.K. and Kelly, J.M., 1991.
UCB/EERC-91/02	"Displacement Design Approach for Reinforced Concrete Structures Subjected to Earthquakes," by Qi, X. and Moehle, J.P., January 1991, (PB93 114 569/AS)A09.
UCB/EERC-91/03	"A Long-Period Isolation System Using Low-Modulus High-Damping Isolators for Nuclear Facilities at Soft-Soil Sites," by Kelly, J.M., March 1991, (PB93 114 577/AS)A10.
UCB/EERC-91/04	"Dynamic and Failure Characteristics of Bridgestone Isolation Bearings," by Kelly, J.M., April 1991, (PB93 114 528)A05.
UCB/EERC-91/05	"Base Sliding Response of Concrete Gravity Dams to Earthquakes," by Chopra, A.K. and Zhang, L., May 1991, (PB93 114 544/AS)A05.
UCB/EERC-91/06	"Computation of Spatially Varying Ground Motion and Foundation-Rock Impedance Matrices for Seismic Analysis of Arch Dams," by Zhang, L. and Chopra, A.K., May 1991, (PB93 114 825)A07.
UCB/EERC-91/07	"Estimation of Seismic Source Processes Using Strong Motion Array Data," by Chiou, S.-J., July 1991, (PB93 114 551/AS)A08.
UCB/EERC-91/08	"A Response Spectrum Method for Multiple-Support Seismic Excitations," by Der Kiureghian, A. and Neuenhofer, A., August 1991, (PB93 114 536)A04.
UCB/EERC-91/09	"A Preliminary Study on Energy Dissipating Cladding-to-Frame Connection," by Cohen, J.M. and Powell, G.H., September 1991, (PB93 114 510)A05.
UCB/EERC-91/10	"Evaluation of Seismic Performance of a Ten-Story RC Building During the Whittier Narrows Earthquake," by Miranda, E. and Bertero, V.V., October 1991, (PB93 114 783)A06.
UCB/EERC-91/11	"Seismic Performance of an Instrumented Six-Story Steel Building," by Anderson, J.C. and Bertero, V.V., November 1991, (PB93 114 809)A07.
UCB/EERC-91/12	"Performance of Improved Ground During the Loma Prieta Earthquake," by Mitchell, J.K. and Wentz, Jr., F.J., October 1991, (PB93 114 791)A06.
UCB/EERC-91/13	"Shaking Table - Structure Interaction," by Rinawi, A.M. and Clough, R.W., October 1991, (PB93 114 917)A13.
UCB/EERC-91/14	"Cyclic Response of RC Beam-Column Knee Joints: Test and Retrofit," by Mazzoni, S., Moehle, J.P. and Thewalt, C.R., October 1991, (PB93 120 277)A03.
UCB/EERC-91/15	"Design Guidelines for Ductility and Drift Limits: Review of State-of-the-Practice and State-of-the-Art in Ductility and Drift-Based Earthquake-Resistant Design of Buildings," by Bertero, V.V., Anderson, J.C., Krawinkler, H., Miranda, E. and The CUREe and The Kajima Research Teams, July 1991, (PB93 120 269)A08.
UCB/EERC-91/16	"Evaluation of the Seismic Performance of a Thirty-Story RC Building," by Anderson, J.C., Miranda, E., Bertero, V.V. and The Kajima Project Research Team, July 1991, (PB93 114 841)A12.
UCB/EERC-91/17	"A Fiber Beam-Column Element for Seismic Response Analysis of Reinforced Concrete Structures," by Taucer, F., Spacone, E. and Filippou, F.C., December 1991, (PB94 117 629AS)A07.
UCB/EERC-91/18	"Investigation of the Seismic Response of a Lightly-Damped Torsionally-Coupled Building," by Boroschek, R. and Mahin, S.A., December 1991, (PB93 120 335)A13.
UCB/EERC-92/01	"Studies of a 49-Story Instrumented Steel Structure Shaken During the Loma Prieta Earthquake," by Chen, C.-C., Bonowitz, D. and Astaneh-Asl, A., February 1992, (PB93 221 778)A08.
UCB/EERC-92/02	"Response of the Dumbarton Bridge in the Loma Prieta Earthquake," by Fenves, G.L., Filippou, F.C. and Sze, D.T., January 1992, (PB93 120 319)A09.
UCB/EERC-92/03	"Models for Nonlinear Earthquake Analysis of Brick Masonry Buildings," by Mengi, Y., McNiven, H.D. and Tanrikulu, A.K., March 1992, (PB93 120 293)A08.
UCB/EERC-92/04	"Shear Strength and Deformability of RC Bridge Columns Subjected to Inelastic Cyclic Displacements," by Aschheim, M. and Moehle, J.P., March 1992, (PB93 120 327)A06.
UCB/EERC-92/05	"Parameter Study of Joint Opening Effects on Earthquake Response of Arch Dams," by Fenves, G.L., Mojtahedi, S. and Reimer, R.B., April 1992, (PB93 120 301)A04.

UCB/EERC-92/06 "Seismic Behavior and Design of Semi-Rigid Steel Frames," by Nader, M.N. and Astaneh-Asl, A., May 1992, PB93-221760(A17).

UCB/EERC-92/07 "A Beam Element for Seismic Damage Analysis," by Spacone, E., Ciampi, V. and Filippou, F.C., August 1992, (PB95-192126)A06.

UCB/EERC-92/08 "Nonlinear Static and Dynamic Analysis of Reinforced Concrete Subassemblages," by Filippou, F.C., D'Ambrisi, A. and Issa, A., August 1992, PB95-192175(A09).

UCB/EERC-92/09 "Evaluation of Code Accidental-Torsion Provisions Using Earthquake Records from Three Nominally Symmetric-Plan Buildings," by De la Llera, J.C. and Chopra, A.K., September 1992, (PB94 117 611)A08.

UCB/EERC-92/10 "Slotted Bolted Connection Energy Dissipators," by Grigorian, C.E., Yang, T.-S. and Popov, E.P., July 1992, (PB92 120 285)A03.

UCB/EERC-92/11 "Mechanical Characteristics of Neoprene Isolation Bearings," by Kelly, J.M. and Quiroz, E., August 1992, (PB93 221 729)A07.

UCB/EERC-92/12 "Application of a Mass Damping System to Bridge Structures," by Hasegawa, K. and Kelly, J.M., August 1992, (PB93 221 786)A06.

UCB/EERC-92/13 "Earthquake Engineering Research at Berkeley - 1992," by EERC, October 1992, PB93-223709(A10).

UCB/EERC-92/14 "Earthquake Risk and Insurance," by Brillinger, D.R., October 1992, (PB93 223 352)A03.

UCB/EERC-92/15 "A Friction Mass Damper for Vibration Control," by Inaudi, J.A. and Kelly, J.M., October 1992, (PB93 221 745)A04.

UCB/EERC-92/16 "Tall Reinforced Concrete Buildings: Conceptual Earthquake-Resistant Design Methology," by Bertero, R.D. and Bertero, V.V., December 1992, (PB93 221 695)A12.

UCB/EERC-92/17 "Performance of Tall Buildings During the 1985 Mexico Earthquakes," by Terán-Gilmore, A. and Bertero, V.V., December 1992, (PB93 221 737)A11.

UCB/EERC-92/18 "Dynamic Analysis of Nonlinear Structures using State-Space Formulation and Partitioned Integration Schemes," by Inaudi, J.A. and De la Llera, J.C., December 1992, (PB94 117 702/AS/A05.

UCB/EERC-93/01 "Seismic Performance of an Instrumented Six-Story Reinforced-Concrete Building," by Anderson, J.C. and Bertero, V.V., 1993.

UCB/EERC-93/02 "Evaluation of an Active Variable-Damping-Structure," by Polak, E., Meeker, G., Yamada, K. and Kurata, N., 1993, (PB93 221 711)A05.

UCB/EERC-93/03 "An Experimental Study of Flat-Plate Structures under Vertical and Lateral Loads," by Hwang, S.-H. and Moehle, J.P., February 1993, (PB94 157 690/AS)A13.

UCB/EERC-93/04 "Seismic Performance of a 30-Story Building Located on Soft Soil and Designed According to UBC 1991," by Terán-Gilmore, A. and Bertero, V.V., 1993, (PB93 221 703)A17.

UCB/EERC-93/05 "Multiple-Support Response Spectrum Analysis of the Golden Gate Bridge," by Nakamura, Y., Der Kiureghian, A. and Liu, D., May 1993, (PB93 221 752)A05.

UCB/EERC-93/06 "On the Analysis of Structures with Viscoelastic Dampers," by Inaudi, J.A., Zambrano, A. and Kelly, J.M., August 1993, PB94-165867(A06).

UCB/EERC-93/07 "Earthquake Analysis and Response of Concrete Gravity Dams Including Base Sliding," by Chávez, J.W. and Fenves, G.L., December 1993, (PB94 157 658/AS)A10.

UCB/EERC-93/08 "Model for Anchored Reinforcing Bars under Seismic Excitations," by Monti, G., Spacone, E. and Filippou, F.C., December 1993, PB95-192183(A05).

UCB/EERC-93/09 "A Methodology for Design of Viscoelastic Dampers in Earthquake-Resistant Structures," by Abbas, H. and Kelly, J.M., November 1993, PB94-190071(A10).

UCB/EERC-93/10 "Tuned Mass Dampers Using Viscoelastic Dampers," by Inaudi, J.A., Lopez-Almansa, F. and Kelly, J.M., December 1993.

UCB/EERC-93/11 "Nonlinear Homogeneous Dynamical Systems," by Inaudi, J.A. and Kelly, J.M., October 1995.

UCB/EERC-93/12 "Synthesized Strong Ground Motions for the Seismic Condition Assessment of the Eastern Portion of the San Francisco Bay Bridge," by Bolt, B.A. and Gregor, N.J., December 1993, PB94-165842(A10).

UCB/EERC-93/13 "On the Analysis of Structures with Energy Dissipating Restraints," by Inaudi, J.A., Nims, D.K. and Kelly, J.M., December 1993, PB94-203619(A07).

UCB/EERC-94/01 "Preliminary Report on the Seismological and Engineering Aspects of the January 17, 1994 Northridge Earthquake," by EERC, January 1994, (PB94 157 666/AS)A05.

UCB/EERC-94/02 "Energy Dissipation with Slotted Bolted Connections," by Grigorian, C.E. and Popov, E.P., February 1994, PB94-164605.

UCB/EERC-94/03 "The Influence of Plate Flexibility on the Buckling Load of Elastomeric Isolators," by Kelly, J.M., March 1994, PB95-192134(A04).

UCB/EERC-94/04 "Insitu Test Results from Four Loma Prieta Earthquake Liquefaction Sites: SPT, CPT, DMT and Shear Wave Velocity," by Mitchell, J.K., Lodge, A.L., Coutinho, R.Q., Kayen, R.E., Seed, R.B., Nishio, S. and Stokoe II, K.H., April 1994, PB94-190089(A09).

UCB/EERC-94/05 "Seismic Response of Steep Natural Slopes," by Sitar, N. and Ashford, S.A., May 1994, PB94-203643(A10).

UCB/EERC-94/06 "Small-Scale Testing of a Self-Centering Friction Energy Dissipator for Structures," by Nims, D.K. and Kelly, J.M., August 1994.

UCB/EERC-94/07 "Accidental and Natural Torsion in Earthquake Response and Design of Buildings," by De la Llera, J.C. and Chopra, A.K., June 1994, PB94-203627(A14).

UCB/EERC-94/08 "Preliminary Report on the Principal Geotechnical Aspects of the January 17, 1994 Northridge Earthquake," by Stewart, J.P., Bray, J.D., Seed, R.B. and Sitar, N., June 1994, PB94203635(A12).

UCB/EERC-94/09 "Performance of Steel Building Structures During the Northridge Earthquake," by Bertero, V.V., Anderson, J.C. and Krawinkler, H., August 1994, PB95-112025(A10).

UCB/EERC-94/10 "Manual for Menshin Design of Highway Bridges: Ministry of Construction, Japan," by Sugita, H. and Mahin, S., August 1994, PB95-192100(A08).

UCB/EERC-94/11 "Earthquake Analysis and Response of Two-Level Viaducts," by Singh, S.P. and Fenves, G.L., October 1994, (A09).

UCB/EERC-94/12 "Response of the Northwest Connector in the Landers and Big Bear Earthquakes," by Fenves, G.L. and Desroches, R., December 1994, PB95-192001(A08).

UCB/EERC-95/01 "Geotechnical Reconnaissance of the Effects of the January 17, 1995, Hyogoken-Nanbu Earthquake, Japan," by , August 1995, PB96-143300.

UCB/EERC-95/02 "The Attenuation of Strong Ground Motion Displacement," by Gregor, N.J., June 1995, PB95-269346.

UCB/EERC-95/03 "Upgrading Bridge Outrigger Knee Joint Systems," by Stojadinovic, B. and Thewalt, C.R., June 1995, PB95-269338.

UCB/EERC-95/04 "Earthquake Hazard Reduction in Historical Buildings Using Seismic Isolation," by Garevski, M., June 1995, PB95-269312.

UCB/EERC-95/05 "Final Report on the International Workshop on the Use of Rubber-Based Bearings for the Earthquake Protection of Building," by Kelly, J.M., May 1995.

UCB/EERC-95/06 "Seismic Rehabilitation of Framed Buildings Infilled with Unreinforced Masonry Walls Using Post-Tensioned Steel Braces," by Terán-Gilmore, A., Bertero, V.V. and Youssef, N., June 1995, PB96-143136.

UCB/EERC-95/07 "Earthquake Analysis and Response of Concrete Arch Dams," by Tan, H. and Chopra, A.K., August 1995, PB96-143185.

UCB/EERC-95/08 "Behavior of Pre-Northridge Moment Resisting Steel Connections," by Yang, T.-S. and Popov, E.P., August 1995, PB96-143177.

UCB/EERC-95/09 "Seismic Behavior and Retrofit of Older Reinforced Concrete Bridge T-Joints," by Lowes, L.N. and Moehle, J.P., September 1995.

UCB/EERC-95/10 "Seismological and Engineering Aspects of the 1995 Hyogoken-Nanbu (Kobe) Earthquake," by EERC, November 1995.

UCB/EERC-95/11 "Studies in Steel Moment Resisting Beam-to-Column Connections for Seismic-Resistant Design," by Blackman, B. and Popov, E.P., October 1995, PB96-143243.

UCB/EERC-95/12 "Natural Rubber Isolation Systems for Earthquake Protection of Low-Cost Buildings," by Taniwangsa, W., Clark, P. and Kelly, J.M., December 1995.

UCB/EERC-95/13 "Analytical and Experimental Studies of Steel Connections and Energy Dissipators," by Yang, T.-S. and Popov, E.P., December 1995.

UCB/EERC-96/01 "Earthquake Engineering Research at Berkeley -- 1996: Papers Presented at the 11th World Conference on Earthquake Engineering," by EERC, May 1996.

U.S. DEPARTMENT OF COMMERCE
Technology Administration
National Technical Information Service
Springfield, VA 22161 (703) 487-4650